Radical-Anion-Photodetachment-Photoelectron-Spectroscopy: Application to a Variety of Molecules with extended π-Systems

Inaugural Dissertation

zur Erlangung des Doktorgrades
der Mathematisch-Naturwissenschaftlichen Fakultät
der Heinrich-Heine-Universität zu Düsseldorf

vorgelegt von
Bernd Kosper
aus Ochsenfurt

Düsseldorf, Januar 2022

aus dem Institut für Lasermassenspektroskopie
der Heinrich-Heine-Universität Düsseldorf

Gedruckt mit freundlicher Genehmigung der
Mathematisch-Naturwissenschaftlichen Fakultät der
Heinrich-Heine-Universität Düsseldorf

Referent: Prof. Dr. Rainer Weinkauf
Koreferent: Prof. Dr. M. Schmitt
Datum der mündlichen Prüfung: 27.01.2022

Meiner Frau

Meinen Eltern

Meinen Großeltern

Erklärung

Hiermit versichere ich, Bernd Günter Kosper, dass ich die dieser Dissertation zugrunde liegenden Arbeiten selbstständig und eigenhändig durchgeführt habe. Des Weiteren erkläre ich, dass die vorliegende Arbeit selbstständig und ohne fremde Hilfe verfasst habe und die benutzten Quellen wörtlich und inhaltlich entnommenen Stellen deutlich als solche gekennzeichnet habe.

Diese Dissertation wurde bisher weder im In- noch Ausland als Prüfungsarbeit vorgelegt.

Düsseldorf, 02. November 2021

Ort, Datum

Bernd Kosper

Danksagung

Die vorliegende Dissertation wurde am Institut für Physikalische Chemie I in der Abteilung für Lasermassenspektroskopie der Heinrich-Heine-Universität Düsseldorf unter der Leitung von Herrn Prof. Dr. Rainer Weinkauf angefertigt.

Besonderer Dank geht an:

Herrn Prof. Dr. Rainer Weinkauf für die unermüdliche und intensive Betreuung während meiner Masterarbeit und die Jahre meiner Promotion. Ebenso bedanke ich mich für meine Aufnahme in den Arbeitskreis im Vorfeld meiner Masterarbeit als wissenschafliche Hilfskraft. Auch für die Zahlreichen fachlichen Diskussionen und die allgemein familäre Atmosphäre, möchte ich meinen Dank ausdrücken.

Herrn Prof. Dr. Michael Schmitt für die Übernahme des Koreferats und seiner Funktion als Mentor während der Promotion.

Herrn Paul Konieczny, für die ausgezeichnete Betreuung während meiner Masterarbeit und die Einarbeitung in das komplexe Thema der Anionen-Spektroskopie.

Andreas Wolters, Fabian Drenkow, Paul Konieczny und Bettina Deckert für die gemeinsame und auch lustige Zeit im Büro, Labor sowie bei externen Treffen/ Essen/ Feiern, aber ebenso für die angenehme und familiäre Arbeitsatmosphäre und die anregenden Gespräche.

Den Mitarbeitern der Feinmechanik-Werkstatt der Heinrich-Heine-Universität Düsseldorf, ohne deren großen Hilfe bei der Umsetzung von Bauteilen diese Dissertation nicht möglich gewesen wäre.

Meiner Frau Alexandra, die mich mit Engelsgeduld jederzeit und mit jeder Faser unterstützt , aufgebaut und immer wieder daran erinnert hat was wir gemeinsam erreichen können.

Meinen Eltern Irmi und Martin sowie Großeltern Käthe und Gottfried, als auch Sara und Martin ohne deren Unterstützung und Liebe ich nicht annähernd so weit gekommen wäre. Kein Ausdruck der Welt beschreibt meine Dankbarkeit für euren Einsatz für mich.

Meiner Schwiegermutter Carmen und ihrem Lebensgefährten Olaf, für die regelmäßige Unterbringung in der Heimat und der vielen Gespräche, insbesondere über meine "unverständliche" Arbeit.

Meinem Schwiegervater Hans für seine Unterstützung, vor allem im Bereich der englischen Sprache bei der Anfertigung der Arbeit.

Den Herren Angelo Altavilla, Mirko Lindic und Peter Brüggemann, für die letzten 9 Jahre. Die besten Kommilitonen und Freunde, die man als Auswärtiger an der HHU finden konnte.

Abstract

In this work the electron affinities and the energetics of low-lying triplet states of a great variety of large molecules have been measured which have extended π systems . Some of the investigated molecules or their variants have potential applications as colour dyes or chromophores in molecular electronic devices.

The approach of this work is, to first form radical anions of the intact sample molecules, select the sample molecule or the molecular cluster by mass spectrometry, then detach an electron by laser excitation and to measure the kinetic energy of the removed electron.

Only the access via the radical anion allows to circumvent optical selection rules valid for neutral molecules, enabling the direct spectroscopy of otherwise "forbidden" states. In total 15 molecules are investigated, for which so far no or only vague values for electron affinities and no S_0 - T_1 transition energies are known. The efficient access to so many molecular systems becomes feasible due to a new method of anion formation. The construction, the realisation, the testing and the properties of the new discharge anion formation is described in this work in detail. The new anion formation method comprises a short-pulsed discharge, which takes place in a pulsed molecule-argon co-expansion, in front of a pulsed gas nozzle. The observed evidences show, that this new anion source is able to efficiently and very stably form intact radical anions, even from those molecules, which can offer only extremely weakly bound states, such as dipole-bound states.

For the first time the measured electronic state order of these manifold molecules allows a systematic comparison and an investigation of the question, how substitutions in different positions of a core chromophore (here mostly anthracene) influence the molecular electronic state energetics. The sample data are compared to literature data and an effort is made to explain already known photo-physics of these sample molecules on the basis of the new results.

In dieser Arbeit wurden die Elektronenaffinitäten und die energetischen Lagen niedrig liegender Triplettzustände von einer Vielzahl von grossen Molekülen mit ausgedehnten π-Systemen gemessen. Einige der untersuchten Moleküle oder deren Varianten, weisen großes Potential in der Anwendung als Farbstoff oder Chromophor in molekularen elektronischen Bauelementen auf.

Das Konzept dieser Arbeit war es, zunächst Radikal-Anionen von intakten Probemolekülen zu generieren, diese Probemoleküle bzw. Cluster mittels Massenspektrometrie zu trennen und dann mittels dem Herauslösen von Elektronen durch Laseranregung die kinetische Energie dieser Elektronen zu messen. Nur der Zugang über das Radikal-Anion ermöglicht ein

Umgehen der optischen Auswahlregeln die für neutrale Moleküle gelten, was eine direkte Spektroskopie von sonst "verbotenen" Zuständen erlaubt. Insgesamt wurden 15 Moleküle untersucht, für welche nur wage oder keine Werte der Elektronenaffinitäten oder der S_0-T_1-Übergange bekannt waren. Der effiziente Zugang zu derart vielen molekularen Systemen war lediglich durch eine neue Methode der Anionenerzeugung möglich. Die Konstruktion, Realisierung, Erprobung und Eigenschaften dieser neuen entladungsgestützten Erzeugung von Anion wurde in dieser Arbeit beschrieben. Die neue Anionengenerationsmethode umfasst eine Kurzpulsentladung, welche in einer gepulsten Molekül-Argon Koexpansion, im Bereich vor einer gepulsten Gasdüse stattfindet. Die Beobachtungen indizieren, dass diese neue Anionenquelle effizient und stabil Anionen generiert, selbst von Molekülen welche nur extrem schwach gebundene Zustände aufweisen, wie beispielsweise dipolgebundene Zustände. Die gemessenen Reihenfolgen elektronischer Zustände so vieler Moleküle, erlaubt ein erstes Mal einen systematischen Vergleich und eine Untersuchung der Frage wie Substituenten in verschiedenen Positionen an Chromophoren (hier vorwiegend Anthracene) die molekularen elektronischen Zustände beeinflusst. Die erhobenen Daten werden mit der Literatur verglichen und ein Versuch der Erklärung von bereits bekannten photo-physikalischer Vorgängen wird auf der Basis der neuen Ergebnisse versucht.

Contents

1 Introduction

During the studies of chemistry, it is easy to become overwhelmed by the information which have been up to now accumulated for innumerable molecules: structural formulas, projection drawings, chemical bond strengths, rotational vibrational and electronic energy levels, time scales of intra-molecular processes, chemical reaction-pathways and other information concerning physical and chemical properties in the gas and various condensed phases.

The major part of this molecular data was gathered by different spectroscopic methods. Spectroscopy in general, is in most cases the measurement and interpretation of these data which can be acquired as a result of the interaction of photons with atoms or molecules. These molecules are either isolated in the gas phase, diluted in solutions or arranged in aggregates of different sizes. The latter can cover the gap from the single molecule to the solid state matter. By using different photon wavelengths, numerous physical and chemical data and properties have been explored over the last 50 years, which allowed to gain specific microscopic information on manifold molecules.

With the accessibility of high-intensity and narrow-bandwidth lasers, countless optical properties of molecules can be investigated with high accuracy and in great depth.

The simplest light-matter interaction is the physical reflection of the light on surfaces, either macroscopic surfaces (the outer surface of an object) or microscopic surfaces (the surfaces between different phases, different crystal modifications or simply crystal orientations) inside a poly-crystal solid state. However, in the latter case only those wavelengths of the light can be reflected, which are not absorbed. Hence, absorption and reflection mainly define the colour of the macroscopic objects in our daily environment.

If the weak light-matter non-resonant diffraction processes are neglected, such as Raman-effects [RAM21], the difference between a direct photon reflection at such a micro-crystal surface and photon emission process from a molecule after a photon absorption is, that in the latter process a time delay and often also a change in colour. Also a lot of possible directions of the outgoing versus the incoming photon is observed. Hence, after absorption the photon energy is within the molecule for a certain time .

As a first expectation, in an analogy to atoms, a re-emission of the same photon or a photon of similar colour, termed in general luminescence, would be the main answer of the molecule. But by a rough check of the light and its colours which are present in our daily environment it becomes evident, that the re-emission of photons from a molecule is not the main process and only happens efficiently in a small fraction of all molecules. In most of molecules the absorbed energy is simply converted from electronic to vibrational energy, which is termed heat in an ensemble of molecules .

A first essential understanding for the non-radiative processes which happen in molecules after photoabsorption was provided by a strongly simplified visualization in the ladder of the electronic states of the molecule, invented by Jablonski and therefore termed "the Jablonski scheme" [Jab33]. In this scheme, the role of the respective excited electronic states and their vibrations for photoabsorption and photoemission can be explained, but more importantly also radiation-less energy deactivation processes can be understood. The main message of this scheme is that the excited electronic states of a molecule (with their energetic order, energetic spacings, electronic wave-function characters, total electron spin and geometries) are the key elements for the understanding of the molecular processes which happen in molecules after a photoexcitation.

For example, after photoexcitation of a molecule to one of the lowest singlet states, fluorescence from the S_1-state and/or –less often– phosphorescence from the triplet T_1-state can happen. This light emission channels carry signatures of the molecular properties and can be investigated in detail in order to derive molecular parameters, such as geometric structures, energies, dynamics of physical and chemical processes and so forth.

However, after photoexcitation non-radiative processes happen in many molecules instead of photon emission: the energy of the photoexcitation is simply converted to heat. Therefore, for these molecules the methods fluorescence excitation spectroscopy and dispersed fluorescence spectroscopy are not applicable. In such cases either the non-sensitive absorption spectroscopy or a resonant enhanced multiphoton ionization (REMPI or RPI) scheme has to be applied to produce well-detectable signals [SBZ21].

Typically from the neutral S_0 ground state of a molecule usually it is not possible to investigate a triplet state by direct absorption or emission, since they are not accessible by photoexcitation from S_0 due to the electron spin conservation during optical excitations. If triplet states are "invisible" and not accessible by photoexcitation, the obvious and important question arises, why is it at all necessary to know more about these triplet states. Do they have any importance for fundamental molecular processes? The number of actual research topics in which triplet states are involved provide the answer to this question.

Triplet states are involved in:

- the deactivation of S_1 state populations in countless molecules
- photo-destruction of molecules by intra- or intermolecular excited state chemistry
- the limitation for the photoemission efficiency in organic light emitting diodes (OLED)
- semiconductors used for triplet-triplet up-conversion [OGMA21]
- electron spin resonance spectroscopy [BAB+19]
- supramolecular photocatalysis, e.g. for [4+2] additions [UOK+20]
- photopolymerisation processes [ABDC20] and
- analytics on biomolecules [GBA+11]

The list above is quite long, but definitely still not a complete collection of the topics were triplet states are playing an important role. As already mentioned in the context of the Jablonski scheme, the relative order of the electronic singlet and triplet states and their character play the most important role for the photophysics of a molecule.

Although some exotic methods exist to determine the energetics of triplet states in solid state, there are just two methods to observe them directly and in isolated molecules in the gas phase. These are:

- i) electron energy loss spectroscopy ([HAAS03])
- ii) the radical anion PD[1]-PES[2] used in this work

Both methods are enabling directly access low-lying triplet states and have the potential to observe otherwise transition-forbidden singlet states.

Theoretically angle- and energy-resolved EELS[3] is even able to distinguish transitions to triplet and singlet states in the spectra ([HAAS03]) by using different energies of the primary electron and different detection angles , a feature PD-PES is not able to provide. However, to the authors knowledge EELS was up to now only applied to small and mediocre-sized molecules without supersonic cooling. This is a strong drawback especially for large molecules which have to be heated up to high temperatures for evaporation. In

---

[1] Photodetachment

[2] Photoelectron Spectroscopy

[3] electron energy loss spectroscopy

addition, since the EELS method is applied directly in the inlet chamber, severe surface contamination with sample molecules is a significant problem ([TVC+98]). In contrast to this the anion PD-PES is performed after mass selection in a separate high-vacuum chamber.

Usually for almost all spectroscopy methods – EELS included – the initial starting state is the ground state of the neutral molecule. Neutral ground state molecules are usually closed-shell molecules, which means that all molecular orbitals are full and the total electron spin is $S = 0$. The multiplicity (degeneracy) of the ground state is one and it is therefore termed as a singlet state S_0.

By using the radical anion as starting position, the initial state for spectroscopy changes from the ground state of the neutral molecule S_0 to an open shell state with an overall spin $S = \frac{1}{2}$, which is a doublet state. Beginning from this state, using photoexcitation to remove an electron the total spin is changed by $\pm\frac{1}{2}$ leading to singlet ($S = 0$) and triplet ($S = 1$) states of the neutral molecule equally. The energy of the emitted electron then carries the information of the neutral molecule to which final state the excitation took place. This is the spectroscopy concept used in this work.

Advantages of the method in comparison to coventional spectroscopy are, that the radical anions can be internally cooled and mass-selected in a time-of-flight mass spectrometer (TOF[4]-MS[5]) prior to photodetachment and photoelectron spectroscopy.

The here presented thesis also features a new efficient method for generating cold, intact radical anions. This new anion formation method drastically reduces the effort and the time needed to run photoelectron measurements. Due to this improvement, the following molecular systems can be investigated:

- heterocyclic species like 5Fi[6], 6Fi[7], DBF[8] and f9one[9]
- polyaromatic hydrocarbons , mostly anthracene derivatives
- the organic complex compound copper(II)phthalocyanine

Numerous EA[10] values and state energies for many triplet T_1 states and some forbidden or only weakly allowed singlet states can be obtained for many molecules, which could not be investigated before.

---

[4] time-of-flight
[5] Mass Spectrometry
[6] 5-Fluoroindole
[7] 6-Fluoroindole
[8] Dibenzofurane
[9] 9H-Fluorenone
[10] electron affinity

In addition it is possible to test and evaluate the new anion generation method. For this previously well-investigated sample molecules were re-measured in the new set.up for comparison (compare 4.2.1 for a reference with pyrene).
This work is organized as following:

- Introduction to required background information to facilitate the understanding of the process of anion formation as well as the principles and physical properties of discharges. this theoretical outline only includes the information necessary to understand the subject of this work.
- Provision of the concept and theory behind the photodetachment process of radical anions.
- Detailed descriptions of the experimental set-up, vacuum system, short-pulse laser as well as other therefor significant components, enabling to form a connection/link between theoretical knowledge and the experiment performed for this work.
- Presentation and assignment of the molecular PD-PE spectra as well as embedding into the context of data already known for the investigated molecules.
- Finally a comparison between the results of molecules with similar chemical structures is performed.

2 Theory

2.1 Discharge Phenomena

One of the most well known examples of discharge phenomena is lightening in thunderstorms. Since the 19th century, artificial discharges and especially their light emission phenomena have been subject of many scientific investigations.
A pulsed discharge in a pulsed, supersonic co-expansion of neutral sample molecules with the rare gas argon is used for the formation of intact molecular radical anions in this work
.
To the knowledge of the author this is the first time that a pulsed discharge in a gas pulse outside the nozzle is used for radical anion formation of intact molecules.
In this set-up, a combination of several exceptional methods is used, which are - as a combination - unique in comparison to previous experiments of others (see Figure 2.1).

The goal of this chapter is to outline first the well-known theoretical and practical aspects of different discharges, in order to subsequently obtain a qualitative understanding of the processes, which happen in the used anion source. In order to be able to pick the relevant information from the following review on the research performed on discharges, it is necessary to know the main elements of the discharge anion source. In Figure 2.1 the set-up of our inlet system is shown as a two-dimensional sketch. It is mounted into a vacuum chamber and consists of 1) a pulsed and heated gas nozzle, which is also the anode, 2) eight Tungsten needles as cathodes, arranged in a concentric symmetry around the nozzle orifice at a distance of $4-5\ mm$ and 3) the skimmer, which selects the middle part of the expansion and the ion cloud and transfers it into the second vacuum chamber where it arrives in the pulsed ion source.
In Figure 2.1 from left to the right the timing of the main three processes is schematically displayed.
In the following the time sequence of the three main processes which are involved in the anion formation is explained (see Figure 2.1):

- Left inset of Fig. 2.1: The gas valve opens, releasing an expanding gas pulse (grey cloud) into the vacuum . The gas contains argon with a contribution of about 3% of sample molecules. The temporal width of the gas pulse is about 200 μs half-width-at-half-hight (hw). At this early time the set-up is still field-free.

- Middle inset: A negative HV-pulse (duration $1-2\ \mu s$) is applied at the needles. The discharge ignites into the expanding gas pulse in the direction of the nozzle head. Primary electrons are accelerated and cause an electron avalanche by multiple

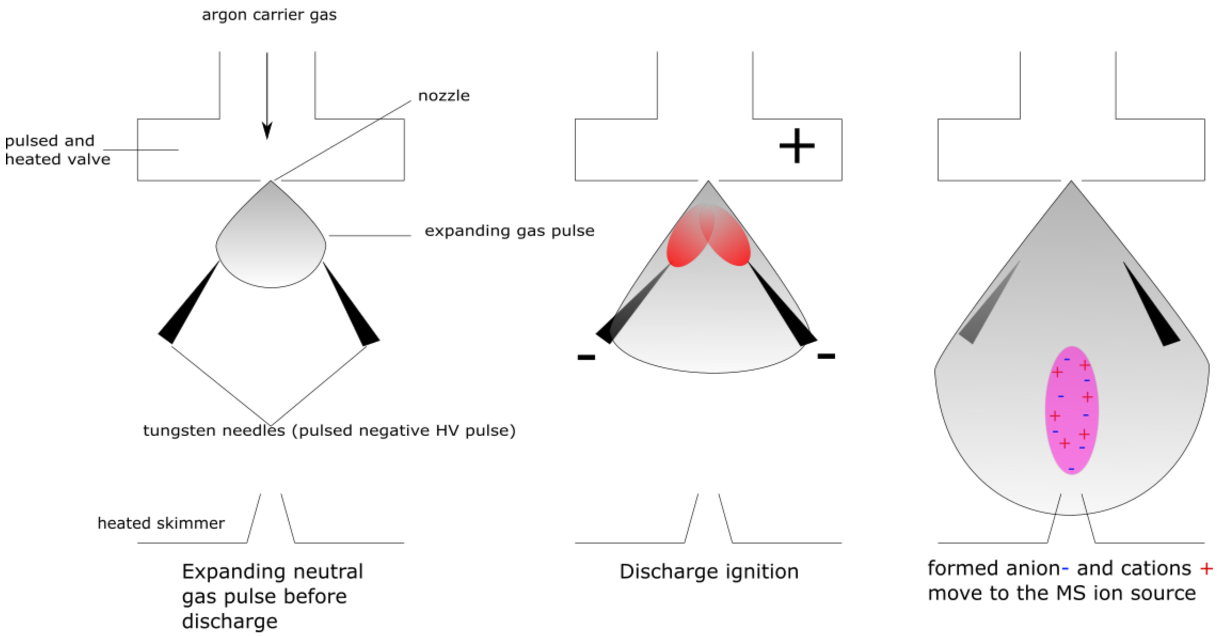

Figure 2.1: Illustration of the timing of the three main processes, taking place in the inlet chamber. The important devices of the set-up are: The pulsed gas nozzle, the needle cathodes and the skimmer for selection ans transfer of the ions to the second vacuum chamber. Left side: Opening of the gas nozzle and formation of the supersonic expansion. Middle: Application of the negative HV pulse at the needles and ignition of the discharge. Right side: After the voltage is switched off the ion cloud drifts downwards to the skimmer (see also text).

sequential ionisation processes. During this time, argon cations as well as sample anions are formed.

- Right inset: The HV-pulse is switched off. In the dense gas expansion the newly formed anions are cooled by collisions with the argon atoms and transported to and through the skimmer into the second vacuum chamber into the pulsed ion source of a mass spectrometer.

In comparison to other typical discharges (see subsequent chapters) the discharge used in this work has a very high complexity due to the fact that:

- The pulsed expansion of the gas through a small orifice results in a strong inhomogeneity of the gas density in time and space.
- The high voltage ($2.5 - 5\ kV$) at the cathode needles is switched on only for $1 - 2\ \mu s$. So prompt ignition of the discharge is necessary.

- The electric field and the gas density during the discharge is extremely inhomogeneous.
- The timing between the gas pulse and the discharge ignition pulse is critical.
- The electric field is switched off in a few nanoseconds, which means that the charge distribution present at the end of the discharge is conserved as it is and is no more distorted by electric fields.

It is nearly impossible to discuss and understand the processes, which happen in such a complex discharge without a detailed and broad knowledge of a variety of discharges, such as for example continuous discharges, discharges in homogeneous and inhomogeneous electric fields and discharges in gas columns of constant gas pressure and discharges in different gases.
Therefore,the for this work relevant part of the basic textbook knowledge on discharges is presented in the following . The described elements will enable a qualitative understanding of the microscopic processes that take place in the discharge anion source used herein.

2.1.1 Electric fields

Before talking about discharges, the basic laws of electrodynamics needs to be recalled. In a discharge, it has to be distinguished between the external field applied between the electrodes, which is necessary for maintaining the discharge and the internal space charge, which is produced by the charged particles moving in the gas between the electrodes.
A charge Q positioned at the origin $(0;0;0)$ of the cartesian coordinate system creates an electric field $E_{el.field}$ at the position $\vec{r}$. This centre-symmetric field can be written with Coulomb's law as [Gob71]:

$$\vec{E}(\vec{r})_{el.\ field} = \frac{Q}{4\pi \cdot \epsilon_0 \cdot \epsilon_r} \cdot \frac{\vec{r}}{r^3} \tag{2.1}$$

$\vec{r}$: position vector $[m]$
r: length of $\vec{r}$, distance to Q $[m]$
$\vec{E}(\vec{r})$: electric vector field $[\frac{V}{m}]$
Q: charge in coordinate origin $[m^2]$
ϵ_0: electric field constant $[\frac{A \cdot s}{V \cdot m}]$
ϵ_r: electric permittivity $[\frac{A \cdot s}{V \cdot m}]$

Recalling that $\frac{\vec{r}}{r}$ is a vector of the length 1, one realises that the electric field decreases with $\frac{1}{r^2}$ when moving away from the centre of the charge. If many charges of the same polarity are arranged in a certain volume, the resulting total electric field is just the sum of the individual field contributions [Gob71] :

$$\vec{E}(\vec{r}) = \frac{1}{4\pi \cdot \epsilon_0 \cdot \epsilon_r} \cdot \sum_{i=1}^{n} Q_i \frac{\vec{r} - \vec{r_i}}{|\vec{r} - \vec{r_i}|^3} \tag{2.2}$$

E: electric vector field $[\frac{V}{m}]$
$\vec{r}$: position vector $[m]$
$\vec{e_r}$: unified vector
Q: charge in coordinate origin $[m^2]$
ϵ_0: electric field constant $[\frac{A \cdot s}{V \cdot m}]$
ϵ_r: electric permittivity $[\frac{A \cdot s}{V \cdot m}]$

The formula above is the result of the super-positioning principle of electric and magnetic fields in electrodynamics. Later-on in this chapter it will be shown that the field caused by a cloud of positive charges, plays an important role for anion formation in pulsed discharges. Although the superposition principle is easy to be understood and to be applied, unfortunately, the field of an arbitrary charge distributions cannot easily be described mathematically for a given experiment because of the numerous charges and their irregular spatial distribution.Time consuming computer-simulations would be necessary which lie outside of this thesis.

In many experiments where discharges have been used or investigated, the electric field, which is applied at the electrodes is constant in time and space. The typical set-up consists of parallel electrodes at which the potential difference U is applied. Neglecting disturbances of the field at the borders of the plates (distance d between the plates is much smaller that the plate geometries), the field inside this plate geometry is homogeneous and can be written as [Gob71] :

$$E = \frac{U}{d} = \frac{Q}{\epsilon_0 \epsilon_r \cdot A} \tag{2.3}$$

E: electric field $[\frac{V}{m}]$
d: distance between plates $[m]$
A: plate area $[m^2]$
Q: charge [a.u.]
ϵ_0: electric field constant $[\frac{A \cdot s}{V \cdot m}]$
ϵ_r: electric permittivity $[\frac{A \cdot s}{V \cdot m}]$

ϵ_r is in the gas phase in effect one. In this set-up of parallel plate electrodes it is not necessary to write the electric field as a vector field, since it is homogeneous and the field lines are all parallel to each other and orthogonal to the plane electrodes. The lines of the electric field and the arrows of the forces on positive and negative charges can be seen in figure 2.2. In this homogeneous electric field, positive particles are accelerated along the field lines to the negative electrode (termed cathode) and electrons would be accelerated to the positively-charged plate, the anode.

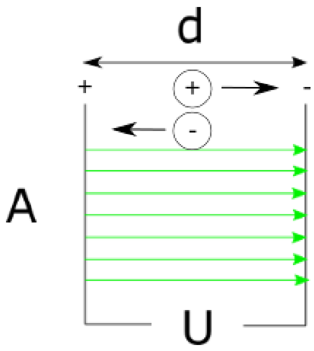

Figure 2.2: Two-dimensional illustration of the electric field lines between two opposite-charged parallel plates as described with formula (2.2). The field lines, displayed as green arrows, are orthogonal to the plates and parallel to each other. Note the field direction from + to − and the forces which act on the two opposite-charged particles. [Gob71]

The last example is the electric field distribution in an arrangement of two long concentric cylinders (see Figure 2.3). This field distribution comes into use in the Geiger-Mueller-set-up and qualitatively with reversed electrodes in the herein used setup. The function of the Geiger-Mueller-set-up will be explained below in detail.

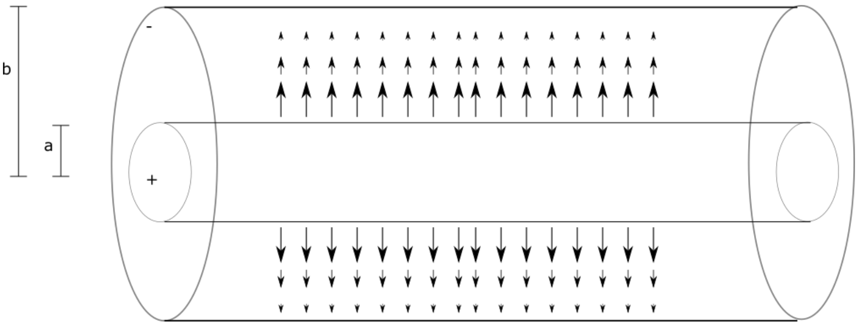

Figure 2.3: Three-dimensional illustration of the electric field lines between two concentric cylinders as described by formula (2.4). The outside cylinder is negatively charged and the inner cylinder (or wire) is positively charged. The electric field between the two cylinders is strongly inhomogeneous. It increases from the outer cylinder to the inner cylinder, which would be the flight direction for free electrons in a discharge.

The electric field between the two cylinders can be written in dependence on r, which is the distance from the centre of the inner wire.

$$E(\vec{r}) = \frac{\rho \cdot a^2}{2 \cdot \epsilon_0 \cdot r} \cdot \frac{\vec{r}}{r} \quad a < r < b, r = b - a, max. \tag{2.4}$$

E: electric field $[\frac{V}{m}]$
r: distance from centre $[m]$
a: inner wire radius $[m]$
b: outer cylinder radius $[m]$
ρ: charge distribution $[\frac{C}{m^3}]$
ϵ_0: electric field constant $[\frac{A \cdot s}{V \cdot m}]$

The electric field between the electrodes is strongly inhomogeneous and proportional to $\frac{1}{r}$. It has its maximum at the surface of the inner cylinder or wire and decreases with the distance from the inner wire.

As noted above, the most common application of this cylindrical electrode set-up is the Geiger-Mueller-Counter which is able to detect ionizing radiation (for details see below).

Conventional continuous discharges

If the distance d between two flat and parallel electrodes (- the anode (+) and the cathode $(-)$ -)is not too large and the voltage difference U is high enough (even at atmospheric pressure) after ignition, then discharges can burn stable. This means that in the gas phase charged particles can move from one electrode to the other. In-between the electrodes, the electrons are accelerated by the electric field $E_{field} = \frac{U}{d}$. If there are not too many collisions with the gas, their kinetic energy becomes high enough ($E_{kin} = q \cdot E_{field} \cdot l$ with l as the flight path of undisturbed acceleration) that they can cause electronic excitation or even ionisation in one of the next collisions with neutral atoms or molecules. When a single electron ionises a neutral atom, afterwards two free electrons exist. Such ionisation processes can happen several or even multiple times between the electrodes. This results in an amplification of the number of charged particles in the gas, which leads to an increase of the current through the gas and by this also stabilizes the discharge [Raj97].

At this point, it is obvious that the ionisation energy (IE) of the gas and its collisional cross section σ for ionisation with electrons comes into account. As already indicated above, the pressure (p) in the gas is an important parameter for discharges as well. Electrons and ions can only gain as much energy in the electric field as needed for the collisional ionisation process, if their flight is not too often decelerated or even stopped by collisions with neutral atoms.

The preceding description of continuous discharges between flat parallel electrodes shows, that already in such straightforward set-ups (continuous discharge, homogeneous electric field) many parameters are involved.

By changing the pressure and keeping the voltage constant, the well-known Franck-Hertz experiment [FH67] directly proves, that the electrons at first have to gain enough energy in the electric field in order to be able to excite or ionize the next neutral collision partner. If voltage and pressure are well-suited, the electron (and the ion amplification) by collisional ionisation can happen multiple times on the way to the attractive electrode. If the charge multiplication happens very often, it is more precisely described as an "avalanche effect".

The initial charge formation

The most relevant question for continuous and especially for pulsed discharges is: how the first free seed electrons are formed. The following scenarios for the initial charge formation can be imagined:

- Ionization of gas atoms or molecules between the electrodes by high-energetic photons or particles which stem from natural sources (see below 2.1.2).
- Ionization at the cathode surface by high-energetic photons or particles from natural sources.
- Spontaneous thermal electron emission by a strongly heated cathode and/or
- Spontaneous electron emission by tunnelling out of the cathode caused by a very strong local electric field at the metal surface.

Natural sources of high-energetic photons or particles are nuclear fission (natural radioactivity) or nuclear fusion processes (extraterrestrial radiation or particles from the sun or other interstellar sources). In former works, it was often assumed that the ionisation by natural high-energy processes takes place in the gas between the electrodes. Due to the much higher density of the atoms in the electrodes in comparison to the gas it seems more reasonable to assume that the first ionisation process takes place at the cathode surface. In the past often β emitters have been included in the cathode material in order to make sure that enough electrons for the discharge ignition are provided. This method is nowadays excluded for safety reasons.

Spontaneous electron emission either by heat or field or both needs very high temperatures or/and very high electric fields, as will be described below.

It is very important to note that the question "how the first free charge is formed" is not so important for continuous discharges but very essential for pulsed discharges. This holds especially for the discharge used in this work, where i) the ignition of the discharge should follow promptly the rise-time of the high voltage applied to the electrodes and ii) no charges are left over in the gas between the electrodes from the previous discharge pulse cycle.

After ignition (first free charge formation), the discharge can only form a stable current through the gas if at least a minimal avalanche amplification effect is present. As evident from the Franck-Hertz experiment the applied voltage, the gas pressure between the electrodes as well as the property of the gas in the electrode gap have an influence on the stability of the burning of the discharge as reflected in its light emission and the current through the discharge.

Since the cross section for the formation of negatively charged molecules and atoms is usually very small and radical anions can typically be only stabilised by energy-loss in low-energetic collisions (see Chapter 2.2) anions play virtually no active role in usual discharges.

One well-known exception is the molecule SF_6 which has a very large electron affinity and a very high cross section for the uptake of an electron [CO01] and therefore can scavenge free electrons. By this it is able to prevent the formation of discharges.

The asymmetric roles of electrons and ions in discharges

The role of the free electrons and the free ions (atomic ion core or radical cation molecule) in discharges is complex and not understood in all facets. First of all, the role of the electrons and the cations in discharges might be different for several reasons. The most obvious differences between an electron and and ion are i) their different masses, but also ii) that ionised and neutral atoms and molecules offer bound states for electrons. These differences have consequences for the microscopic processes happening in discharges. In a discharge, due to its small mass an electron in collisions with neutral atoms or molecules

- Cannot transfer a significant amount of kinetic energy to the kinetic energy of a heavy neutral atom or molecule as a whole: Low-energetic electrons are therefore expected to be scattered elastic (no loss of kinetic energy, just a change in the flight direction) as long as their kinetic energy is not too high.

- High-energetic electrons, however, can directly interact with the bound electrons of the neutral atoms or molecules: they can excite the neutral to an electronic excited state but can also directly ionize.

Because i) the mass of an ion is much higher, ii) it is positively charged and iii) can offer bound states to electrons:

- The interaction of radical cations with neutral molecules is more complex than that of electrons with neutrals.
- The cross section for a purely mechanical ion-neutral collision is much higher (note that twice the radius of the atom has to be considered) than the cross section for an electron-neutral collision.
- Since the cation and neutrals of the gas in the discharge have practically the same masses and diameters, kinetic energy transfer is expected to play a very important role. The motion of a cation can be completely stopped in one cation-neutral collision.
- Charge transfer from the cation to a neutral especially between the same atomic and molecular species is known to have a very high cross section [BBST81] . This means that fast ions can efficiently transfer the charge to slow neutrals. This can lead to a situation where the cations, in the worst case, can not at all or only with a small fraction contribute to the charge amplification in a discharge. They should, however, still be able to create one or two new free electrons by ionisation of the cathode surface, which has a much smaller work function than the ionisation energy of the neutral rare gas atoms.
- The fact that in a cation-neutral collision in the gas phase the electron has to escape from two positive charges, to be available as free electron. This is an extremely improbable process since double ionisation energies typically lie above 30 eV [DM61].

Due to the mentioned reasons, a direct ionisation and formation of a free electron by ion-neutral collisions in the gas phase seems to be extremely improbable.
With the described asymmetry between electrons and ions and the consequences thereof in mind, it can attempted to interpret former experiments of others. In a usual discharge set-up, it is not so easy to separate the contributions of the electrons from the contributions of the ions to the discharge.

From pulsed discharges with repetition rates in the kHz range, it is known [Git40], that even after a time gap of more that 100 μs, the re-ignition of a subsequent discharge pulse profits from the presence of radical cations which are still present form the previous cycle. This is assumed to be due to their high masses and the resulting relative slow motion between the electrodes in comparison to electrons. It is also possible that after switching off the voltage the fast ions transfer resonantly the charge to slow neutrals (see above), and these now thermal ions stay and survive between the electrodes for a relatively long time. Due to this,even after more that 100 μs there are still some ions present in the gas. To clarify the role of these remaining radical cations for the restart of the subsequent discharge pulse, the gas phase ionisation versus the surface ionisation has to be weighted at the cathode. For this, there are several important effects to consider. On one hand, there is the above-mentioned efficient charge transfer from the fast ions to the slow neutrals, which makes it improbable that ions in the gas make it to produce free electrons. On the other hand there is the low work function of the cathode metal surface as well as the high atom density in the cathode. Hence, one can imagine that the impact of one, two or a few cations on the cathode surface eject each one or two electrons, and by this can initiate the observed easy re-start of the subsequent discharge pulse at relatively low voltages.

The question is now, whether an experiment which selectively enlightens the role of the electrons can be found. The key for this experiment is the Geiger-Mueller-tube.

2.1.2 The Geiger-Mueller-tube

The basic set-up of a Geiger-Mueller tube (see Figure 2.4) can be described as following: It consists of a vacuum sealed tube filled with a gas at low pressure. The tube contains two electrodes, which can be fed with voltages. Inside the tube, there is a hollow-cylindrical cathode. Concentric to the cylinder is a wire-like anode in the centre.

As previously discussed, this electrode set-up produces a very inhomogeneous electric field. It increases with $\frac{1}{r}$ when moving from the outer negative cylinder electrode (high r) to the positive inner wire (low r). Typically neon or argon gas at a low pressure is used as a medium inside the tube. Figure 2.4 displays the basic set-up of a Geiger-Mueller tube. Gamma radiation, enters the tube via the glass window and is able to ionize at the electrode or the carrier gas.

The electric field strength and the gas density in the tube are chosen is such way, that a single primary electron is accelerated to such high kinetic energy that in the next collision

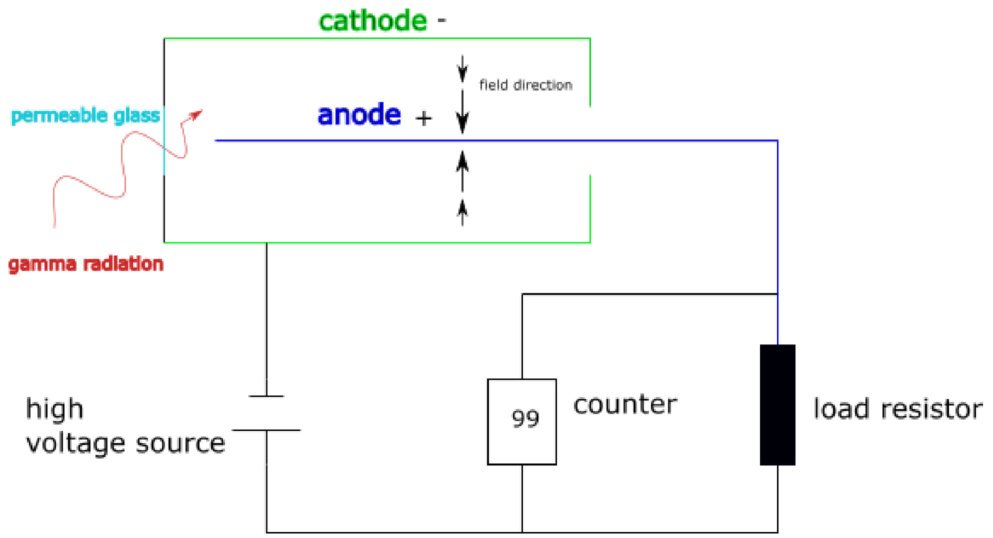

Figure 2.4: Two-dimensional illustration of a Geiger-Mueller-Tube. Note that the outer electrode is a hollow-cylinder. The gamma radiation can enter through the permeable glass. A single ionization event triggers an electron avalanche. Electrons and cations are moving in opposite directions in the field. The electron discharge stops, when the electrons reach the centre electrode. The pulsed electron signal can be used as input signal for a counter. Sketch based loosely on [Kor12]

with a neutral atom it can eject an electron. In the next step, primary and secondary electrons are accelerated and are each able to ionize in their next collisions with neutral atoms. This results in four free electrons. These four electrons are again accelerated ... and so forth.

This cascade is repeated multiple times resulting in an efficient free electron amplification process. Because the electric field increases as closer the electrons come to the inner electrode ($E_{wire} \approx \frac{1}{r} \cdot \frac{U}{d} \cdot \frac{1}{\epsilon_0}$) the stronger the secondary and tertiary and so on electrons are accelerated. This enforces the formation of an electron avalanche.

In contrast to the active role of the electrons in the Geiger-Mueller tube the role of the cations is passive:

- They are accelerated to the outward cylinder.
- In the next collision they can efficiently transfer their charge to a slow neutral atom. This basically prevents that positive cations can become fast in a gas-filled tube.
- Principally the ionization of a neutral atom by an ion is extremely improbable because of its positive charge, as was discussed in 2.1.1
- Due to of the decrease of the electric field with increasing distance from the centre,

the many collisions and charge transfer processes the ions become slower and slower.

- At the end they are so slow that they can not ionize the cathode.

This special set-up achieves that if a single primary free electron is formed the electron avalanche starts, but the current flow ends if the electrons reach the inner wire. The discharge ends because the ions can not contribute to the formation of new free charges. Hence, one primary ionization event results in one single short negative pulse.
These numerous electrons are captured by the middle electrode and can be detected by a counter. Normally the counting signal is linked to a loud speaker, which generates the well-known ticking noise. One tick indicates a single primary ionization event.
In conclusion, with the Geiger-Mueller counter, which is easy in function and relatively cheap, it is possible to detect even low activity of gamma radiation[Kor12].
For this work, the function of the Geiger-Mueller-counter is a proof that the above-listed asymmetry of the roles of the electrons and the ions in a discharge is qualitatively right. Figure 2.5 illustrates a primary ionization event by gamma radiation and the formation of the electron avalanche, which is then captured by the inner positive electrode.

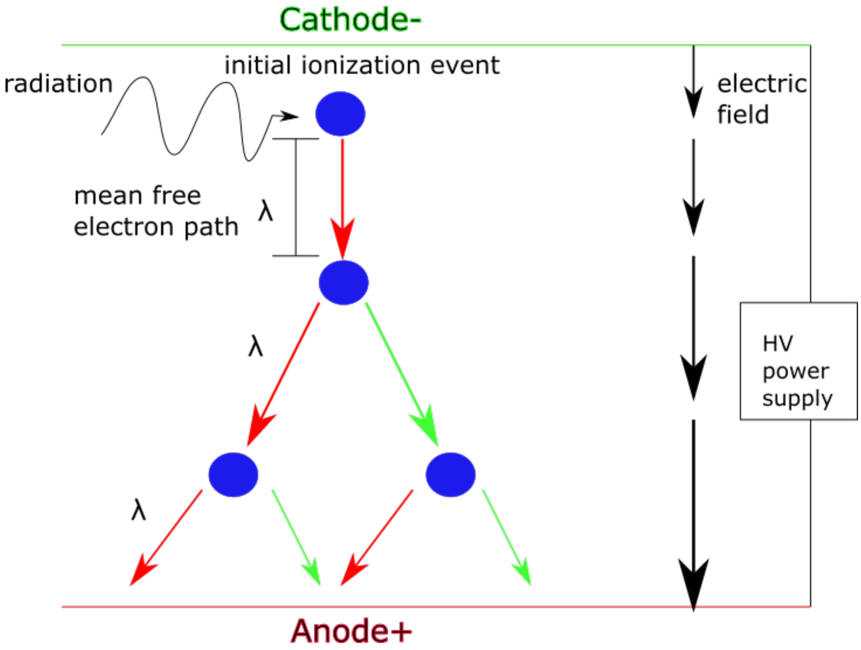

Figure 2.5: Sketch of the electron avalanche formation in the Geiger-Mueller-counter. The electron avalanche captured by the anode superimposes to a short negative pulse, which can be detected by a counter. Sketch based loosely on [EH40]

Historical classification of discharges

While using a relatively extraordinary method of a pulsed discharge for anion formation in this work, it is nevertheless necessary to also submerse somewhat in the discussion of some well-investigated classical types of continuous or semi-continuous discharges.

Continuous discharges are characterized by the gas properties, the gas pressure and the current which flows through the gas. The latter depends on the number of atoms between the electrodes - which means the pressure in the discharge - , but also on the voltage difference applied at the electrodes. Because charge flow and voltage correlate monotonously and in former times three-dimensional plots have been impossible, in the past gas discharges have been characterised only by pressure and current density (see Fig. 2.1). Note that this classification is rough and not sharp [Mid02]. This classification can be subdivided into

- Dark discharges at low pressures and low currents up to 1 μA and high pressure and high current also known as Townsend or avalanche discharge. [TB21]
- Glow Discharges, at not too high pressure, but high current from 1 mA to 50 mA
- Arc discharges, at medium pressure and current above 50 mA

All of this gas discharge phenomena have different applications from welding metals (i.e. arc discharges), the production of UV-lamps, the detection of atoms and molecules by their fluorescence to the determination of electron affinities. As already outlined above, the widely known Geiger-Mueller-Counter is a very useful device to detect weak levels of ionizing radiation and radioactive processes [GM28].

Dark discharges have small numbers of charges per volume and therefore need ionization events caused by external sources to keep ongoing. As already outlined above, external sources for free charge formation can be high- energetic cosmic photon or particle radiation (see Geiger-Mueller-counter above) or even ultra-violet light.

In a discharge, the current through a gas of constant pressure depends monotonously on the applied voltage. In a discharge, in the low-voltage range the increase of the current with a rise in voltage is rather steep. Above this range, if the voltage is further increased, the current starts to saturate and only increases slowly. From that point on the discharge does not need any further ionizing stimuli from outside. Now the discharge can be classified as an independent dark discharge respectively a Townsend discharge. The nomenclature "dark discharge" refers to the fact that the light emission from the discharge is so weak,

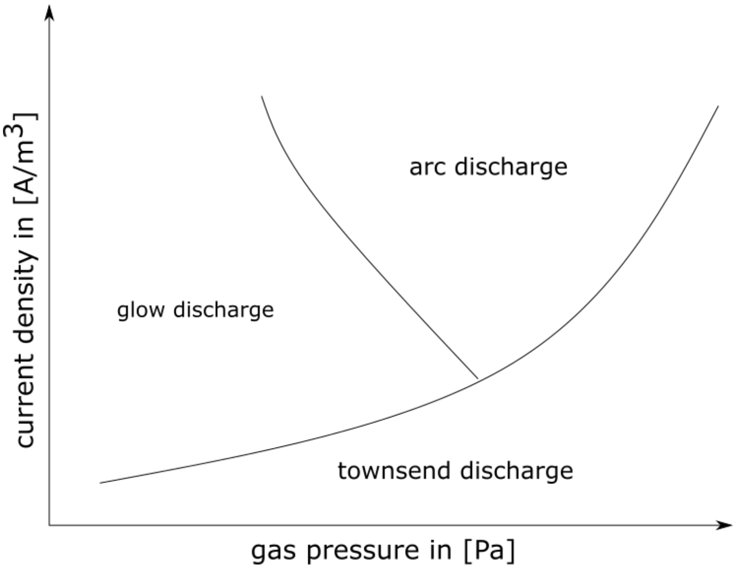

Figure 2.6: Illustration of the different types of discharges depending on the pressure and current density. The transition from the glow to an arc discharge can be provoked by increasing the pressure. The transition form a Townsend discharge to an arc discharge can be achieved by an increase of the current density (by increasing the voltage). Sketch based loosely on [Gob71]

that it is practically invisible. The transition to a glow discharge is achieved by a additional increase of the current. It is now possible to observe a strong light emission from the discharge. When the pressure in the gas is further increased and the current density is high, the temperature of the cathode strongly increases and thermionic emission of electrons occurs at the cathode. This type of discharge is then termed "arc discharge". Arc discharges can be recognised by their steady and strong light emissions and the glowing electrodes.

Since in Figure 2.6 the voltage applied to the electrodes is not included, the impression occurs that it may be of minor importance. This, however, is not the case, as the following chapter shows.

2.1.3 Paschen's Law describing the minimum voltage necessary for a stable discharge

For some technical applications of high voltages for example in photo-multipliers, particle detectors, in Geiger-Mueller counters as well as in electron microscopes and other high voltage electronics, it is important to know at which voltages, distances and gases stable discharges can occur. It should be noted that such knowledge is important, because for example in mass spectrometers one short discharge in an ion detector can destroy all the subsequent expensive electronics for data acquisition.

After an ignition process with a certain voltage, the discharge is expected to start burning constantly. The amount of voltage required is given determined by Paschen's law. Experimental conditions such as the electrode distance d, gas pressure p (which correlates to the mean free path length until the next collision happens) and properties of the gas such as the electron-atom collisional cross section σ and the IE[1] of the gas influence the minimum voltage at which a stable discharge can evolve. All the above parameters are included to a greater or lesser extent directly in Paschen's law[Pas89]:

$$U = \frac{B}{ln(\sigma \cdot p \cdot d) - ln[ln(1 + \gamma^{-1})]} \cdot p \cdot d \qquad (2.5)$$

U: Voltage [V]
σ: cross section electron-gas [$\frac{1}{Pa \cdot m}$]
B: $= \frac{\sigma \cdot IE}{e}$ [$\frac{V}{Pa \cdot m}$]
p: pressure [Pa]
d: electrode distance [m]
γ: third Townsend coefficient [a .u.]

This equation is crucial to understand that for a given gas and given distances specific parameters such as gas pressure and voltage can be used to control and maintain discharges. The minimum voltage for a discharge depends on electrode distance d and pressure p on the electron-neutral cross section σ and the constant B, which is the product of σ with the ionisation energy of the gas IE/e, given in electron volt. It should be noted that the influence of the third Townsend coefficient is very small.

If the minimum voltages for stable discharges - as given by equation (2.5) - are plotted versus the gas pressure (as can be seen in figure 2.7) for several gases, it turns out, that over a broad range of pressures the rare gas argon is the gas for which the voltage for a stable discharge is the lowest.

Luckily, argon is inert and heavy and therefore also well-suited as carrier gas for atom-molecule co-expansions and is thus used in this work as carrier and discharge gas for the pulsed co-expansion through which the pulsed discharge is ignited.

Most of the previously mentioned laws and considerations apply for discharges with constant voltages. There are also discharge phenomena where voltage and current are alternating or unidirectional and pulsed.

However, a pulsed discharge - as used in this work - which is realized by a pulsed inho-

---

[1] ionization energy

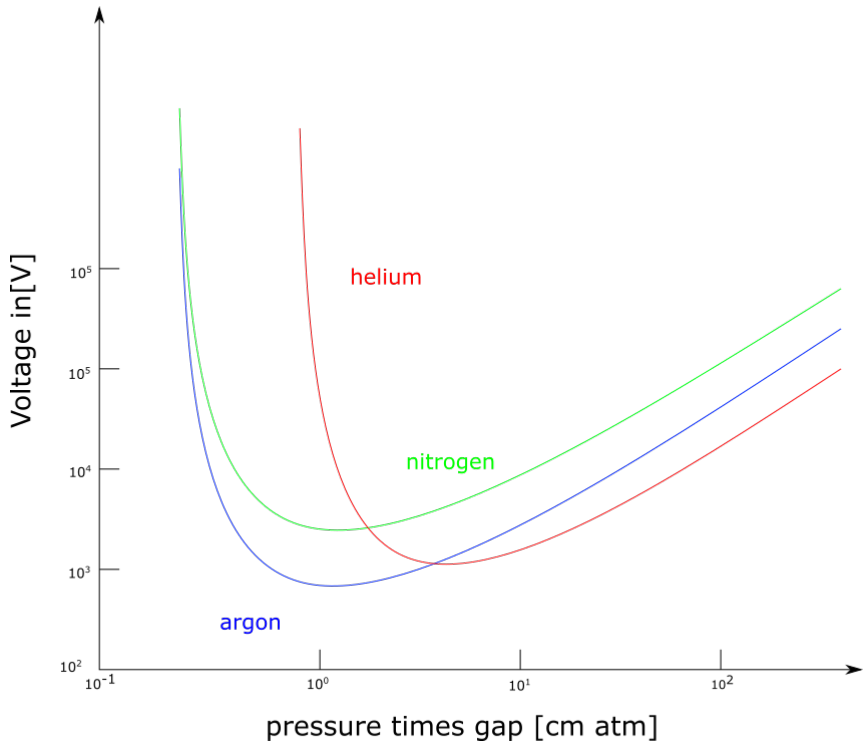

Figure 2.7: Sketch of the paschen curves for argon, nitrogen and helium. Note that discharges in argon, which was used in this work, need the lowest voltage over a wide pressure range. Sketch based on [LL94]

mogeneous electric field in a pulsed Argon gas cloud needs further detailed discussion. Intending to use the numerous free electrons which are formed in a discharge for radical anion formation, it is immediately understandable the necessity for a pulsed discharge as will be outlined in the next section.

2.1.4 Pulsed discharges and intact anion formation

Pulsed discharges have previously been used in countless experiments. The discharge was mostly aligned perpendicular to a channel, which was placed in front of a pulsed nozzle. In such discharges molecules and solid state material were fragmented to atoms and in the expansion reassembled to form atomic clusters or exotic molecular species as anions or cations [CKM10].

The aim of this work is, however, to form radical anions of intact molecules. As the example of previous work shows, discharges usually provide a crud and high-energetic environment.

In the following the discharge set-up is presented with further details and the peculiarities as well as the functions of the involved devices are explained. At the end, a possible scenario for the time sequence of the microscopic processes is proposed.

The detailed experimental set-up of the anion source

Before attempting a microscopic explanation of the processes, taking place in the pulsed discharge of this work, it is necessary to provide a more detailed understanding of the experimental set-up. Figure 2.8 shows a sketch of the inlet chamber used in this work. In this chamber the electrodes for the pulsed discharge and a pulsed gas valve for the supersonic argon-molecule co-expansion are mounted. The whole electrode and nozzle set-up is mounted inside an aluminium vacuum chamber, which is pumped by two turbo pumps. In the following the devices of the set-up will be described one by one.

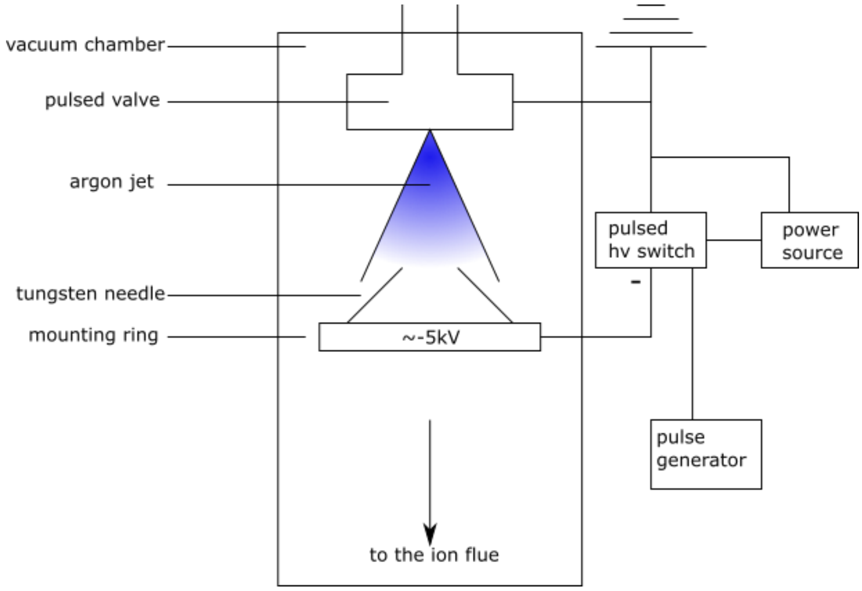

Figure 2.8: Simplified illustration of the needle electrodes (negative cathode), the pulsed-discharge (blue) and the pulsed gas valve (positive anode). Eight Tungsten needles are arranged concentric at $4-5\ mm$ in front of the gas nozzle orifice. A high negative voltage($\approx 4\ kV$) pulse (duration: $1-2\ \mu s$) is applied in order to inject seed electrons into the expansion gas. The seed electrons initiate an electron avalanche in the argon gas to the nozzle. It should be noted that the electric field is strongly inhomogeneous at the negatively charged needle tips. This field-inhomogeneity is opposite to the Geiger-Mueller-tube (see chapter 2.1.2) where the field strength increased when going to the inner positive wire. For further explanations see text.

The nozzle: The heated and pulsed gas valve contains the sample molecules and is kept under approximately 30 *bar* excess of argon pressure. It is typically heated to a temperature below the estimated melting point of the sample, in order to just sublimate sufficient amount of sample molecules into the gas phase. The mixture of argon carrier gas and sample molecules (maximum five percent) expands from 30 *bar* to vacuum ($5 \cdot 10^{-5}$ *mbar*). The pulsed valve is activated ten times per second. The electric steering pulse is a high-current pulse of 70 *V* which is led into a copper-wire-coil (30 turns about 6 *mm* inner coil diameter) with a isolating coating. The coil is wrapped on a magnetisable hollow-cylinder which is also the housing of the nozzle. The resulting pulsed magnetic centre-symmetric field attracts the magnetic plunger which then moves from outside the field into the coil. By this it draws back the poppet and opens the orifice (diameter $\approx 300\ \mu m$). The resulting gas pulse has a time-width at half height of estimated 120 μs to 200 μs.

The gas co-expansion: During the expansion through the orifice and still some millimetres downstream, the nozzle orifice, first the neutral sample molecules and later the newly formed anions are strongly cooled internally. Cooling of the vibrations of the sample molecules is performed by a transfer of vibrational energy to the argon translational energy in low-energetic argon-molecule collisions.

The Tungsten needles (the cathodes): Eight tungsten needles are used as cathodes. They are arranged centre-symmetrically , pointing to the hole of the nozzle at a distance of about $4 - 5$ *mm* from the nozzle surface. It is essential to keep a suitable distance between the tungsten needles and the stainless-steel front plate of the valve: They need to be close enough to the nozzle to keep the electric field high and to reach into a suitable pressure domain and far enough to prevent that the gas pressure at the needles is still so high, that the mean free path length is still so short that avalanche effect fails.

The inhomogeneous electric field: The voltage applied to the needles is about $2-4$ *kV*. Since the needle tips have only a radius r of about 20 *mum* and the electric field at a tip is proportional to $\frac{1}{r}$ it follows that the electric field at the tip is particularly high and very inhomogeneous. The immense electric field at the tips might be essential for the formation of the first free electrons which ignite the electron avalanche effect (see below). It should be noted also, that in contrast to the Geiger-Mueller-tube the electric field increases when moving to the negative electrodes.

The timing: To allow the electron avalanche effect to take place, the electric field and the argon gas pressure must be suitable. It is necessary to emphasize that i) the pulsing of the gas valve and ii) the time-correlated fast pulsing of electric field provide the key elements for the formation of an efficient discharge and therein the formation of cold anions. The pulsed gas valve produces a Gaussian-like temporal pressure distribution in front of the valve. It is important to understand that the density of the gas decreases with the distance from the nozzle. This pressure-variation in time and space allows to choose the right pressure-condition for the ignition of the discharge and the formation of the electron avalanche. This needs a perfect, reproducible timing between the nozzle opening and the electric pulse. Whereas the HV-pulse can be controlled in time and pulse width with a nanosecond accuracy, usually the temporal reproducibility of the mechanical gas valve is miserable. In this work a high reproducibility was achieved by several changes at the gas nozzle, which are described in the experimental section (see Chapter 3.2.1).

The double function of the argon carrier gas. As already mentioned, the function of argon as a carrier gas is twofold:

- i) By its efficient ionization in the electron avalanche, it acts as electron multiplier.
- ii) It serves as a collision gas, which cools the vibrations of the freshly formed hot sample anions.

Regarding i): Due to the high gas density in the argon jet and the large cross-section for electron ionization in argon, plenty of electrons are formed in the pulsed electron avalanche. Because there are many electrons formed, nevertheless the number of low-energy electrons is still high. Preferentially only these low-energetic electrons are able to efficiently attach to neutral molecules and form radical anions. Regarding ii): The argon atoms are heavy enough to be able to accelerate the sample molecules until they have the same velocity as the argon atoms. Then the argon-molecule collisions are low-energetic and the cooling of vibrations of the freshly formed hot anions sets in.

The sequence of processes: Some tenth of μs after the valve is electrically addressed it opens and the gas expands from 30 bar into vacuum ($5 \cdot 10^{-5}$ $mbar$ before the valve opening). It should be noted that in general, in agreement with the theory of gases, the average velocity of the argon gas is only slightly increased by increasing the pressure in the nozzle. The density of the gas cloud directly at the nozzle orifice increases over time to a maximum and then decreases until the valve closes again. The pulse width at half height is about 200 μs which results about in a 10 cm long gas cloud. In a distance of approximately $4 - 5$ mm the jet hits the cathode needles which are oriented towards the orifice (tip radius about 20 μm) of the valve. The high-voltage pulse for the discharge at the needles is synchronized to that gas density, which is ideal for the ignition and the avalanche process. The high-voltage pulse is switched-on shortly before the gas density at the needles reaches its maximum. About 1 μs after the high voltage ($2 - 4$ kV) is applied, at an oscilloscope which monitors the discharge pulse, a small voltage drop can be observed. This drop is interpreted as the time at which the discharge is fully evolved. An avalanche of free electron is formed by electron ionisation of the argon carrier gas. It burns into the gas expansion and to the valve front plate, especially to the orifice. Directly in front of the nozzle orifice the gas density is so high and the mean free path lengths becomes so small, that numerous collisions occur, which moderate the electron velocity and prevent further ionization. Nevertheless, the countless electrons reach the nozzle front surface. After the electron avalanche is fully evolved, the HV and hence the discharge is shut-off in 10 ns. Due to this, the electric field can no longer disturb neither the cooling effect nor the direction of the ion flight path. The remaining charge cloud consists of cations, anions and electrons. It is reasonable to assume, that at this time because of their small mass most of the electrons have already disappeared. The cloud travels now with the velocity of the neutral gas through the skimmer and to the ion acceleration area of a Time-of-flight-MS where they can be separated by mass and detected.

This set-up generates sufficient amounts of anions, which then can be analysed and investigated by PES.

The following subsection is dedicated to attempt an understanding of the specialities of this discharge ion source.

An attempt of a microscopic understanding

As noted above, anions usually do not play an active role in discharges. Besides the fact that not every gas has a positive electron affinity, it can also be assumed that the conditions in a discharge are too harsh, in order to form radical anions by electron capture. Here a pulsed discharge with argon as carrier gas which contains up to five percent of sample molecules is used. It is known that electron-capture by molecules preferentially works for low-energetic electrons (see chapter 2.2), which should be usually sparse in number in a discharge. An obvious reason for this is the presence of the high electric field driving the discharge. A second aspect is that the excess energy of the electrons which approaches the molecule has to be removed by low-energetic collisions of the argon gas, in order to stabilize the newly formed anion, which is internally hot due to the electron attachment process. It should be pointed out that the electron affinity is converted to vibrations of the anion ground state, which have to be removed in order to obtain simple PE spectra. Because of the electric field during the discharge, also the anions are immediately accelerated against the neutral gas, leading to high-energetic instead of low-energetic collisions with the neutral argon atoms.

As the experiment here shows anion formation in a pulsed discharge of a pulse width of $1 - 2\ \mu s$ performed in a pulsed rare gas cloud is very efficient in anion formation.

As a consequence, there have to be extraordinary characteristics of a pulsed discharge in

a dense argon cloud, which have been not yet considered in the previous sections.
It is important to note that due to the application of an ultra-fast high-voltage switch (Behlke HTS12, circuit plan in chapter 3) the high voltage for ignition and driving the discharge can be switched on and off with very fast rise and fall times of about $10-20$ ns. There are several motivations to use a pulsed discharge, especially those with an ultra-fast fall-time of the high voltage for anion formation:

- The ultra-fast switching-off of the electrode voltages freeze out the charge situation, which is actually present at the end of the discharge.
- If it is assumed, that a sufficient number of anions and/or electrons are formed during or after the discharge, the switch-off of the electric field, prevents a further acceleration of the anions and the electrons.
- By this, a low velocity of the anions can be realised, which results in small velocity differences between the anions and the neutral argon atoms. This allows the neutral argon atoms to stabilize and cool the anions internally.
- If the pulse of the electric field is short enough, it can be assumed that predominantly the electrons move and initiate an electron avalanche in the discharge.
- In contrast cations which are formed close to the needle cathodes are strongly accelerated by the immense attractive inhomogeneous field of the tip and gain enough energy that they can eject electrons from the needle and by this help to increase the number of seed electrons and maintain and stabilize the electron avalanche effect.
- The pulsed electron current through the gas can be pushed to the maximum, since with the support of storage capacitors the high-voltage power supply can provide energies of up to mJ in one μs. Ageing of the electrodes due high temperature and erosion by sputter processes can be nearly avoided.
- The presence of a high number of free electrons is very suitable for anion formation: its probability clearly increases with the number of attempts the molecule has to capture a free electron. This obviously increases with the number of free electrons.
- In contrast to the electrons, because of their large mass, the ions stay (for a relative long time) in the gas expansion. After some time this leads to an excess of positive charges. As a result, they form a positive coulomb trap for the anions and interestingly also the low-energetic electrons.

- The formation of a coulomb trap for the low-energy electrons considerably increases the number of attachment attempts and prolong the times scale for anion formation.
- The coulomb space charge cloud drifts downwards with the neutral gas atoms through the skimmer into the ion source and keeps the anions together. Especially the repulsion between the anions is compensated for.

The above list shows that the microscopic effects in a pulsed discharge, as used in this work, are very different in comparison to a continuous discharge. It also shows, that there are many advantages of such a set-up for the formation of molecular anions.
One last question is, how the first free electron are formed, which then start the avalanche process.

2.1.5 The first free electrons

It should be noted, that the emission of electrons from the tip surface depends on several parameters:

- The size of the work function (see below).
- The field strength at the surface of the tip.
- The temperature of the tip.

In the following we discuss these effects and their contribution to the formation of the first free electrons.

Field emission of electrons

The formation of the first free electrons is a very crucial point, since the discharge has to fully evolve in the duration of the electric pulse, which is only $1-2\ \mu s$. Hence, the first free electrons have to be ejected rather promptly after the rise of the HV-pulse. Background radiation from radioactivity or UV-radiation can be ruled out here because i) the discharge happens inside an alumina vacuum chamber and ii) the pulse length of $1-2\ \mu s$ is too short to allow a ignition by background effects.
At immense electric fields at the cathode tips electrons may be able to leave the metal and initiate the discharge.
For this very high electric fields ($\frac{U}{d} = E_{field}$; U = voltage difference at the electrodes, d = electrode distance) as achieved by high voltages, small electrode distances and sharp cathode tip geometries ($E_{field} \approx \frac{1}{r}$, while r is the radius of the tip of the cathode electrode)

have been used. A more precise description of the electric field generated by a needle tip is given by the following equations. Under the assumption of a perfect tip with a field direction along the gap axis the field at the tip can be written as[ASNM07]:

$$E(r) = \frac{U}{R}\frac{cos(\theta_1)}{ln(cot(\frac{\theta_1}{2}))}\frac{1}{sin^2(\theta)} \qquad (2.6)$$

U:	applied Voltage [V]
R:	gap distance [m]
$tan^2(\theta_1) = \frac{r}{R}$:	ratio radius to distance [a.u.]
r:	distance from tip [m]
$cos(\theta) = (R - r) \cdot \frac{\theta_1}{R}$:	circle distance relation[a.u.]

Due to the high field densities at the tip of the tungsten needle and between the the tip and the orifice of the valve it is possible that electrons are ejected by field-supported electron emission from the tungsten needles. As can be seen in figure 2.9 the electric field vectors are also directed into to argon jet. So the initial electrons leaving the tip surface can be accelerated and start the avalanche process. This means the question, how the initial free electrons are formed can be possibly answered by field emission of electrons from the Tungsten tip surface. This effect is well known and applied for example in the scanning tunnelling microscopy [CBP12]. In the following the field-assisted electron emis-

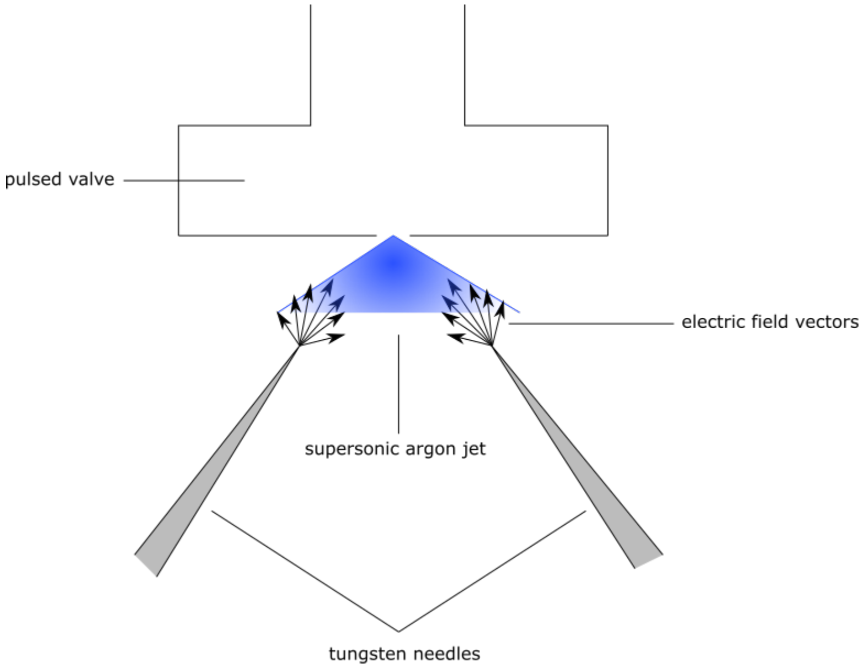

Figure 2.9: Simplified Illustration of the pulsed-discharge pulsed-valve system used in this work. The highly negatively charged tungsten needles generate enough initial free electrons to trigger an electron and ion avalanche in the argon gas entering the vacuum chamber. Because of the high gas density plenty of free electrons are formed. Electrons which have suitable energies are able to form radical sample anions and cations while hitting the sample molecules in the jet.

sion is described.

Electron field emission from metal surfaces needs very high electric fields in the order of $10^9\ \frac{V}{m}$ or more. It can be understood as the tunnelling probability of an electron through the fermi barrier out of the bulk into the continuum. The field emission current can be written as[GM56]:

$$G(b_0, B) = 2\sqrt{2m} \cdot \frac{1}{\hbar} \int_{b_0}^{B} \sqrt{M} dx \quad (2.7)$$

$$M(b_0, B) = b_0 - eBx - \frac{e^2}{16\pi\epsilon_0 x} \quad (2.8)$$

G: escape probability [a.u.]
b_0: zero field height [eV]
B: barrier field [eV]
$\hbar$: Planck's constant [eVs]
$M = (U(x) - E_n)$: electron motive energy [eV]
$U(x)$: potential energy [eV]
E_n: electron total energy [eV]

The thermionic electron emission

In case the temperature of a metal wire (usually tungsten enriched with elements of low-work-function) is very high, electrons can leave the metal alone by their thermal energy.

Regarding first the pure thermionic emission. As mentioned before the jet valve needs to get heated in order to sublime enough sample molecules. The molecules in this work are without exception relatively large polyaromatic hydrocarbons and as such have different sublimation temperatures. For example, it is possible to obtain spectra of 5-Fluroindole at about 70°C, but samples molecules like Pentacene need temperatures close to 300°C to evaporate efficiently. Because of the close distance to the nozzle and the skimmer (typically heated 50°C above the nozzle temperature to circumvent surface adsorption), it is reasonable to assume that over time the needles and their mountings are heated up close to the valve temperature. To understand the influence of temperature on the emission of electrons in the following we indulge somewhat in the thermionic effect.

The relation between electron emission and temperature in solids can be described by Richardson's law[Ric13] :

$$J = A_g \cdot T^2 \cdot e^{\frac{-W}{kT}} \tag{2.9}$$

J: current density [$\frac{A}{m}$]
A_g: material constant [$\frac{A}{m^2 \cdot K^2}$]
W: work function [eV]
kT: Boltzmann energy [eV]

This means for a heated wire that higher temperatures lead to higher electron currents out of the surface. However, the thermal energy kT has to be at least a fraction of the work function. Since the latter is at best in the range of $3 - 4\ eV$ extremely high temperatures are necessary, which are far beyond our nozzle temperature. Since the temperature of the needles always stays below the temperature of the nozzle (at maximum $650\ K$), a pure thermionic emission is ruled out.

A concerted action of field and temperature

One could, however imagine that temperature and field can work together. This means that the current of the field-emitted electrons rises with temperature[DD54]. With respect to that, the term M can be corrected by the Schottky approximation ($\frac{e^2}{16\pi\epsilon_0 x}$), which describes a remodelled barrier function. This suggests that most electron emissions out of solids are combined processes of field emission and thermionic emission. To include both kinds of mechanisms Walter Schottky introduced a correction term to describe field regimes below $10^9\ \frac{V}{m}$ [MG56]:

$$J = A_g \cdot T^2 \cdot e^{\frac{-W-\Delta W}{kT}} \tag{2.10}$$

J: current density [$\frac{A}{m}$]
A_g: material constant [$\frac{A}{m^2 \cdot K^2}$]
W: work function [eV]
kT: boltzmann energy [eV]

While the correction term ΔW takes the electric field into account by :

$$\Delta W = \sqrt{\frac{e^3 \cdot E}{4\pi\epsilon_0}} \qquad (2.11)$$

e: elemental charge [C]
E: applied electric field $[\frac{V}{m}]$
ϵ_0: electric permittivity $[\frac{As}{Vm}]$

On one hand, by this formula the transition between the different types of electron emissions are described and on the other hand it shows how two effects can cooperatively determine the electron current from the metal surface. For this work it can be assumed that the regime of the above-mentioned method lies within the Schottky area of the phenomena. Figure 2.7 illustrates how the regimes behave in a qualitative way. If the field is zero solely thermionic emission remains. With increasing electric field intensity the curve will transform to a regime where the field emission becomes predominant as can be seen in Figure 2.7. With that in mind, it is reasonable to to assume that the pulsed discharge used here lies within the gap of the Schottky regime. This means both field (strong contribution) and thermionic effects (minor contribution) add up to the primary charge carrier generation.

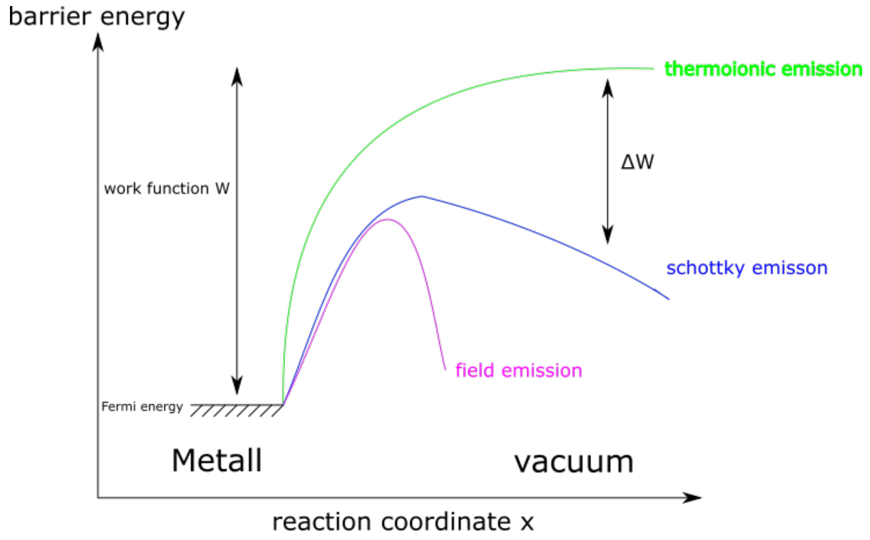

Figure 2.10: Simplified Illustration of the emission barrier under the influences of temperature and electric field effects. Just thermoionic emission is the less effective. When the field densities rise, it will transition into a Schottky emission. When the estimated electric field threshold of $10^9\ \frac{V}{m}$ is reached the field emission curve becomes dominant. Sketch loosely based on [DGA+12]

One of the most important parameters is, however, the work function of the metal.

The work function of the cathode

The work function of a metal describes, how much energy is needed to remove an electron from the metal surface, if no electric field or temperature is involved. The appearance of the work function in the previous formula means that the choice of the right metal is crucial, as the work function is a material constant. The work function can be measured by the photo-effect[Ein05]. It can be described as [KW96]:

$$W = -\phi \cdot e - E_F \tag{2.12}$$

W: work function [eV]
ϕ: electrostatic potential $[\frac{eV}{C}]$
e: fundamental charge of an electron [C]
E_F: fermi energy [eV]

It is necessary to mention, that the electrostatic potential, is the electrostatic potential at the immediate vicinity of the surface to vacuum and can be derived by the line integral[Gri13]:

$$\phi = -\int_{A_s} E dl \tag{2.13}$$

ϕ: electrostatic potential $[\frac{eV}{C}]$
A_s: surface area $[m^2]$
dl: line length [m]
E: electric field [m]

The Fermi energy E_F and the work function W are material properties. Thus the solid state material of the cathode used to generate initial charge carriers in form of electrons should be thoroughly selected. Figure 2.8 illustrates the work function and the Fermi level in relation to the vacuum energy. When within two metals the work function in one metal

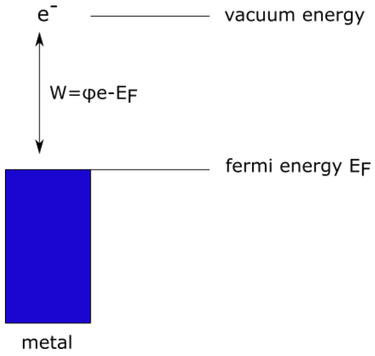

Figure 2.11: Simplified Illustration of the work function of a metal.The lower the Fermi level the more energy a electron needs to get ejected. Sketch loosely based on [DGA$^+$12]

is lower than in the other it is easier to remove an electron from the metal of lower work function into vacuum. Table 2.1 shows work function of several pure metals.

Table 2.1: Overview of some work functions of different metals. It can be well stated that the work functions differ strongly. Based on[RBD20]

metal	work function [eV]	metal	work function [eV]
Al	4.30	Au	5.10
Ti	4.33	Ir	5.27
V	4.30	Os	4.83
Cr	4.50	W	4.55
Mn	4.10	Ta	4.25
Fe	4.70	Hf	3.90
Co	5.00	Ru	4.70
Ni	5.15	Rh	4.98

There can be, however, surface effects that drastically change the work function. Adsorption (physisorption) of molecules at the surface or chemical surface modifications can have an influence on the work function of a given metal surface.

Taking a closer look at the chemical behaviour of tungsten, which is used here as cathode material, one can see how the work function of clean tungsten (4.66 eV) can be changed by chemistry. Because in our discharge gas also molecules are contained physisorption and even surface chemistry can take place. If for example organic compounds are fragmented near a metal electrode, carbo-metals can be formed. Such a reaction can build-up a tungsten-carbide surface layer, whose work function of 3.73 eV is considerably lower in comparison to pure tungsten (4.55 eV).

Since the formation of a tungsten-carbide surface on the needle tip considerably eases the process of releasing electrons [JZS$^+$02].

Interestingly also chemical compounds with negative electron affinities can lower the work function of a material when adsorbing on the surface. For example is known that pyridine on zinc-oxide decreases the work-function from 4.5 eV to 1.6 eV [HDX$^+$13].

In conclusion, a discharge in an atmosphere of argon enriched with aromatic molecules and tungsten cathodes, as used in this work, are ideal preconditions for field electron emission. Hence, in conclusion, it seems that the initial seed electrons of the pulsed discharge can leave the tungsten metal surface because: i) the work-function of tungsten is lowered by sample-molecule-induced surface effects, ii) by thermal heating and mostly iii) by field emission.

Conclusion

It has been a complex question, why and how the pulsed discharge in combination with an argon-sample gas pulse are able to generate many more intact radical-anions in comparison to classical anion formation methods. In this chapter a variety of reasons has been found, explaining why the new anion source works so well. It seems, however, that all these reasons even constructively work together, which explains the extraordinary success of the new anion source.

2.1.6 Closed Shell Versus Open-Shell Anions

In general negatively charged molecules, termed anions, can be formed either by:

- removal of a proton (a hydrogen cation), meaning deprotonation, a chemical change of the molecule or
- Attachment of a surplus electron to the intact molecule and the formation of a radical anion.

It should be noted that molecular radical anions are open shell species, whereas deprotonated molecules are closed shell species. The latter are usually more stable, but strictly seen a chemically modified version of the initial molecule. Usually the site of deprotonation is known by chemical intuition, but may be unclear in special cases, especially in larger peptides or proteins.

Even in the gas phase stable anions can be formed by deprotonation of neutral molecules. This is performed in electrospray ionization mass spectrometry (ESI-MS[2],[YF84]) and in matrix assisted laser desorption/ionization mass spectrometry (MALDI-MS[3],[TWI+88]). In ESI-MS one uses negative electrospray of sample solutions enriched with some base. In MALDI one uses suitable matrices which act as photo-bases. The anion formation is performed by proton transfer to the solvent or the matrix, a process which is per definition a chemical reaction

.

They are closed-shell anions, which means that in their ground state their electron spins are anti-parallel paired. As a result the anion ground state is a singlet S_0 state. If then an electron is removed by photo-excitation a neutral open shell molecule is formed. Since closed-shell molecules are more stable than open-shell molecules-also known as radicals, the energy difference between the anion and the neutral, which is defined as electron affinity (compare the following paragraph) is relatively big with about $3 - 4\ eV$[ZKC+04].

In ESI-MS also multiply negatively charged molecular anions are observed if several well-spaced deprotonation sites are present. Such singly and multiply deprotonated molecular anions have been investigated by photo-detachment by Lai Sheng Wang and co-workers [WW00]. They found many new effects such as relatively small stable multiple charged anions, coulomb barriers and emitted electrons that had more energy than the photon, which induced the detachment.

---

[2] electrospray ionization mass spectrometry

[3] matrix assisted laser desorption ionization mass spectrometry

These new effects are without doubt very interesting, but the focus in this work lies on the formation of radical anions which we use as starting point from which we perform photo-detachment photo-electron spectroscopy and determine

- The electron affinity of intact neutral molecules and
- The energetics of the low-lying excited states of the neutral molecule, especially their T_1 and sometimes even their T_2 triplet states.

For this aim it is needed to start with the radical anions of the intact sample molecules as is described in the next chapter.

2.2 The Electron Affinity (EA) of Intact Molecules

Radical anions are formed by attachment of an electron to an intact neutral sample molecule. The anion ground state possesses typically the electron spin $\frac{1}{2}$ and forms therefore a doublet D_0 ground state. Hence, if by photo-excitation an electron (spin $\frac{1}{2}$) is removed from the radical anion ground state, singlet states such as S_0 and S_1 as well as triplet states T_1 and possibly T_2 of the neutral molecule can be addressed with a similar probability.

However, this type of spectroscopy can only be performed for molecules which are able to stabilize a surplus electron.

The electron affinity (abbreviated: EA) of an atom or a molecule is defined as the binding energy of a surplus electron. If the EA-value is positive, then a surplus electron can be stabilized within the atom or the molecule. If the EA of a molecule or an atom is negative, then it can not stabilize an electron in an orbital. For molecules with high dipole or quadrupole moments it is possible to bind a surplus physically mostly outside of the molecule in dipole- or quadrupole-bound states (see Chapter 2.3 dipole bound states).

Here the main focus lies on valence-bound electrons, which means molecules with a positive EA.

In the following it has been tried to provide an understanding where the binding energy for the surplus electron comes from. For example it is well-known that halogen atoms have high electron affinities[Per63]. This can be understood with classical chemical intuition: the neutral fluorine atom is the atom i) with the highest-charged ion core of the second row of the periodic table, which ii) has still a free position in the $2p$-orbitals. In order to saturate and close the orbital an additional electron is needed. Since the three p

sub-orbitals p_x, p_y and p_z are perpendicular to each other i) the electrons can efficiently avoid each other and ii) they can well participate at the positive charge of the core (the shielding of the core charge by the other p-electrons is weak).

This means that in the fluorine atoms the fact that the "participation at the positive charge of the core" overrides the repulsion between the other $2p$ electrons is mostly, due to the fact that the electrons can efficiently avoid each other.

Another effect, which is also present in the fluorine atom, but of minor importance there and not needed for the understanding of its high EA is the correlation of the electron motions. This means that the electrons (- due to coulomb repulsion -) within their orbitals and between orbitals avoid each other as much as possible in order to minimize the electron-electron repulsion. This complex correlation of electron motions is termed electron correlation

The best example that in some atoms that electron correlation can be the main effect is the atomic hydrogen anion. In a simplified consideration it can be assumed that the hydrogen atom is not able to stabilize a surplus electron: there are two negative electrons and only one positive charge at the nucleus. The fact that the electron affinity of the hydrogen atom, however, is about 1 eV [Pau], shows that there must be a binding effect, which is not considered in this simple picture just outlined. This effect - as already indicated - is the electron correlation: The two electrons in the $1s$ orbital avoid each other as much as they can. As a result of the coulomb repulsion, they are always on opposite sides of the positive nucleus in average. Remembering that the Coulomb law for the electrostatic potential energy of a three-body system can be composed as the sum of the two-body potentials between all charges and it has a $\frac{1}{r}$ dependence on distance. This causes the attraction of the electron No. 1 by the positive nucleus is stronger as the repulsion by the opposite and further away electron No. 2. Clearly as a result the attraction by the nucleus is predominant.

For large molecules with extended π-systems the situation becomes more complicated because of the numerous electrons, but has the same origin as in the hydrogen anion. The electrons avoid each other in such a way that also the surplus electron is allowed to participate at the positive charges of the nuclei, and the attraction predominates. In conclusion (in conjugated hydrocarbons) the binding effect of the surplus electron is supposed to come from

- The electron correlation.
- The existence of a low-lying un-occupied orbital (abbreviated LUMO)

As already mentioned above, not all molecules have a positive EA, which means that not all molecules are able to stabilize a surplus electron. By substituting one or two hydrogen atoms by halogen atoms in such a molecule, it can be expected that its electron affinity is shifted to a positive EA. Sulphur and oxygen are expected to act similar, but not so strong as halogen atoms.

However, if a conjugated molecule has a certain size of the π orbitals it should have a positive EA. For example, whereas naphthaline does not have a positive EA, antracene has (500 meV[Pau17]).

EAs of many, especially large conjugated hydrocarbons are up to now not determined by direct measurements.

As outlined above, measured EA values can serve as calibration points for theoretical calculations and may be also helpful for experimentalists to understand the energetic position of intermolecular charge transfer states [WSM+96]. It also seems that molecules with very high electron affinities (above 3 eV) are strongly biologically active and therefore can hold a high toxicity or are cancerogen [EE17],[DPTP96]. Of course the major role in toxicity/cancerogenity plays the chemical structure itself, but a high reactivity due to electron affinity can be a partial aspect.

Preconditions for the PD-PES

As already mentioned above, the reason for the interest in forming intact radical anions and apply a complicated and expensive sequence of methods is, that the intact radical anions have spins $\frac{1}{2}$ and therefore a doublet ground state. If an electron is removed the molecular spin is changed by $+\frac{1}{2}$ or $-\frac{1}{2}$. This leads to over-all spins of either zero or one in the neutral molecule. Because electrons from lower orbitals than LUMO can also be removed, if the laser photon energy is high enough, singlet and triplet states can be addressed by photo-detachment equally. This means that via the radical-anion by using photo-detachment spectroscopy (PD-PES) one is able to circumvent most of the classical optical selection rules which exist if one would start spectroscopy from the neutral ground state, as usually performed.

For a given sample molecule, there are, however, several preconditions which have to be fulfilled in order to be able to apply the PD-PE spectroscopy:

- It has to be brought into the gas-phase as an intact molecule.

- It has to be able to form a valence-bound radical anion, where the electron resides in the LUMO of the molecule.

- The laser photon energy has to be high-energetic enough in order to be able to reach the neutral exited states from the anion.

This means that the neutral states of such molecule which can not form a valence-bound radical anion, cannot be investigated at all by PD-PES. Due to the limited photon energy in this experiment (213 $nm \approx\ 6.25eV$), also molecules which have a very high electron affinity only allow excitation to the S_0 ground state. In an ideal case electron affinities and especially the lowest triplet states up to the S_1 state can be investigated.

2.2.1 Definition of the Electron Affinity

Consider reading the IUPAC gold book compendium of Chemical Terminology[NJK+] there can be found two well-suited definitions of electron affinities [NJK+]:

$$X^- \rightarrow X + e^- \tag{2.14}$$

X^-: radical anion X
X: atom X
e^-: electron

In the first definition the EA is the minimum energy required to remove an electron from a radical anion and form its neutral ground state. The second definition is opposite to the first one and more frequently used. It just reverses equation 2.14 and is the

$$X + e^- \rightarrow X^- \tag{2.15}$$

X^-: radical anion X
X: atom X
e^-: electron

maximum energy which is released by a molecule when the surplus electron attaches. Both EA definitions can be calculated as the energy difference between the anion ground state and the neutral ground state S_0.

For atomic species the electron affinity is just a value depending on local effects of the shell. Regarding molecules, it can be assumed that huge π-systems should have positive EA's and that the EA values are monotonously increasing with the molecular size. In general for molecular systems the prediction of the EA by a simple guess, can be much more difficult due to global and local effects [SWNS98]. A more recent example for an extraordinary high EA can be found, when looking at benzoide cyanocarbons. Their EA's can exceed the EA of fullerene, which has an EA of 3.53 eV [ZLI+06]. In general, the determination of EA's is a subject of theoretical, as well as experimental investigations.

2.2.2 The Formation of Radical-Anions

The formation of radical anions in the gas phase is a complex process, which is not understood in detail. In parts it was already described in section 2.1. It can be stated that the size of the EA is a first important factor for the formation of stable radical-anions. In order to successfully detect the anions of a given sample molecule, the newly-formed anions have to be stable for a certain time. Depending on the mass of the anion, in a time-of-flight mass spectrometer this are usually several 100 μs.

The fact that in vacuum radical anions can loose the electron after some time again , meaning that they are metastable, needs further explanation. For this, it has to be considered that the processes which occur during or right after the electron capture process. Since the free electron has some kinetic energy before it attaches to the neutral molecule, due to energy conservation, the newly-formed molecular anion has an internal energy lying above the detachment threshold.

The reason that the internally hot anion does not immediately decay to the neutral plus a free electron is,

- That the excess energy is stored in molecular vibrations.
- That obviously the re-conversion of the vibrational energy into the electronic energy of the surplus electron is slow .

To understand the variables and the parameters, which determine the time scale of the metastable auto-detachment, the size of the EA has to be considered. If the surplus electron makes it to stay in the molecule, its kinetic energy and the electron affinity has to be stored in vibrations. If the molecule has a high number of vibrations - say 20 normal modes - and an EA higher that 0.5 eV, the density of the vibrational states at the level of the neutral ground state is very high. This is due to the many states resulting from the many possible combinations of quanta of the normal modes. The statistics that the energy finds back to the surplus electron is small and depends on the number of accessible vibrational states in the hot anion[KC78].

Even in vacuum, if the excess energy of the freshly-formed anion over the detachment threshold it not too high, it can possibly stabilize itself by the emission of infra-read radiation. In a gas co-expansion with argon vibrational cooling of the anion can be performed by the many low-energy collisions with the argon atoms.

Removing just the excess energy from the newly-formed anion would be sufficient to make the anion forever stable, but would not be sufficient for the subsequent photo-electron spectroscopy.

Starting the spectroscopy in vibrational excited anions would result in manifold hot-band transitions and broad photo-electron spectra, as shown in section 4. This should be avoided under all circumstances.

If the anion formation takes place in a co-expansion with argon, the countless collisions with the rare gas cause an efficient jet-cooling effects (as is described in section 2.1 and can be seen in the experimental part of this work).

The above considerations do, however, not jet explain how the electron manages to stay in the molecule and how it converts so quickly its kinetic energy and the EA to vibrations. The efficient electron capture in liquid fluorinated or chlorinated hydrocarbons is technically used in high-voltage applications, in order to capture and bind free electrons (as formed by high energy particles or photons from natural radioactivity or extraterrestrial origin) into molecular anions and by this avoid discharges.

In liquids the mean free path length for electrons is minuscule, so that even in a enormous electric field the electrons undergo so many collisions that i) they can not gain kinetic energy and ii) after anion formation the excess energy can be very efficiently transferred to neighbouring molecules.

In contrast to this, the formation of radical anions in vacuum is a very different process. It is performed by attachment of a free electron with some kinetic energy to an isolated neutral sample molecule. Since the energy equilibration effect of the liquid is missing, the gas phase process is more complex and not understood in detail at all.

Also experimentally the electron attachment in the gas phase and the cooling of the anion is difficult to perform for several reasons:

- Since the sample molecules are neutral they do not attract free electrons.
- Thus many electrons have to be offered to a single molecule in order to result in a reasonable electron capture result.
- In most of molecular samples the kinetic energy of the incoming electron has to be very small, to allow its stabilization in the molecule at least for an interval long enough, which allows cooling by other processes.
- Once the surplus electron is at least temporarily stabilized in the anion has to be efficiently cooled.

In PD-PES the EA and the kinetic energy of the incoming electron has to be removed by cooling either due to

- Cooling by dissociation of a already existing molecule-argon complex .
- By collisional cooling in the co-expansion with the argon carrier gas.

The most crucial/critical, not jet explained step of the electron attachment is the first stabilization mechanism of the incoming electron (third item in the list above). It should be noted that the electron is fast even if it has a minuscule kinetic energy. For example if an electron has a kinetic energy of 10 meV, it would only need about 1 fs to pass the sample molecule. In this time interval only the electrons of the molecules can react to the approach of the additional electron. The motions of the atoms of the molecule are too slow to be able to immediately react to the new electrostatic situation.

In order to make the additional electron stay in the molecule for a relatively long time or in terms of a real binding, in the gas phase, during the half collision of the attachment process, the kinetic energy of the incoming electron has to be immediately

- Removed by a third particle, presumably an argon atom
- Stored in other degrees of freedom in the molecule

Clearly the probability of a three particle collision electron-molecule-argon is diminishing and does not explain the efficient anion formation in the discharge. The attachment of the electron to a molecule-argon cluster could indeed lead to a situation where the argon is able to remove the excess energy of the electron. However, such a mechanism is not obvious since the electronic energy has to be converted on an ultra-fast time scale to a translational motion of the argon. Nevertheless, it is important to note, that the usage of argon at very high pressures leading to complex formation at this position of the expansion might be dominant.

As already mentioned above, the most plausible possibility to store energy for a relatively long time are the vibrational states of the molecule. Because large molecules have many normal modes and especially very many combination states of these normal modes, the vibrational density at the level of the EA can be so high, that it allows to fulfil the energy conservation law and accept the electronic energy. However, what is the mechanism which converts the kinetic energy of the incoming electron to vibrations of the anion ground state on a ultra-fast scale. If this is achieved, the vibrational hot anion is stabilized and cooled by offering as many rare gas collisions as possible. The time scale on which these collisions have to take place can be a much longer time scale, as outlined above.

Since this energy conversion from the kinetic energy of the incoming electron to the vibrations of the anion has to be fast, there are not so many possibilities, It could be from the starting situation "free electron plus a neutral molecule" to the iso-energetic vibrations of the anion ground state

- An internal conversion process of a short-lived anion excited state
- A direct iso-energetic Franck-Condon-transition to the high vibrational states of the anion.

. Since, for the internal conversion (IC) also a overlap of vibrational wave functions is necessary, essentially both choices are similar. Indeed the example of Benzoquinone has shown [SW99], that anion excited states can act as acceptor states, which enhance electron capture. Obviously these anion excited states are able to convert the energy of the incoming electron on a ultra-fast time scale to iso-energetic vibrational states of below-lying anion excited states or directly to the iso-energetic anion ground state vibrations.
This process is a classical IC: The conversion of electronic energy to vibrations of the lower electronic state. However, if not the situation of a molecular distortion and a conical intersection is present (which may be the case in benzoquinone), IC processes typically take place on a time scale of several nanoseconds, far too long in comparison to the time interval of an electron-molecule collision even for low-energetic electrons. Considering the work of Smirnov and Illenberger [IS98] One can approximate the time t_e for electron capture within the framework of the Born-Oppenheimer approximation and under the assumption of autodetachment-states as

$$t_e <<< \frac{1}{\omega} \tag{2.16}$$

t_e: electron capture time
ω: vibrational energy difference

While $\hbar\omega$ is the energetic difference between the closest vibrational states in the molecule. Assuming electron attachment as a direct Franck-Condon process (similar to photon absorption or emission, but just iso-energetic), there has to be a wave-function overlap between iso-energetic vibrational wave-functions of the highly excited anion ground state with the wave-function of the neutral ground state. If this overlap is too small, the conversion process would fail and so would the stabilization of the surplus electron.
A well-known molecular example for a good Franck-Condon-overlap for such a case is

sulphurhexafluorid SF_6^-[Bor07]. In this molecule, the electron attachment causes a large geometrical change for the anion in respect to the neutral molecule. Since in general the vibrational wave function of high quantum numbers (in the SF_6^- anion at about 2.5 eV) peak at the inside and outside turning points of the Morse-potential and the anion-to-neutral geometry-shift is large, the Franck-Condon overlap of the isoenergetic vibrational levels with the neutral ground state wave function is exceptional. This explains that SF_6 is known to be the most efficient scavenger for low-energetic electrons.

The role of inhomogeneous charge distribution (dipole and quadrupole moment) in the molecule may be important to stabilize the electron in the molecule a little longer than a simple transition time, and thus enhance the electronic to vibrational energy conversion. However, nothing is known about such effects.

The first steps of anion formation, the electron approach and the attachment process, cannot be directly influenced by experimental parameters except that one tries to offer as much as free electrons as possible, as much low-energetic electrons as possible and as much as argon atoms either to form an argon-molecule-complexes or to perform collisions. Since presumably also the energy of the free electrons may be moderated or controlled by argon collisions (see chapter 3.3.2 for evidence and further discussion),the argon particle density in the anion formation zone in front of the nozzle could be a crucial parameter. In this work the back-pressure in the valve was therefore set between 10 and $30 bar$.

2.2.3 Methods to determine electron affinities

electron-capture detection ECD

One of the earliest methods to determine electron affinities in the gas phase is the capturing of electrons after a ionization process by measuring the current after the impact on an electrode, short the ECD[4]. The basic principle of this kind of detection is the ionization of a target molecule inside a carrier gas like argon or xenon which gets hooked to a gas chromatograph.This setup was firstly proposed by J.E Lovelock[Lov58] and was the start for a experimentation series with R.Becker and E.Chen[BC66]. The function of this detector relies on a pre separation via gas-chromatography. After the GC the target molecule will be carried in argon gas entering the detector. The walls are coated in Strontium 90 metal. This substance is a weak β-emitter generating initial electrons. The target substance as well as the argon will form ions. If the target molecule has a positive electron affinity (see 2.15) radical-anions will be formed. The resulting current will decrease

---

[4] electron capture detector

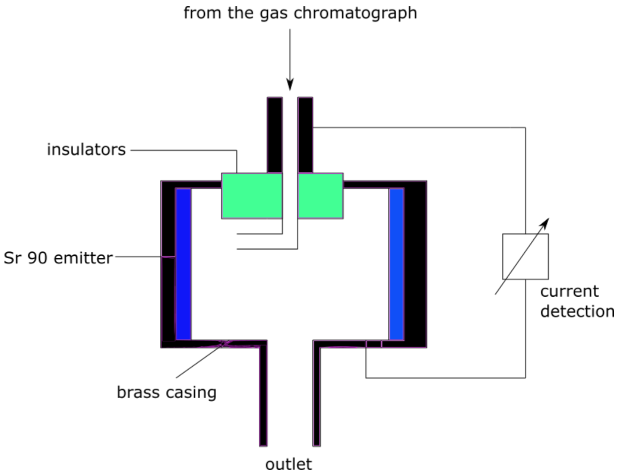

Figure 2.12: Simplified Illustration of the ECD. The gas flows with the target substance into the detector at normal pressure. The β-radiation from the Sr^{90}-surface ionises the carrier gas and the target molecule. The resulting current can be used to determine the EA of the substance. Sketch loosely based on [Lov58]

in comparison to just the argon jet. The drop in current then can be linked to EA after calibrating the detector. This methods gets more sensitive the higher the EA of the target molecule is and is therefore suited to detect most environmental pollutants, which mostly consists of halogenated hydrocarbons. Nevertheless this also means that the ECD is not the most suitable method for measuring substances with smaller EA because of this relation. The EA´s in organic compounds can vary drastically which makes other methods more reliable depending on the EA value. This can be explained by the electron absorption coefficient which describes the effectiveness of electron attachment and is gained by relating data of the ECD with flame ionization detector data[KD70]. The following table shows some of the data of [KD70] and reveals the correlation between substance class and electron absorption efficiency.

This clearly indicates that the probability of forming an Anion is dependent on the local effects and the respective electrophores. Halogenated substances therefore tend to have a higher EA due to local effects and can be detected more sensitively.
Other methods also have been used in the past but most of them function in a similar way and a kind of mass spectrometry or other optical methods.
Of course the laser photoelectron spectroscopy is a valid method to determine EA's too, as can be seen in the next chapter.

Table 2.2: Overview of some electron absorption coefficient depending on functional groups.Based on[KD70]

electron absorption coefficient [a.u]	species
$0,01$	aliphatic-compounds, dienes, benzene
$0,01-0,1$	ethers, esters, naphtalene
$0,1-1$	aliphatic alcohols, ketones, amines, aldehydes
$1-10$	enols, oxalat esters, dichloro, hexafluoro, monobromo-compounds
$10-100$	trichloro-compounds, benzaldehyde, anthracene
$100-1000$	Azulene, benzophenones, monoiodo, dibromo, tri/tetrachloro-compounds
$1000-10^4$	quinones, 1,2-Diketones, polyhalogenated compounds

2.2.4 The formation of radical anions regarding the pulsed discharge

To the authors knowledge, the combination of a pulsed supersonic co-expansion with a pulsed discharge outside of the nozzle is new experimental concept, which is used for the first time in this work . Pulsed discharges have been used in a channel in front of the pulsed nozzle. The discharge provides charges but also evaporates atomic material from the metal rod, which in a pulsed supersonic rare gas expansion reassembles to atomic clusters, which carry a positive or negative charge[WPTM06]. Also outside the valve a continuous discharge (corona discharge[JBD01]) has been used too for small molecular radical anions and cations. It is, however, well-known that continuous discharges can be controlled and stabilized in their behaviour.

Pulsed discharges on the time scale of several microseconds-as used in this work-usually suffer from instability. As explained above, a reproducible ignition time and a reproducible current strength of pulsed discharges strongly depend on

- The existence or formation and number of the first charge seeds.
- The gas pressure between the electrodes

To solve the first mentioned problem, often radioactive materials mixed into the electrode materials or a permanent low-current discharge (simmering: compare flash lamps in Nd:YAG lasers) are used. They inject permanently charged particles (electrons or ions)

into the space between the electrodes. These charges are then instantaneously available to immediately ignite the high current-discharge at exactly the time when the high voltage pulse is switched on. As for point 2): Since beside the charge seeds the gas pressure is a critical parameter for the ignition and maintenance of the discharge, it is thinkable that the distance of the electrode tips to the nozzle (note that the gas density in an expansion decreases with $\frac{1}{L^2}$ with the distance L from the nozzle orifice) and the timing of the high voltage pulse referred to the gas pulse (typical pulse lengths $100-200\ \mu s$) are very critical. Because gas valves, although electrically addressed, open the nozzle orifice by mechanical motion of a poppet, their opening characteristics undergo fluctuation from pulse to pulse. Having the $1-2\ \mu s$ time scale of the high voltage pulse in mind (leading frequencies in a Fourier analysis of the high voltage pulse: $1-0.5\ MHz$), due to mass inertia any motion of mechanical parts is slow ($5-10\ kHz$). Even worse, in addition the mechanical motion undergoes a fluctuation concerning the time difference between the electric addressing of the valve and its mechanical answer.
Another problem may arise from the fact already mentioned above, that if the valve is open, the gas density changes with time but also decreases with $\frac{1}{L^2}$ according to the distance from the nozzle. This means that the average collision-free path-length of the electrons until they duplicate by ionization of an argon atom decreases the closer they come to the valve orifice. It is imaginable that there might be a point close to the nozzle orifice where the ionization processes might stop due to the high number of collisions. In the worst case this could lead to an interruption of the discharge or at least to a insufficient cooling of the anions. For an efficient cooling of the freshly formed molecular anions it is desirable that the anions are formed as close to the nozzle orifice as possible.

Knowing these unfortunate preconditions, you would hesitate to combine a pulsed discharge outside of a pulsed gas nozzle. It turned out, however, that once adjusted in means of the timing and pulse length it became possible to form numerous radical-anions. The very details of the setup can be seen in chapter 3.3.2 where the electrical framework and the geometric boundaries are further explained. But so far, several assumptions regarding the process itself can be made.

Presumably, for most of the sample molecules used in this work, the electron attachment process works best if the electrons are slow. In a discharge, however, the electric field has to be strong in order to start and maintain the charge flow. This means that electrons and ions are accelerated enough in order to be able to ionize and form secondary charge carriers in one of the next collisions. In such a high electric filed (driving voltage at the electrodes: $2000 - 5000\ V$, electrode distance: $2 - 3\ mm$) despite many free electrons may be present in the discharge, the number of low-energetic electrons (say $0 - 100\ meV$) is expected to be very small. Hence, if low-energetic electrons play the mayor role in the anion formation process, their small number would be in contradiction to the fact that in this experiments quite a lot of molecular anions are formed.

The important question resulting from this controversy is, by which process the anions are formed. In general there are the following possibilities:

- I) The attachment of energetic electrons takes place in a three-body mechanism either a three-body collision process (electron molecule and carrier gas atom) or the electron attachment to a preformed molecule-carrier gas complex. In such a process the third partner, an argon atom, could theoretically carry away the electron kinetic energy before the collision and at least a part of the binding energy (electron affinity) if the electron is stabilized in the molecule.
- II) The attachment of energetic electrons is resonantly enhanced by anion excited states of the sample molecule, which lie well above the neutral ground state. In order to form stable anions via this pathway, the anion-excited state - instead of quickly releasing the electron again (this process is termed auto-detachment) - has to undergo an ultra-fast internal conversion process to the vibrations of a below-lying electronic state.
- III) Close to the nozzle the carrier gas density increases so enormously that the electron energy is strongly diminished despite the still existing high electric field. The low-energetic electrons then can efficiently attach to molecules.
- IV) Since the electrons in a typical discharge move very fast and disappear in the anode, at the end of the discharge, when the field is switched off in some tenths of nanoseconds, a positive net charge in form of argon ions remains. This positive ion cloud forms (by its space charge) a Coulomb-valley, in which the still existing free electrons are trapped. These electrons can be caught long enough to be moderated in energy by collisions or/and to have multiple trials for attachments to sample molecules. The coulomb-valley starts to build-up during the discharge and in about $150 \mu s$ drifts down into the ion source.

None of the authors experiments can clarify exactly which of the four process (or a combination of them) is or processes are the most predominant ones in our discharge. A direct proof for the existence of the coulomb-valley is the high electron signal at very short flight times, which can be observed in the backward time-of-flight mass spectrometer (see chapter 3.3.2). That this signal is brought by electrons can easily be proven by deflection using a magnetic field. The presence of the space charge trapping would also explain why in one discharge event (duration about $\approx 1\ \mu s$) are for some sample anions able to transport the high number of more than estimated 1000 to 5000 anions downwards through the skimmer into the ion source of the time-of-flight mass spectrometer. This transfer needs about 150 μs, during which – if the positive charges are absent - the anion would experience a charge repulsion between each other. This should cause a strong loss in the anion intensity, which is obviously not observable.

As already mentioned above, the experiments cannot directly clarify the processes taking place in our discharge anion source, it seems that the high back-pressure in the nozzle and the high current in the pulsed discharge create unique conditions such as a very high gas density in front of the nozzle and the formation of many positive ions (and electrons). These conditions could indeed favour the scenarios III and IV.

2.3 Photodetachment Photoelectron Spectroscopy at Radical Anions

The experimental set-up for radical-anion PD-PES consists of a sequence of different sub-set-ups, each of them using different methods and dedicated to fulfil a certain task. To achieve the main aim this consecutive sequence of methods in order is used , which is the determination of the molecular EAs and the spectroscopy of neutral states otherwise not accessible. In the following sub-chapters the background of the the anion formation, the mass-selection and specifically the principles and boundaries of PD-PES will be outlined.

Overview over the sequence of methods

Basically the PD-PES experiment consists of six sub-set-ups. 2.14 shows the whole prototype as an overview. In the following the sub-set-ups are presented according to their timing in the measurement cycles:

- A heated and pulsed gas nozzle releases argon and sample molecules through a small orifice into the vacuum.
- Intact radical anions of the sample molecules are formed in front of the nozzle by a pulsed discharge, which takes place through the expanding sample-argon gas mixture.
- Directly after anion formation vibrational cooling by the Argon jet expansion takes place.
- The ions pass a skimmer for pressure reduction and enter the pulsed extraction unit of the TOF-MS.
- When the extraction voltage is switched on, the anions are accelerated into the direction of the PE spectrometer and the ion detector.
- In the time-of-flight PE spectrometer the pulsed laser hits the selected anion cloud and performs photodetachment.
- Photoelectron spectra are recorded by measuring the electron flight time for the 60 cm long field-free drift tube to the electron detector.
- To control the mass of the detached anion and the quality of the anion formation process, the mass-spectrum is amplified by a MCP particle detector behind the PE spectrometer and displayed and recorded by a digital oscilloscope.

Every single point in this recital is crucial for the success of the PD-PES method.

The anion formation

It is self-explaining, that without the generation of a sufficient number of cold anions, it is not possible to record PE[5] spectra. In the past, before this work was started, the anion formation in the group of Prof. Weinkauf was also performed in the supersonic co-expansion but it was induced by electrons from a laser-fed pulsed electron gun [Pau17]. This electron gun was mounted on one side of the first chamber in such a way, that the electrons could be injected from outside the expansion into the supersonic co-expansion to the nozzle orifice [Ste15].

In contrast to this, in this work a pulsed discharge in front of the nozzle is used for anion formation. This means that the discharge which provides the electrons for the attachment process and the anion formation take place at the same site in the supersonic co-expansion. In chapter 4 it is shown, that this new anion formation method works more stable and reliable than the electron gun used before. Surprisingly the highest peak in the mass spectra is always the parent anion and only a few fragments with small intensities or some complexes with water or dimers and trimers are observed. Since the new anion formation with the pulsed discharge is very efficient, it is tolerable that less per cent of sample molecules occur in the expansion and therefore the use considerably lower temperatures for the sublimation process in the nozzle head is possible.

The Supersonic Co-expansion of Sample Molecules with Argon

In the chapter two it is speculated that there may be a mechanism for anion formation in which three-bold collisions of the type electron-molecule-argon may be involved. And that this process can be one mechanism which contributes to the efficiency of the anion formation of the discharge in the supersonic co-expansion. This is unproven speculation, but without doubt it is crucial for this experiment, that the newly formed anions are stabilised and cooled. This means that for the neutral and the anionic sample molecules all internal energy in form of vibrational energy should be removed as much as possible.
It should be noted that in the set-up at two positions cooling is needed:

- First for the neutral molecules, which are brought into gas phase at temperatures between 80° Celsius and 350° Celsius, have to be cooled to be prepared for the acceptance of a surplus electron. This happens in the orifice channel and directly behind the nozzle orifice.
- After electron attachment the anions are internally heated again, because the excess

---

[5] Photoelectron

> energy of the incoming electron as well as the electron affinity is converted to vibrations. This energy has also to be removed as much as possible. Because this has to take place already some 100 μm outside of the nozzle, we use a high pressure in the nozzle and the expansion: The hope by doing this, is that one can prolong the collision zone in front of the nozzle.

The collisional stabilization and cooling of the anions is crucial, because as long as they are internally hot they can eject the electron again, which of course is not desired. A cooling effect beyond the anion stabilization is, however, also very essential to obtain sharp and non-congested PD-PE-spectra. The vibrational (and rotational) cooling in co-expansions is often used in laser spectroscopy of poly-atomic molecules [SK13].

The concept of using a supersonic co-expansion consisting of about five percent sample molecules mixed with a rare gas, here argon, is, to achieve a vibrational cooling by the very many low-energetic collisions of the sample with argon atoms.

In order to get an understanding of what happens in the co-expansion, recalling first that the thermal velocity of different masses in a thermal equilibrium, as present in the nozzle head, is different: bigger masses are slower than smaller masses. In this experiment, the big mass is always the sample molecule and the smaller mass is the carrier and expansion gas. If the nozzle opens, the bigger masses are accelerated by the many collisions with the carrier gas atoms. This acceleration starts to happen already on their way out though the orifice channel into the vacuum. In this acceleration phase, the sample-argon collisions are relatively high-energetic. In order to keep the distance over which the acceleration happens as small as possible, a heavy carrier gas has to be used so that the initial sample-to-carrier-gas velocity difference is not too big. The best expansion gas would be theoretically xenon. Beside that xenon is very expensive, it tends to form extensively complexes with molecules, and this even more if the molecules carries a charge. This latter complication is the reason that in our experiment argon (40 Da) is used as carrier gas.

It is typically assumed that the acceleration and most of the cooling is over at some 100 μm outside the nozzle. Because the cathode electrode-to-nozzle distance is only about $3 - 4$ mm, we assume that the anion formation by the discharge happens at $0.2 - 1$ mm above the orifice. Since a $20 - 30$ bar argon backing-pressure in the nozzle is used, the density of the expansion is supposed to be still high enough at the site of the anion formation, so that the internally - due to the attachment process - hot anions are still cooled by collisions with the argon atoms.

It should be noted that due to the dynamics in the on-going atomic expansion (see below) the sample velocities more and more adapt to the atomic velocity so that the molecule-atom collision energies become smaller and smaller until the zone is reached, where all velocities are the same (zone of silence). In this zone all sample anions cations and neutral Argon atoms drift with the same velocity without collisions. This stepwise down-regulation of the collisional energy and the zone of silence ensure that the anions are cooled and stay cold, well-prepared for spectroscopy.

Seen from a theoretical perspective, the cooling of intra-molecular vibrations by collisions with argon converts vibrational energy to translational energy of the atoms. Because the density of the vibrational states is relatively low in comparison to the very high density of the translational states at the energy level of the vibration this process is highly driven by entropy and is a unidirectional process.

The Supersonic Expansions of Atoms

In order to better understand the dynamics of the co-expansion indulging in the dynamics of an atomic rare gas supersonic expansion is needed. A supersonic expansion always occurs when a rare gas of high pressure through a small orifice suddenly enters an area with a very low pressure. The name "supersonic expansion" stems from the fact, that for rare gas atoms at the end of the expansion the velocity of the expanded gas is higher as the average speed in the nozzle before. Therefore the velocity after the expansion is supersonic in comparison to the velocity in the nozzle. The best way to describe the process is by using the Mach-Number which simply is the ratio of the speed after the expansion divided by the standard sonic-velocity in the respective medium.

In textbooks it is noted that due to expansion a cooling effect occurs. The definition of this cooling in the atomic expansion is in principal, however, purely artificial. If the main direction of the expansion follows the z-axis, the extreme cooling of the translation in the direction x- and y-axes is only observed because one uses a skimmer in order to select the centre part of the expansion. If one considers the translational velocity in the z-axis then the velocity is increased. This would be even a heating. Only by trying to describe the narrow velocity in the z-direction in the zone of silence by a thermal velocity distribution (which is a pure artificial fitting procedure, because the average velocity is subtracted) one finds low temperatures.

Additionally the above described effect has nothing in common with the Joule-Thomson cooling effect. This effect comes from the fact that suitable gases under high pressure already have attractive intermolecular van-der-Waals interactions, which are broken if the pressure and the gas density suddenly decreases. To break the bonds energy is needed which is taken from the translational energy of the gas. The Joule-Thomson cooling does not work for helium, the supersonic expansion and the molecular cooling in a supersonic co-expansion, however, with helium does work.

$$M = \frac{v}{\sqrt{\kappa \cdot \frac{R}{M} \cdot T}} \tag{2.17}$$

M: Mach-Number $[a.u.]$
k: isotropic exponent $[a.u.]$
R: gas constant $[\frac{kg \cdot m^2}{s^2 \cdot mol \cdot K}]$
M: molar mass $[\frac{mol}{kg}]$
v: gas velocity $[\frac{m}{s}]$

This means the transition from a effusive jet and a supersonic or sonic jet depends mostly on the relation between the diameter D of the reservoir orifice and the collision-free path-length of the respective gas λ_0. So if the ratio between those numbers reaches the point where $D >> \lambda_0$, the jet will become supersonic, in terms of the mach number $M > 1$ and on the opening of the reservoir at least $M = 1$. If this is the case the velocities equilibrate and the zone of silence exists. Otherwise the gas expansion is just an effusive gas flow, where the equilibration of the velocities fails.

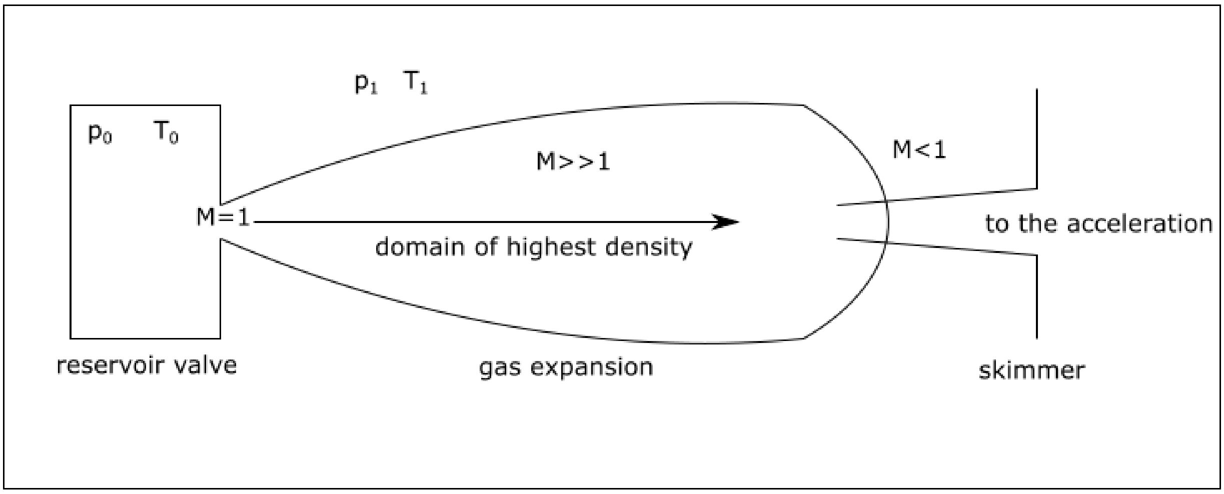

Figure 2.13: Illustration of a continuous supersonic jet expansion. The process can be divided in several sections: i) The reservoir with the high gas pressure, ii) the orifice of some 100 μm diameters, iii) the cone of the expansion gas and iv) the vacuum chamber. In the centre area of the expansion the gas density is the highest. This is the area where the anions undergo many collisions the velocities equilibrate and where the coldest molecular anions are found. This part of the gas passes the skimmer to proceed to the ion source of the ToF-MS. Sketch loosely based on [HS83].

The supersonic expansion is solely formed if the pressure difference between the nozzle and the vacuum is very high (from 15 bar to high vacuum $5 \cdot 10^{-6}$ bar).

As outlined above, for the molecular cooling the mach number of the atomic gas is not the important parameter, since the translational cooling of the atomic gas and the vibrational cooling of the molecules are completely different processes. Important for the vibrational cooling of the molecules is, that the argon density in the middle of the jet is extremely high. Meaning that there the impact probability is enormously high so that vibrational energy can now be transferred out of the molecules by collisions with the argon. In addition the collision energy between molecules and argon is first relatively high and becomes miniscule during the course of the expansion. By this, it is possible to cool the neutral molecules first, which in the nozzle have been brought into gas phase by heating. When the electron capturing happens, the anion is internally heated and needs a second cooling in the ongoing expansion.

It is necessary to ad, that if the expansion is loaded with too many sample molecules or too many ions the formation of an undisturbed expansion fails, which results in an imperfect vibrational cooling.

For further processing of the anions, a skimming of the jet is needed, because i) the molecules outside the centre of the expansion are not cold and ii) a vacuum pressure-reduction is needed in order to stay collision-free in the second vacuum chamber especially at the site of the acceleration into the TOF-MS instrument.

Selection of the Sample Anions of Interest

Mass selection prior to spectroscopy is essential to guarantee that only the species of interest will be analysed and not a fragment or an aggregate. This especially holds for the anion formation in a discharge in a supersonic expansion: i) Discharges are known to impose harsh conditions in which molecular fragments can occur and ii) supersonic expansions are also known to support the formation of complexes, such as the sample molecule with water, sample molecular dimers or clusters with the carrier gas argon.

The most-efficient and most-used method for selection of ions is mass spectrometry. Because of its high transmission, a linear time-of-flight mass-spectrometer (TOF-MS) is used in this work . With certain changes, such as for example reversing the polarity of the acceleration voltages and some detector voltages, the usual TOF- MS set-up, as known from cation mass spectrometry can be also applied for anion MS. By a high voltage pulse applied to the plates of the extraction unit (the orifices at the centre of the plates are covered with copper grids) in the extraction unit, the anions are accelerated to the TOF flight path crossing the photoelectron spectrometer perpendicularly and end at the MCP particle detector. Because of their polarity the cations fly exactly to the opposite side and can be detected in a short TOF. This allows to control the functionality of the discharge.

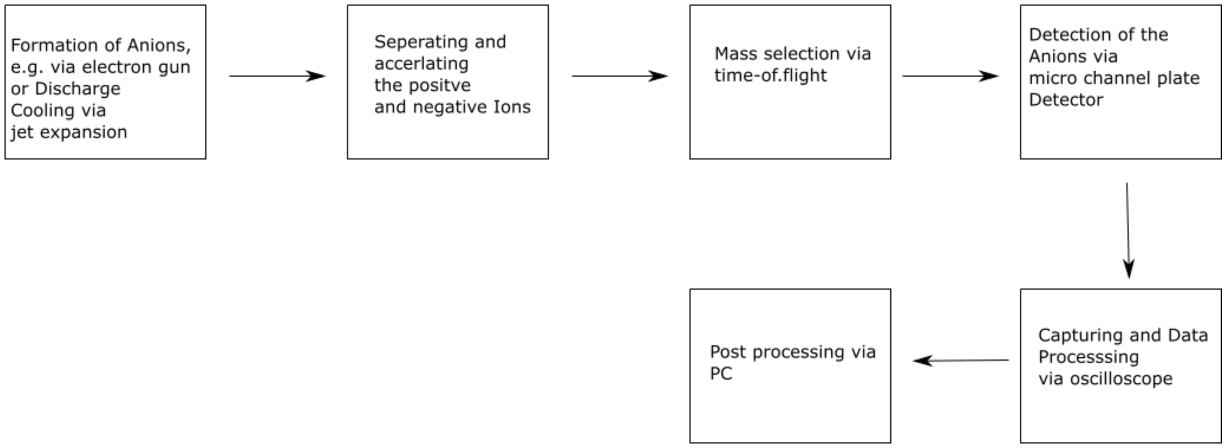

Figure 2.14: Illustration of the linear time-of-flight mass spectrometer for mass selection of negative ions. After arriving in the extraction unit of the TOF-MS, the anions are accelerated by a high voltage pulse into the flight path of the TOF-MS, which crosses perpendicularly the photo-electron spectrometer. Detection happens by a fast two-stack micro-channel-plate detector. The post processing and data collection takes place by a digital oscilloscope and a PC.

The anion cloud passes several electrostatic lenses, two quadrupole deflection systems and the post source acceleration. before the photoelectron spectrometer the anion cloud is, shaped by cylindrical lenses into a cigar-like form for a better overlap with the laser beam. The laser comes perpendicular to the ion flight path and the photoelectron spectrometer. The ion flight-time is measured, when the anions hit the ion MCP detector at the end of the flight path. It is possible to directly observe the full mass spectrum on the digital oscilloscope. The flight time of the ions can be correlated with their masses (see below). This oscilloscope can be also used to digitize and store mass spectra /PC.
The timing of the photodetachment laser pulse is adjusted in such way that the anions are detached in the middle of the photoelectron spectrometer.
The arrival time of a molecular species of mass m in a linear TOF can be computed as following:

$$E_{electric} = E_{kinetic} \tag{2.18}$$

$$e \cdot U = \frac{1}{2} \cdot m \cdot v^2 \tag{2.19}$$

$E_{electric}$: electric energy $[J]$
$E_{kinetic}$: kinetic energy $[J]$
e: electron charge $[C]$
m: mass $[kg]$
U: voltage $[V]$
v: velocity $[\frac{m}{s}]$

Simple transforming of the equation 2.19 to the flight-time t results in:

$$t = \frac{s}{\sqrt{2U}} \cdot \sqrt{\frac{m}{e}} \tag{2.20}$$

Since theoretically (see below) all ions of all masses are accelerated to the same constant energy, the above equations show, that the flight time t is just dependent on the mass of the molecule. So an observed ion peak can be assigned to a certain mass simply by its flight time and with some intuition assigned to a given molecular species or a complex.
It is always important to know the mass resolution of the spectrometer, which is defined as $\frac{m}{\Delta m}$. The 50 percent definition of the mass resolution assumes i) that two neighbouring mass peaks, which can still be identified as two peaks, have the same height and ii) they have a mass difference Δm exactly so, that the two 50 percent levels of the inner signal wings overlap at the same point. Then the so-termed 50 percent mass resolution is $\frac{m}{\Delta m} = \frac{t}{2} \cdot \Delta t$. The mass resolution of the here used TOF-MS is about $200 - 500$ and depends on mass and especially on the intensity of the ion peak. The latter is due to the coulomb repulsion between the ions during their flight to the detector. For intense signals, this repulsion causes a time-broadening of the peaks.

Usually in a mass spectrometer the attempt is made to let all ions start at the same position of the extraction field in the acceleration unit. If this would be fulfilled and all ions start at the same potential energy line, they would all have the same energy. In the set-up this is, however, not the case. There are two reasons for that. One reason is that the volume where the anion formation takes place may have a diameter of one mm. The other reason is that supersonic expansion also expands in diameter when moving away from the nozzle: the nozzle orifice is like a point source of particles and the expansion forms a cone-like structure. In the set-up the cone diameter selected for admittance to the TOF extraction unit, is given by the position of the nozzle in respect to the skimmer (distance: nozzle to skimmer orifice about 20 mm) and the diameter of the skimmer orifice (diameter ≈ 4 mm). Due to this, the ion cloud may have a diameter of $7mm$ or even more between the extraction plates. This means, that the ions - even the ions of the same mass - start at different equipotential lines in the extraction plates and are accelerated to different energies. They therefore do not arrive at the same time at the detector. In the case of an initial spatial width of the ion cloud of 7 mm the time error caused by the energy error is huge. As a first measure, it can be reduced by using two extraction fields (three plates): First a small electric field and then a high electric field is applied.

The energy error of the starting ions in the first small field is then small, much smaller than it would be in the case of using only one field (two plates). According to Wiley and McLaren[WM55], if the two electric fields are well-chosen, the ions meet in a point outside the extraction unit (typically at $20-30$ cm from the extraction unit). This point is termed space focus. This is, however, much too close to the ion source in order to efficiently use it for a considerable increase of the mass resolution in a linear TOF-MS. Weinkauf et al. could show, that when in addition the distances between the extraction plates plates is adapted in the right way, one can shift the space focus to relatively long distances. This is the mode in which we record our mass spectra.
Once the right peak of the sample of interest is identified we further sharpen this ion package in time by the so called "post source focussing effect" (PS[6]) found by Garry Kinsel [KJ89]. This is necessary in order to compress the ions in order to hit as many anions as possible with the detachment laser. The focal size of the detachment laser is about 1 mm in diameter. The idea of this PS method is to post-accelerate the ions of one mass or a small mass range by an accelerating electric pulse at a site of the ion flight path where the low-energetic ions already lag behind. At this point the ions are again accelerated between two plates with a high-voltage pulse, in such way that the slower ions have the longer distance in the field and therefore gain more energy than the faster ones. By choosing the right delay and the right voltage of the PS-pulse the flight errors between the ions of one mass can be mostly compensated for. With both methods applied, and by reducing the ion number, peak widths of down to 50 ns width at half height are achievable (the absolute flight time is about $100-150$ s).

Fast Anion Detection

The detection of anions (in this work also electrons) can be accomplished by using MCP[7]-detectors. MCP's are basically plates (typically made from a non-conductive glass) with a tremendous high electric resistance ($500-1400$ $M\Omega$). In these plates, minuscule channels (diameter 10 μm or less), are etched and coated with semi-conducting material (possibly oxidized lead). The plate itself has typically a diameter of 3 cm (depending on the application up to 40 cm) and a thickness of 1 mm. The centre-to-centre hole distance of the channels is so small that 60 percent of the MCP's surface are open. Front and rear side of the plate are metal coated to which a difference voltage of approximately 1 kV is applied. For single particle detection typically two MCPs are used in series [Wol81]. In combination

---

[6] post source focussing effect

[7] micro channel plate

with a CCD[8]-Chip as a collecting anode for example, they can be also used to obtain an efficient amplification of particles while maintaining a spatial resolution [OSS⁺01].
In order to use MCP'S as a mass detector, especially for anions and electrons, a few features have to be added, as the MCP's themselves are just secondary electron multipliers. For application as fast and sensitive a detector, a grounded copper grid is mounted in front of the first plate. This keeps the flight path free from electric fields. Also a contacted anode is mounted behind the rear side of the second MCP, in order to collect the electron avalanches and deliver the signal to the digital oscilloscope.
As can be seen in figure 2.15, the channels are slightly tilted (about 15° against the ion flight path). Due to this, the entering particle hits the wall in the front part of a channel and kicks out one or two electrons. Because of the applied voltage across the length of the channel, they were accelerated, hit the wall again and create more free electrons. This process repeats many times, so that an electron avalanche moves through the channel. Typically two MCP plates in series are needed to amplify the signal of one ion or electron to 10 mV at 50 Ohm.
By the applied voltage at the front side of the first MCP (U_1 position in Figure x), it is possible to use this set-up for cation (U_1 negative) as well as anion/electron (U_1 positive) detection.

This ion detection by MCPs is applied for the short TOF-MS (positive/negative-mode), for the long TOF-MS (neg. mode only) and the photoelectron spectrometer (negative mode only). The signal is displayed and digitized by a digital oscilloscope and recorded via a pc interface.

---

[8] charge coupled device

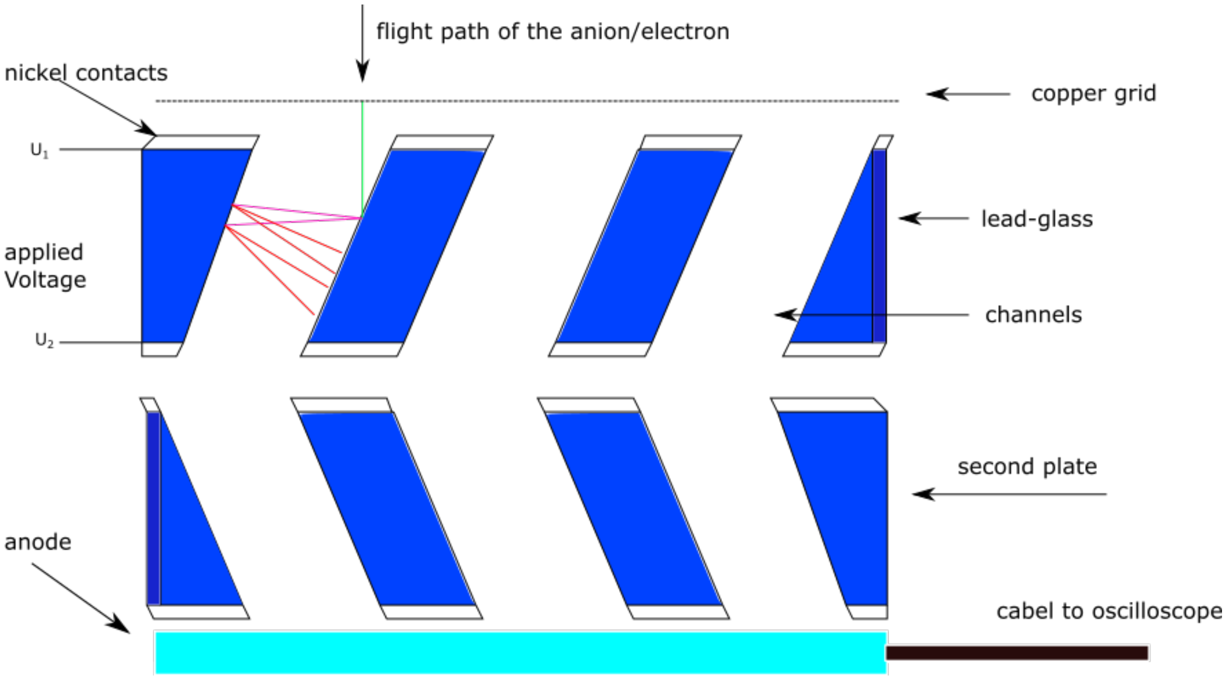

Figure 2.15: Illustration of the dissection of a MCP. The nickel surface coverage reassure a good contact for the applied voltage. The copper grid in front of the MCP keeps the flight path free of electric fields. The entering charged particles are accelerated between the grid and the front side of the first MCP. The ions are converted to a electrons if they hit the inner wall of a channel. In the channel the primary electrons are accelerated and can when colliding with the wall create secondary(violet) and these tertiary electrons(red) and so forth. The electrons of the first MCP are typically post-amplified in a second MCP. The electron signal is collected at an anode which is connected to the signal cable. Sketch based on [Ber17].

Calibration of the Mass Spectra

In mass spectra (especially PES), the confident assignment of peaks to their masses is of utmost importance. For PD-PES, it is crucial to be certain about the anionic species which will be detached. To calibrate a mass spectrum, a well-known sample which does not show complications should be used. Wanting to get one step further and exclude any potential error it is possible to choose a sample molecular anion which is well-characterized by PD-PES in terms of the energetics of the neutral excited states. Thus, the reproduction of the well-known PE-spectrum of the species (here for example pyrene, PES) provides the ultimate certainty that the TOF peak picked for the detachment is the parent anion, which was assigned before by mass spectrometry. If masses and flight time are known for several masses, one can calculate the calibration parameters with equation 2.20. If the mass calibration is complete, one can assign also the unknown masses in the time-of-flight spectrum. Due to its already known PES spectra, the pyrene anion (202.26 Da) to calibrate the

TOF-MS was used. The flight time of the pyrene mass peak at a flight time of 76.3 μs was correlated to its mass 202.16 Da by applying equation 2.20. The result led to the equation:

$$t_{TOF} = \sqrt{\frac{1}{2} \cdot \frac{\frac{m_{sample}}{N_a} \cdot l_{TOF}^2}{e \cdot (U_{applied} + k)}} \cdot 10^6 \tag{2.21}$$

t_{TOF}: flight-time $[\mu s]$
m_{sample}: mass of the sample$[\frac{kg}{mol}]$
N_a: Avaogadro's constant $[a.u.]$
l_{TOF}: length flight path $[m]$
e: elementary charge $[C]$
$U_{applied}$: voltage ion source $[V]$
k: voltage correction $[V]$

The reproducibility of this empirical equation derived from equation 2.20 was consistent with almost all samples, with an estimated error of about 2 %. To fit the mass values to the time-of-flight mass spectra, a correction voltage had to be added to the applied voltage ($k = 100\ V$). The reason is, that because of the many ion lenses and deflection plates the ions arrive earlier as if the drift length would be field-free. This means that in reality equation 2.20 is just an approximation, which needs some correction.

2.3.1 The Laser Photodetachment Spectroscopy

For the presentation of this sub-chapter in this work, it is necessary to emphasize, that already several thesis have been submitted, in which the anion photodetachment spectroscopy had been described thoroughly before [SWNS98][Sie11][Vog12][Ste15][Pau17]. As this work does not contribute fundamental new approaches regarding the theory of laser-photodetachment, the explanations are kept brief.

In general, the photodetachment spectroscopy of anions is a direct and systematic way to investigate unknown EA's as well as transitions to so-called forbidden states of the neutral molecule such as the triplet states, T_1 and sometimes also T_2. Since the energetic positions of the S_1 state are usually already known, they can be used as a further validation of the PD-PES-method.

The basic effect of the photodetachment is the outer photo-effect [Ein05]: a bound electron is ejected as a result of the absorption of a photon (laser-radiation). Due to energy conservation, the energy of the ejected electron is intimately correlated to the photon energy and the energy of the final state of the neutral molecule:

$$E_{neutral} = E_{anion} - E_{electron} + h\nu \qquad (2.22)$$

$E_{neutral}$: energy of neutral species$[eV]$
E_{anion}: energy of anion species$[eV]$
$E_{electron}$: electron energy $[eV]$
h: Planck´s constant $[\frac{eV}{s}]$
ν: frequency of the photon$[\frac{1}{s}]$

Therefore, if the energy of the electron is measured, the energy of the final neutral state of the detachment process can be found. The energy of the electron is determined by measuring the flight time from the detachment site to the electron detector (distance of 62 cm). There are other possibilities to measure electron energy such as slow electron velocity imaging [HKW$^+$12] or a scanning technique using the deflection in-between two half-bowls. The advantage of a TOF measurement is, that the full electron energy range is covered for each laser shot. Hence, fluctuations in the anion formation do not influence the relative intensities of the peaks in the PE spectra. The disadvantage of a TOF measurement is the low transmission: Because the electrons are statistically ejected in all directions, only a small fraction of the electrons hits occidentally the detector. The transmission is only about 10^{-2}, which means that the data acquisition for one spectrum need some hours. The resolution of the spectral PE-features theoretically only depends on the accuracy of the flight time measurement (about 2.3 ns) and the absolute flight time, which means the energy of the electrons. The energy resolution is best for low-energetic electrons. In reality, however, also surface charges of the tube wall, repulsion effects of the electrons by the anions and other imperfections of the field-free drift tube play additional roles. As a result, one has to work at low anion numbers and the spectrometer has to be heated from time to time to over 130 °C in order to remove the non-volatile molecules, which are absorbed and accumulated on the inner surface of the flight tube.

If all aspects are well considered, the starting point from the radical anion provides the possibility to circumvent or bypass most of the classical optical selection rules, speaking of:

- Transitions to triplet states (spin selection rule).
- To dipole-forbidden states and
- To some symmetry-forbidden singlet states.

Nevertheless, not all electronic states of the neutral molecules can be addressed, since a photon can only excite and address one electron [Ein05]. That means if one starts in the anion with the electron in the LUMO and two electrons would have to be moved in order to form an excited state of the neutral molecule, than this state is not observed in the PE spectrum. Further effects like a lack of overlap of the electronic wave-functions can also lead to a non-appearance or a very weak intensity in the obtained PE spectra. The latter for example would hold for a n to π^* excitation.

This said, the major difference between anion PD-PES and conventional methods, is the starting point from the doublet D_0 state of the anion ground state instead of the usual singlet S_0-state of the neutral molecule.

$$m_s = 2S + 1 \tag{2.23}$$

m_s: spin multiplicity [a.u.]
S: total spin[a.u.]

Recalling that in the neutral molecule an optical transition has to follow the electron spin selection rule $\Delta S = 0$. Starting in the neutral ground state of the molecule, with a total spin of $S = 0$, the only accessible states have again spin $S = 0$, such as for example the S_1.

Because the ground state or the radical anion is a doublet state, with a total spin of $S = \frac{1}{2}$, if o an electron by photodetachment is removed in the molecule a spin change $+\frac{1}{2}$ or $-\frac{1}{2}$ is caused. This means that neutral states with a total spin of zero or one can be addressed. This results in the fact, that from the anion in general triplet states and singlet states of the neutral molecule can be addressed equally.

Because electronic excitations are very fast, the photo-excitation processes takes place at such a fast time scale, that during the excitation the molecular atoms do not move. Due to this, the excitation problem can be separated with the help of the Born-Oppenheimer-approximation into an electronic transition moment and an overlap of vibrational wave-functions:

$$\mu_{transiton} = \mu_{electron} + \mu_{core} = -e\sum_i x_i + e\sum_j z_j x_j \tag{2.24}$$

$\mu_{transiton}$:	transition dipole moment $[Cm]$
$\mu_{electron}$:	electron dipole moment $[Cm]$
μ_{core}:	core dipole moment $[Cm]$
e	elemental charge $[C]$
x_i:	electron position $[m]$
z_j:	number of core charges [a.u.]
x_j:	core position$[m]$

The dipole transition moment describes the strength of a photo-excitation. It consists of the integral over the product of the total wave-function of the excited state (ψ_2) multiplied by the transition dipole operator and the total wave-function of the lower state (ψ_1):

$$P_{transition} =< \psi_1|\mu|\psi_2 >= -e\sum_i \int_\tau \psi_1 \cdot \mu \cdot \psi_2 d\tau \tag{2.25}$$

μ:	transition dipole moment $[Cm]$
$P_{transition}$:	transition probability [a.u]
ψ_1:	wave function state 1 [a.u.]
ψ_2:	wave function state 2 [a.u]
e	elemental charge $[C]$
τ:	integration volume $[m^3]$

Starting from equation 2.25, one can use the Franck-Condon principle to split the integral into products by separating the two total wave functions in a vibrational and electronic part with $\psi = \psi_{electronic} \cdot \psi_{vibrationally}$

$$P_{transition} =< \psi_{1,\nu}|\psi_{2,\nu} > \cdot < \psi_{1,e}|\mu_e|\psi_{2,e} > \tag{2.26}$$

The first factor (squared) is the so termed Franck-Condon-factor[FD26][Con26], describing the vibrational overlap of the wave functions and the second factor describes the oscillator strength of the electronic transition. The FC-factor determines how many vibrational states can excited with which intensities $I \propto FC^2$).

If in the detachment process the excitation of the removed electron goes to the detachment

continuum, then the intensities in the electronic anion-to-neutral transitions would allow to directly derive what kind of a geometry-change happens between the two involved electronic states.
It turns, however, out, that in some cases the detachment laser does not directly excite to the continuum but to an anion excited state. Typically high-lying anion excited states are very short-lived and therefore better termed anion excited resonance. Since such an anion excited state may have a different binding situation as the anion ground state, the FC-factor to the neutral state is then manipulated by this intermediate anion excited state. This effect is usually causing the excitation of many vibrations, which unfortunately often make the spectra ambiguous.

The Typical Situation of the Neutral Excited States

After this introduction, it is necessary to explain the typical electronic state situation in a neutral molecule. Figure 2.16 displays a typical Jablonski scheme for a "normal" molecule. It should be noted that also the anion ground state is added as well as the photo-detachment of an electron. Traditional spectroscopy methods such as laser excitation of neutral molecules start in the S_0-state. Violet arrow: The neutral molecule is excited for example into a vibrational state of the S_2. After this excitation, the molecule can undergo internal conversion to the S_1 state. From The S_1 state either fluorescence can be emitted, or the molecule undergoes an inter-system crossing to the T_1 state. In some molecules from the T_1 a long-lasting weak phosphorescence is observed. Sometimes both types of radiations - phosphorescence and fluorescence - can be detected after excitation. Nevertheless not all molecules shows a fluorescence or phosphorescence, but instead very fast deactivate the excited state to heat. The molecule in the S_1 state can deactivate by efficient IC. In general the emissions of triplet T_1 state are challenging to detect because often in parallel to phosphorescence the molecule deactivates the T_1 state by a reverse ISC to the ground state.

If the PD-PES method is applied, the starting state is the anion ground state, a doublet D_0-state. If an electron is detached into the continuum, the final state depends from the MO from which the electron is removed. The MO where the electron hole is formed determines which neutral state with the corresponding MO configuration is formed.
Usually, in the anion the surplus electron resides in the LUMO orbital. If then the LUMO electron is removed the neutral ground state is formed. If an electron from the HOMO is removed it depends whether the electron has the same spin as the electron in the LOMO or the opposite spin. In the first case a triplet state, presumably T_1 is formed and in the

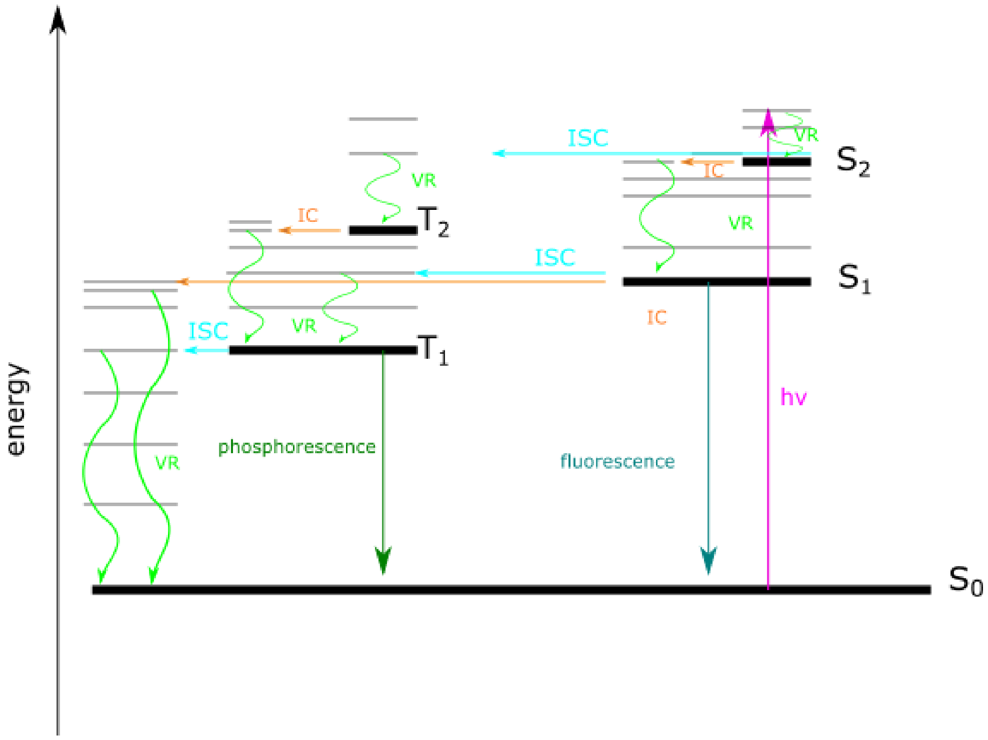

Figure 2.16: Illustration of the typical situation in solvent. Illustrated are all radiating and non radiating processes as well as an overview of the detachment channels. The violet arrow represents an higher-state excitation and the subsequent processes as fluorescence phosphorescence and non-radiative processes like internal conversion (IC,orange), inter-system-crossing (ISC,cyan) and vibrational relaxation (VR, light green). Sketch loosely based on[Jab33][SWNS98][Pau17].

latter case a singlet state, presumably the S_1 state is formed. Some neutral molecules have a S_1 state electron configuration which does not correspond to a hole in the HOMO and an electron with anti-parallel spin in the LUMO. Such electronic states might be more difficult to be addressed by PD. Just the removal of a single electron might be not sufficient to reach some neutral excited electronic states. If so, this neutral state cannot be observed at all in the PD-PE-Spectra or only with this MO contribution of the state which is accessible from the anion.

Therefore there are still molecules which can not be perfectly analysed by PD-PES.

These considerations are all focussed on the direct PD-process: The photo-excitation into the continuum. But also indirect photo-detachment is possible via a anion excited state (also termed auto-detachment-states). The probability of addressing one of these state seems to be higher, the bigger and complexer the molecule is, as can be seen in the spectra of this work, where often anion excited states change the expected anion-to-neutral Franck-Condon-factors (compare chapter 4). Due to this, it is necessary to describe the origin of theses states in the next chapter.

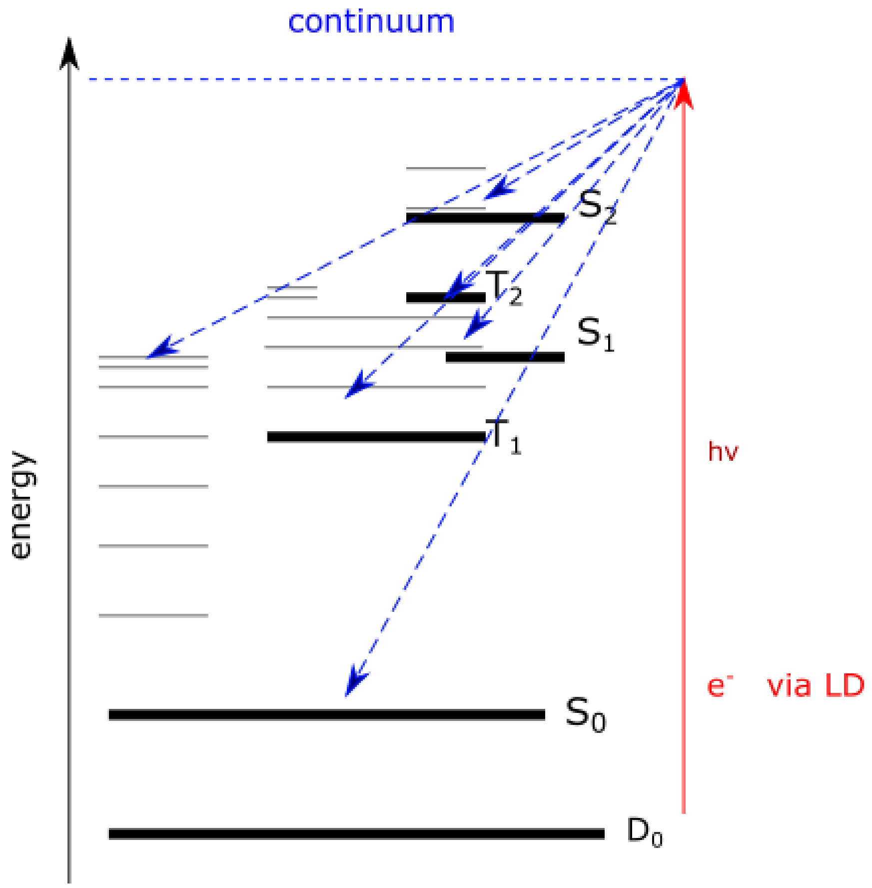

Figure 2.17: Illustration of the typical detachment channels reachable by PD of the anion. Even triplet states can be reached. The red arrow shows the detachment process starting from the doublet anion ground state. The blue arrows shows exemplarily the reachable states, sketch loosely based on[Jab33][SWNS98][Pau17].

Other values also can influence the PD-process, like the effective cross section of a molecule, as well as the polarisation of the radiation of the detaching laser (compare the dipole bound state of 5Fi in chapter 4). The cross section of a molecule is strongly energy-dependent and depends on the angular momentum of the emitted electron, but also on the excess-energy of the respective process. The latter is known as Wigner's threshold law[Wig48]. Wigner described generally the cross-sections for detachment and ionisation processes. Since between the neutral molecule and the electron no coulomb attraction exists, the process is highly dependant on the angular momentum and the energy of the emitted electron

$$\sigma \sim (\Delta E)^{l+\frac{1}{2}} \tag{2.27}$$

σ: cross-section $[fm^2]$
ΔE: energy difference threshold/photon $[eV]$
l: angular momentum quantum number [a.u.]

The type of detachment can be termed s- or p-detachment, depending on the angular quantum number of the leaving electron. At an excess energy which is not far above the threshold, the s-detachment is the more efficient, as the p-wave detachment. As can be seen in the chapter "Results and Discussion", which detachment type provides the better results cannot be answered easily. There are two reasons for this: i) the certainty whether the polarisation direction is maintained by the quartz windows (note that there might be locally birefringent crystals in them, they are pressed against the sealing and heated) and ii) auto-detachment states can be involved. In this case the Wigner threshold laws are not applicable, since they are only valid for transitions to the continuum.

The Influence of Anion Excited States on the PD-PE-spectra

As noted before apart from the direct detachment into the continuum, resonant excitation and detachment via short-lived anion-excited states can happen. This means, that a photon of the detachment laser at a fixed wavelength accidentally excites an electron of the anion to an excited electronic state of still the anion which now lies above the energy of the neutral ground state. From this state the electron then can detach (this process is termed auto-detachment) and release the molecule in a neutral state. Not being involved in anion photodetachment spectroscopy could lead to the assumption that such a case appears rarely. This is, however, not the case as can be seen in Chapter 4.
There are two reasons for this:

- Most of the anion excited states are broad due to their short lifetime.
- The number of anion-excited states increases with the density of molecular orbitals, which is a critical point for the molecules with extended π-systems investigated in this work.
- There are several types of anion excited states.

Excited states of anions above the detachment threshold can be formed by different effects:

- i) Dipole or quadrupole-bound states, which lie close below the neutral state to which they belong.
- ii) Shape resonances where the electron is excited into an electronic orbital above the detachment threshold,
- Feshbach resonances, where the molecular anion has enough internal energy to make an electron leave, but the energy is distributed over two electrons, and

- the electron is excited to a relatively long-lived anion-excited state which converts the electronic energy to vibrations and then cooks-off the electron.

Each of the above cases needs some explanation. The nature of dipole and quadrupole-bound states is explained below in a separate chapter. Similar to Rydberg states, the electron is physically bound mostly outside of the molecule. Theoretically a whole set of dipole-bound state would exist for each electronic state of the neutral molecule and its vibrational states.

The "shape-resonance" got well-documented in detachment processes of Ca^- anionic atoms quite thoroughly by Walter et al [WP92] and for ionisation of neutrals also by Zobel et al, by investigating Rydberg-states of CO[ZMJ$^+$96]. Shape resonances have been also observed in larger molecular anions, such as for example in benzoquinone[SW99].
A shape resonance is due to an excitation to a higher unoccupied molecular orbital (LUMO + n). Since the orbital is, however, not able to stabilize the electron these states are extremely short-lived and appear as broad features in photodetachment-spectra, where the laser wavelength is scanned and the number of detached electrons is recorded. By its presence in case of a resonant excitation it just causes a higher transition moment than the excitation to the continuum. So only for a miniscule amount of time, the electron is in the excited orbital, which is energetically higher than the detachment threshold and it then leaves the molecule. The residence time in the orbital is supposed to be so short, that the excited anion cannot undergo vibrations. Nevertheless the anion "experiences" for this very short time the properties of the anion-excited state (which is presumably less bound than the anion ground state). As a result the anion-excited state still can manipulate the Franck-Condon-factors between the anion ground state and the neutral states, occasionally causing broad vibrational features in the PD-PES spectra.

The other above-mentioned anion-excited state is termed "Feshbach-resonance" mentioned first by Herman Feshbach in his work [Fes58] and is still subject in today's research [YCW$^+$20]. The background of these resonances is more complex than that of the shape-resonances. In Feshbach states above the detachment threshold, the electronic energy is so distributed on two or more electrons that neither of them has the energy to leave. For example if in the ground state of the anion the surplus electron is in the LUMO orbital and a second electron is excited from the HOMO-2 to the LUMO orbital. So two paired electrons are in the LUMO but there is a hole in HOMO-2. In total, the energy of this anionic state is above the detachment threshold, but neither of the electrons in LUMO can leave. Only if one electron of the two LUMO-electrons or another electron of a higher occupied MO fills the hole in HOMO-2 and transfers the energy to one of the electrons in the LUMO, this electron can leave. In Röntgen-innershell excitations and photoelectron spectroscopy one would term this detachment process a shake-up process. Because in molecular anions the energetics and the size of the molecule is different in comparison to an atom, this two-electron process is assumed to take some time, in agreement with longer lifetimes. In benzoquinone Feshbach states with lifetimes of some *ps* have been found[SW99]. This is long enough for an electronic state to exhibit vibrational states. If such a state is accidentally excited by the detachment laser it completely determines the Franck-Condon-factor to the neutral molecule.

Unfortunately the variety of such Feshbach resonances is so high and complex, that their energetic positions cannot be predicted. One can solely state, that as denser the MO-ladder in a molecule is as more Feshbach resonances should exist.

Usually all anion-excited states are short-lived and would appear as more or less broad excitation resonances in photodetachment spectra. Since the geometry of the anion excited states is different in comparison to the anion ground state, the anion-excited states are indirectly observed in PD-PE-spectra as unexpected vibrational structures. For large molecules with large π systems one has usually the expectation that Franck-Condon-factors between the anion ground state and the neutral electronic states are mostly diagonal.

If a strong vibrational activity is observed in the PD-PE-spectra it can be assumed that an anion excited state contributes to the excitation. Even more, the accidental excitation of one of these anion-excited states, can extremely complicate the interpretation of PD-PES spectra as the relative positions of the vibrational states caused by the auto-detachment can interfere with the peaks of other electronic state origins. The only possibility to circumvent addressing of these states, is to shift the detachment-laser wavelength, best done with a dye-laser. Due to the already very complex set-up the use of a dye-laser was avoided, by simply changing to another wavelength of the fundamental or a higher harmonics of the Nd:YAG laser.

Figure 2.18 shows a PD-PE-spectrum, where an excited auto-detachment state manipulates the Franc-Condon-factors.

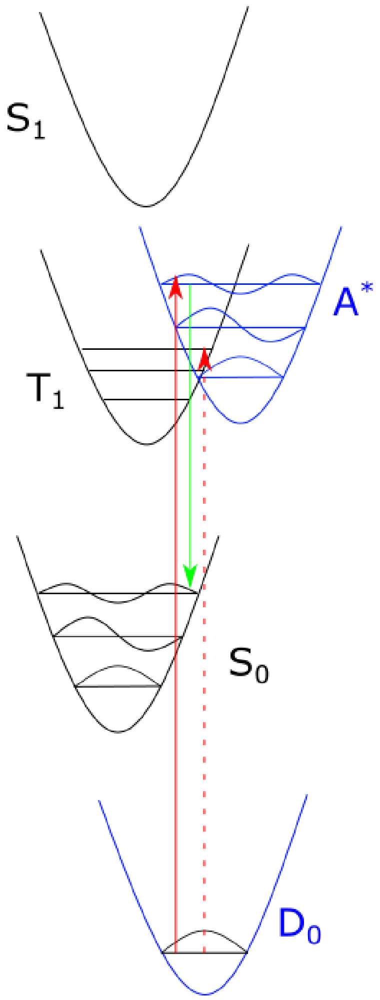

Figure 2.18: Illustration of the effect of the accidentally excited anion excited states on the PD PE spectra. Note that direkt PD and the indirect PD typically happen both in an ensemble of anions. The observed PE spectrum is then a superposition of the two processes. For further explanation see text.

Dipole-Bound States

The dipole- and quadrupole-bound states still need further consideration, since dipole-bound anions have been also investigated in this work. It was theoretically predicted that molecules with a dipole moment of more than 2 Debye should have dipole-bond states [ACBD$^+$97] or $\mu > 2.5\ D$ [LCG$^+$20]. In these states the surplus electron always resides on the positive side of the molecule and is mostly outside of the molecule in a very large diffuse orbital. Therefore, molecular rotation and the binding conditions by the positive charge are correlated, leading to a finite number of dipole bound states, typically just one for each neutral state.

A closer look to the concept of dipoles and multi-poles shows, however, that the approximation to describe an inhomogeneous charge distribution in a molecule by a dipole

or a quadrupole is an approximation, which is only valid with a high accuracy at large distances from the molecule. Strictly seen, this is not the case for the electrons bound in such states. Nevertheless the nomenclature dipole-bound and quadrupole-bound provide a good description of the physical binding effects in these states. Dipole-bound states have been found by many groups[LML84],[CLG+18],[YZQ+21]. To the authors knowledge quadrupole-bound states have been only found up to now by Bowen and coworkers [LCG+20]. In this work the dipole-bound 5-Fluoroindole anions was accidentally investigated and its water clusters, as well as dipole-bound 6-Fluoroindole anions. In general, molecules with hetero-atoms integrated in their π-systems or molecules with electron-withdrawing substitutions, often have a very pronounced charge separation in their electron-density. When this occurs, a dipole-moment (or a higher multipole moment) can be assumed as an approximative description. This can be even extended to water-clusters, which can have relative large dipole moments due to a suitable collective arrangement of all dipole moments of the individual water molecules [Hab94].
As stated already above, in dipole-bound states the excess electron is trapped on the positive site of the dipole-field (see the work of Lykke, Lineberger et al. [LML84]). In this state the surplus electron is also only very weakly bound and resides in a large diffuse cloud mostly outside of the molecule. Because the MO´s do not contribute to the binding of the surplus electron, these states are characterized as physical-bound states, in contrast to valence bound states, where the surplus electron resides in a MO of the molecule.
Thus, it is probable to find DB-states in molecules or molecular complexes with a high dipole moment. The size of the dipole moment of a complex than interestingly also depends on the structure of the complex. Structural research in molecular clusters with dipole-bound electrons has been performed in the group of Kit Bowen by a combination of Rydberg electron transfer and PES.
In the PD-process of DB-states the direction of the electron emission is found to strongly depend on the polarisation of the laser radiation (see chapter 4.1). This polarisation behaviour can be even used as a proof for the DB-character of an anionic state. DB-states typically have very small binding energies in a range from several meV up to a few hundred meV.

To form those dipole-bound anions, electrons of very low kinetic energy are needed. In this work, by chance, it was possible to form DB-states in 5-Fluoroindole and its water-clusters as well as in 6-Flouroindole. Even though this works major aim is to investigate the triplet states of neutral molecules, the dipole bound states of those two molecules revealed that the new discharge method for anion formation, is capable of producing electrons with such a small kinetic energy that they are able to form DB-states. This is surprising, as discharges are considered to be a very harsh electron formation method. This finding supports the conclusion drawn in chapter 2.1 that the very fast switching-off of the discharge may be the crucial point in order to achieve soft conditions for the electron attachment.

3 The experimental set-up

The experiment "photo-detachment photo-electron spectroscopy on radical anions" is a prototype spectrometer, which has been set-up in a first version in the year 2000 and has been constantly changed and optimized during the last twenty years. Except turbo pumps, pre-pumps, high-voltage power supplies, digital oscilloscopes, the basic laser components and the personal computers most of the other components are home-built or consist of commercial products, which have been modified by Ph. D students or the chemistry machine shop. As a result, the handling of the experiment is quite delicate and time-consuming. The set-up is very complex in many ways. It has especially many knobs to turn and many switches to set. Its handling needs la long time experience, many technical skills and a perfect reproducibility of user during the switching-on and switching-off processes: A single user error can cause severe damage or even destroy the complete experiment.

The key component of the experiment is clearly the anion source:

- If the anion source does not always work reliably, it may happen that during the up-heating of the nozzle the temperature window for the sublimation of the sample molecule is missed and the temperature is increased too much. As a consequence the sample would be destroyed by thermal decomposition.

- If the number of anions at the photo-detachment site is too small, the photo-electron spectra will be very noisy and it will be difficult to find and assign the electronic transitions. This holds especially for higher excited states, which lie in an energy range where the density of electronic and vibrational states is high and the intensities due to Wigner´s law are low (see chapter 2).

- If the anion signal is not stable enough, it is very difficult to adjust the detachment laser in time and space: In case of a stable anion signal, the right adjustment of the detachment laser can be observed as a small decrease of the anion signal. Such a control is impossible, if the fluctuation of the anion mass signal is too high.

- If the anions are not cold, the spectra contain numerous hot-band transitions, which unfortunately lie mostly on the blue side of the origin transition and are not distinguishable from cold bands. They can form a broad background-like structure on which it may be difficult to identify weak electronic transitions, such as for example the T_2 state. Unfortunately, however, one would like to know whether the T_2 state lies below or above the S_1 state, because this might be highly relevant for the understanding of the S_1 dynamics.

First in the following section the previous set-up is described and in a second section the changes made in this work are outlined.

3.1 The experimental set-up at the beginning of this work

The experimental set-up of the anion photo-detachment photoelectron spectrometer was developed in evolutionary steps over more than 20 years. Each Ph.D. student improved specifics details of the experiment, such as for example the resolution of the mass spectrometer, or of the resolution of the photo-electron spectrometer. Minor improvements of local components have been performed by several bachelor- and master-students, supervised by a Ph.D. student.

Most of the previous improvements have been already described thoroughly in the dissertations of Paul Konieczny[Pau17] and Stefan Vosskötter[Ste15]. The major changes and improvements performed in the course of this work concentrate on the inlet vacuum chamber, where the formation and cooling of the radical anions takes place. It is natural therefore, that the following chapters mainly deal with the improvements, which have been implemented in this work.

3.2 Overview

In Figure 3.1 the complete experiment is displayed in an overview sketch. The machine is subdivided into four vacuum chambers in order to be able to improve stepwise the vacuum pressure from the inlet chamber 1 to the photo-electron spectrometer in chamber 4. This is necessary, because the back-pressure in the nozzle is 20 *bar* and due to this many atoms and molecules enter chamber one during a single pulse of the gas valve.

The first vacuum chamber one contains the pulsed and heated gas valve, the discharge electrodes and the skimmer. Here the formations of molecular radical anions takes place. After the formation of the molecular anions, they are cooled by the argon-molecule co-expansion and transported through the skimmer (orifice diameter about 4 mm) into chamber two. By collisions the anion velocity is adapted to the supersonic velocity of the argon expansion (about 500 $\frac{m}{s}$). In chamber two the ions enter the two-stage ion source perpendicular to the flight path of the mass spectrometer. In order to have maximal transmission a Wiley-McLaren time-of-flight TOF mass spectrometer with some modifications is used. In Figure 3.1 this TOF-MS is drawn to the right side and passes chamber three and four, where the anion-MCP detector is mounted. The voltages applied at the plates of the ion source can be exchanged by a switch in such a manner, that the anions fly to the left into a short TOF-MS with very high transmission. This means that, when entering the ion source, the anions can be either accelerated into the direction of the photo-electron spectrometer (chamber 4) or in the opposite direction to the short flight path by just switching the polarity of the ion source. The high-transmission TOF with its MCP-mass-detector on the left hand side can be used to easily monitor the anion formation process: this is important because the two quadrupoles adjustment units and the manifold lenses are difficult to adjust and also reduce considerably the transmission. Alternatively the short TOF can be also used to detect the argon and the sample cations which are also formed in the discharge. For this it is possible to switch the polarity of the MCP-detector accordingly.

The application of the cation detection mode needs some explanation, since the major interest lies in anions: for some molecules it is unknown, whether the EA is positive or negative. Unfortunately for uncounted large conjugated molecules it is also unknown at which temperature their vapour pressure will be sufficiently enough for a measurement. Since the formation of radical cations is always possible, the observation of the radical cations of the sample molecules indicates, that there are in general enough molecules in the gas phase for a measurement. If then under the same experimental conditions no anions are observed, it seems plausible to assume that with a high probability this molecule does not have a positive EA. The details of the operating principle of the high-transmission TOF is described in detail in a master thesis [Ber17].

3.2.1 Chamber 1

As can be seen in 3.1, Chamber 1 hosts the inlet and anion formation set-up. It consists of a stainless steel tube for the supply of the argon gas which allows to maintain a steady argon gas pressure of $5-20$ bar inside the valve. The pulsed and heatable gas valve opens with an electro-magnet which is steered by an electric pulse of $+70$ V, several amperes

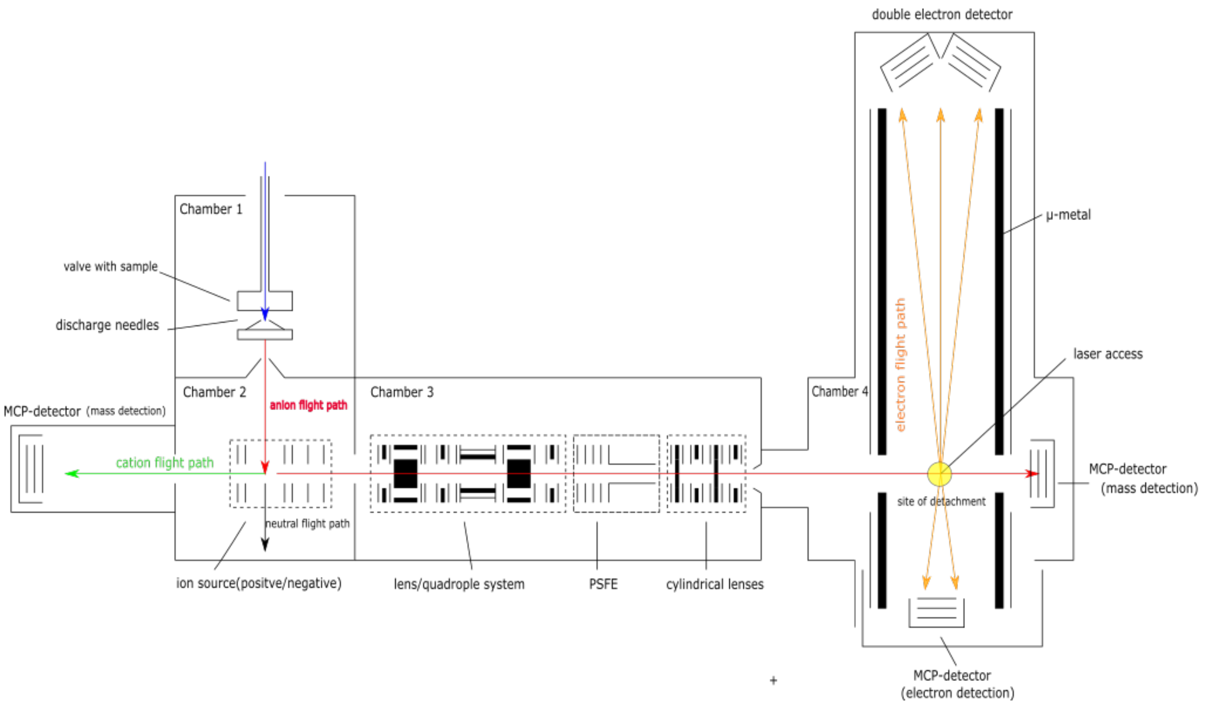

Figure 3.1: Schematic Illustration of the PD-PES set-up. Chamber 1 contains the pulsed valve and the pulsed discharge electrodes. The ions (red arrows) enter the ion source in chamber 2. By exchanging the pulsed voltages at the plates of the ion source, two possible flight paths can be chosen: Either along the short or along the long flight path through the photo-electron spectrometer. Chamber 3 contains two quadrupole steering systems and many rotation-symmetric and some slit lenses. The goal of the beam shaping is the only these anions enter chamber 4 which can be hit by the laser beam (yellow dot, the laser comes from above the plain). The laser-photo-detachment, the electron and the mass detection takes place in Chamber 4. For further explanations see text

and a pulse width os $15 - 25\ \mu s$. The nozzle can be heated to more than 300 °C in order to achieve sufficient temperatures for sample sublimation within the valve. The nozzle is enclosed by a brass block which can be cooled by water flow from the outside. This is necessary because the magnetic material of the nozzle is heated by the attached heated nozzle head (wherein the sample resides) and the electric energy which drives the opening motion of the valve. In order to keep the susceptibility of the coil core constant, cooling to about 60 °C is necessary. The pulsed discharge needles are directly mounted to the pulsed valve in a tip-nozzle-head-distance of approximately 2.7 mm. Right below the valve in a distance of approximately 1.5 cm is a heated skimmer with an orifice of 4 mm. On one hand the skimmer acts as a differential pressure reduction stage between the first two chambers, on the other hand it selects the mid area of the beam, where the coolest ions are and deflects all other particles to the walls. In operation of the valve with a repetition

rate of 10 Hz, the average pressure inside the first vacuum chamber is approximately $2-4\cdot10^{-5}$ $mbar$. This, however, means that for the short time of the opening of the valve the pressure goes strongly up, possibly to 10^{-2} $mbar$ or even higher. Two close-mounted turbo pumps with a pumping speed of 500 litre per second each ensure that the pressure will be again in the range of 10^{-5} $mbar$, so that a collision-free condition exists, when the next gas pulse follows.
The processes taking place in chamber 1 are :

- Heating of the nozzle head to achieve a sufficient vapour pressure of the sample by sublimation.
- Opening of the valve for a determined period of time (≈ 200 μs)
- Switching-on the high-voltage pulse of the discharge at a suitable time ($100-200$ μs) after the opening of the valve. The pulse width of the HV-pulse is $200-300$ ns)
- Ignition of the discharge into the argon jet
- Formation of cations and anion by the electron avalanche in the argon jet
- Transition of the middle part of the co-expansion through the skimmer into chamber two.

Figure 3.2 shows on the left hand side (a) a more detailed schematic set-up of the devices in chamber 1 and on the right hand side (b) a photo taken of the valve for comparison. As can be seen in (a), the valve set-up is mounted on a flange plate which is in two axis adjustable. This flange has several feed-throughs for the gas inlet, the water cooling, the HV pulse, the valve steering pulse, the nozzle heating and the PT 100 temperature sensor. The flange separates the valve set-up which reaches into the vacuum and the supply media on the outside which connect to the feed-throughs. Through two metal springs and screws it is possible to adjust a concentric relative position of the valve and the skimmer. This way, it is possible to guarantee a perfect alignment in order to only transmit exactly the middle area of the jet into chamber 2. Beside the argon gas inlet, the flange has a water in- and outlet which allows the water to circulate through the brass plate. The cooled brass plate tightly encloses the electromagnetic coil housing and by this also cools the coil via the water flow. Also every necessary cables are conducted through the cover plate, as needed for a pt 100 temperature sensor, the heating itself and the high-voltage pulse cable. Right under the hull of the coil is the head of valve with the sample and the orifice. The nozzle head cannot be seen in inset (b) because it is embedded in the heating ring (note the thick metal coated cable going to the right) The Pt 100 temperature sensor is directly mounted at the heating (note the thinner metal-coated cable, which goes to the left).

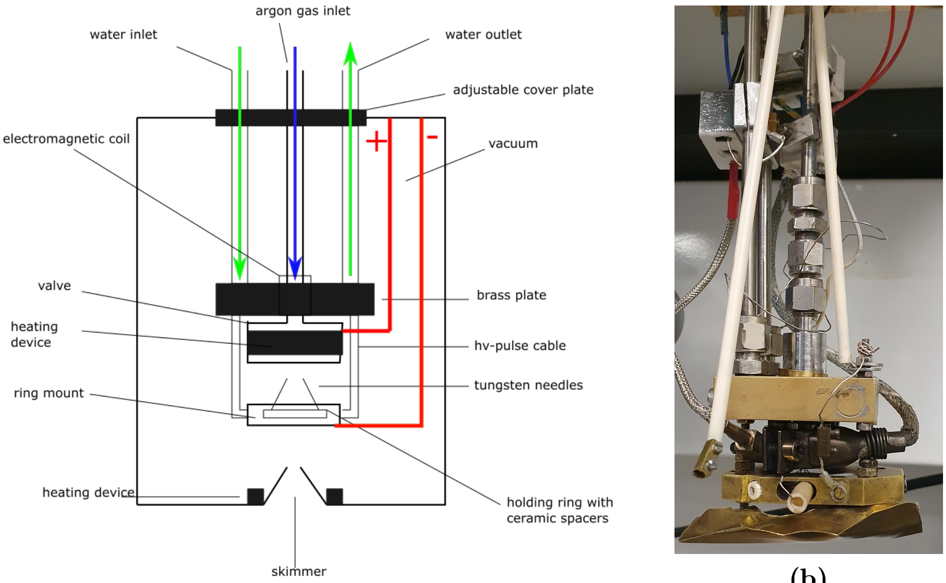

(a)

(b)

Figure 3.2: a) Schematic Illustration of the devices in chamber 1. The valve with its heating ring and the below mounted discharge ring is right above the heated skimmer. Details of the devices and the processes are described in the text. b) Photo of a part of the valve set-up shown in a)

The Reproducible Gas Valve

The gas valve is based on a valve of a former company named "General Valve" (type: Series 9). Several modifications were made and new parts were added. First a new valve head was constructed which has enough room to host the sample. A intermediate spacer part was added, which is mend to better thermally insulate the valve coil from the nozzle head. By this and the cooling of the coil the nozzle head and the sample was heated to above 340 °C. To be able to use this distance part, the new poppet had to be extended considerably.

The function of the nozzle is as following: Inside the valve, there is a magnetic plunger between two springs. The plunger is moved backwards into the coil if current flows though the coil and produces a strong centre-symmetric magnetic field. When moving backwards the plunger draws back the poppet, which then frees the orifice in the nozzle head. This part of the nozzle set-up is described further in detail in the work of Stefan Vosskötter [Ste15].

Since the discharge only can ignite if the gas pressure at the needles it suitable, it is urgently needed that the valve reproducibly opens for each gas pulse at exactly the same time. Since this was originally not the case and there was a considerable time jitter between the electric steering pulse and the valve opening, the valve had to be modified.
After a detailed analysis of the valve opening mechanism, in this work a small modification of the nozzle was made. A small brass screw with a cylindrical head was added above the upper spring, which is pushing down the poppet which closes the valve orifice. Since the poppet lies inside the plunger also the plunger is pushed downwards. The head of the screw was chosen to have the outer diameter of the spring. The thread part of the screw fits loosely inside the spring. If the screw is mounted, the head of the screw extends the spring. Since in the assembled valve the space for spring plus the screw head is about the same as it was before for the spring only, the prolonged spring is now stronger squeezed and the force on the poppet is somewhat higher. It should be noted that, however, it seems that it is not only the higher force on the poppet, which improves the performance of the modified nozzle. Obviously the "longer spring" causes the magnetic plunger to be moved somewhat more outside of the electro-magnet of the pulsed coil and this slightly new position seems to be more favourable for the reproducibility of the valve opening.
This very small change of the valve had a huge impact on the stability of the jitter of the delay which the valve shows between the electric steering pulse and the real gas pulse. It seems that this improvement was crucial for the success of the pulsed discharge in a pulsed argon expansion as a new anion source.

Right below the valve is the mounted discharge device in approximately 2.7 *mm* distance. Here the jet coming from the pulsed valve gets hit by the initial electrons out of the discharge and the ion formation takes place. The ions pass the skimmer to the next chamber. Due to the major changes in terms of ion formation, the discharge device will be further described in the next sub-chapter.
Moreover the pressure needs to be maintained in the given range, otherwise the discharge will not ignite properly (meaning a regular opening behaviour is also crucial). Furthermore the cooling by co expansion can solely be efficient if the velocity of the newly-formed ions is not further increased after after the ignition. A higher argon pressure results in many more collisions of the anions with argon atoms and can only resolt in a good vibrational cooling if the velocity differenced between the anions and the argon atoms is not too big and is quickly equilibrated.
The exactness of timing the trigger events of the pulsed valve and discharge is also of

utmost importance. If the time-sequence is out of certain time windows, the formation of ions is not efficient any more respectively not taking place at all. The key to the successful formation of ions is a small time jitter of the nozzle and the fast switching off of the high-voltage pulse right after the ignition of the discharge. If the width of the high voltage pulse is too long, the electric field of the discharge is able to accelerate the formed anions, leading to a less efficient cooling or a deflection of the ions of their destined flight path through the skimmer in the worst case .

The skimmer itself also needs to be heated, to keep the surface of it free of sample substance. Otherwise there could form monolayers of the sample substance which are insulating. An insulating surface can get charged up by the ions and then cause an electric field which could also perturb the flight path of the following ions. After this processes the cations, anions and neutral molecules in the centre part of the expansion proceed to next chamber.

3.2.2 Chamber 2

The anions, cations and neutral molecules enter chamber 2 at approximately sonic speed. The separation of the species and the acceleration of the anions into chamber 3 takes place within the ion source. Some modifications of the ion source made it possible to switch the polarity of lens 1 and 2. This is a desirable feature, because it is possible to direct any species to the short flight path with the micro channel plate detector. This short flight path is intended to act as a easy and effective way to control the proper formation of ions. The necessity of this flight path is based on the historical development of the discharge-method and the need to validate the proper function of the discharge as well as the possible other difficulties that occurred in the past resulting in a non appearance of any signal at the mcp detector in Chamber 4. Those can be:

- Maladjustments of the long flight path.
- Insufficient temperatures inside the valve.
- Absent formation of ions (due to negative electron affinities).
- Malfunctions of the formation system(discharge/or the former electron gun).

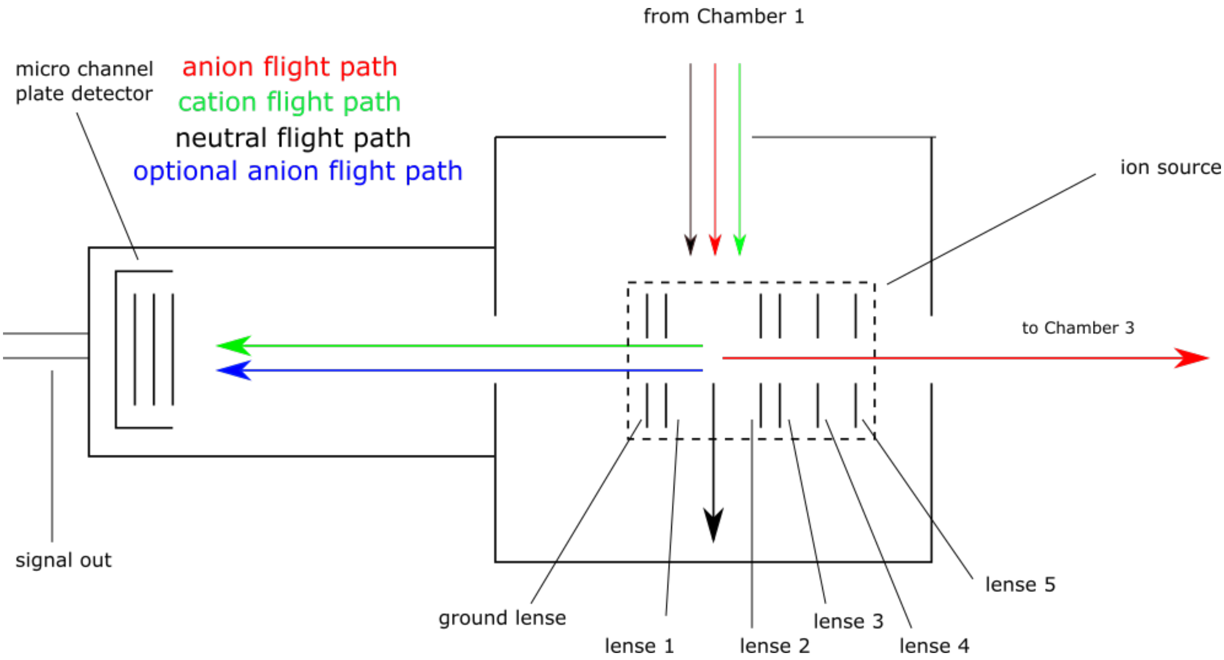

Figure 3.3: Schematic sketch of chamber 2. The cloud consisting of anions, cation an neutral molecules enters the ion source. With the bipolar ion source it is possible to direct cations or anions to the short flight path to verify a proper anion. Normally for PD-PES the anion acceleration takes places into the direction of chamber 3.

Those insecurities made it quite difficult to get a hold of the exact reason why a certain sample does not appear on the anion mass detector in chamber 4. So it is an easy way to direct the ions to the short flight path with the intention of observing solely the ion formation. With entering the ion source ($\approx 130\ \mu s$) after the ignition of the discharge) the cloud which is now exactly between the lenses 1 and 2, can be separated by applying a pulsed electric field between lens 1 and lens 2. If the polarity is negative, 100 percent of the voltage ($613\ V$) is applied to lens 1 and about 66 percent to lens 2 resulting in an acceleration of the anions towards chamber 3 (PES mode). Lenses 3 to 5 then act as a deflection lenses. To check the proper function of the formation of ions 2 modes are now possible. If it is desired to direct the anions to short flight path, on lens 2 100 percent of the voltage is applied and the 66 percent to lens 1, so the anions can be directed to short flight path. By switching polarity it is possible to detect cations properly on the short flight path. Of course it should be possible to detect the cations in the short flight path simultaneous while the anions transit to chamber 3, but was not possible due to geometrical deviations of the exact flight path (the left path lies vertically under the right one). In conclusion this short flight path offers a quite easy method of monitoring the ion formation to guarantee the anion-formation of a new sample molecule or respective the ruling out of a too small or negative electron affinity for example. It has to be pointed out, that it was necessary to attach a neodym-magnet on top of the feed-through of the left flight path to suppress a very prominent electron peak. This peak vanished by applying a magnetic field instantly and led to the conclusion it has to be free electrons trapped in the ion cloud. Without magnetic suppression the electron peak led to a saturation of the MCP detector.

3.2.3 Chamber 3

Chamber 3 hosts a system consisting of two quadrupoles and a system of lenses. Basically it is a modified version of a Wiley-McLaren TOF-MS. This system is described in detail by several former PhD-canditates as can be seen in [SWNS98], [Pau17] and [Ste15]. This part of the setup is necessary to separate all the formed anions to gain certainty of detaching only the desired species of anions. Due to the cleaning routine of the valve-system it is possible to form anion clusters consisting of ethanol or water and the sample molecule aside of the sample molecule itself. The mass spectra resolution can reach $\frac{m}{\delta m} \approx 190$, which allows to distinguish between clusters and the sample anion. Furthermore the lens system has the capability to compensate small deviations in the ion beam and correct its direction towards chamber 4. The post source focussing system [KMMJ91] is intended to further separate the desired molecule from all other occurring masses in a spectrum and is described in detail in [Ste15]. Its function is to isolate a given peak by post acceleration of the peak at the time the mass passes through it. That way it is possible to enhance the resolution and therefore the intensity of said peak as can be seen in [Pau17]. The cylindrical lenses right after the post source focussing system is intend to form the anion cloud. The desired form of the cloud would be a perfect cylinder orthogonal to the flight direction, so it would be in perfect overlap with the beam profile of the detachment laser. Thus the lenses can skim the ion beam in a horizontal direction and widen the ion beam in a vertical direction. The following horizontal slit is built in to force the ion beam mechanically into the said shape. After passing the slit the ion beam transits to chamber 4.

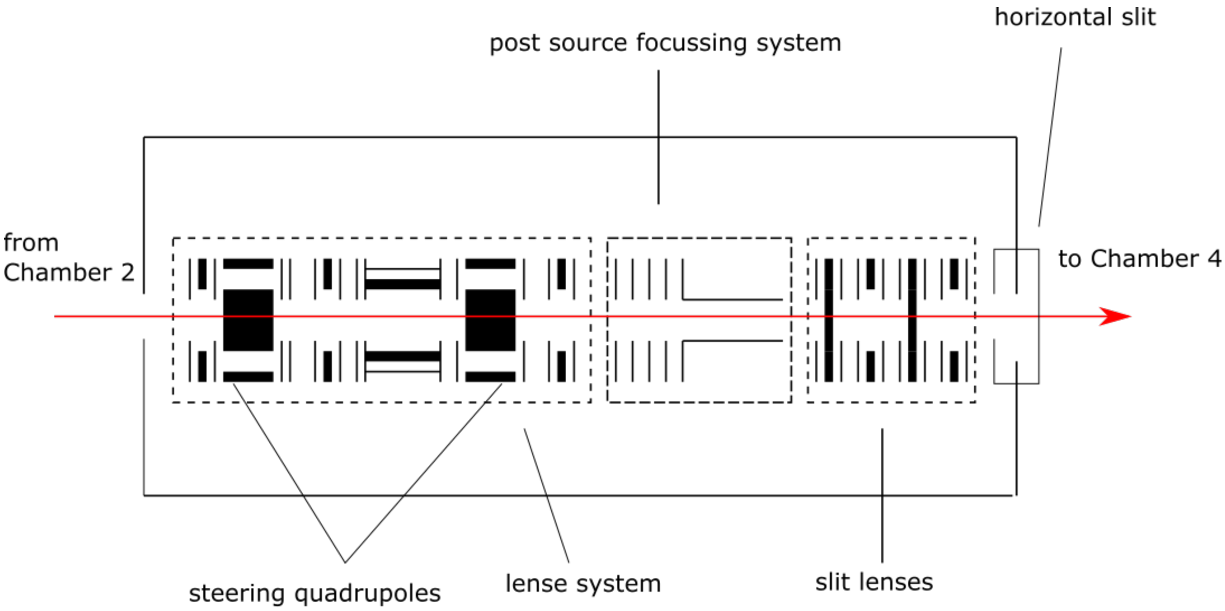

+

Figure 3.4: Schematic Illustration of chamber 3, hosting the modified Wiley-McLaren TOF-MS, the post source focussing system and the cylindrical lenses. The intention in this chamber is to direct the ion beam towards the detector and enable a decent mass selection. By different lenses the ion beam can be formed into a cylindrical shape which is optimized for laser overlap and detachment.

3.2.4 Chamber 4

Chamber 4 hosts all the essential detection systems needed to record photo electron spectra, mass spectra and a uv-permeable window for laser access. The pressure need to be maintained in ranges of $3 \cdot 10^{-8}\ mbar$ to $5 \cdot 10^{-9}\ mbar$ to guarantee an optimal mean free path for the electrons. To achieve this pressure regime, two molecular pumps and a kryo-pump is attached to Chamber 4. The external heating ($\approx 60^\circ\ C$) drives water out of the inner surface of the chamber to avoid reflections of electrons from the water layers. The entering anion cloud passes through the μ-metal-shielding and is directed to the MCP-mass-detector. The green cross marks the laser-detachment spot. The shielding is necessary to block any magnetic field from the outside of the apparatus to avoid distraction of electrons. The ejected electrons from the detachment site emit in spherical shape. Normal measuring mode, uses the double electron detector with a small angle, to get a better cone-cut-out of the spherical emitted electrons (detailed description in [Ste15]). The signals of both detectors are merged afterwards and analysed with a LE Croy 500 MHz oscilloscope after passing a constant fraction system and recorded via a MathLab routine (see[Pau17]). The energy of the electrons can be determined by their time-of-flight. The short flight path to the other detector is intended as a monitoring system during measurements with low count rates or to measure the signal-noise ratio while using deep UV wavelength to easy the critical geometric adjustment of the detachment laser. The MCP mass detector is functioning as the one mentioned above and is mainly used to separate mass signals in order to guarantee the detachment of the desired species.

3.2.5 The detachment laser

Due to the nature of this kind of TOF-electron measurements the timing and positioning of the laser-access is of utmost importance. This means the durance of the laser-pulse marks the start and the stop in terms of timing for the electron-spectra.3.6 shows the laser system used for detachment. The diode-laser ($\approx 800\ ps$) generates a pulsed infrared laser beam ($\approx 1065nm$). This beam is directed trough a focusing lens(2)) and a Faraday-Rotator. The Rotator has the purpose to block unwanted reflections back to to the diode laser. Thus, after passing the polarisator the beam enters via a polarised two-way mirror the laser head of a Innolas Spitlight 600 laser head. It passes the first Nd:YAG rod in a first amplification process, while the second amplification takes places while it is reflected by another polarised mirror (8)). Then it is directed toward the other rod for a third amplification process. Right behind the laser head is the higher harmonics generation

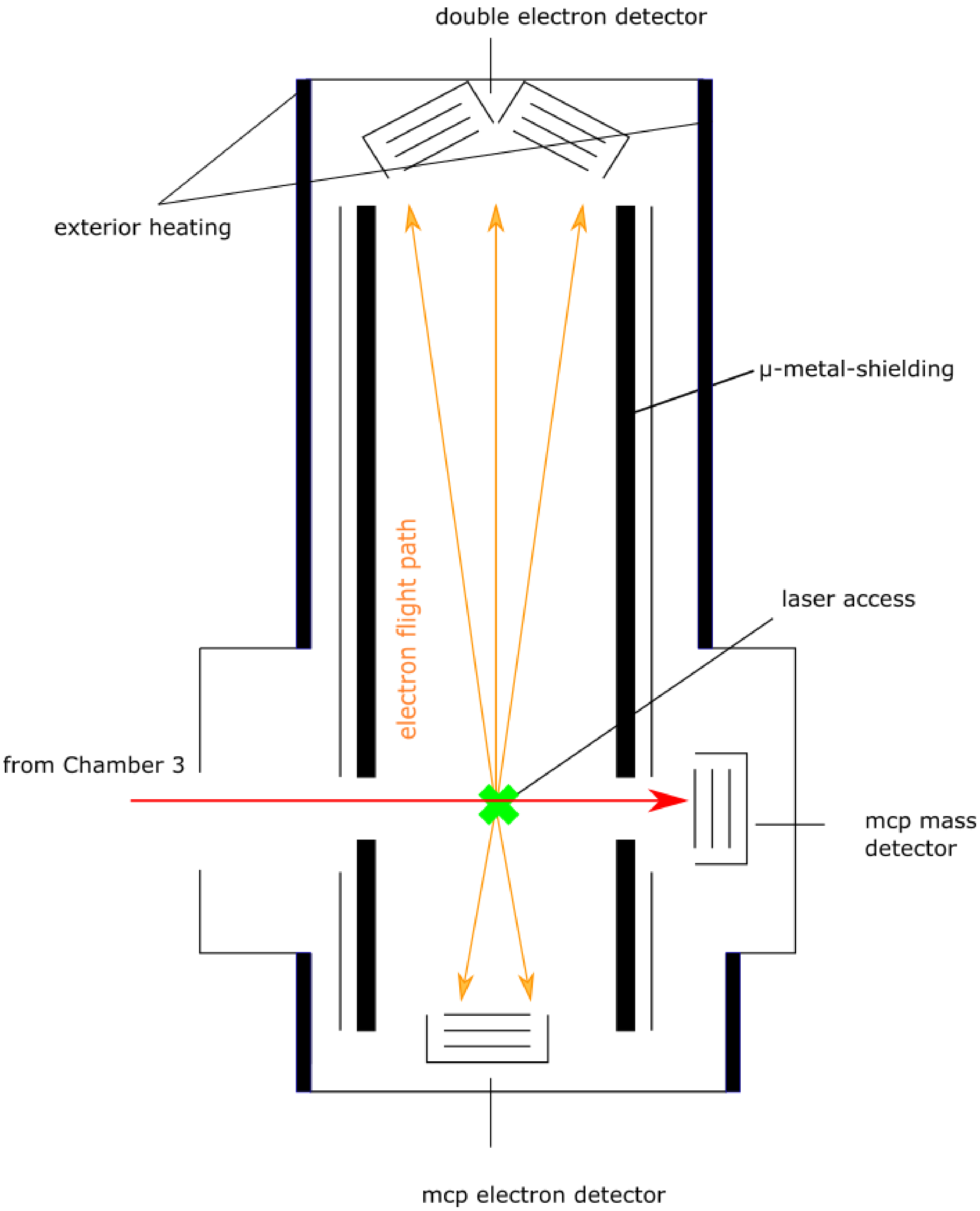

Figure 3.5: Schematic Illustration of chamber 4 with the detection systems for electrons and molecular ions. The detachment takes place in the area of the green cross. A short flight path with high transmission is installed at the bottom. It serves for back-ground optimization in case of UV photodetachment is performed.The long flight path is used for actual TOF photoelectron energy measurements. The fast ion detection takes place on the right hand side.

system, where several crystals can be used to gain the wavelengths 1064 nm (without crystal), 532 nm (doubling 1064 nm), 355 nm (mixing first and second harmonic), 266 nm

(doubling 532 nm) and 213 nm(mixing second and fourth harmonic). After passing a Pellin Proca prism the laser can be direct towards Chamber 4 via another mirror-system. To fix a starting point of the electron counting system, a diode-sensor catches the reflexes of the laser beam and triggers the counting system. The pulse energy of a single pulse ranges from 40 mJ (1064 nm) to 0,8 mJ (213 nm) which is a amplification of approximately times 1000 regarding the diode-laser pulse. Due to the critical nature of overlapping the laser-focus and the ion beam as well as in terms of timing and geometry, it is necessary to control the laser beam in terms of energy and shape. The beam form is also strongly dependent on the adjustments of the system and must be controlled regularly. The laser beam then is able to enter the apparatus via a three-mirror system. Before entering chamber 4 via the window it is possible to rotate the polarisation and adjust the laser focus with a collecting lens to optimize the spatial conditions of detachment.

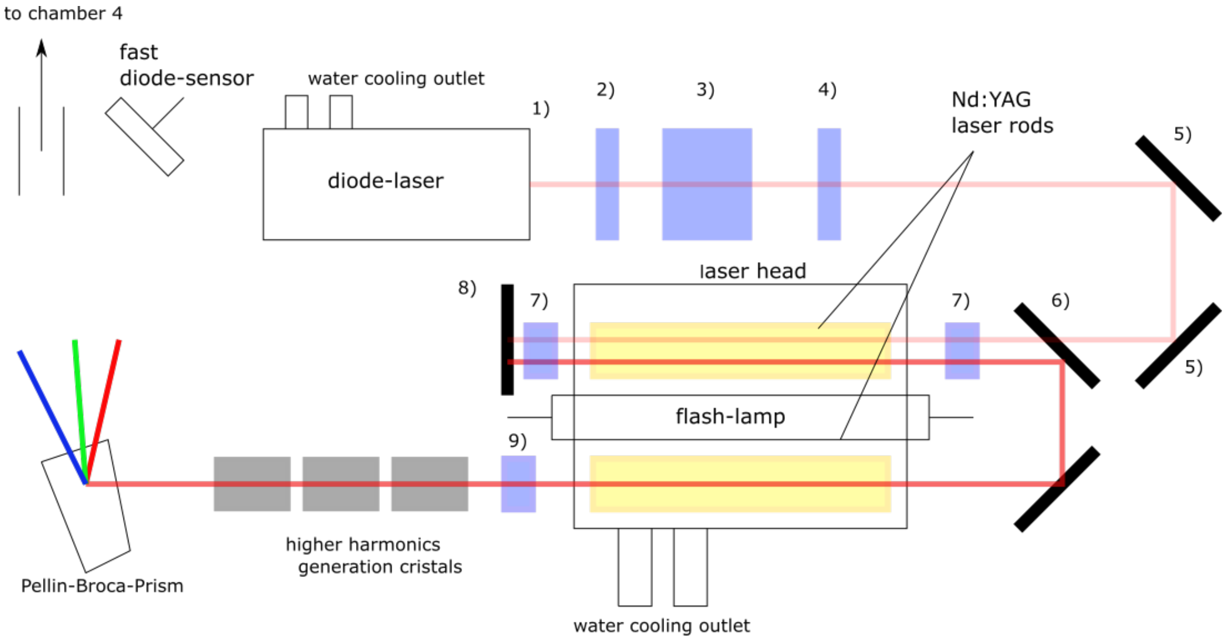

Figure 3.6: Schematic Illustration of the photodetachment laser system. 1)ps-diode laser "picolo"; 2)lens; 3)optical diode:Faraday-rotator; 4)Fresnel-Rhombus to rotate the polarisation to be perpendicular to the table; 5)100%-mirror; 6)polarised 100%-mirror; 7)$\frac{\lambda}{4}$-plate; 8)polarised 100%-mirror; 9)$\frac{\lambda}{2}$-plate;The ps-laser pulse from the diode laser passes three times trough the Nd:YAG rods and is amplified by about a factor of 1000. With the prism the wavelengths are separated and directed to the PD-PES apparatus. A fast diode sensor triggers the electron counting system. Sketch based on [Pau17].

3.2.6 The timing sequence of the setup

As mentioned before, the timing sequence of the whole setup is crucial for a successful measurement. The setup works with a repetition rate of 10 Hz and the trigger signals are based on 5 V-TTL-logic pulses all over the setup, steered by a Stanford Research Delay generator Model DG. To gain a better understanding of the complexity of the Anion-PD-PES method, it is helpful to understand the timing in detail. All triggering signals are five volts TTL-logic based. The timing sequence is illustrated in 3.7, while the colour systems refers to the single components used in the system. The initial triggering starts within the Stanford Research Delay generator. The first 100 μs gap is the time between the initial electronic signal and the mechanical response of the valve(see3.7 green).The valve then opens for a total time of approximately 800 μs and the opening behaviour resembles a gaussian function regarding the time and the pressure with a peak around 400 μs. That is the reason why the delay for the discharge pulse is around $380-500$ μs(violet). The discharge pulse is then active for around $0.8-3$ μs for an effective anion formation as mentioned above. This timing is variable and must be optimized manually for an optimal mass signal and need to be adjusted as needed. The travelling time for the ion cloud to the ion source is around $100-200$ μs, so the electric pulse steering the ion source pulse (orange) follows the discharge time with approximately $120-180$ μs. The duration of

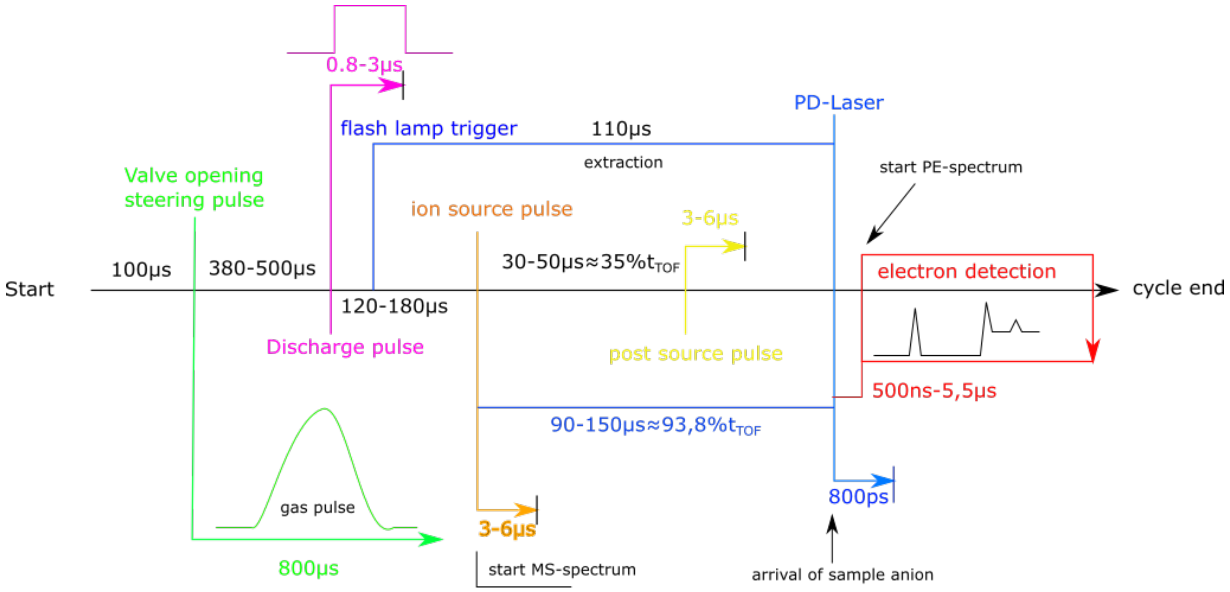

Figure 3.7: Scheme of the timing sequence. Different parts of the setup are separated by colours. After the electric steering pulse the valve opens with some delay. The discharge ignites at a suitable gas pressure at the needles;The ion source pulse acts starting time for the post source focussing, the laser trigger and the mass spectrum. The electron detection takes place 500 ns to 5.5 μs after the detachment.

the ion source pulse ($3 - 6$ μs) is based on the actual geometrical size of the ion cloud because it directly refers to the horizontal expansion of the cloud and also needs to get readjusted depending on the effective mass signal. $30 - 50$ μs after the ion source pulse follows the post source trigger (yellow) which is basically a second ion source with a similar timing to the ion source. The exact timing also needs to be adjusted depending on the time-of-flight (t_{ion}) of the desired mass with around 34 percent of the effective time of the respective peak. The blue coloured arrows illustrates the timing sequence of the laser. The flash lamp trigger of the laser system needs to be triggered 110 μs before the ion source to guarantee the laser pulse to be released just in time for the passing anion cloud approximately 94 percent of t_{ion}. To generate well resoluted spectra, the laser pulse width needs to be as narrow as possible, here around 800 ps. The laser itself triggers finally the electron detection which takes place 500 $ns - 5.5$ μs after the laser pulse. During a measuring session it is needed to adjust the timing depending an the effective mass signal and electron counts, to guarantee optimal count rates.

3.3 The Mounted-Discharge-Valve

3.3.1 The Evolution of the Mounted-Discharge-Valve Setup

During the completion time of the thesis, several bachelor and master thesis got involved with different problems concerning the discharge method as such. Those thesis have been stages in the evolution of the Mounted-Discharge-Valve-Setup. A brief overview of this evolution is described in the next paragraph.

Inspired by several other methods utilizing a discharge source([Wol]), it was possible to circumvent certain problems with the previous setup. It turned out, that the amount of anions produced by the previous setup had been inferior to the discharge setup. Manifold other problems, like the directing through the apparatus by using a discharge source, several other problems had to be solved in order to achieve a well working setup for the application used in this work. Thus several Bachelor and Master thesis revolved around the discharge method to overcome those mentioned problems.
The first attempt in utilizing discharges as a anion source, has been made in the work of Marco Schmidt[Mar17]. Two tungstens needles were applied to a copper ring mounted to an adjustable swivel arm. This arm could be moved in proximity to the pulsed valve. By applying a constant high voltage (approx 5 kV) it was possible to obtain the first mass spectra of anions and cations. Due to the constant voltage, the ion cloud got distorted right after formation and the time-of-flight was flickering. This made calibration of the spectra quite difficult. The conclusion was made to pulse the high voltage applied to the needles.
By using a Behlke high voltage double bridged switch (HTS-121) in another bachelor thesis ([Fra18]), it was possible to pulse the applied voltage and thus enabling to calibrate the spectra because the ion cloud got no longer distorted by the electric field. Furthermore, it turned out that more needles are more effective (now using eight) but finding the perfect distance between valve and needle setup had been difficult.
Still not being quite confident with the setup, further experiments took place in two other thesis. One of them tried to use the needle setup as a feeding source for a electron gun ([Lau18]). The other one made use of the needle setup to get anion and cation spectra out of the surface of the valve ([Jan19]). The latter thesis enabled the generation of the first well interpretable spectra as can be seen in a first pentacene spectrum in figure 3.8. This was the first spectrum with a recognisable parent ion. Noticeable is also the strong fragmentation and other peaks like OH^{-}-anion originating from leftover water at the valve

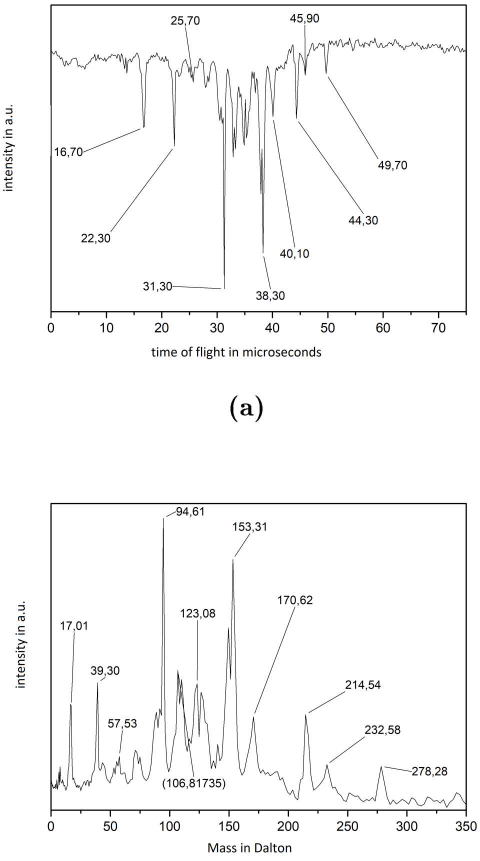

(a)

(b)

Figure 3.8: a) Time-of-flight anion spectrum of pentacene (argon). The baseline variation can be repatriate to the manifold peaks . Parent ion at 44.30 μs b) Respective anion mass spectrum with well recognisable fragmentation and parent ion at 278 Dalton

itself as well several water clusters of the parent ion. These peaks are withdrawing electrons during the process of anion formation and this can be an explanation for the low parent ion intensity.

The main idea here was to use a double high voltage pulse to firstly bring the substance off the surface and with the second pulse to ionize the molecules inside a argon jet. As can be seen, the intensity of the parent ion (44.30 μs) is quite low, due to the fragmentation of the parent ion and water cluster formation. Nevertheless this work marks a essential evolution stage in the development of the mounted discharge valve because the spectra became interpretable in reproducible manner.

In further approaches ([Nik19]) it was decided to use a single pulse again, as well as mounting the discharge setup to the valve itself, to facilitate the adjustment of the distance between the valve and the tungsten needles. In this thesis the short flight path was utilized for the first time for monitoring purposes. Now the most fitting values for the distance between the valve and the needle mount as well as the timing for the high voltage pulse became determinable. After this master thesis the set-up evolved to the current system.

3.3.2 The current Mounted-Discharge-Valve

The framework of the discharge Mount

With the last paragraph in mind, a very crucial dimension for a proper working anion formation is the distance between the valve and the plane of the tungsten needle tips as can be seen in figure 3.9. The optimal distance is between $2.5 - 3$ *mm* and seems reproducibly stable at 3 *mm* varying a bit from one substance to another. As discussed earlier, the distance determines factors like the mean free path regime of the gas jet, but also the voltage needed for proper operation. Too close to the valve the discharge is burning through the valve instead of into the jet. This results in an absence of ions frequently due to the flashover. Too far from the valve results in an total absence of the discharge because of the bigger mean-free-path of the gas molecules. Figure 3.10 shows the ring mount of the tungsten needles. The high voltage is directly applied to this ring. It contains holes to put the needles through as well as deepenings for holding the ceramic screws. Figure 3.11 shows the complete blueprint of the mounting ring. The needle holes are about 0.4 *mm* in diameter, the needle tips itself are a bit smaller(varying). The distance between two facing needles is about 1 *mm*. Also crucial is the angle of the holes (needles) respective to the valve orifice here about 34°. Also the diameter of the ring is important to maintain a fixed electric field distribution, as the geometry of the ring also has an impact on it. It

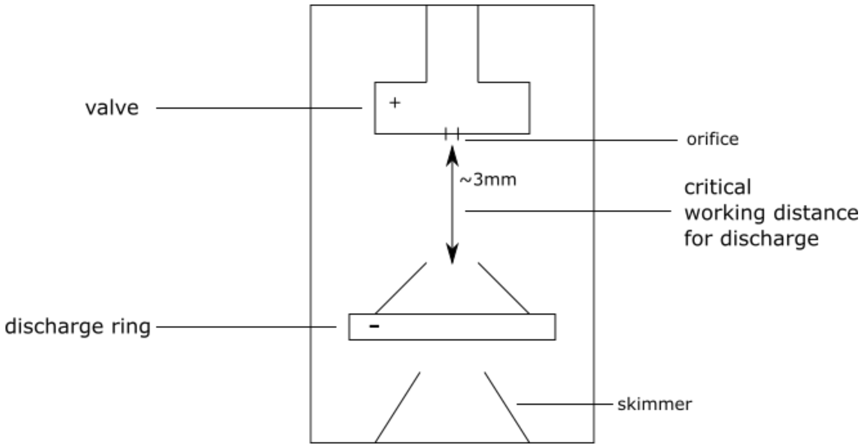

Figure 3.9: critical distance between the needle tips (cathode) and the valve (anode).The distance is fixed before bringing the valve into chamber 1.

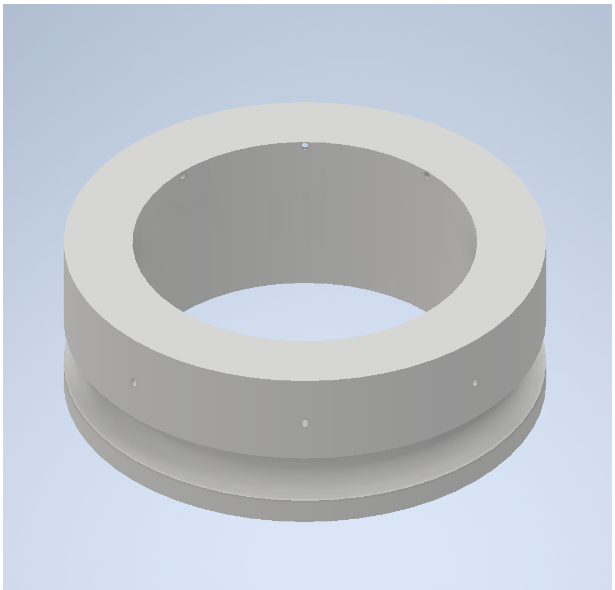

Figure 3.10: 3D modell of the needle mount.

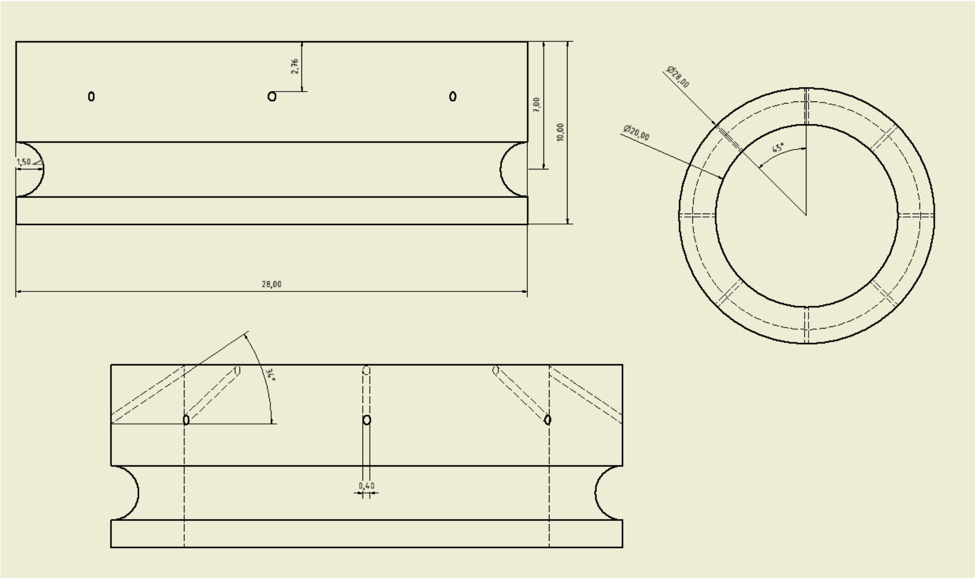

Figure 3.11: Blueprint of the needle mount.

was chosen by the size of the valve and became a bit smaller during the evolving process for an easier handling. Probably a bigger diameter could result in a more fitting electric field distribution. The eight holes for the needles are distributed in an angle of 45° around the ring. The mounting plate can be seen in Figure 3.12. The edges were cut out to be better fitting through the feed-trough as the valve and the mount are designed as a dive-in-system which gets lowered down into chamber 1 from the upside. The boreholes at both sides are intended for threaded rods. With those it is mounted to the cooling plate of the valve. The three boreholes in the horizontal axis are for ceramic screws to

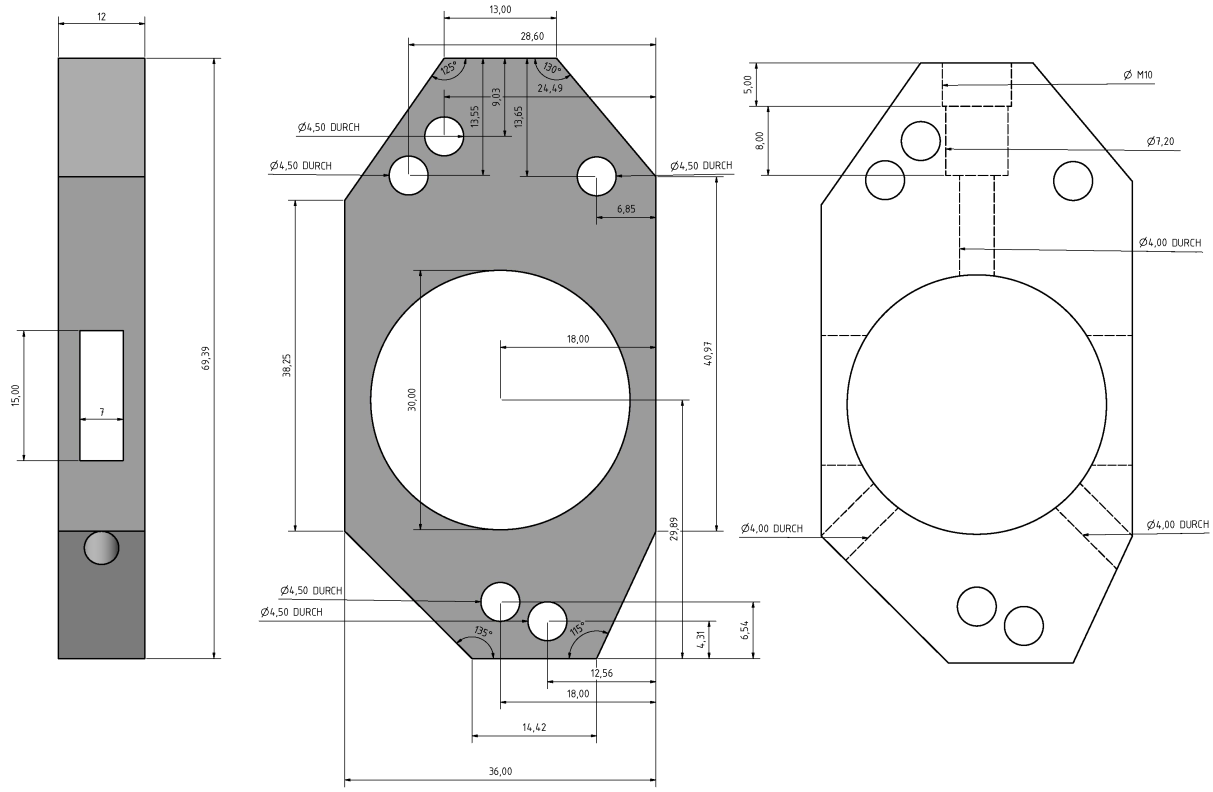

Figure 3.12: Blueprint of the ring mount.

fix and insulate the mount versus the high voltage applied to the ring. The mount is on the same electrical ground level as the rest of the valve. The ceramic screws also enable an adjustment of the needle tips in a horizontal plane in respect to the orifice. As can been seen earlier the needles are positioned in a centro-symmetric way around the orifice. This assures a symmetric field and therefore a proper symmetry of the anion formation regarding the setup geometry in chamber 1.

It has to be said that the majority of the geometric values got improved step-by-step using the trial and error method during the several thesis mentioned above. The key to be able to improve the method, finding fitting ways of monitoring the behaviour of

- The anion (cation) formation by rusing the short flight path.
- The electronic behaviour of the discharge itself.

Both items mentioned on the list above shall be explained in a detailed manner in the next subsections.

Besides the geometry, the electronic setup is also important. To apply a negative high voltage pulse it is necessary to use a fitting switch. It must be able to operate at a frequency of 10Hz, with negative polarity, as well as being able to trigger with 5V TTL-pulses as the other devices also get steered by TTL-pulses. The switch used here is a Behlke HTS 121-01-HB-C, with a maximum voltage reference of $-12kV$. With the intention to use voltages around $-5kV$. It turned out that it is necessary to stay below the maximum voltage to prevent flyback pulse damaging the switch. Those pulses can occur after the ignition of the discharge when a flashover happens between the needles and the valve. Those flyback pulses can overlap with the next incoming pulse and add up, resulting in a higher voltage than applied and therefore damaging the switch. The circuit diagram in Figure 3.13 shows the used circuit in this application. The Behlke switch itself is in the middle (green ring) of the circuit. The transformer and the wheatstone-bridge on the left side with the following capacitors grant a proper source voltage for the switch. Under the switch there is the circuit for the incoming high voltage with a small circuit just at the output of the circuit. This protects the switch from the above mentioned flyback spikes coming from the discharge. Not pictured is the TTL input which is just directly at the Behlke component itself. All ground levels are brought to the same level. This circumvents any outside coupling of distorting signals into the cables. Directly behind the output is a pick of where the effective signal can be illustrated with a time resolution on a oscilloscope. Through this it is possible to monitor the timing behaviour of the applied negative high voltage pulse. Usual voltages are between $2-5\ kV$ with a strong dependency on the framework situation of chamber 1.

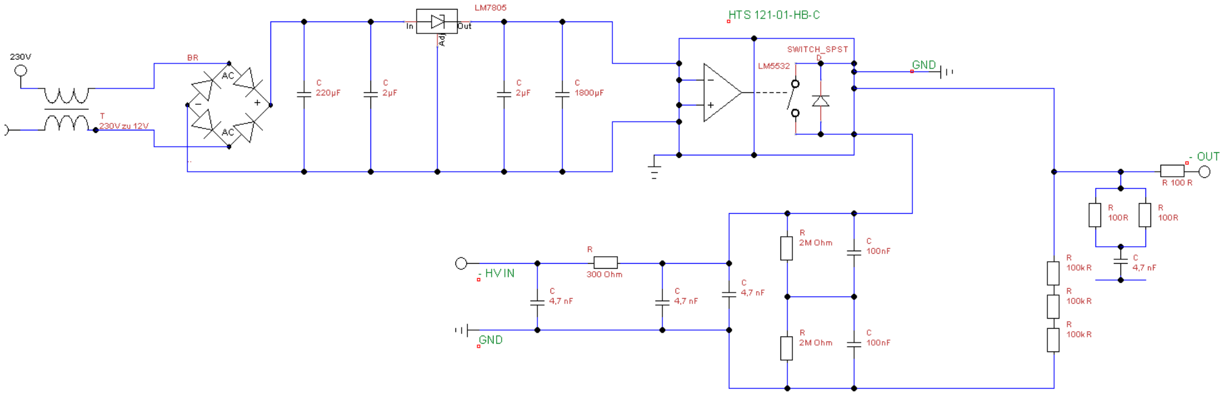

Figure 3.13: Circuit diagram of the pulsing device for the pulsed discharge.

The monitoring of the discharge

As mentioned before the effective monitoring takes place in two instances. It is important to observe the behaviour of the discharge at all times during a experiment. Several conditions can influence this specific behaviour:

- The working distance (valve vs needle plane).
- The back-pressure of the carrier gas.
- The applied voltage.
- The timing of the discharge and its length.
- The opening behaviour of the valve (consistency/timing).
- The temperature of the valve.

Although the temperature is dictated by the sample substance and cannot be adjusted at will (with the exception of ranges of about $5-10^{\circ}$ Celsius). The opening behaviour of the valve is strongly dependent on the mechanical conditions and can vary to a certain degree from experiment to experiment. The tightness of the valve in standby has to be nearly perfect as a possible control value for the proper functioning. The working distance can solely be adjusted between two experiments and just turned out to be fitting at the mentioned 3 mm value.

The back-pressure as well as the applied voltage, and the timing can be adjusted on the fly during a running experiment. It can be modified depending on the mass signal and stability and has to be modified manually. So the other above mentioned items on the list can be adjusted during the experiment. To guarantee a stable running experiment, several monitoring instance can be consulted.

One of these is the monitoring of the applied high voltage pulse via the above mentioned pick off. The interpretation of the resulting signal on the oscilloscope can be seen in Figure 3.14. Three situations can occure while monitoring the pulse. On the left a simplified illustration of the pulse when the valve is not working is displayed. If that is the case, the pulse can be recognised as a simple negative rectangle signal. If during this state, anything is not functioning properly - like a too close distance to the valve-, it can be recognised right away.

The graph in the middle describes the pulse during a proper functioning measurement. The rectangle pulse is a bit cut off on the right side, because of the ignition of the pulse into the gas. This situation leads to the assumption that the setup works without any

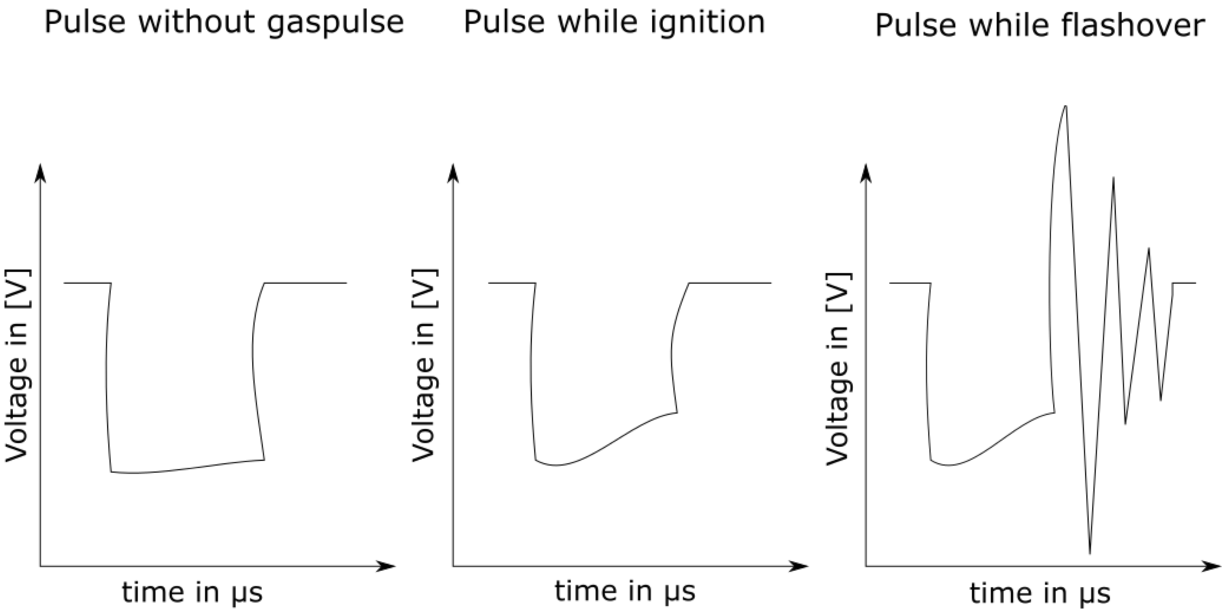

Figure 3.14: Schematic Illustration of the monitoring of the discharge pulse via the oscilloscope.

problems.

The right illustration shows the signal if anything is not working properly. This can for instance be a too large voltage on the needles, which causes the discharge to burn right to valve (instead of into the gas pulse), resulting in a flashover. This behaviour can also be caused by a too small distance between the needles and the valve, as well if the valve is opening improperly or unstably (or the valve simply is not sealed properly). Additionally, a non fitting timing overlap between the high voltage pulse and the opening time of the valve can cause this distorted signal. However, this means that it is possible to adjust the above mentioned values solely with this signal. The timing, as well as the applied voltage, can therefore be adjusted to always fit the situation illustrated in the middle picture. This can be used as a reference to maintain the mass signal, which is the very foundation for the following photo-detachment. It turned out that it is not possible to gain a stable mass signal, if the high voltage pulse signal is not resembling the middle picture. Also the stability can be monitored with this signal. In border regions of the timing/voltage/distance, it is possible to monitor how stable this situation can be sustained and necessary adjustments can be made. Typical working ranges had been

- for the voltage : $2-5\ kV$ (at $1\ mA$ current)
- for the high voltage pulse length : $800\ ns - 3\ \mu s$
- for the timing between valve and high voltage pulse : $200-500\ \mu s$

It has to be emphasised that the sustaining of the high voltage pulse was easier with a sample molecule in the argon jet than without a sample (empty valve), which led to the assumption that the sample molecule must have an impact on the discharge itself.

Even with this instance, it is possible that no mass signal is detected. Possibly because most of the sublimation temperatures of the sample molecules are not well known or not known at all. This adds temperature as a possible unknown value. This value can not be controlled by electrical means, but the short flight path with its MCP detector can be extraordinarily useful when it comes to determine fitting sublimation temperatures (as well if a substance is not forming anions at all). Furthermore, the obtained mass spectra from the short flight path can be indicating a proper anion formation as well as reaching the correct sublimation temperature. In figure 3.15 an early mass spectrum of dibenzofurane can be seen . Just with reaching the temperature of 71° Celsius, the marked parent ion peak appeared. The peaks left to the parent ion peak could be determined to

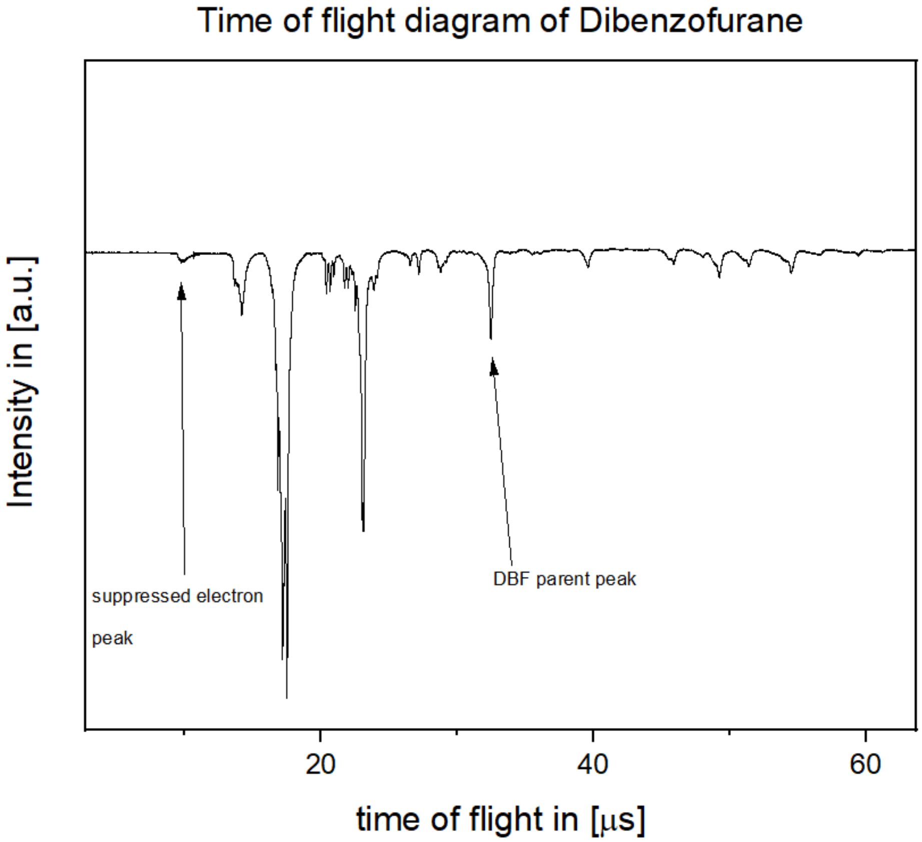

Figure 3.15: Time of flight spectrum of the anion formation of DBF. The parent peak loses intesity due to fragmentation and cluster formation

be aluminium as well as OH^- and impurities of the setup. Special attention has to be given to the first occurring peak. The peak could be nearly suppressed completely by applying an weak magnetic field from the outside and therefore led us to the assumption that this peak represents the presence of free electrons in the ion cloud. This contributed to several assumption regarding the attachment process as mentioned in section 2.2.4 .

3.4 Mass-selection via Time of flight

Since the radical anions carry a charge they can be analysed by mass in a mass spectrometer. A prototype-build time-of-flight mass spectrometer (TOF-MS) is used for this, because of its construction and its high transmission. The advantage of mass separation is (before performing the laser spectroscopy) that it can be ensured that the right molecular species and not a cluster nor a fragment anion is investigated by photo-electron spectroscopy. Beside its high transmission, a further advantage of a TOF-MS is the fact that the anions of one mass can be compressed in time and thus also in space. This compression of the molecular anions in a small volume is very favourable for the laser access needed in the photo-electron spectrometer. The disadvantage of a linear TOF-MS instrument as used in this work is its typical malign mass resolution in comparison to other types of MS spectrometers. The ideal concept of TOF-MS is that all ions start at the same time at the same position in the ion source. If all ions obtain the same energy, then ions of small masses come first and ions with bigger masses come later. Whereas the timing of the acceleration can be well controlled by an accurate fast high-voltage pulser, the starting position of the anions is very broad. This is due to the large volume in which the anions are formed and the large skimmer orifice. In this work, the diameter of the anion cloud at the start position is estimated to be $4-5\ mm$ along the direction of the ion flight path in the MS-spectrometer. As a result even the ions of the same mass are accelerated to different kinetic energies.
A reflectron TOF-MS instrument ([Mam01] , [BNWS82]) would compensate the effect of the ion energy distribution on the flight time and thus provide a much better resolution than a linear TOF-MS. However, it would – due to the longer flight path and the typically used grids - lead to a considerable loss of anions at the site of the laser access. It also would need a more complicated PE-spectrometer, because the anion flight path has to cross two times the PE-spectrometer.

As outlined above , the spatial ion distribution in the pulsed ion source results, if the electric field is switched on, in energy differences between the ions of the same mass and is the reason for the relatively bad mass resolution. A two-stage ion source with a first small electric field and a second strong field helps to reduce the energy error caused by the different starting positions in the first weak field ([WM55]) . Weinkauf et al.([Wei89]) have shown that the mass resolution in such a concept can be further improved by choosing the right acceleration path lengths in the two-stage ion source and use suitable voltages allowing to compensate the errors in flight time to the second derivative. Because in the used setup the spatial distribution in the ion source is so enormously large the ion cloud at the laser interaction site is still too big to lie fully in the laser-interaction volume. Garry Kinsel at al.([KJ89]) could show that for a part of the mass spectrum an improve in mass resolution by post-source focusing (PS-focussing) is possible. This means, that far downstream the ion source, the ion cloud of one mass is a second time accelerated. This is performed in a way that the slower ions – lying back - receive more energy than the fast ions – flying ahead -. This PS-focussing even works for a section of about five per cent of the mass spectrum. By this post-source-acceleration the ion cloud of one mass (here the mass of the anion of interest) is so strongly compressed in the direction of the flight path, so that all ions can be hit at the detachment site by the slightly focused laser beam (focal size $1-2\ mm$ diameter). The anions are further accelerated in front of the detector and detected by a micro-channel-plate (MCP) detector (consisting of two stacked micro channel plates). The signal is then displayed and stored by a digital oscilloscope (bandwidth 100 MHz, Tektronic/LeCroy).

3.5 The PD-Laser in the context of anion spectroscopy

Since the number of parent anions in one cycle of measurement (the repetition rate of the experiment is 10 Hz) is not very high (about 50-200 ions) and the transmission of the TOF-photoelectron spectrometer is only 10^{-3}, the photodetachment efficiency should by as high as possible. Virtually this depends on many factors such as

- i) The detachment cross section of the orbital from which the electron is removed.
- ii) The anisotropy of the electron emission and the polarisation of the laser radiation.
- iii) The excess energy of the detachment photons over the final neutral state.
- iv) The temporal and spacial overlap between the detachment laser beam and the ion cloud.
- v) And evidently the pulse energy of the detachment laser.

Whereas i) is given by the molecule, the size of its orbital (π-system, or localized lone pair orbital) or the type of excitation (single excitation or contribution of double excitation (see Chapter 2)) and cannot be improved, all the other factors can be influenced by the by the experimentalist. For example, if the electron emission does not take place isotropically over the angle of 4 π, (see ii) above) (but is for example preferentially directed along the polarization of the detachment laser), then at least two different laser polarisations have to be used, to make sure that this transition is missed. According to Wigner´s law the detachment efficiency also depends on the angular momentum of the emitted electron and the photon excess energy (see iii) above and chapter 2). Especially if a π wave detachment takes place the detachment cross section in dependence on the excess energy is first very low (low excess energy) and then only rises very flat for higher excess energies. Since the wavelengths which are available for photodetachment are limited (see chapter 3 and below), it could be that low-energetic photons can just detach to a neutral electronic state. If this state, shows a π-wave detachment then this transition would appear to be very weak in the according PD-PES or would be even completely missing in the case the laser polarisation is wrong (Wigner's Law.). The best possibility to improve the intensity of this transition is to increase the photon excess energy by choosing a higher harmonics of the Nd:YAG laser.

The spatial and temporal overlap (iv) above) can only be achieved by a careful adjustment of the laser beam and the anion beam. The ideal situation is that all ions can interact with the detachment laser. Due to the fact that the laser beam typically has a gaussian spatial profile, the interaction of the anions with the outer area of the laser beam is usually small. This can be simply improved by increasing the laser pulse energy (i.e. the number of photons). This can be easily realized in the fundamental and the lower harmonics 532 nm and 355 nm. The only precondition is that the laser does not perform laser desorption of metal atoms or cause a laser plasma at the inner surfaces of the spectrometer. For the fourth and fifth harmonics the situation is more complex: the requirement for a good beam quality and technical reasons limit the maximum intensity and thereby also the laser pulse energy. The reasons are that

- i) If photons with a wavelength below 300nm hit the inside spectrometer wall, they can produce background electrons, which can destroy the PD-PE-spectrum.
- ii) The entrance windows of the spectrometer start to absorb and can be destroyed.

In the above discussion still one aspect is missing. This is the aspect of the time accuracy, with which the time of flight of the electrons can be measured. In a former work a laser pulse of $12-15$ ns (depending on the harmonics) was used for the detachment, resulting in a flight time accuracy for the electrons which was practically completely limited by the laser pulse width itself. In a second step a laser set-up with a shorter pulse width was used in order to improve the over-all flight time error to 2 ns (see explanations below and Reference [Ste15]).
In conclusion the anion photoedachment photoelectron spectroscopy experiment imposes the following requirements for the detachment laser:

- The fundamental and all harmonics up to the fifths harmonics (212.7 nm) have to be available for the detachment.
- The laser beam quality has to be taken care of to reduce or avoid laser desorption and background electrons.
- The laser pulse width should be in the order of a few ns, in order to not limit the electron energy resolution.

In order to ensure a short laser pulse width, a diode-pumped Nd:YVO$_4$ seed-laser with a pulse width of 800 ps was used and post-amplified in a home-build amplifier. This amplifier was mainly based on the pump chamber of a regular Nd:YAG laser in our case the Spitlight 600 of the German laser company Innolas.

The complete laser set-up is described in the following (see also figure 3.6). In order to fit in the importance of the laser system in context of the experiment, further explanations are necessary The laser Spitlight 600 was still functioning in its basic functionalities, except that the pump chamber is mounted outside the original laser into the home-build amplifier. The pump-chamber has one flash-lamp and two Nd:YAG rods. When the Spitlight 600 is switched on, the flash-lamp is brought into a pulsed low-current discharge mode, which is necessary to ensure that enough charge carriers are still between the electrodes if the high power discharge is initiated: It is essential that this main discharge starts instantaneously with full lamp-light intensity. The light of the lamp directly or by reflection from the pump-chamber inner walls enters from all sides into the two laser rods. During the 110 μs of the main lamp discharge this light creates a strong energy level population inversion in the two Nd:YAG rods. This complete pump-chamber set-up including the electric wires and the water cooling for the flash-lamp and the laser-rods have been taken out of the Spitlight laser and posed onto a separate aluminium plate, which allows to freely mount additional optics.

The post-amplification of the 800 ps laser pulse of the Piccolo was necessary because its pulse energy is in the order of 30 μJ, far to low for our application.

The requirement concerning the detachment laser were, that about 30 mJ (800 ns pulse width) are available at 1064 nm. This requirement comes from the need to produce the fourth´s and fifth´s harmonics. Note that for the production of the fifth´s harmonics the 1064 nm has to be a first time frequency-doubled to 532 nm then again frequency-doubled to 266 nm and finally mixed with the fundamental to 212.7 nm. Hence three non-linear processes are necessary in order to create 212.7 nm radiation. In order to end up with a sufficient pulse energy of about 500 μJ at 212.7 nm, the above-mentioned 30 mJ should be available in the fundamental.

This means that the pulse energy of the piccolo has to be amplified by about a factor of 1000. These requirements define the specifications for the amplifier:

- i) Light amplification by a factor of 1000
- ii) Preservation of the 800 ps pulse width, especially no double pulses or continuous radiation.
- iii) Good beam and polarisation quality to allow efficient higher harmonics generation.
- iv) Exact triggering with an accuracy of better that 1 ns.

- v) No destruction of the Piccolo laser by amplified back-reflections.

In order to fulfil the requirements of the above list the follwing concept and tools were used:

- In order to achieve the amplification of about 1000 (see i) above) the seed-beam was three times send for amplification thorough Nd:YAG rods.
- In order to preserve the pulse width (see ii) above) of the seed-laser great care was taken that the seed laser does not have a continuous back-ground. In addition all optical surfaces were slightly tilted in order to avoid reflections, which could result in a second pulse (note that 1 ns light travel time corresponds to about a 30 cmdistance).
- In order to avoid destruction of the Piccolo by amplified back-reflections an optical diode (Faraday rotator) was used.

In the following for one laser shot the formation of the detachment laser pulse is described. In the beginning the laser flash-lamp is ignited 110 s before the laser pulse is needed. During the 110 μs the flash-lamp has enough time to create an inversion in the two amplifier laser.

If the laser pulse is needed, the Piccolo laser is triggered by a 5 V TTL-pulse. Inside the diode-pulped Nd:YVO$_4$ laser an optical deflection element allows lasing for a very short time. Since the cavity length of the Piccolo laser is only 2.5 cm the round-trip-time is very short and a pulse with abut 800 ps pulse width evolves. This pulse is transmitted through the Faraday-rotator acting as an optical diode. Since the polarisation is turned by the Faraday-rotator, afterwards a Fresnel-rhombus is used to rotate the polarisation to the plane of the table. Two dielectric 45° mirrors for 1064 nm allows to adjust the Piccolo beam in order to become collinear to the left laser rod. On its way to the left Nd:YAG rod, the beam passes straight a polarisation-dependent mirror aligned in a mechanical 45° orientation to the beam. The beam of the Piccolo then runs through the left laser rod for the first time and is amplified by that. Its polarisation is then rotated by 45° by a $\frac{\lambda}{4}$ plate and reflected in itself by a 0° mirror. By passing the $\frac{\lambda}{4}$ plate the second time, the polarisation is again rotated by 45° so that in total the polarisation is now rotated by 90° against the original orientation. After passing the left laser rod a second time for a second amplification, it is now deflected by the polarisation-dependent mirror to the right, again deflected by 45° and fed into the second laser rod. After the third amplification the laser passes a $\frac{\lambda}{2}$, which allows to suppress spontaneous emission and distorted laser light contributions. The higher harmonics are created from the fundamental of the Nd:YAG laser (1064 nm) by using the right polarization of the laser and non-linear crystals tilted to the right angle and heated to the right temperature. They have two different refractive indices for the two perpendicular polarization directions of the different colours allowing to synchronize the speed of light in the crystal for the involved wavelengths. The second harmonics (532 nm) is formed by using a doubling crystal. The third harmonics (355 nm) is created by mixing the fundamental with the second harmonics. The fourth harmonics (266 nm) results from the frequency doubling of 532 nm. The fifth harmonics (213 nm) is formed by mixing the fundamental with the fourth harmonics.

The laser light with the desired colour is selected by a Pellin-Broca prism by rotation of the prism and via the different exit angles of the different light components.

The laser pulse of the right colour is adjusted via three dielectric mirrors into the PE spectrometer from above. Different lenses and orifices are used to optimize the bean quality. The laser pulse energy is measured on a regular basis, to ensure that the pulse energy is roughly right. A fast photo-diode is used to feed a constant fraction unit, which forms the trigger pulse to start the flight time measurement for the photoelectrons. Since also the electron signal passes though a constant fraction unit and the cable lengths are exactly measured, the zero-time for the photoelectron measurement can be determined. Typically the first time point in the spectrum corresponds to 500 ns.

As already indicated the adjustment of the laser in time and space can be first only performed by following a typical adjustment procedure. Typically one of the wave-lengths 1064 nm, 532 nm or 355 nm is used, because the laser pulse energy is then so high that a considerable amount of the anions can be detached. As a result the anion signal at the mass detector decreases. This decrease then allows optimization of the temporal and spatial laser-anion overlap. If after such a measurement a fourth or fifth harmonics is used for photodetachment, one can be sure that at least the timing between laser and anions is right, so the main adjustment that is then that of the spatial anion to laser overlap under the precondition that a minimum of back-ground electrons is created. This requires a good beam quality and a perfect adjustment of the beam without hitting internal surfaces.

4 Results and Discussion

The sample molecules investigated in this work were preferentially large polycyclic conjugated hydrocarbons, which may be interesting for organic electronic devices. The general aim of this work was, to determine electron affinities and the energy of such electronic excited electronic states of the neutral molecules, that are otherwise transition forbidden from the neutral S_0 ground state. With this knowledge, we possibly can contribute missing links to the discussion and understanding of photo-physical and photo-chemical processes in these molecules.

To achieve this goal, the intact sample molecules were

- Brought into the gas phase by thermal heating.
- Co-expanded in a supersonic jet with argon .
- Transformed into radical anions in a pulsed discharge.
- Cooled by the on-going co-expansion.
- Mass-selected.
- Photo-detached by a short laser pulse.
- Measured regarding their photo-electrons.

All the points of the above list are described in detail in Chapters 2 and 3. The formation of cold radical anions and their mass-selection as well as the laser-excitation are expensive components which are also difficult to handle. But, as outlined above, only the approach via the radical anions allows a systematic circumvention of most of the selection rules which are otherwise valid in neutral molecules.

It is well-known in science that the difficulty of a prototype experiment increases with the number of steps by which a sample is prepared, selected and treated. This is also the reason why the output of this experiment is usually low. In addition, time-consuming improvements have to be made and constant maintenance work is necessary.

The Results for the investigated sample molecules were:

- The determination of the up to now unknown electron affinities.
- The spectroscopy of the up to now unknown triplet states T_1.
- Possibly energies of T_2 states.
- Energies of intra-molecular charge transfer states.

In this chapter for the molecules investigated in this work,

- The chemical structures are presented.
- Previous experimental and theoretical investigations are reviewed.
- Specialities concerning the electronic structure or unusual photo-physical or photo-chemical properties are highlighted.
- The PD-PE spectra are presented, described and as far as possible assigned.
- The extracted electronic state data are listed in tables and compared to the results of previous works.
- For molecules of similar chemical structure the energetic electronic state positions and the state orders are compared and discussed.

Data Processing and Presentation of the PD-PE-Spectra

In the following, it is described with which wavelengths the PE-spectra have been recorded, how the sub-spectra have been assembled to obtain one complete spectrum, why PE intensities of different electronic transitions are difficult to be compared, and how the spectra have been calibrated.

The Composition of the PE-Sub-Spectra to one Complete Spectrum.

The PD-PE spectra cover up to 6.25 eV of energy. Due to using a time-of-flight PE spectrometer and its energy-resolution strongly depends on the velocity of the electrons (see chapter 2/3), several laser wavelengths have been applied for the detachment. By this the energy of the removed electrons is limited to a certain range in a certain section of the PE-spectrum . The intention of this was to achieve optimal energy resolution for each electronic state of the neutral molecule which was identified. Hence, the featured overview PD-PE spectra are composed of several sub-spectra, recorded with different laser wavelengths. The wavelengths used for photo-detachment were the fundamental and the higher harmonics of the ps-Nd:YAG laser (see chapter 3):

- 1064 nm
- 532 nm
- 355 nm
- 266 nm
- 213 nm

The formation of higher harmonics of the fundamental wavelength of the Nd:YAG laser is described in section 3.6.

The positions at which the spectra are composed are marked by arrows in the respective figures and the wavelength used are given below the respective section.

Transition Intensities in the PD-PE-Spectra

The peak intensities of the PE spectra are difficult to compare in general, since according to Wigner´s law [Wig48], the intensity of an electronic transition to the neutral molecule should increase with the photon excess energy over the final neutral state. A result of this methodical artefact is, that in principle low-lying electronic states of the neutral molecule, such as S_0 and T_1 states, have typically considerably higher intensities than higher-lying electronic states (for example T_2 and S_1), which lie close below the photon energy (the photon energy is added to the anion ground state).

As a result of this, in PD-PE spectra electronic transition intensities can be only interpreted, if:

- The two electronic states lie very close in energy.
- They have been recorded with the same detachment wavelength.
- Their intensities are significantly different.

This intensity problem is very unfortunate, since the transition intensities could - with the help of theory - give hints, which molecular orbital might be involved in the transition (see chapter 2).

Time-of-flight to energy conversion

As in the thesis of Vosskötter [Ste15] and Konieczny [Pau17], also in this work PE spectra have been recorded by measuring simultaneously the complete kinetic energy range of the photo-electrons for each data acquisition cycle (see Chapter 3.6). This was performed in a time-of-flight photo-electron spectrometer. The TOF spectrum (electron intensity versus flight time) was first recorded and afterwards converted to an energy spectrum (electron intensity versus electron energy). Because of the non-linearity between flight time and energy ($t \propto \frac{1}{\sqrt{E}}$) great care was taken to convert the intensities in such a way that the number of electron counts which have fallen in a certain flight-time window are exactly filled into the corresponding energy window.

It should be noted that this procedure fails in the case of a metastable, delayed electron emission (see the 5Fi molecule) or in the case of background electrons which stem from a laser surface interaction. In the latter case, this background signal could be subtracted without loosing information.

The intensities of the electronic states are presented as realistically as possible. Interestingly in some cases the intensity effect (this corresponds to the area under a peak) as caused by Wiegner´s law is at least optically compensated for by the fact, that the energy resolution is better if the electron energy is low. This means that the peaks become sharper and even if the intensity (area under the peak) is small it becomes considerable high.

If possible, overlapping peaks in neighbouring spectra are used to adapt the y-scales of these spectral sections.

Since the number of anions known in the overlap between laser and the anion beam is not exactly, the y-axis is displayed in arbitrary units. In most of the cases this procedure is justified since mostly the energetic position of a respective electronic state is of interest and not the absolute intensities.

The energy calibration.

Unfortunately photo-electron spectrometer suffer from surface ageing by adsorption of molecules or pump oil. All these surface contaminations produce electric stray fields which cause a time-of-flight shift resulting in a falsified energy. Heating of the spectrometer can help to minimize or heal such effects. It turns out that a full recovery to the old status cannot be achieved. In former works photo-detachment spectra of the atomic iodine anion recorded with the fourth and the fifth harmonics have been used for calibration, as is described extensively in the thesis of Konieczny[Pau17].

The atomic iodine anion is formed by dissociative electron attachment to iodo-methane. Because of the hazardous nature of this substance, we decided to use the well-known S_0 and T_1 states of anthracene as calibration points. They have been calibrated before with iodine. As a result, the calibration constants for converting the PE spectra from flight time to energy were adapted to shift the spectrum of anthracene to the right energies.

Comparison of the Old and New Anion Formation Methods

In Figure 4.1 two PD-PE spectra of the neutral S_0 ground state of anthracene recorded with the detachment wavelength 1064 nm are shown. The spectrum in red has been recorded with the old anion formation method by using electrons from a MCP-electron gun and the black spectrum with the new anion formation method (MDV) using the pulsed discharge in combination with a pulsed argon co-expansion. Compare the good agreement in the vibrational structure and the intensities. The black spectrum has a slightly better resolution, but also a somewhat higher hot-band contribution in comparison to the red spectrum. The hot band at the left side lies about 400 cm^{-1} below the origin transition. This should be a non-symmetrical out of plane vibration, which has in the anion a lower frequency than in the neutral S_0 state. It should be noted that the sequence hot-bands with the anion-to neutral vibrational quantum numbers 1-1 and 1-2 lie on the high-energy side of the cold-band transitions because the neutral molecule is stronger bound than the anion.

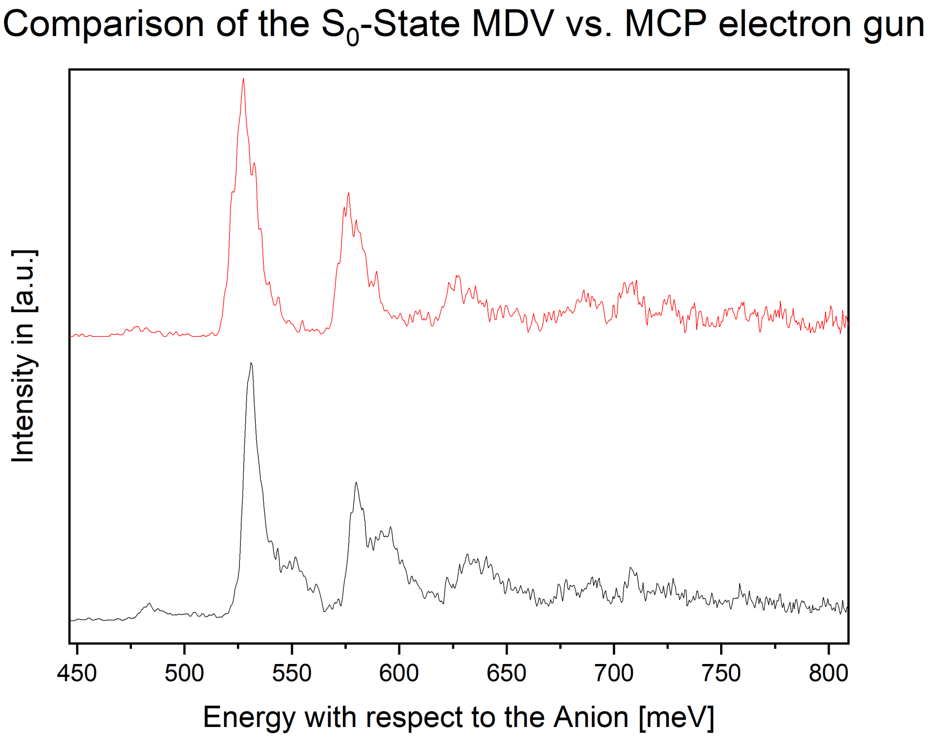

Figure 4.1: Photoelectron spectra of the anthracene radical anion. Red PE spectrum: Anions generated with the MCP-based electron gun. Black spectrum: Anions formed with the pulsed discharge. Note the hot-band contribution. For comparison see text.

Overview Over the Investigated Molecules

In this work 15 molecules have been investigated by PD-PE spectroscopy.

This chapter is organised as following:

- A first section is dedicated to the investigation of poly-aromatic hydrocarbons.
- A second section reports on the results on hetero-cyclic hydro-carbons.

4.1 Molecular Samples and the Subjects of Investigation

The major focus of the here presented spectroscopic measurements on the investigated neutral sample molecules is to determine electron affinities (EA) and the energetic positions of up-to-now not or only rarely investigated low-lying excited electronic states, such as for example especially the T_1 states and in some molecules also the T_2 state.

4.2 Heterocyclic Conjugated Compounds

Heterocylic compounds are molecules, which consist of π conjugated ring structures and therein embedded heteroatoms, such as for example oxygen, which could on one hand contribute orbitals to the π system, but could on the other hand also have lone pair orbitals which are supposed to stay local and not contribute to the de-localized π orbitals. Due to the hetero atoms, they i) can form hydrogen bonds to their environment, ii) have a enhanced chemical reactivity at the site of the hetero atom and iii) have a complex and dense excited state structure.

In this work the major interest lies in the electronic state effects, since after photo-excitation of the molecule they define the subsequent molecular answer such as photo-emission, photo-induced chemistry or simply deactivation of electronic energy to heat.

The excited electronic states of heterocyclic conjugated compounds can have two type of MO characters either $\pi\pi^*$ or $n\pi^*$. Since the absolute energies of these two types of states react differently on the increase of the π system or the position of the heteroatom, these derivatives offer a great variety of photophysics and photochemistry and therefore play an important role in various applicative fields of chemistry and physics.

In practice, heterocyclic compounds can be found in many kinds of research fields, for example:

- As pharmaceuticals [BBLN11]
- In key elements of molecular electronics (organic semi conductors, transistors and field effect transistors) [Ron92]
- As luminophores and fluorophores in OLEDs and organic solar cells[OSS+20]
- As dyes for biochemical investigations by imaging methods [OBP+]

- In preparative chemistry [JM08]

For most of these applications, a detailed knowledge of the electronic properties of the molecular compounds is necessary. Different spectroscopic methods have been used, in order to be able to gather a complete set of data on molecular properties, which then can be used by the researchers of the different fields .

Two molecules in which this effect was explicitly studied have been N-methyl-acridone (NM-AC) and N,N-dimethyl-quinacridone (NNM-QAC). The results on these two molecules are published in a master thesis by Jan Meissner and an article in JPC [MKMW21]. The author of this Ph. D. thesis was also involved in these measurements and is therefore co-author of the latter publication. The details of the results on NM-AC and NNM-QAC are not part of this work, but are mentioned in order to demonstrate the main effects which occur in hetero-cyclic molecules.

4.3 Molecules with Conjugated π Systems

Since Stefan Vossköter [VKMW15] and Paul Koniezcny [Pau17] already investigated medium-sized to large conjugated cyclic hydrocarbons, it is only consequent to enlarge the list of PAHs. In this work, it was tempting to simply continue the investigations of the same molecular class, but also to increase the size of the molecules as much as possible.
Especially interesting from a methodical point are those results which can be compared to results formerly achieved with a different anion source (see section above: 4.1).
Previously, it has been found out that some of the investigated molecules show quite an exceptional behaviour regarding the size of their singlet-triplet splitting [VKMW15]. Such a behaviour was found in the azulene molecule und could be explained by the overlap of the electron densities between the involved MOs.
So for this work the question was, whether it would be also possible to find new concepts or even rules by conducting broad investigations on different classes of sample molecules. In order to observe gradual changes, the sample molecules have to possess the same or similar molecular motives or core structures, but need to have systematic variations. The latter could be for example the substitution of phenyl rings in different positions or a simple increase of the π system.

4.4 Excited State Properties relevant for the Photophysics of a Molecule

As already motivated in the introduction, there are some properties of excited electronic states of molecules which are of primary importance for the understanding of the molecular dynamics after a photoexcitation. They are:

- The total electron spin of the state, typically for closed shell molecules either 1 or 0 .
- The energetic order of the electronic states, especially what triplet states lie below S_1.
- The relative energy difference between energetically neighbouring states, because close states can more efficiently couple.
- The molecular orbital character of these states (see below).

The most important key information is (see point 1) in the list above) the spin character of the individual electronic states: It is either a singlet ($S = 0$) or a triplet state ($S = 1$). The total electronic spin of the electronic states determines the efficiency with which they can be optically excited from the ground state S_0. Additionally, after the population of an excited state its decay by fluorescence or possible transfers between the excited states and to the S_0 state also influence excitation. Inter-spin processes are typically (with the exceptions below) less efficient than processes between states of the same spin. This statement holds for radiative processes such as absorption and fluorescence emission, but especially also for non-radiative processes such as intersystem crossing (ISC). Because for most of the molecules the excitation energies of the S_1 and possibly higher singlet states are known –for example by UV-Vis spectroscopy –, the question whether in a PD-PE spectrum a transition ends in a singlet or a triplet state can be directly answered: the singlet states should appear in the PD-PE and the UV-Vis spectra, but the triplet states should do s only in the PD-PE spectra.

The second key information is (see point 2 in the list above) the knowledge of the energetic order of the excited electronic states: only these molecular processes are efficiently possible, which energetically lead downhill. If an assignment of the structures in the PD-PE spectrum is found for a molecule, the order of the electronic states is known. If then for example the T_2 state lies close below the S_1 state, it can be assumed that in this molecule the fluorescence efficiency is considerably reduced by an ISC process to the T_2 state.

The third key information (see point 3 in the list above) is the orbital character of the electronic states: It could be for example either a $\pi\pi^*$ or a $n\pi^*$ state character. According to the rule of El Sayed ([ES68]) the ISC is considerably enhanced between singlet and triplet states of different MO character: ICS from a a $\pi\pi^*$ singlet to a $n\pi^*$ triplet state or in reverse the ICS from a $n\pi^*$ singlet to a $\pi\pi^*$ triplet state is in both cases very efficient and mostly prevents the fluorescence of the corresponding molecule. The orbital characters can typically not be derived from our PD-PE-spectra. The MO character of a state is hidden in subtle spectral features or can be only determined by theoretical calculations. For example the agreement or the disagreement with calculated Franck-Condon-factors from the anion ground state to an excited electronic state of the neutral molecule can give hints about the bond strength in the experimentally observed excited state (please note Chapter 2.3.2 anion excited States).

4.5 Experimental Problems Arising with the Investigation of Large Sized Molecules

Because the herein investigated sample molecules have extended, conjugated π-systems, they have all a positive EA, which is the main precondition for the application of anion PD-PES.

However, it has to be mentioned that severe problems can occur when one tries to transfer compounds into the gas phase, which have one or more hetero atoms incorporated :

- Most of the organic compounds with one or more hetero atom have very high sublimation temperatures.
- Unfortunately, in most cases nothing is known about their sublimation points, which could vary over a large temperature range.
- Some of them cannot be vaporized without chemical decomposition or denaturation, such as isomerisation or decay.
- Due to forming hydrogen bonds to a second identical sample molecule or water the monomer signal can be weak.

The above list motivates why spectroscopy on conjugated and hydrocarbons heterocyclic compounds is experimentally difficult and presumably also a reason for why such molecules have been not extensively investigated up-to-now.

4.5.1 Fluoro-Substituted-Indoles

Indole is the chromophore of the amino acid tryptophane. It has a high optical cross-section at about 300 nm and is supposed to play a key role in the photo-damage and photo-protection processes in skin [WS97]. The still unsolved problem in the neutral indole molecule is the exact electronic state order of the two lowest excited singlet states l_a and l_b. In un-substituted indole in the gas phase the l_b lies below the L_a state [BKP+10]. However, this electronic state order is reversed in polar solvents, because the L_a state is considerably more polar than the L_b state and therefore more strongly stabilized by the solvent dipoles.

In order to investigate this question in more detail, Michael Schmitt and co-workers [WWB+17] investigated 5-fluoro-indole 5Fi and 6-fluoro-indole 6Fi by high-resolution UV-laser-induced fluorescence excitation spectroscopy combined with rotationally-resolved Stark spectroscopy. The concept behind the usage of different fluorine substitution sites was, that the relative energetics of the electronic states and possibly even the electronic state order may be changed. For the structure and the numbering of the possible substitution sites see Figure 4.2.

Schmitt et al. [WWB+17] found out, that a change of the position of the fluorine atom resulted in a change of the mixing of the L_a state with levels of the L_b state. A direct observation of the L_a state origin was impossible up to now : it is assumed that its geometry differs so much from that of the S_0 state that its origin transition cannot be vertically excited. Due to the scientific and geographic vicinity of our two research groups, we became interested in this problem and investigated 5Fi and 6Fi with PD-PES.

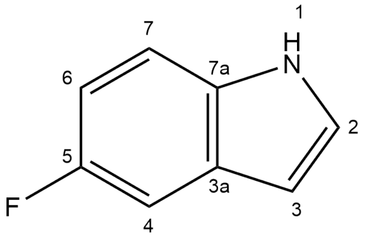

Figure 4.2: The structure of the 5-fluoro-indole (5Fi) molecule with the numbering of the other possible substitution sites (IUPAC).

The focus of this investigation was to solve the excited state riddle in indole, or even to observe the L_a state origin directly for the first time. This latter desire was based on experiences from the cold anion ground state the origin transitions of the neutral ground state and of the excited states are typically the most intense vibronic peaks. This can be understood by the fact that for molecules with large π systems typically the anion ground state geometry lies in-between the geometry of the S_0 state and the geometries of the excited electronic states of the neutral molecules (see chapter 2).

As mentioned above, our main motivation to investigate fluoro-indoles by anion-PD-PES had been the hope to directly access the up-to-now not observed origin transition of the L_a state. In addition to this, one could as side effects determine the EA and the excitation energies of the two triplet states which by MO configuration correspond to the L_a and the L_b singlet states.

These triplet states have great importance for the photo-stability of tryptophane. In an ensemble of tryptophane molecules 30 per cent of a produced S_1 population undergoes ISC, presumably first to T_2 which by subsequent IC relaxes to the T_1 state. This lowest triplet state has an unusual long lifetime of seconds and can undergo intermolecular spin exchange for example with O_2 [WS97] or intermolecular chemistry.

Since indole itself is supposed to have a slightly negative EA [BBX+16] and is therefore not able to stabilize a surplus electron, our expectation was, that one substituted fluorine atom should withdraw electron density from the π system and by this bring the EA to a positive value. The surplus electron would then reside in the LUMO π^*, and by this form a valence-bound radical anion.

This expectation turned out to not be the case, neither for 5Fi nor for 6Fi. As reported in the next Chapters, for both molecules we only observed anions where the surplus electron is very weakly bound, presumably by a physical binding in a dipole-bound state.

A molecule can offer a dipole-bound state for a surplus electron if the dipole of the molecule exceeds 2.0 Debye [ACBD+97],[LCG+20]. It is a state where the surplus electron is embedded in a very large diffuse orbital and always remains on the positive side of the molecule. Hence molecular rotation and the electron motion are coupled, which leads to the situation that typically only one dipole-bound state is possible . This is in contrast to Rydberg states, where the electron can orbit the positive core and the number of Rydberg states reaches infinity.

Because dipole-bound states are rather seldom and are therefore rather exotic, here the reversal of the typical order in which experimental results and their theoretical consequences are presented was applied. In the following, a first listing of the special properties of dipole-bound anions and the corresponding experimental findings, which support and prove the dipole bound character in 5Fi and 6Fi are displayed.

The dipole-bound nature of the surplus electron in the fluoro-substituted indoles is derived from the facts that:

- The dipole moments of both molecules exceed the threshold value for the existence of dipole-bound states (details see below).

- The EA observed in the PD-PE spectra is very small.
- The anion-to-neutral geometry change derived form the vibronic transitions in the PD-PE spectra is very small and
- The photodetachment behaviour follows a p-wave detachment, as expected for the detachment of dipole-bound states (see below) [San14].

The most important point in the above list is that high-resolution gas phase data of M. Schmitt and co-workers [WWB$^+$17] showed that the dipole moments of 5Fi and 6Fi in their neutral ground states have values of 3.27 and 2.53 Debye, respectively. Hence, the dipole moments of both molecules considerably exceed the theoretical threshold of 2.0 Debye for the existence of dipole-bound states (see Chapter 2.3). This experimental finding is already the proof that dipole-bound states exist for both molecules. The experimental findings to the other three points in the above list then prove that these dipole-bound states can be indeed populated and stabilized by the discharge anion formation method.
The fact that for 5Fi and 6Fi only dipole-bound anions have been found is an unfortunate situation regarding the initial goal to access the neutral excited states by PD-PE spectroscopy. In a dipole-bound state the surplus electron is essentially outside the molecule. The removal of this weakly bound electron or an other electron from an occupied molecular orbital does not result in a MO configuration of an excited electronic state. Hence PD-PES applied to dipole-bound molecular anions does not provide data on excited electronic neutral states.
It turned out, that in the pulsed discharge many low-energy electrons are formed, which can be efficiently captured into a weakly bound state. This turned out to be interesting for itself. The main question here is, how a discharge, which up-to-now was assumed to be always crude and brutal, can efficiently produce such weakly-bound dipole-bound molecular anions.

4.5.2 The Influence of the Discharge Pulse Width on the Anion Mass Spectra of 5Fi

Usually, if discharges are used for ion formation, the observation is, that manifold fragment ions are formed. This is presumably caused by the fact that in discharges the charged particles are strongly accelerated by the high voltage ($3-4\ kV$), which is needed to ensure the ignition of the discharge. In such a high-voltage driven discharge the ions and electrons become fast and high-energetic and can easily form fragment ions by collisions . As shown in the following, this expected scenario is in strong contrast to our observation for a short-pulse discharge within a molecule rare gas co-expansion.

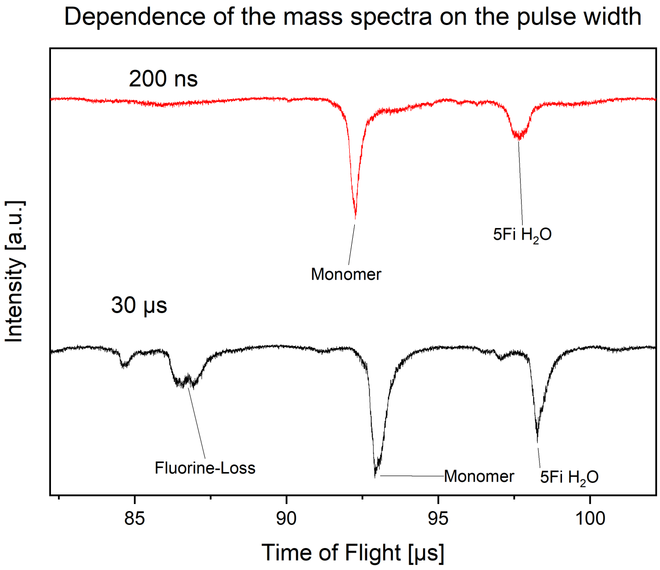

Figure 4.3: Two anion mass spectra of 6Fi when using different discharge times for the anion formation. MS spectrum with 200 ns (red spectrum at the top) and MS spectrum with 30 µs discharge time (black spectrum at the bottom). Nearly no fragments are observed in the red MS spectrum. The two very close-lying fragment peaks in the black spectrum are due to the loss of atomic fluorine. For further explanations see text.

To investigate the influence of the duration of the discharge in front of the pulsed inlet nozzle on the anion mass spectra, discharges of different pulse widths were ignited trough a pulsed co-expansion of 5Fi with argon in a separate experiment. Thereby for each discharge pulse width, the time delay of discharge pulse was optimized with respect to the gas pulse. The two traces for the ion intensity versus flight time in Figure 4.3 show that the fragment intensities in anion mass spectra which stem from pulsed discharges are in general relatively weak and dependent on the pulse width of the discharge used for the anion formation. The two most extreme cases of these experiment are displayed in Figure 4.3. For the mass spectrum on the top (red line) the discharge pulse width was 200 ns. For the spectrum at the bottom (black line) the discharge pulse width was 30 μs. The fragment ion intensity, the width and the positions of the peaks is affected by the discharge pulse length. The reason for the latter two observations is that the lower spectrum is about five times more intense: the broader pulse widths and the peak shifts result from the Coulomb-repulsion between the enormous number of anions. In the lower spectrum, the broad peak at a shorter arrival time can be attributed to indole fragment anions, where a loss of fluorine and/or possibly also a loss of hydrogen-flouride had taken place. The small single peak at shorter flight times could be due to loss of C_2H_2.

Whereas in general the fragmentation is an undesired side effect, the loss of the fluorine substituent may open up a new access route to deprotonated anionic species: If the fluorine-substituent is lost, a deprotonated indole molecule remains. Presumably the unsaturated site of the deprotonated indole is located at the former position of the fluorine substituent. It should be noted that this observation could be used as a novel pathway to access anions (as for example nucleic acid bases) with well-defined specific sites of deprotonation: simply using a precursor molecule in which a fluorine atom is substituted at a specific position, say position number 5. In the discharge then the fluorine atom is lost presumably as an anion. Under suitable conditions the remaining dehydrogenated molecule then can subsequently accept an electron and ends up to be nothing else but an indole-molecule deprotonated at the position number 5. Although not thoroughly investigated in this work, this could be a possible access to the spectroscopy of closed shell anions formed by deprotonation at a specific position. Other methods such as electrospray ionisation [WW00] would produce a deprotonation at the most acid site or if two sites have similar deprotonation energies and would lead to a statistical distribution.

Although the peak intensities in Figure 4.3 are much higher for the broad discharge pulse width, the usage of discharge pulses with widths of $200 - 350\ ns$ are applied for several reasons. One reason is that at these conditions practically no fragment ions are formed, which also indicates that the molecules are internally not heated intensively. The origin of this is the short on-time of the high voltage pulse used for the discharge: it transfers only a relatively small kinetic energy to the anions. Because the velocity difference of the anions against the neutral argon atoms is relatively small:

- In the on-going co-expansion a velocity equilibration between the sample anions and the argon carrier gas is achieved by the many low-energetic collisions with argon atoms.

- This velocity equilibration ensures that in the course of the expansion the anion-argon collisions become more and more low-energetic which results in a good internal cooling of the anions.

- The deceleration of the velocity of the anions by the argon is also important for quality of the the anion beam in the MS spectrometer. The velocity the anions still have after the formation process is perpendicular to the ion flight path of the TOF-MS. If this transversal velocity would be high, it would provoke extensive adjustments in order to not loose too many anions in the TOF flight path.

The fact that the ion signals in the MS are smaller and sharper in time when using the short discharge pulse is not a disadvantage for PD-PE spectroscopy: it is compressed in time and space allowing to acces all anions with the detachment laser. In case the ion cloud would be larger, not all anions would interact with the laser, but contribute to a space charge which would cause an electron energy error due to the Coulomb repulsion.
In conclusion, a short discharge pulse-width is used to reduce the fragment ion intensity and improve the cooling of the newly-formed internally hot anions.
This result is very important for a systematic adjustment of the pulsed discharge.

4.5.3 5-Fluoro-Indole

Although not a natural compound, 5Fi is of biological interest: it has been used as a mimic for DNA-bases and natural indole. Furthermore, in biochemistry it had been subject of extended research, for example as a growth-inhibitor in different fungi [Til78]. It is also a possible agent for an anti-bacterial bio-film and acts anti-viral. It also interferes with the quorum sensing systems of a manifold of bacterial pathogens [SSK$^+$20].

The PD-PE Spectrum of 5Fi

In Figure 4.4 the PD-PES spectrum of 5Fi recorded with the detachment laser wavelengths of 1064 nm is displayed. The spectrum features one predominant peak, which is attributed to the photodetachment from the vibration-less ground state of the 5Fi anion to the origin of the ground state of the corresponding intact neutral molecule. Only very small vibronic transitions are observed. The characteristics of the spectrum indicate that in the 5Fi anion the surplus electron resides in very weakly bound state, presumably in a dipole-bound state. The spectral features which support the presence of a dipole-bound state are are:

- The very low binding energy of 180 meV.

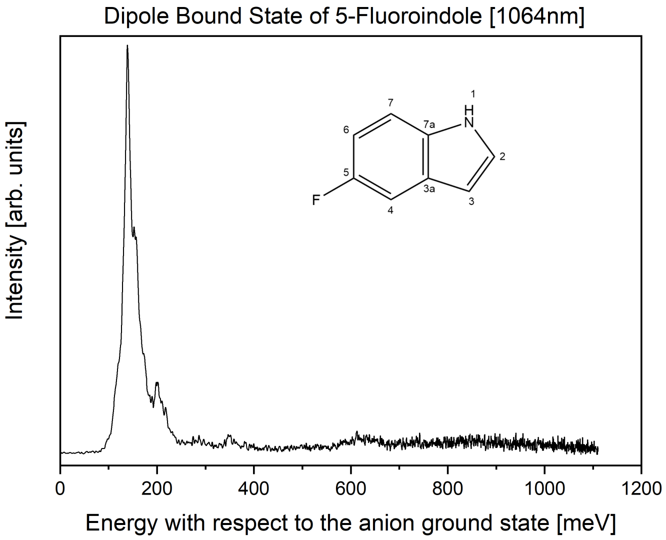

Figure 4.4: The PD-PE-spectrum of 5Fi. Note the small electron binding energy and the low vibrational activity in the transition

- The anion-to-neutral Franck-Condon-factors, which strongly prefer the transition to the origin of the neutral ground state. This shows that the anion and the neutral molecule have essentially the same valence bond character.

- The measured *p*-wave detachment (see Fig4.5), which is typical for dipole-bond anions.

For the third point on the list above, the angle of the linear polarized 1064 *nm* light of the laser beam was rotated with respect to the direction of the electron detection through some angles and the corresponding electron intensities were measured (see Figure 4.5). Remembering the detachment laser beam is perpendicular to the ion beam and the direction of electron detection. The laser polarization is then rotated with respect to the direction of the electron detection from 0° (parallel to the electron detection) to $-90°$ and $+90°$ (perpendicular to the electron detection). The electron detachment count rate in dependence on the angle was then recorded for some angles. As Figure 4.5 shows, the rotation of the laser polarisation greatly affects (approximately times five) the electron count rate. This is a clear *p*-wave detachment, as expected for a dipole-bound state. The angular distribution of photoelectrons is described in general by the equation[San14]:

$$I(\theta) = \alpha \cdot [1 + \beta \cdot P_2(cos(\theta))] \tag{4.1}$$

$I(\theta)$:	Intensity $[a.u]$
α:	normalization constant $[a.u]$
β:	anisotropy constant $[a.u]$
θ:	Polarisation angle [°]
P_2:	second order legendre polynom

The second order Legendre-polynome is defined by $P_2(cos(\theta)) = \frac{1}{2} \cdot (3cos^2(\theta) - 1)$. The normalization constant here is proportional to the resulting intensity and the β-constant is ranging from -1(for a perpendicular transition) uo to $+2$ (for a parallel transition).

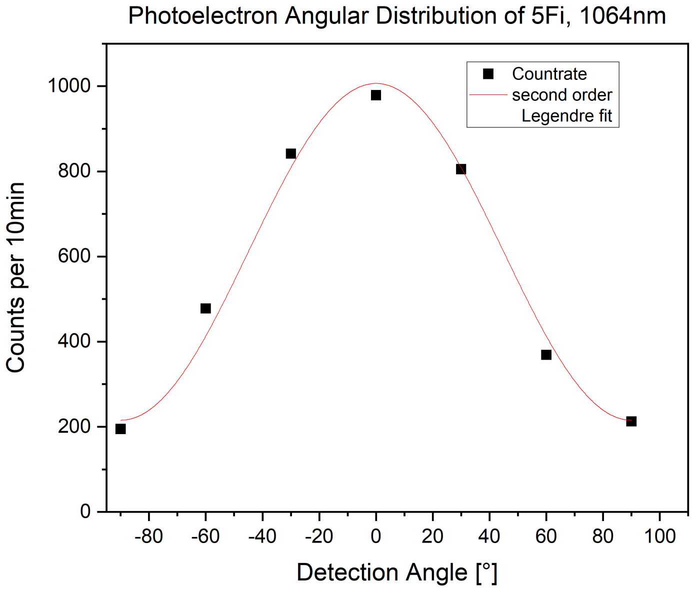

Figure 4.5: Detachment intensity versus the direction of the linear polarisation of the laser. The count rate of the photo-ejected electrons strongly depends on the polarisation angle of the linear polarized light of the laser. This clearly further supports the electron binding in a dipole-bound state. The fitting curve is given by equation 4.1 .

From the polarization data, the β-value 1.10 is determined. This means a strong preference for an electron emission process parallel to the laser polarization. This behaviour supports a detachment from a dipole-bound state.

In conclusion, since the 5Fi and 6Fi molecules (see below) have a suitable dipole moment and their anions show all properties of a dipole-bound states, it can be assumed that in the pulsed discharge dipole-bound anions are formed.

Unfortunately, from the electron configuration of the dipole-bound anion it is not possible to accesses triplet states of the neutral molecule: the removal of the dipole-bound electron only leads to the ground state of the neutral molecule. To access higher excited electronic states the excitation of electrons in the neutral core are needed. By this excitation to dipole-bound states of the S_1 state [YZQ+21] could occur, which then ejects the electron after some time. Since the molecular core of the anion is neutral, the optical spin selection rules of the neutral molecule are also valid for the excitation of dipole-bound anions. The only advantage of such a anion photodetachment spectroscopy over UV-Vis spectroscopy of the neutral molecule is the mass-selection prior to spectroscopy and the access to open shell neutral molecules when one starts in deprotonated molecular anions.

The fact that in a pulsed discharge quite a great amount of dipole-bound anions can be formed is interesting in itself and was very surprising. In other groups (compare [LCG+20]) the formation of theses states is only possible by offering very low energetic electrons or even Rydberg electrons [CLG+18] for the attachment.

This leads to the conclusion that the short-pulsed anion formation method in a discharge can well produce many low-energy electrons.

Since in the mass spectra, water clusters as well as homo-multimeres (up to the trimer) appear, we also investigates the monomer-water clusters and molecular dimers by PD-PES.

4.5.4 PD-PE-Spectra of 5-Fluoro-Indol clusters

Since 5Fi has already a high dipole moment of 3.27 Debye, it is evident, that if further dipoles, such as that of a water molecule (1.8 Debye [GCL+97]), are attached to it the resulting total dipole of the cluster complex is a question of the geometrical structure of the molecular complex. In principal the individual dipole vectors of all molecules in the complex sum up in a vector summation. Hence, the total dipole moment of the complex can become smaller (below 2.1 Debye: no dipole-bound state possible) or considerably larger (a stronger-bound dipole-bound state exists) but theoretically also many cases in-between are possible.

If other effects are neglected two rod-like electrical dipoles would arrange head to tail and form either i) a linear configuration or ii) a side by side structure. In practice, however, an important additional restriction for the molecular cluster formation is, that the water molecule - if possible - tends to go to that site of the molecule which is best suited for a hydrogen-bonding. This could 5Fi theoretically be in the positions at i) the nitrogen atom or ii) at the fluorine atom. Presumably the most stable H-bond would be to the flourine atom. In this case one could speculate that also the dipole moments add almost constructive, assuming a in-plane geometric bounding.

Remembering that an anion solvation by a solvent dipole could also result in a valence-bound anion state of the sample molecule [SWS98]: the solvation energy of the surplus electron in the localized LUMO by the solvent molecule could be so high that this structure is lower in energy than that of the state "electron bound to a larger dipole ". This valence-bound effect shows up in the PD-PES of clusters as a very broad structure. This broadening can be well understood: the solvation energy of a localized charge is high in the anion, but the solvation energy in the neutral complex is small. This leads to different molecule-solvent equilibrium distances and orientations in the anion and the neutral complexes. This anion-to-neutral geometry shift in the intermolecular coordinate causes a broad spectrum for the electron detachment ([SWS98]). In conclusion: Sharp PD-PE spectra and small binding energies are a signature for a dipole-bound electron in the molecular comples and broad PD-PE spectra and high binding energies are typical for valence-bound electrons in the sample molecule stabilized by the solvent molecule.

In figure 4.6 the PD-PE spectra of the 5Fi monomer and five clusters are displayed.

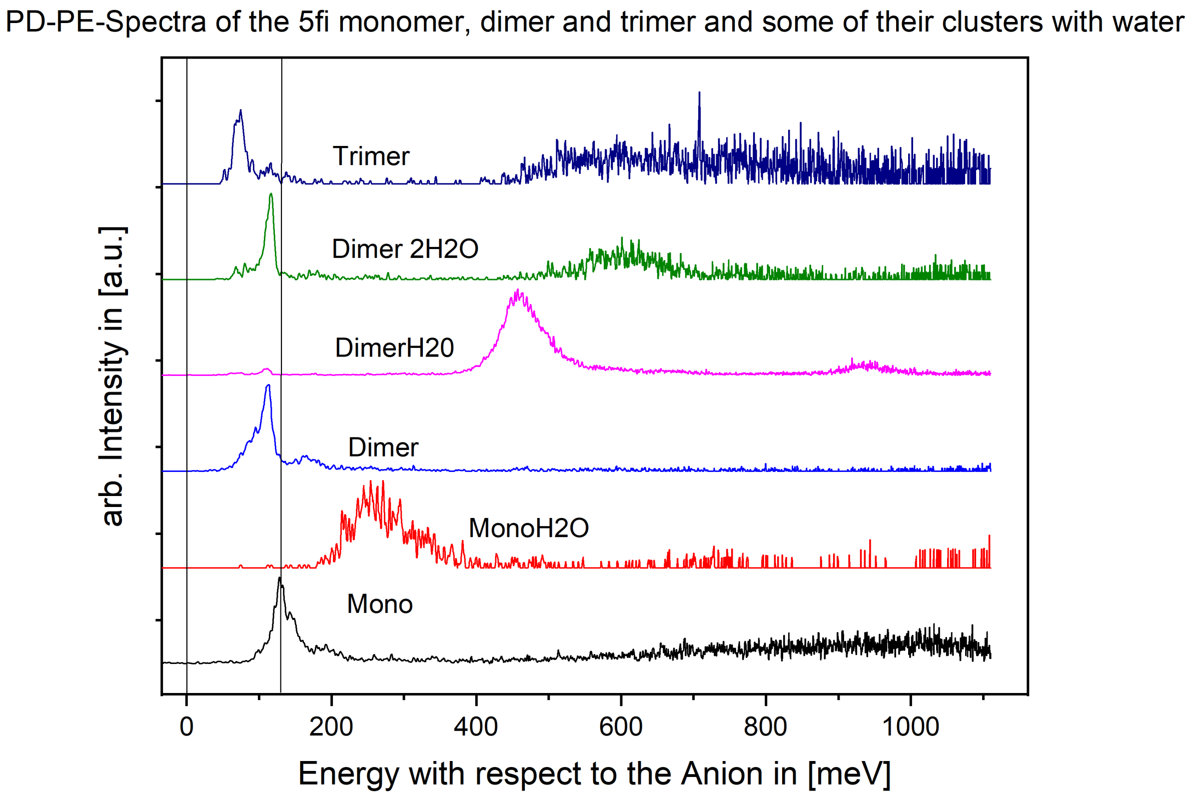

Figure 4.6: Juxtaposition of the PD-PE spectra of the monomer and some of its homo and hetero clusters. Note especially the changes in the electron binding energies: The binding energies decrease and increase.

In Figure 4.6 at a first glance its observable that for some complexes the EAs increase and the spectra become broad and for some cases the EA's differ not very much from that of the monomer but are somewhat smaller and the spectra are sharp. All EA values of the monomer and clusters are also collected in table 4.1.
At the bottom of 4.6, for comparison, the PD-PE-spectrum of the 5fi monomer (black) is repeated. The activity between $700 - 100$ meV seems to be due to a small vibrational excitation, a metastable auto-detachment or noise.
The red plot visualizes the PE spectrum of the $5Fi - H_2O$-cluster. Note the shift of about 150 meV to a higher energy in respect to the monomer and the remarkable increase in the width of the first peak. The electron is obviously stronger bound in the cluster than in the monomer anion. The EA of about 220 meV is rather high for a dipole-bound state. The width of the peak can be due to the high flexibility of the single attached water, which results in many low-energetic non-resolved vibrations. Since, the vibrational activity concerning intra-molecular 5Fi vibrations is still small, the removed electron seems still to come from a dipole-bound state.
The light blue curve is the spectrum of the 5fi dimer. Its S_0 origin position is slightly shifted to a lower-energy in comparison to the monomer and the structure is very sharp, much sharper than in the monomer-water cluster. This leads to the conclusion that i) the dimer complex forms a rigid structure ii) in which the electron is less bound than in the monomer and iii) the dimer does not form a charge resonance complex [PMLK14], which should result in a much higher EA and a broad spectrum. In conclusion, the electron is trapped in a physically bound state of a rigidly bound dimer. This could be a π stacked dimer structure in a head-tail conformation. In this case speculation is possible whether the electron is bound in a quadrupole-bound state [LCP+19]. This would at least explain the sightly less binding energy in comparison to the monomer.
The 5Fi-dimer-water-cluster (magenta) PE-spectrum comprises a big surprise. It shows a large increase of the EA to 500 meV and a broader peak as the 5Fi monomer and dimer. This value is surprisingly different from that of the dimer and the monomer, and is very large for a dipole-bound state. This and also the presence of a molecular vibration may be an indication that the structure of the 5Fi dimer is considerably changed by the one water molecule attached. This tempts to propose that the dipole moments of the three molecules cooperatively bind the electron. The alternative, a charge resonance effect or a valence-bound state is, seems implausible, because one then would expect to see more vibrational activity in the intramolecular and intermolecular modes. In the case of a charge

resonance anion one would also expect a resonant excitation from the bound CR ground state to the anti-bonding CR state, leading to auto-detachment or dissociation. In the latter case the formed monomer anion could be detached by a second photon which can not be observed.

The green spectrum shows the PES of the dimer-2 $\cdot$ H_2O-cluster. Interestingly its EA position jumps back to that of the 5Fi dimer. This energetic agreement is so striking, that one could think of a two-photon detachment: First an anti-bonding charge resonance state is excited with a first photon and then the anion cluster decays and with a second photon the remaining dipole-bound monomer is detached [SWS98]. This riddle can, however, not be solved without theoretical calculations.

In this series, the 5Fi trimer seems to offer the weakest binding of all investigated clusters for the electron. This could have many reasons, such as for example that the trimer forms a three-dimensional triangle structure, trapping the charge within the three fluoro-substituents.

A more precise interpretation on the structure of the clusters can not be made so far, as there are no computational data available concerning the structures of the complexes.

Such calculations would be, however, very important since the "dipole moment" is an approximation for the electric field a polar molecule causes, which strictly applies only in the far-field. This means that distance in which the approximation can be used should be considerably larger that the size of the dipole ([Dra08]). Strictly seen in a dipole-bound anion this distance requirement is violated.

In a dipole-bound state the electron can indeed move in a rather large and diffuse orbital. However, the question arises, whether the electron indeed is far enough outside of the molecule most of the time or the cluster in order that the dipole approximation is reasonable. The same question arises also for the clusters where the dipole possibly increases in geometric size by a factor of two in comparison to the monomer. We cannot solve this problem on the basis of our measurements. The plots of the EA values of the clusters, however, show that interesting effects are going on and might be worth to be investigated.

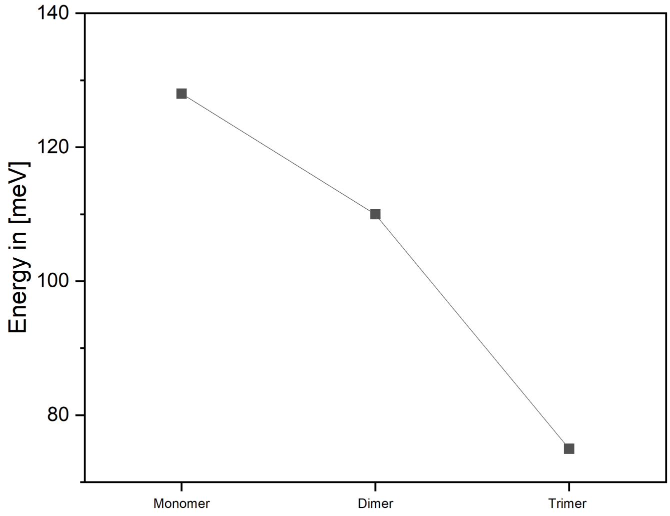

Figure 4.7: Plot of the binding energies of the species. Note the steady decrease in binding energy up to the trimer.

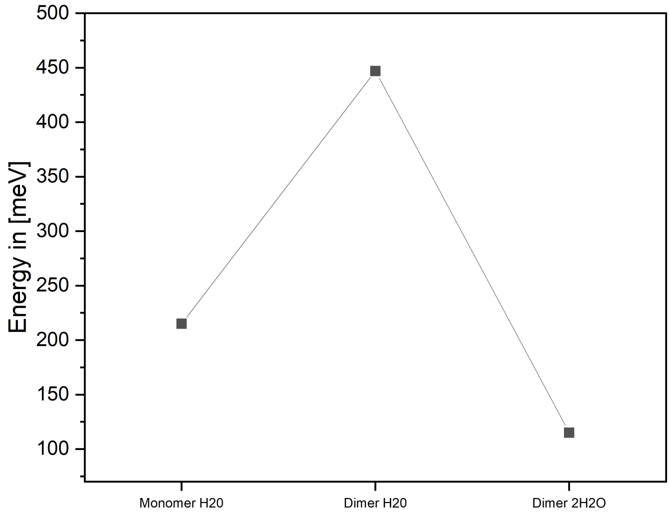

Figure 4.8: Plot of the binding energies of the species. Note the extraordinary increase in binding energy in the dimer-water cluster.

In a direct comparison, the transition from the monomer to the dimer and to the trimer of 5Fi results in a decrease of the electron binding energy, a weaker stabilisation of the additional charge. This is difficult to understand, if one thinks about possible cluster

Table 4.1: energy values of the 5Fi clusters.

species	energy [meV]
$5Fi$	128
$5Fi \cdot H_2O$	215
$5Fi_2$	110
$5Fi_2 \cdot H_2O$	447
$5Fi_2 \cdot 2H_2O$	115
$5Fi_3$	75

structures which produce gradually lower dipole moments with the increase in the cluster size.

Interestingly the first attachment of a water molecule to 5Fi considerably increases the binding energy, but a second water brings this effect to zero. This clearly has to be due to a cooperative effect of the two molecular dipoles. Unfortunately the trimer-water cluster and the monomer-$2H_2O$-cluster had only a minuscule peak height in the mass spectrum, so that it was impossible to record detachment spectra.

Although it has to be emphasized, that the main subject of this work is the access to triplet states of neutral molecules, it seems that we accidental entered a new interesting research field. Due to the limited time available, this research was put aside and instead a proposal for a cooperation with Prof. Kit Bowen was made, who is an expert in the field of dipole-bound and quadrupole-bound molecular anions.

6-Fluoroindole

As already mentioned above, the main interest of this work is to unravel energetic positions of excited electronic states. The possibility that 6Fi has a valence-bound anion in addition to a dipole-bound state could not be ruled out. Hence 6Fi is a logical follow up species after the analysis of 5Fi. 6Fi got also characterised concerning a $L_a - L_b$-mixing by Schmitt and co-workers.

It also has - similar to 5Fi - an application as inhibitor of the bio-synthesis of indole-3-acetic acid in plants[LMDCQ10]. Nevertheless the spectrum again only featured a dipole bound state, although its value is a bit higher with around 203 meV which is featured in Figure 4.10. It is possible that the higher energy value, indicates that the stability of the DB-state is increased compared to 5Fi.

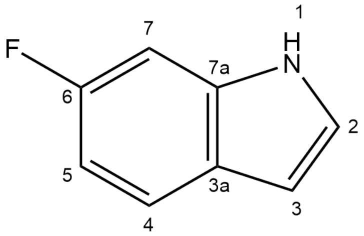

Figure 4.9: Atomic numbering of the 6FI molecule (IUPAC).

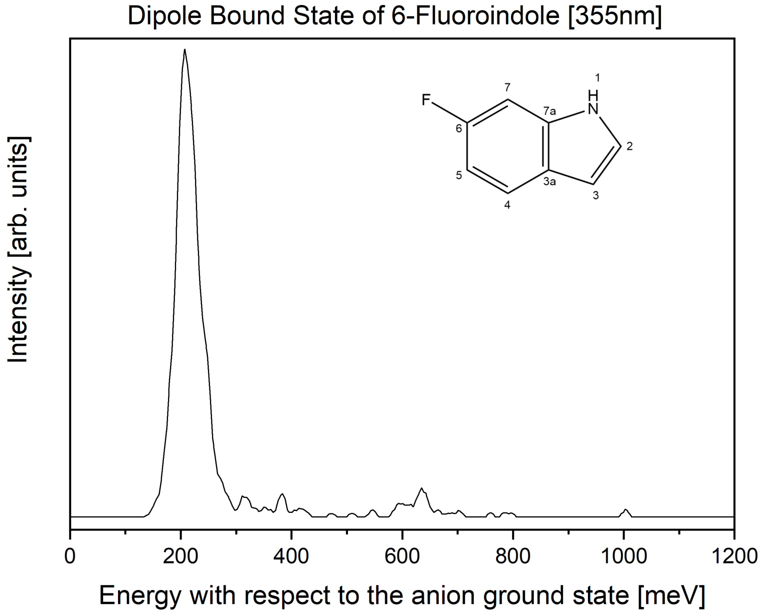

Figure 4.10: PD-PE spectrum of 6Fi: The small binding energy and the low vibrational activity indicates that a dipole-bound anion is detached.

Conclusion

Taking the measurements of 5Fi and 6Fi, it is for both molecules obviously not possible to form valence-bound anions. It was possible to gain some insights into the properties of the pulsed-discharge anion formation method. Surprisingly even states with a minuscule binding energy for the surplus electron can be formed. This was not expected beforehand, as in discharges usually very harsh conditions exist. This means, the short-pulse discharge in front of a pulsed high-pressure gas nozzle seems to be a valuable tool for the formation of all kind of intact radical anions. Furthermore the cluster PD-PE spectra of 5Fi with other 5Fi units and with water molecules provide significant shifts which are correlated to structural motives of the clusters but may also correlated with new binding situations which lie beyond dipole and quadrupole approximations. To obtain a more detailed understanding whether the explanation of the above cluster spectra has more a geometric or an electronic background high-quality calculations of the anion clusters are needed.

4.5.5 9H-Fluorenone

In general 9H-fluorenone (often simply termed fluorenone, see Figure 4.11) is used as a dye for liquid chromatography due to its yellow bright colour. But also other research fields are interested in this molecule, such as biochemistry and medicine. Fluorenone is assumed to be carcinogenic, which so far was not explicitly confirmed [Nik02]. The mitogenic activity of fluorenone and its derivatives is the reason that they are tested as virostatica [CDA$^+$13]. They also gained popularity in organic electronics as material which shows a thermally activated delayed fluorescence with an orange emission[YTG$^+$19].

Interestingly f9one is one of the molecules in which the fluorescence intensity strongly depends on the polarity of the solvent environment. It has a S_1 lifetime of 0.4 ns and a very low fluorescence quantum efficiency of 0.04 % in cyclohexane and a lifetime of 17.8 ns and quantum efficiency of2.7 % in acetone.[GMK$^+$14] Because the S_1 state has a n^* character [MIH02], this solvent behaviour is expected in the gas phase because the T_1 state is a $\pi\pi^*$ state. Hence, fluorenone fulfils the El Sayed rule ([ES68]) conditions for a fast ISC (see also Chapter 4.1). The situation seems to be, however, more complicated because also a $n\pi^*$ triplet state should be situated below S_1.[GMK$^+$14] Ghosh et al. [GMK$^+$14] even proposed that in gas phase three triplet states are be below S_1.

Figure 4.12 shows the PD-PE composite spectrum of 9H-fluorenone (f9one), for which two PD-PE spectra recorded with 532 nm and 213 nm have been mounted together (see arrow at 2000 meV). The first distinctive broad hump between 1000 and 2000 meV has a sharp peak at its beginning at 1072 meV. This peak is attributed to the transition from the cold anion to the origin of the S_0 state of the neutral molecule. The energetic position of this peak is the EA value of f9one. The EA of f9one is relatively high in comparison to other heterocyclic compounds [VKMW15]. Right after the onset of the S_0 state appears a very broad structure (termed AD) which has no corresponding equivalent behind the origin transitions of the excited electronic states in the spectrum. This indicates that its appearance is an effect of the wavelength of 532 nm, which was used for the detachment

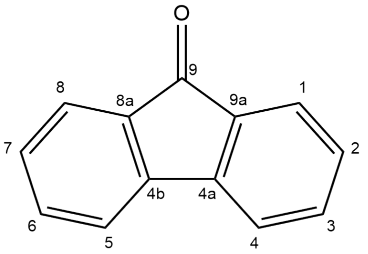

Figure 4.11: chemical structure and atomic numbering of 9H-fluorenone

when recording this part of the spectrum. The "hill" is therefore attributed to electrons, which stem from auto-detachment (AD) from an anion excited electronic state, which was obviously accidentally excited by the detachment laser: the excited vibronic states of this anion-excited state strongly influence and determine the Franck-Condon factors to the S_0 state. This auto-detachment results in the broad structure. In conclusion, for the PD-PE spectrum recorded with 532 nm there are two contributions: i) the direct detachment into the continuum, which provides the sharp origin transition to S_0 and ii) an indirect detachment via vibrations of an anion excited electronic state, which provides the broad hump.

The next steep onset corresponds to the origin transition of the triplet T_1 state at 2056 meV above the S_0 state (upper scale) with some vibrational progression. This value agrees well with the literature value 2207 meV in paraffin at low temperatures. [?] It is probably followed by the second excited triplet state T_2 with a very distinctive sharp peak at 2472 meV. The shape of this peak is so different to the first peak of the T_1 state that a possible assignment to a $n\pi^*$ transition is tempting. Note that Ghosh et al. postulated that such a triplet state should lie below S_1 [GMK+14]. The next rise behind the sharp peak could then be T_3(marked X), which is then expected to have again $\pi\pi^*$ character. The assignment of T_2 and T_3 is clearly speculative and inspired by the work of Ghosh et al.: the signal to noise ratio is not very good in order to postulate tree triplet states.

Remarkable is then the onset of the S_1-state at 2984 meV which is somewhat higher than the previous peaks.

So far regarding the obtained spectrum, the excited electronic states are embedded into a background structure. This structure is ether due to an AD[1] state or due to photo-induced background electrons from the inner walls of the spectrometer. In table 4.2 all literature values as well the values determined in this work are listed. The position of the singlet S_1 state as determined by PD-PES is in good agreement with previous data. Concerning the triplet T_1 there is some discrepancy with the literature value. Looking at Figure 4.12, assuming that the first steep onset after the S_0 state and the AD structure should be the first excited state – the triplet T_1 state is possible. Soep et al.[SMB+16] have been performing two-colour multi-photon-ionization with two time-delayed femtosecond laser pulses. The first laser populates the S_1 state, which then decays – if one follows our assignment – by ISC to the T_2 and then presumably by IC to the T_1 state. The second laser pulse then performs ionization from the T_1 state to the cation. The energy balance of the photons and the kinetic energy of the electron then gives an upper limit of 2311 meV for the position

---

[1] auto detachment

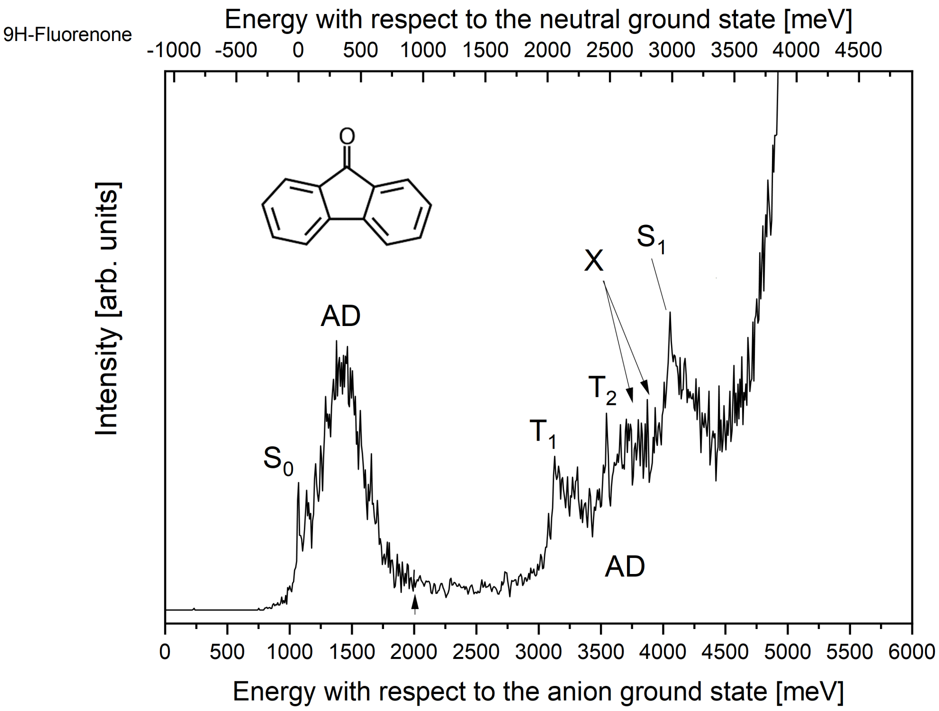

Figure 4.12: PD-PE overview spectrum of 9H-Fluorenone. For this spectrum two spectra recorded with the detachment wavelengths 532 nm and 213 nm have been mounted together at the arrow (2000 meV). Note the two energy scales which refer to the neutral ground state S_0 (upper axis) and to the anion ground state (lower axis).

of the T_1 state position. This value is 255 meV higher than the measured value, which is no contradiction, since it was termed "upper limit". Considering that their experiment took place in the gas phase, it becomes evident that due to energy conservation, after ISC and IC their T_1 state is enormously vibrational hot (932 meV or more vibrational energy), which could well account for the deviation. Also the T_2-state in Figure 4.11 fits the expectation of being a distinct peak as a $n\pi^*$-transition which should be "bright" in the PD-PES spectra. This is the first time that a triplet state with a lifetime shorter than 200ns [SMB+16]) was observed by PD-PES. Note that the intensities and shapes of the spectra do not rely on lifetime as long as a few picoseconds are not fallen short of. In the gas phase the S_2 $\pi\pi^*$ state is assumed to be very close above S_1 state which has a $n\pi^*$ character [MIH02]. Since no observation of two independent structures in this energy range took place and since the splitting of the two states should be small, it can be assumed that due to the limited resolution of about 5meV both states seem to be superimposed in this spectrum. The most prominent peak in that energy range of the PD-PES lies at 2984 meV and therefore 107 meV too high in comparison to the accurate value determined in the gas phase with laser excitation. This deviation motivates to assign the peak at 2984 meV to the S_2 $\pi\pi^*$ state, which should be also considerably more intense than the S_1 $n\pi^*$ state. The S_1 state than could be one of the small peaks in front of the transition to S_2 (Area marked X.). Without further investigations (theoretical computations mainly) a reassuring assignment of the excited states above the T_1-state cannot be made.

Table 4.2: Overview of the electronic states of f9one. The values without citation are from this work. All values are indicated in meV

electronic state	configuration (ratio)	literature		experimental	
		theory	experiment	ΔE_{S_0}	ΔE_{D_0}
S_0/eA	-				1072
T_1	$\pi\pi*$	2220[d]	2311[a], 2200[e]	2056	3128
T_2	$n\pi*$	-	-	2472	3544
T_3	$\pi\pi*$	-	-	X	X
S_1	$n\pi*$		2877 [a]2918[b]2877[c]	X	X
S_2	$\pi\pi*$		-	2984	4056

[a] [SMB$^+$16] multiphoton ionization
[b] [ZBV74] in hexane matrices
[c] [MIH02] gas phase fluorescence
[d] [KHF$^+$11] TD-DFT at B3LYP
[e] [GMK$^+$14] in solvents

4.5.6 Dibenzofurane

As other heterocyclic compounds, also dibenzofurane (DBF) is subject of current research. Concerning the chemical structure see Figure 4.13. Beside the fact that different spectroscopic methods have been applied to DBF, it is also a test sample investigated and used in biochemical experiments. It is tested in regard of the inhibition of the bio-synthesis in lichens under cadmium exposition and in consideration for a possible application in biomedicine as a transition product of the medulla [MMT16]. Its structural similarity to 9H-fluorenone (f9one) made it interesting for a comparison of the electronic state systems of the two molecules. In the Ph. D. Thesis of Fabian Drenkow –a former member of our group– [Fab] DBF was ionized with two-photon REMPI[2]. The electrons removed in this step have been analysed by photoelectron spectroscopy and the ions by mass spectrometry. This means that this molecule was also well-known in the authors working group, an additional reason to decide to investigate DBF with PD-PES. Since nothing was known concerning the first triplet states of DBF, it was desirable to obtain new insights regarding the position of the excited states. The PD-PES overview spectrum of DBF is presented in figure 4.14. It is composed of sections of three spectra recorded with the wavelengths 1064 *nm*, 266 *nm* and 213 *nm*. The transition points are marked by arrows. The first peak corresponds – as always – to the transition from the anion ground state to the S_0 state of the neutral molecule. Its first peak energy of 359meV defines the EA of DBF. The strongest and sharpest peak of the spectrum lies on the very right of Figure 4.14. Due to the work of Drenkow and others, who found the S_1 state at an excitation energy of 4173 meV above the S_0 state, it is straight forward to assign this sharp and intense PD-PE peak to the transition to the first excited singlet state S_1. This resulting S_0 -to- S_1 transition energy of 4207 meV which is quite somewhat higher than the literature value. The resulting PE energy error of 34 *me*V seems at first thought quite large. Considering that this value is determined as a difference between the EA value and the S_1 energy in respect

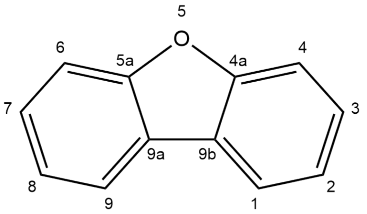

Figure 4.13: The chemical structure and the atomic numbering of dibenzofurane (DBF)

---

[2] resonance enhanced multi photon ionisation

to the anion ground state. Hence the PES error appears twice. In the neutral molecule this S_1 state is formed by excitation of an electron from the n_O lone pair orbital to the π^* orbital. This excitation is fully allowed. Since from the anion the transition to the S_1 state is just the removal of an electron from the lone pair orbital, the binding situation in DBF is by this nearly not changed. It is therefore reasonable to assume that the geometries of the anion and the neutral S_1 state are very similar and that the corresponding FC factors should strongly prefer the origin transition, resulting in one sharp peak. This seems to be the case, since it seems that no vibronic transitions in the S_1 spectrum is observed. A closer look, however, makes clear that the electrons corresponding to the vibronic states of S_1 would be so low-energetic that they are no more detected.

This S_1 assignment suggests that the two peaks at lower energies, are the triplet states T_1 and T_2. The transitions to the first and the second triplet state have both distinct onsets, but are both broad. The onset of the first triplet state at 3073 meV and that of the second triplet state at 3769 meV above the S_0. The fact that both electronic transitions possess a broad non-resolved vibrational structure in the PD-PE spectrum is strange since one of the two –presumably T_2 – has the same MO configuration than S_1 and should therefore be sharp. Concerning the $\pi\pi^*$ triplet state –presumably T_1 – forwarding the argument that the broad PD-PES structure is due to the true FC factors from the anion seems possible. Note that the π system of DBF is not yet so large that the surplus electron is already so strongly diluted in the molecule that its effect on an individual C-C bond is completely washed out - as expected for very large π systems. This argument does, however, not hold for T_2. This means that there has to be in addition also a contribution of auto-detachment to this spectrum. Which of the two effects is predominant for which state remains unclear. Taking the symmetry character of both triplet states into account, it is not surprising that they have not been observed before: they are both from the S_0 state spin- and symmetry-forbidden. The reason that they can be observed in this PD-PE spectrum, is that the molecular orbital configuration of the anion is such that in both cases the excitation of one electron accesses directly the relevant triplet state.

Most probable a wavelength could be found which is more suitable and would allow to avoid the AD-states. A tuning of wavelengths is unfortunately currently not available. In the 213 nm section of the PD-PE spectrum the S_2-state appears as a very sharp peak on top of a huge background. It is slightly red-shifted in comparison to the literature value 4975 meV [BVZ73].

In conclusion, it was for DBF possible for the first time to measure the electron affinity, as well as the energetic positions of the first two triplet states. The agreement of the

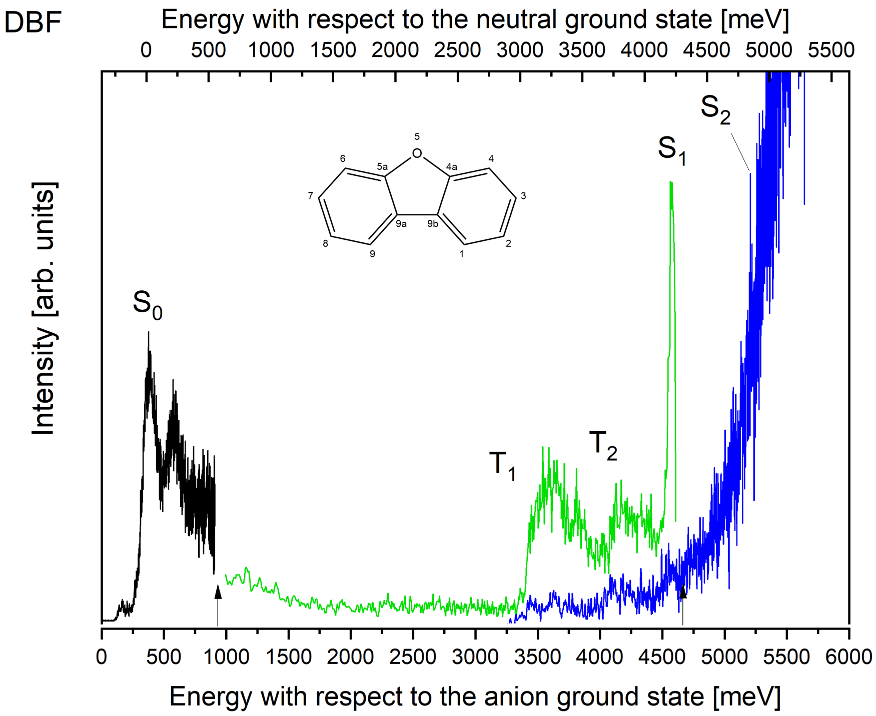

Figure 4.14: PD-PE overview spectrum of DBF. For the three sub-spectra the wavelengths 1064 nm, 266 nm and 213 nmhave been used. The connection points lie at 1000 meV and 4600 meV.Additionally the 213 nm spectrum is below the 266 nm to visualize the accordance of the spectra.

Table 4.3: Overview over the electronic states of DBF. The non-cited energy values stem from this work. All values are given in meV

electronic state	configuration (ratio)	literature		experimental	
(symmetry)		theory	experimental	ΔE_{S_0}	ΔE_{D_0}
$S_0(^1A_1)$/eA	-				359
$T_1(^3B_2)$	-	3379[b]		3073	3432
T_2 $(^3A_1)$	-	3921[b]	-	3769	4128
S_1 $(^1A_1)$		4442[b]	4173[a]	4207	4566
S_2 $(^1B_2)$			4975[c]	4849	5208

[a] [Fab] REMPI
[b] [GKKN09] model of vibronic induced spin-orbit coupling
[c] [BVZ73] in n-heptane

PD-PES energies of the first two singlet states with the literature values is acceptable. The computed energies of Bree et al. overestimate the excited state energies [Fab], by a systematic error of $+260 meV$.

4.5.7 The Comparison of DBF and f9one

The two substances DBF and f9one have both two conjugated rings and an extended π system. They differ, however, in the way the oxygen can participate at the π system: In DBF the oxygen is integrated into the ring system and in f9one it is in the keto-group, which can with the C=O π bond participate at the π system . In Figure 4.15 the energies (y axis) of the electronic states (abstract x axis) of DBF and f9one are compared. The S_0 state is chosen as zero point of the energy y scale. The electronic states are aligned in equidistant units from left to right (x axis). Concerning the EAs (see energies at D_0): f9one has the higher EA of 1074 meV and the EA difference to DBF is 713 meV. An EA difference of this high value is rather unexpected. It was clear that there should be a difference, as in f9one i) the keto-group participates at the π system increasing its size and ii) the oxygen is able to considerably draw electron density out of the ring system. Thus facilitating the binding of an additional electron in the π^* orbital. Nevertheless the value seems quite high, as it is in the range of the EA of pentacene (see next chapter).

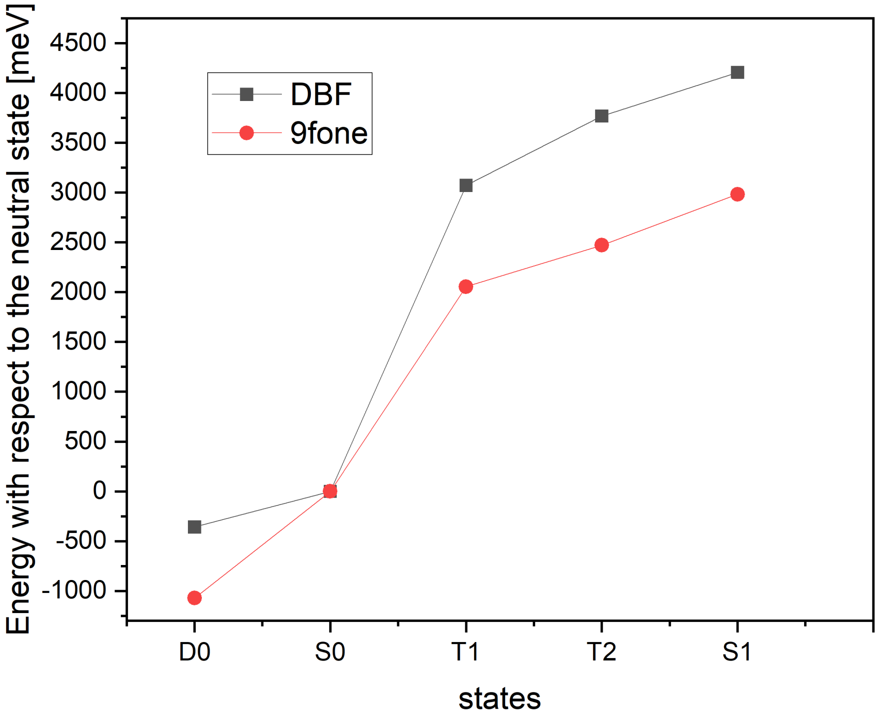

Figure 4.15: Comparison of the electronic state energies in DBF and f9one: On the x-axis: EA, T_1, T_2 and S_1. On the y axis the energy in meV. Note that the S_0 state is the energy reference point "zero energy" for both molecules.

The much smaller EA in DBF could be due to the fact that the lone pair electrons of the oxygen directly participate at the π system thus providing a higher electron density to the ring system. This seems to hamper the hosting of a surplus electron, leading to a smaller EA.

In both molecules two triplet states are below the first singlet state. The fact that in f9one versus DBF the excited states lie systematic lower in respect to the S_0 state is interesting. One question arising from this observation, which is a direct result of the scheme in Figure 4.15, is, whether the low anion ground state energy is correlated with the low excited state energies in f9one. In any case one should keep this in mind, in order to see whether there might be a systematic rule in this. The state-to-state energy increase of both molecules seems to follow a linear growth with a slope of 0.3 eV per state.

4.6 Poly-Aromatic Hydro-Carbons (PAH's)

In the last few years PAH[3]'s gained more and more attention due to their carcinogenicity and –as a result of this–, their relevance in environmental analytics. They are typically present as waste products in practically all forms of combustions of organic materials, such as for example wood, oil, plastics or tobacco. In the meantime they are even used as benchmark molecules to characterize the level of urban pollution[PSO+17]. They are conjugated hydrocarbons, which consist of several up to numerous conjugated annealed rings. The rings can form complex structures (see coronene) and they can carry all kind of substitutions in different positions. In a sub-class of such hydrocarbons benzene rings are substituted in different positions. While the smaller PAH's are volatile at 100 or 150 °C, the larger ones are practically non-volatile and also quite difficult to be solved in solvents[CS13]. These larger PAH's are often adsorbed on small dust particles or even form such dust particles. Inhaling them can cause on the long term health problems.

Because of the very high temperatures which is needed to transfer them the into gas-phase (up to 350 °C) they were simply not found in former analytical mass-spectrometrical investigations.

As indicated above, many of the PAH's either are classified as "carcinogenic" or are - because they have not jet been characterized in detail - at least in suspicion of being hazardous. Benzo[a]pyrene for example is the main PAH component in cigarette smoke and is known to be highly carcinogenic [DPTP96]. Recent studies [MRS+20] propose a regular investigation of the PAH concentration in urine of adolescents and children as a marker for the pollution level in their immediate environment.

As a consequence, it is not surprising that PAH's are subject of numerous research works in many laboratories and in different scientific fields.

The Relevance of Electron Affinity and Excited Electronic States

Most of the applications of PAH's rely on the interaction of photons, or charges and both photon and charges with the molecules in a solvent or condensed phase.

PAH's are quite interesting as chromophores in dyes and are subject of investigations for the applications in organic solar cells, in organic light emitting diodes OLED[4], in organic electronic devices and in photochemistry. For example, it was shown that a ter-pyridine-substituted chyrsene has a high potential as electron transport layer in high-performance

---

[3] Poly aromatic Hydrocarbons

[4] Organic light transmitting Diode

OLED's recently[5].

As already discussed previously, the understanding of electronic and photo-physical properties of molecules is only possible if at least the order, the spin of the electronic states and even better the MO character would be known. As already outlined in chapter 2, due to the spin selection rules, singlet states are able to directly absorb or emit photons and triplet states only participate indirectly in the form that deactivate the population of the singlet states. The interplay between singlet and triplet states in excited state dynamics is complex and still a subject of intense investigations.

If it comes to the application of molecules in electronics, mostly properties such as the conductivity and charge separation are involved. For the electron conductivity and the charge separation in molecular dimers properties such data as ionisation energy and electron affinity are important. Whereas due to the many investigations with analytical mass spectrometry the ionization energies of many PAH's are known, only a few EA values exist taking typical databases into account like the NIST.

Concerning inter- or inter-molecular charge transfer states in PAH's, the number of experiments is very sparse. It is a fact that in many homogeneous crystals of hydrocarbons the fluorescence is very efficiently quenched and the molecules stay dark. In contrast to this, if the same molecules are isolated in solution they show a strong fluorescence. Many authors correlate this phenomenon with the existence of excitonic couplings between the S_1 states of neighbouring molecules. What is mostly over-locked is, that molecules with large π systems have low ionisation energies and high electron affinities. If the neighbouring molecules then are π-stacked and are close to each other, the intermolecular charge transfer state can lie below the S_1 state and efficiently cause its depopulation and quench the fluorescence. The assumption, that this mechanism is present in most of the non-fluorescing organic crystals can be made. Interestingly, in some of them the fluorescence can be re-gained by cooling the crystal. In a here proposed model, this means that the CT-state is slightly above the S_1 state at the neutral dimer geometry. Only by vibration the two molecules come for a short time closer to each other so that the energy of the inter-molecular CT state – which is strongly distance dependent – shifts below the S_1 and depopulates it. If the crystal is then cooled, the amplitude of the inter-molecular vibrations diminishes. It is then only a question of temperature that the CT fails and the fluorescence recovers. It is evident that for the calculation of the energy of the intra- or inter-molecular charge transfer states beside the ionisation energy – which is often known– the EA value is necessary.

---

[5] [OSS$^+$20]

In addition beside providing data for applications, experimental values of electron affinities of large aromatic molecules provide benchmark data for the theorists. Since electron affinities are mostly due to electron correlation effects, and since molecules with large π-systems have many electrons, the calculations of electron affinities is a test for the quality of theoretical methods.

4.6.1 Pyrene

The chemical structure of pyrene – also known as benzo-phenanthrene – is shown in the inset of Figure 4.16. It can be found in fuels and is a waste-product of combustion processes for example in tobacco- and oven-smoke. In the latter, the concentration is especially high, when wood with oleaginous materials are burned. It is likely to be carcinogenic and can be accumulated in organisms especially in the grease. The reason for this is its non-polarity, its high chemical stability and therefore its long biological persistence. Due to this special combination of properties it is considered as a dangerous PAH [MPW$^+$09].

Pyrene has been subject of several spectroscopic investigations in solution [KRH$^+$21] as well as in the gas phase [TR97]. Pyrene as a monomer shows a strong fluorescence at $455nm$ and has been used as a probing substance for the examination of local molecular organization [JFV$^+$10].

Pyrene dimes and multimers are especially interesting due to the excimer-formation (excited-dimer-formation) and the resulting strong red-shifted emission [FK54].

This excimer effects might have been the reason that the pyrene monomer and its homo-complexes have been subject of two independent investigations conducted also with the radical-anion PD-PES method. The group of Ando et al. were the first to investigate the electron affinities of pyrene and its homo-clusters [AKMN04]. Similar work was performed somewhat later by Kim et al. [KLS09]. The focus of these two investigations were not on the excited states of the monomer, but the question whether in the anion complexes the surplus electron is either shared by two or more active pyrene molecules or the electron resides on one pyrene molecule and the other molecules passively act as "solvents". Because of this goal the authors used only detachment wavelengths down to 355 nm and therefore only observed the T_1 state for the monomer. In addition their energy resolution was so low that the EA and energetic position of the T_1 state can only be vaguely determined.

One trivial reason to re-investigate pyrene in this work was the fact, that there were already publications to which the results can be compared. This decision was important for this work at that time, because recording the PD-PE spectra with i) the new discharge anion formation source and ii) with a photoelectron spectrometer which has a considerable higher resolution in comparison to the previous investigations was insightful. The primary goal was to investigate the properties of the pulsed discharge combined with a pulsed co-expansion of sample molecules with a high pressure of argon, as a novel source for intact and cold molecular radical anions.

In figure 4.2 our PD-PE spectrum of pyrene recorded with the above-described methods is shown. Three sharp peak structures with an at some distance following vibrational activity are observed, which are due to the transitions from the anion ground state to the S_0, the T_1 and the S_1 states of the neutral molecule. The assignments of these intense peaks can be directly derived from the fact that the S_1 position is already known [TR97]. The question is why for the electronic transitions such a strong vibrational activity is observed or whether there are other electronic states hidden under these structures. Note, that especially the transition to the T_2 state should also lie in this observation window. The spectral activity behind the T_1 state looks similar to that behind the S_1 state and both seem to be due to vibrations only. Note that interestingly the PD-PE spectrum looks similar to a typical REMPI spectrum of a molecule with a conjugated polycyclic rigid ring system: behind the origin transition there is a gap and then the intensity increases because there very many vibrations simultaneously contribute. The distances between these latter transitions is so small that they are not resolved and create a hump with sharp peaks on top. The gap between the origin transition is due to the fact that the molecule is rigid, and there are non many vibrational levels in this low.energetic energy range. Despite this possible scenario, since in such a large π system already almost diagonal FC factors are expected, the observed vibrational activities behind the origin transitions can also be due to the influence of an anion-excited state: a part of the laser excitation does not go to the continuum but excites resonantly an anion-excited vibronic state. This excited state of the anion is far above the detachment threshold and therefore un-stable and short-lived. When it emits the surplus electron the FC factors between this excited anion state and the neutral final state come into play. The probability that an excitation with a fixed laser frequency excites a vibration of this state and not the origin is rather high. In this case the resulting Franck-Condon factors for the subsequent electron emission to the neutral states provokes the excitations of many vibrations.

The intense peak at the right could be an experimental background or the transition to T_2 or to S_2. If this peak would be due to the S_1 state, immediately the question would arise where T_2 is located. Since there is also this spectral hump-like activity in the energy range between the T_1 and the S_1 states and above the S_1 state, you cannot derive, whether there is still the T_2 state hidden in this structure. Unfortunately theoretical data which could help to find the right assignments are missing.

The nature of the high peak at the end of the spectrum is unclear and therefore marked with a question mark. Theoretically it can not be fully excluded that it is due to an unusual mono-energetic electron background effect. Recent theoretical work of Inagaki and

Shirai [SI20] reports that the S_1 state is in fact the ${}^1L_b$ state. Since the ${}^1L_a$ state should be not so much above S_1, one could propose that the strong peak at 4200mev would be the ${}^1L_a$ state. If so, the structure of the T_2 state would be missing. In this case it has to be either in the vibronic hump structure of the T_1 or of the S_1.

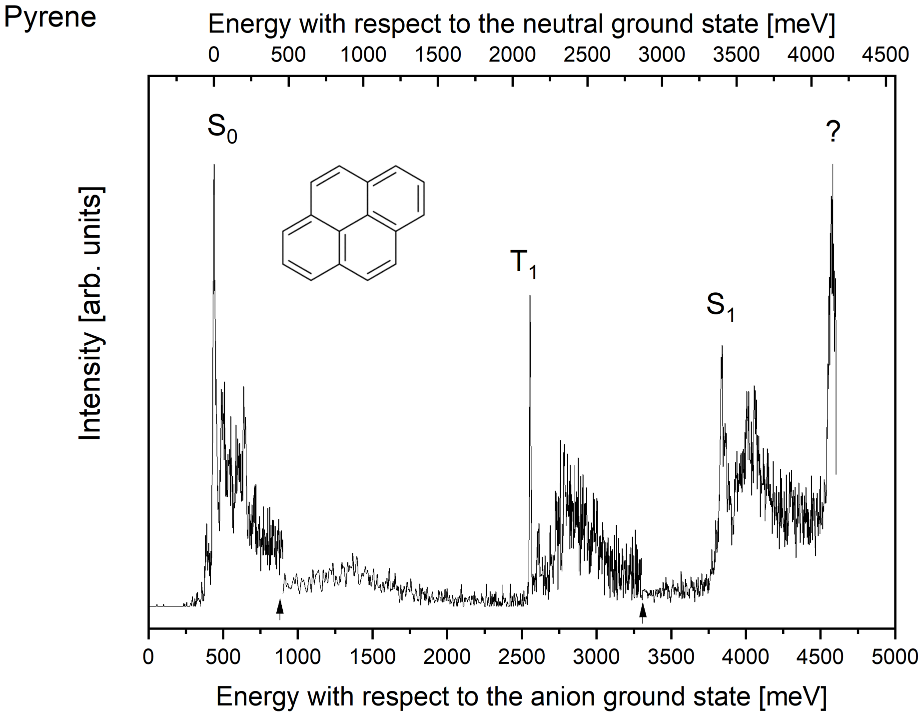

Figure 4.16: PD-PE overview spectrum of pyrene: It consists of three sections each from a spectrum recorded with different wavelengths: 1064 nm, 355 nm and 266 nm. Note the sharp origin transitions and the following dense vibrational structure. For further explanations, see text

Table 4.4: Overview of the electronic states of pyrene. The non cited values are out of this work. All values are indicated in meV

electronic state	configuration (ratio)	literature		experimental	
(symmetry)		theory	experimental	ΔE_{S_0}	ΔE_{D_0}
S_0 $(A_g)^{\mathrm{a}}$	-		450^{b}		440
$T_1(B_{1g})^{\mathrm{a}}$	-		$2570(\Delta E_{D_0})^{\mathrm{b}}$ $2554(\Delta E_{D_0})^{\mathrm{c}}$	2114	2554
S_1 $(B_{3u})^{\mathrm{a}}$	$H \rightarrow L+1(0.33), H-1 \rightarrow L(0.32)^{\mathrm{a}}$	3400^{a}	$3800(\Delta E_{D_0})^{\mathrm{c}}$	3400	3840
S_2/ T_2	-		-		4582?

[a] [SI20] Theory (multi-reference perturbation theory methods)
[b] [KLS09] MS-LPES(magnetic bottle technique)
[c] [AKMN04] MS-LPES (magnetic bottle technique)

4.6.2 Benzanthracene

The chemical structure of benz[a]anthracene – or benzanthracene – is shown in Figure 4.17. Benzanthracene, as numerous other PAHs, can be found in manifold processes involving combustions. The most common appearance is in cigarette smoke. It is carcinogenic as most of the PAHs investigated in this work. Derivatives of benz[a]anthracene have potential applications as fluorescence marker for oncologic applications [WSW98]. Due to the fact that it contains the same number of conjugated six-rings as pyrene, it also attracted the authors interest as a sample molecule for comparative studies conducted with radical-anion PD-PES.

Some time ago benzanthracene gained spectroscopic interest because it can perform p-type delayed fluorescence in a homogeneous crystal. The delayed fluorescence in the wavelength regime of visible light is the result of a triplet-triplet annihilation process. The energy of two triplet T_1 excitations on neighbouring molecules combines to populate a higher excited singlet state S_n on a single molecule. This S_n state then relaxes to S_1, which then can emit a photon [Nic74]. This effect sounded extremely interesting for the application as a wavelengths conversion process of invisible IR light to visible photons. Unfortunately this effect it is not very efficient and therefore did not end in a technical application. Nevertheless the data of this investigations [Nic74] can be used to estimate the energy of the first triplet state T_1 as 2070 meV.

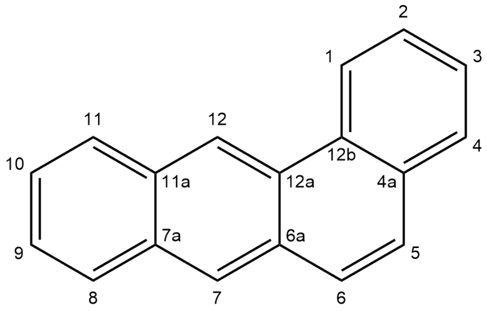

Figure 4.17: Chemical structure of benzanthracene (IUPAC).

Nakajima et al. [Nak72] investigated the two lowest-lying singlet states by laser-induced fluorescence in the gas phase. The origin state energies for the S_1 state 3248 meV and for the S_2 state 3583 meV, respectively (see Table 4.5). In their spectrum, you are able to find a small signal onset below of the declared S_1 energy position. This small peak lies approximately 24500 $\frac{1}{cm}$ (3037 meV) above the S_0 state.

In Figure 4.18 the PD-PE overview spectrum of benzanthracene is presented. It consists of two sections of two spectra recorded with 1064 *nm* and 266 *nm*. Again as for all investigated molecules the first peak, here at 572 *meV* (lower scale), corresponds to the transition from the anion ground state to the S_0 state of the neutral molecule and defines the electron affinity of benzanthracene. This EA value does not match the EA value of 630 *meV* determined by Becker et al. [BC66]. Since the error of our electron energy measurement should be smaller than ± 10 *meV*, it seems that the method "electron capture detection" used by Becker et al. determines systematically too high values and thus provides at best only an upper limit for the EA.

In figure 4.18 only a small vibrational activity and a small background is observed between the S_0-state and the first triplet-state T_1. This indicates that auto-detachment via anion excited states is with the excitation by 266 *nm* photons can be neglected, in strong contrast to pyrene (see above) and benz[a]pyrene (see next section). The T_1 energy position (upper scale) derived from the PD-PES is 2076 *meV* above S_0. In comparison to this, the indirectly determined T_1 value of Nickel et al. [Nic74] is 2070 *meV*. This indirectly determined value in the crystal, is surprisingly close to the PD-PES gas phase value.

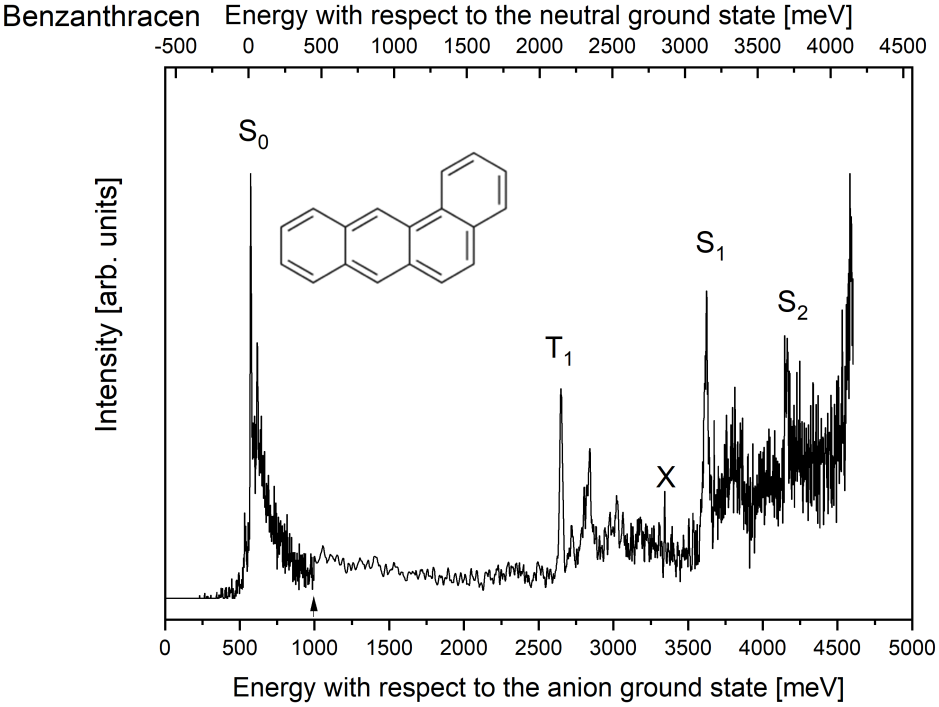

Figure 4.18: PD-PE overview spectrum of benzanthracene. The spectrum is composed of two sections of two spectra recorded with 1064 *nm* and 266 *nm* as detachment wavelengths. For assignments see text.

The minuscule, very sharp peak at 2772*meV* (upper scale) in front of the next intense

transition lies far behind the vibronic transitions of T_1 and could possibly be the transition to the T_2. This assumption relies upon typical peak patterns, which we observed in earlier works [VKMW15],[Pau17]. In these former investigations also small peaks in front of the S_1-state have been observed, which could be in most of the cases identified as a triplet-state with the help of theoretical calculations (Marian et al.).
The S_1 state energy derived from the PD-PES lies at 3052 meV. The value determined by Nakajima et al. [Nak72], however, is 3248 meV. This large difference of about 200 meV is far outside our experimental error.Therefore it can be postulated that the small structure found in the spectrum of Nakajima et al. [Nak72] at 3037 meV is the true S_1 origin and the other peaks at higher energies are vibronic transitions of S_1. The next electronic transition observed in the PD-PES lies at 3574 meV (upper scale). Taking a closer look to the publication of Nakajima, reveals that the values of the graphics and the tabular, where the values are assigned, are inconsistent. My work is referencing the assigned values in the tabular. This time this value is in very good agreement with the value for the S_2 state origin of Nakajima et al. of 3583meV[Nak72]. The very good agreement of the S_2 energy value with the literature value supports the PD-PE accuracy, and indirectly supports the newly proposed S_1 origin transition energy. Note that the S_2 state has a considerable contribution of double excitation [Pro17], which cannot be used for the photodetachment from the electron configuration of the anion. Nevertheless the PD-PE transition to this state is clearly detectable. In Table 4.5 the PD-PE energy data are compared to the available literature values.

Table 4.5: Overview over the data of the electronic states of benzanthracene. The numbers without citation stem from this work. All values are given in meV

electronic state	configuration (ratio)	literature		experimental	
		theory	experimental	ΔE_{S_0}	ΔE_{D_0}
S_0/eA			630[a]	-	572
T_1	-	-	2070[b]	2076	2648
T_2	-	-		2772?	3344?
S_1			3248[c]	3052	3624
S_2			3583[c]	3574	4146

[a] [BC66] electron capture detection
[b] [Nic74] laser excitation
[c] [Nak72] fluorescence excitation gas phase

In conclusion, the above-shown PD-PE spectrum of benzanthracene provides i) a much more accurate EA than previously published, ii) for a first time the accurate gas phase energy of the T_1 state, iii) a new transition energy to the S_1 origin and iv) confirms the literature energy value of the S_2 state.

Comparison of the results: Benzanthracene versus tetracene

In previous PD-PES work, Koniezcny[Pau17] measured and compared the polyacenes compounds tetracene and anthracene. As the empirical formula of both species benzanthracene and tetracene are the same, it would be interesting to compare their electronic state properties. The only structural difference between them is the different position of one ring in the ring-systems. The question is, how this relatively small change shifts the electronic state energies. In the following for simplification and as a test we assume that the electronic properties of such type of molecules can be described by a "particle in the box" model. Clearly from anthracene to tetracene the "box" is enlarged, which predicts an energetic drop of the MOs in agreement with the PD-PES observations [Pau17]. A first assumption for the comparison between tetracene and benz[a]anthracene could be, that in the latter the "linear box" of tetracene is only slightly distorted leading to a slight energetic decrease of all neutral excited electronic states.
Table 4.6 is a juxtaposition of the excited state energies and the EA values of the two molecules. By comparison of the data in Table 4.6 it becomes evident on a first glance that all excited state energies of benzanthracene in comparison to tetracene shift considerably upwards in energy and even the anion ground state shifts up with respect to the neutral S_0 state and causes a considerably smaller EA value. This means that the slightly distorted particle in a box model completely fails.

Table 4.6: Comparison of the EAs and the electronic state energies of tetracene and benz[a]anthracene. All values are given in meV, with respect to the neutral ground state.

electronic state	tetracene	benz[a]antracene	difference
S_0/eA	1055[a]	572	-483
T_1	1332[a]	2076	744
T_2	2616[a]	2772	156
S_1	2777[a]	3052	275
S_2	3021[b]	3574	553

[a] [Pau17] radical-anion PD-PES
[b] [Pro17] theoretical investigation

Also the simple concept that the molecules with the same size of their π systems should have similar excited state energies fails. Obviously the theoretical effects which stay behind

the electronic differences of the two molecules are much more sophisticated than expected. Looking at the T_1-states, one finds the biggest energy difference. In tetracene the configuration for the first triplet state consist mostly of a HOMO[6]-LUMO[7]-transition (0,92 [Pro17]), which leads to a nearly perfect overlap of the wavefunctions [Pau17]. This situation must be obviously very different for benzanthracene, resulting in a higher excited T_1 state energy. Also the the T_1/S_1-splitting leads to this conclusion, as it is bigger in tetracene as in benzanthracene. The T_2-state difference of 156 meV between the two molecules is relatively small, the S_1 state energy difference increase to 275 meV and finally the S_2 state energy difference is with 553 meV again large. Despite that the S_2 excitation is dominated by a double excitation [Pro17] it follows the same trend than the the states which have only single excitations.
The comparison of benzanthracene to tetracene can be concluded as following: In comparison to tetracene benzanthracene has:

- systematically higher excited state energies
- a smaller T_1/S_1 gap, meaning a smaller HOMO-LUMO overlap and
- a smaller stabilization for a surplus electron

The large differences between the electronic state energies of the two molecules show that the "particle in a box" model is by far not sufficient to describe the situation in the two molecules. Also the fact that the two molecules have the same number of conjugated rings and the same sizes of the π systems is no argument for similarities. One consequence of the above comparison is, that the question arises whether one could generate a smaller T_1/S_1-splitting if one would arrange the rings in such ways that the linear geometry is even stronger disturbed. A small S/T splitting would be interesting for an application as TADF[8]-molecules, which need a small singlet/triplet splitting to enable a thermal-induced reverse intersystem crossing from the T_1 to the S_1.

---

[6] highest occupied molecular orbital
[7] lowest unoccupied molecular orbital
[8] thermally activated delayed fluorescence

4.6.3 Benz[a]pyrene

The chemical structure of benzo[a]pyrene (termed also 3,4-benzpyren, abbreviated BaP[9]) is presented in Figure 4.19. In comparison to benzanthracene or pyrene is has an additional annealed conjugated six-ring . It is as many other PAHs also found in incomplete combustions. Because of its high toxicity and its potential to promote tumors, its concentration is constantly monitored in the environment by several national and international institutes [Dab99]. It also can be found in higher amounts in charcoal-grilled meat and is one of the main reason of the health risk of barbecues [AK05]. The toxicity lies not in the molecule itself, but in the diole-epoxide, which is enzymatically formed in a metabolic reaction

. Although it has been spectroscopically studied for almost 80 years, the excited state data on BaP are sparse and limited to the energetic position of the S_1-state [ZHHK11]. It is considered to have a C_3 geometry in the ground state of the neutral molecule. The overview PD-PE-spectrum recorded in this work is shown in Figure 4.20. It is composed of two sections of PD-PE spectra recorded with the detachment wavelengths 532 and 266 *nm*. The peak positions and the assignments are collected in Table 4.7. The electron affinity is given by the S_0 onset and is 760 *meV*. The minuscule peaks in front of the steep and high onset of S_0 are interpreted as hot-band transitions. The unresolved structure right behind the S_0 origin peak is unexpected, since BaP is so large that the presence of a surplus electron should not much change the structure of the neutral molecule. As an effect the origin transitions of the electronic excited states should be by far the highest peaks and the vibrational activities should be small. This situation is found for the transitions to the T_1 state and the T_2 states. It is therefore assumed that the reason for this high spectral activity behind S_0 is not due a D_0 to S_0 geometry change but due to the accidental excitation of vibrations of an anion excited state with 532 *nm* photons of the detachment

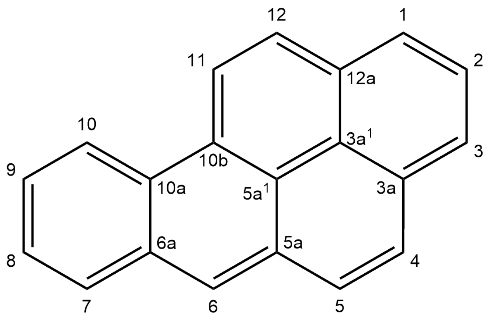

Figure 4.19: Chemical structure of benzo[a]pyrene (IUPAC).

---

[9] Benz[a]anthracene

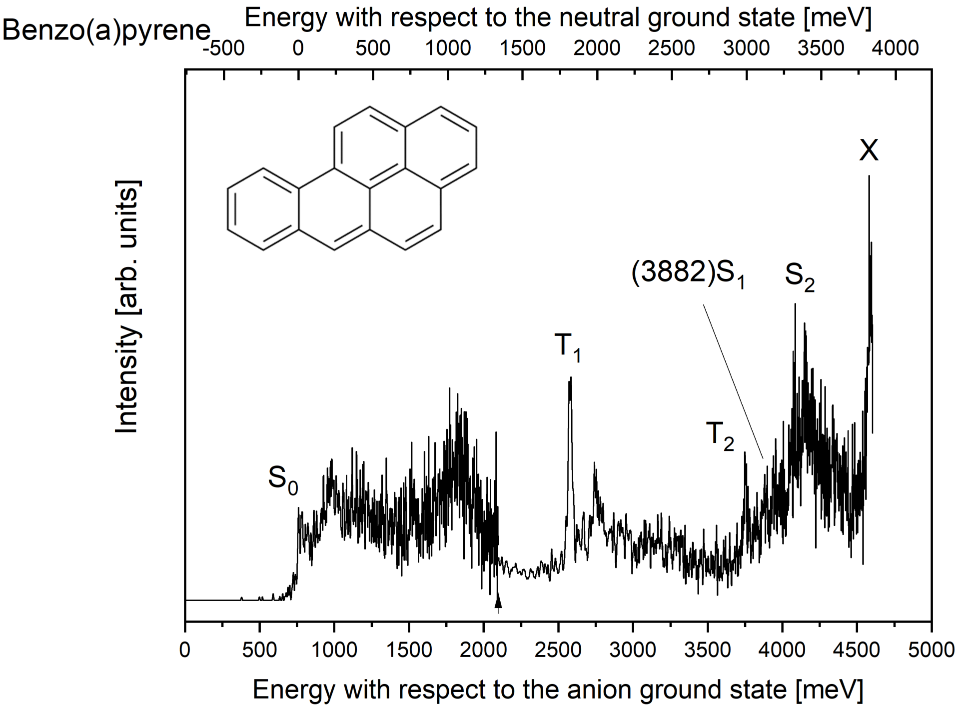

Figure 4.20: PD-PE overview spectrum of benzo[a]pyrene. Note that the complete spectrum is composed of the two sections of spectra, recorded with 532 *nm* and 266 *nm*. The energies of the transitions to the T_1, the T_2 and the S_2 states haven´t been known before. For further explanations see text.

laser.

The vibronic states of the anion excited state then have two possibilities for decay:

- i) they can either decay to the neutral molecule by electron emission to many S_0 vibrational levels of the S_0 ground state, or
- ii) they stay to be anions and decay by IC to iso-energetic vibrations of the anion ground state.

Because in the case ii) the vibrational levels of the anion ground state, which lie iso-energetic to the energy level of the anion excited state, lie far above the detachment threshold, they can undergo thermal auto-detachment by a delayed electron emissions. Such a delayed emission should follow an exponential decrease with a time scale of $1 - 100\ \mu s$. Note that this delayed emission of electrons destroys the concept of the calculation of the electron energy from the time-of-flight measurement. Usually, electrons which arrive at a later time at the detector of the TOF PE spectrometer are interpreted as low-energy electrons. The correlation between the detector arrival time and the electron energy, however, does not exist any more in the case of a delayed electron emission. Even worse, because the PE spectrometer is unsuited for that the transmission of the electrons is optimized for a detachment in the middle of the spectrometer tube. Since the anions fly in about 4 μs out of the spectrometer tube, the intensity modulation at 1750 meV can be a pure transmission artefact. It is assumed that both mechanisms i) and ii) are active.

The next very sharp and distinct peak is the transition to the T_1-state at 2572 meV. In contrast to S_0 the transition to T_1 shows only some weak vibrational progression, which is moderate in length and intensity. These vibrational excitations seem to be not affected by an other AD-state, resonantly excited with 266 nm.

The interpretation of the spectrum above the T_1 state is more difficult. The next peak about one eV behind the T_1 origin is labelled T_2 because it does neither fit the energy known for S_1 nor for S_2

Just taking intensities into account, thinking that the peak marked with S_2 should be the first excited singlet state S_1. Zhang et al. [ZHHK11] had determined that from the anion the S_1-state position above S_0 with 3125 meV (lower energy scale). In a theoretical work [WW08] it was calculated that the S_2 state may be very close above the S_1 state at 3330 meV and that the weak transition to the S_1 state gains intensity from this nearby S_2 state. The distinctive peak at 3326 meV fits this value perfectly and hence, could be the transition to the S_2 state.

The question is now, where is S_1? The minuscule peak already termed with the label S_1 in our spectrum indeed fits the S_1 value of Zhang et al. (compare Table 4.4), meaning the peak just below it at 3748 meV should be another triplet state, most likely the T_2 state. As a result the energetic difference between the first two singlet states is very small.

The S_1-S_2 energy difference was already predicted by Wang to be about 1935 cm^{-1} (240 meV) in good agreement with the gained value $\Delta E_{S_2-S_1} = 202\ meV$. Note that the energies of the transitions to the T_1, the T_2 and the S_2 states haven´t been known before. Since the transitions to T_2, S_1 and S_2 lie in the same PD-PE spectrum and the states are energetically close, it is tempting to interpret the intensities: based on their small intensities, proposing that T_2 and S_1 have both electron configurations which are difficult to excite from the anion ground state configuration. Since the S_1 is practically invisible proposing that it may have configurations which strong contribution of a double excitation, such as $HOMO^0LUMO^2$ can be done. Note that due to the fact that the transitions to T_1 and S_2 are intense and the transitions to T_2 and S_1 are weak, feeds the idea that the two pairs might be corresponding singlet triplet pairs and have the same or similar electron configurations. If so, the T_1-to-S_2 splitting would be large (1514 meV) and the

T_2-to-S_1 splitting very small (134 meV).

Table 4.7: Electronic state data of benzo[a]pyrene. The values without citation are from this work. All values are given in meV

electronic state	configuration (ratio)	literature		experimental	
		theory	experimental	ΔE_{S_0}	ΔE_{D_0}
S_0/eA			680[a]	-	760
T_1	-	-	-	1812	2572
T_2	-	-	-	2988	3748
S_1			3125[b]	3122	3882
S_2		3330[c](L_a)	-	3326	4086

[a] [BC66] electron capture detector
[b] [ZHHK11] REMPI/ZEKE
[c] [WW08] TDDFT

In conclusion, by PD-PES for benzo[a]pyrene three excited electronic state positions have been identified for the first time, which have been determined not even vaguely up to now. The comparison of the electronic state schemes of benzo[a]pyrene and benzanthracene show that there is no easy way to predict the electronic state order and their energy spacings from the chemical structure by using hand-waving arguments.

4.6.4 Dibenz[a,h]anthracen

1,2,5,6-dibenzanthracene or dibenz[a,h]anthrace is in this work abbreviated DBahA. Its structure is shown in Figure 4.21. DBahA is in the focus of oncological studies since the 1930´s[See34]. In solid state, it is a white to light yellow crystalline powder. Because it is known to intercalate into bacterial as mammalian cell systems, it can easily trigger mutations and it therefore can also cause carcinoma and sarcoma [Lor40]. Since long it is therefore under investigation by different environmental agencies, such as for example the international agency for cancer research [IAR85]. It is also – as most other PAH´s – a waste product of practically all combustions and therefore can be found as pollutant around all kind of industries. Its concentration in the air is also under permanent surveillance and control, similar to many other PAH´s (see above).

In chemistry and physics, DBahA gained interest in organic mixed n-trap crystals for triplet exciton fusion, e.g. in naphthalene as host and in DBA as a guest system [BGLR87]. The research for superconducting materials investigates DBahA and other PAH concerning their conducting properties in the range of $5 - 7\ K$ [ZCL19]. The interest of the authors working group in DBahA is inspired primarily by its similarity to benzo[a]pyrene and other molecules which appear in this work. The literature concerning the excited state properties of DBahA is surprisingly rare or completely missing. Most of the research at DBahA deals with crystal structure spectroscopy [BGLR87] and only a few groups work with DBahA in solution [PA99] or in the gas phase [BC66].

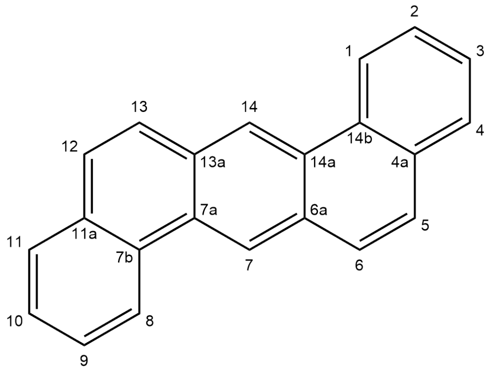

Figure 4.21: Chemical structure of dibenz[a,h]anthracene (IUPAC).

In Figure 4.22 the overview PD-PE spectrum of DBahA is presented. It consists of two sections of two spectra, recorded with 532 nm and 266 nm. The peak positions are collected in Table 4.8 and compared to literature values. The S_0 origin transition peak (first peak) is high and absolutely sharp with a clear, perfect onset. With its position at 544 meV it defines the EA of DBahA. This value is somewhat lower in energy as the value 595 meV

previously measured by Becker and Chen with the electron capture method [BC66]. As already discussed above, it seems - and this is confirmed also here – that with this method only a upper limit of the EA can be given.

Behind the S_1 origin a vibrational progressions of the S_0-state follows until suddenly the signal rises and ends in an intense, broad structure termed AD. The energy of this hump is definitively too low to be due to an electronic excited state and is due to autodetachment (see above).

The next intense PD-PE peak is very exceptional in intensity and shape. It lies at 2324 meV (upper scale) and should be due to the transition to T_1 or. Since the energetic position of the S_1 state is known to be 3178 meV [PA99] and this value agrees well with the position of the third large peak in the PD-PE spectrum. This transition is termed accordingly S_1. With this S_1 identification automatically the assignment of the T_1 state is confirmed. Note that this is the first direct observation of the T_1 state. Its remarkable higher intensity in relation to that of the transition to the S_1, should be partly caused by to the threshold problem for different electron excess energies [Wig48]. The fact that the intensity difference is so great, could, however, also be a result of different electron configurations of these states. Clearly this question cannot be answered without theoretical data. One could speculate, whether a strong contribution of a double excitation in S_1, which is not accessible from the anion ground state and which is not possible for the T_1 state, causes the observed extreme intensity ratio. The minuscule peak (marked with X) lies just before the S_1-transition. It is very sharp, and low in intensity. An assignment of its nature is without additional information impossible. It could be for example the T_2-state. Such a situation that the T_2 state is very weak and lies just below the S_1 has already been observed for other PAH species, and obviously occurs rather frequently.

Right behind the S_1-state the vibrational activity and unfortunately also the background of stray electrons increases. This makes a proper discussion of the section Y difficult. It seems, however, that there could be other transitions as e.g. the S_2-state.

In conclusion, for DBahA it was possible to determine an accurate EA value, to observe the first triplet state and to confirm the position of the S_1-state. To evaluate the nature of other unassigned weak peaks in the PD-PE spectrum, further theoretical studies are required.

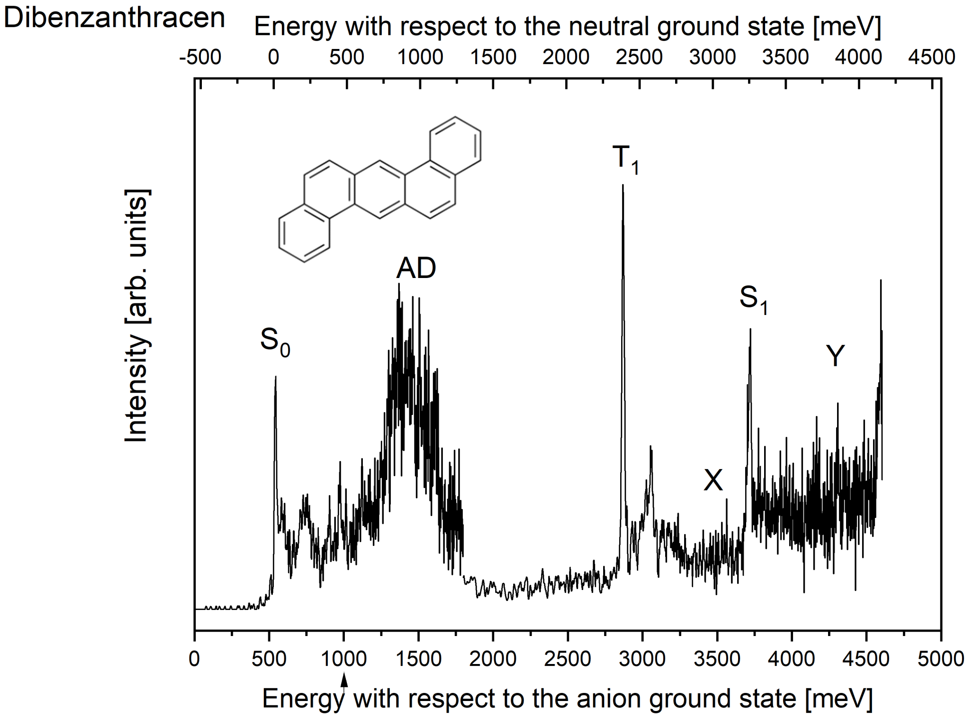

Figure 4.22: PD-PE overview spectrum of dibenz[a,h]anthracene. The spectrum consists of two sections of two PD-PE spectra recorded with 532 *nm* and with 266 *nm*. Note the strong auto-detachment (AD) when 532 *nm* photons are used for the detachment.

Table 4.8: Overview of the electronic state energies of DBahA. The values without citation stem from this work. All values are given in *meV*

electronic state	configuration (ratio)	literature		experimental	
		theory	experimental	ΔE_{S_0}	ΔE_{D_0}
S_0/eA	-	595[a]		-	544
T_1	-	-		2324	2868
T_2	-	-	-	3020 ?	3564 ?
S_1			3148[a]	3178	3722
S_2			-		

[a] [BC66] electron capture detection

[b] [PA99] linear dichroism spectroscopy, in n-hexane

4.6.5 Pentacen

In the past decade pentacene (abbreviated 5-Ac[10]) gained high interest in photochemistry and polymer chemistry. Its chemical structure is shown in Figure 4.23. As it is highly conjugated, its application as a semiconductor material (as a thin film or as single crystal) has been investigated [Kha20a],[Kha20b]. For the crystal first a triclinic crystal structure was reported [CRT62], but it was difficult to reproduce these results later. It seems that different triclinic structures co-exist in a single crystal (polymorphism) [MDB+01]. It was argued that molecular impurities negatively influence the perfect crystallisation process of pentacene. In addition it also seems that the exact crystallisation temperature is an crucial parameter[SBH+07].

The most remarkable optical property of 5-Ac in a homo-crystal is its ability to perform singlet fission. This process can be described as a process where a singlet-state excitation on one molecule is split into two triplet excitations on two neighbouring molecules. This process can only work if the S_1 energy is larger that twice the triplet-state energy: $\Delta E(S_1 - S_0) \geq 2 \cdot \Delta E(T_1 - S_0)$ [SJS+65]. For the first time reported in the 1950 [BMS49], it still attracts immense attention, as a way to circumvent the Schockley-Queisser limit (limiting loss effect in solar cells by radiative recombination). [SQ61]

This means, that a singlet exciton formed in the layer p-n element of a solar cell can be converted in one step into two triplet state excitations, without the subsequent possibility of a radiative recombination by photon emission. If it would be possible to use the two triplet excitations to achieve the separation of two charge pairs in a solar cell, this would be an elegant way to push forward the efficiencies of organic solar-cells [FRE18]. To be able to optimize this genius concept also in other molecular crystals, the energetics of the involved singlet and triplet states is crucial, a great motivation for this work.

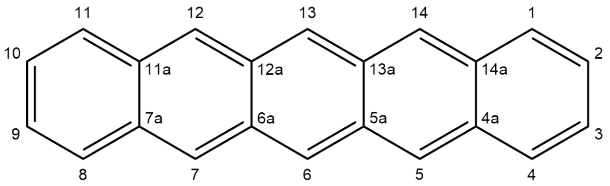

Figure 4.23: Chemical structure of pentacene (IUPAC).

Still open question concerning the singlet fission is, what exactly is the pathway for singlet-fission. Either it is a direct transition from the S_1-state to the corresponding T_1-states, or the transition is mediated by a bimolecular charge-transfer-state.

In a previous work Konieczny [Pau17] investigated anthracene and tetracene by PD-PES,

---

[10] Pentacene

so the pentacene spectrum in this work completes the series of linear acenes.

Nakajima et al. [MSN16] already performed Radical-Anion PD-PES for pentacene. They determined an EA and the first excited states of the neutral molecule. Due to the different spectrometers used, electron gun and magnetic bottle PE spectrometer by Masubuchi, and discharge anion source and field-free PE spectrometer in this work, it is nevertheless interesting to reinvestigate pentacene.

Figure 4.24 displays the overview composite PD-PE spectrum of pentacene. It consists of two sections of two spectra recorded with the detachment wavelength 355 *nm* and 266 *nm*. The PD transition from the anion to the S_0 state shows a very unexpected structure:

- i) It does not rise as steep as expected for a molecule with such a large π system (see for comparison the shape of the transition to T_1)
- ii) It has a well-resolved low-energetic substructure in the rise and close behind the maximum and
- iii) It and has a strong vibrational activity right after the maximum.

The effects mentioned in iii) stem from an accidental excitation to a vibration of an anion-excited state. This anion state then obviously undergoes fast auto-detachment. In this process the vibration excited in the anion excited state dictates the FC factors which rule the auto-detachment process to the vibrations of the neutral S_0 state (see chapter 2). Obviously in the anion excited state a low-energy vibration is excited, resulting in the neutral S_0 state in a structure of many peaks with a very low-energetic energy spacing. An un-complete cooling and the resulting hot-band transitions doe not account for the not so steep rise simply because no hot-bands are observed for the transition to the T_1 state.

The EA of pentacene is determined by taking the energy value at half height of the rise ($\approx$ 1392 *meV*) of the transition to S_0. This procedure follows the assumption that due to the above problem the origin transition of S_0 is not the highest peak but lies before the maximum. To take the energy value at half height is – one has to admit – somewhat arbitrary since the quantum numbers of the vibrational states are not known.

The previous PD-PE spectrum provides an EA value of 1430 *meV* [MSN16](EA at 1392 *meV*) is 38 *meV* higher in energy. This error could have the simple reason: Masubuchi et al. could not resolve the low-energetic vibrations in S_0. They therefore presumably took the position of the maximum of the first peak for the EA value. This maximum lies at a higher energy, what might explain their higher EA value. The perfect agreement of the EA value here with the value of Crocker and Wang, also 1392 *meV*, seems to be accidental, because they use the electron capture set-up, which usually gives higher values too [CWK93]. The

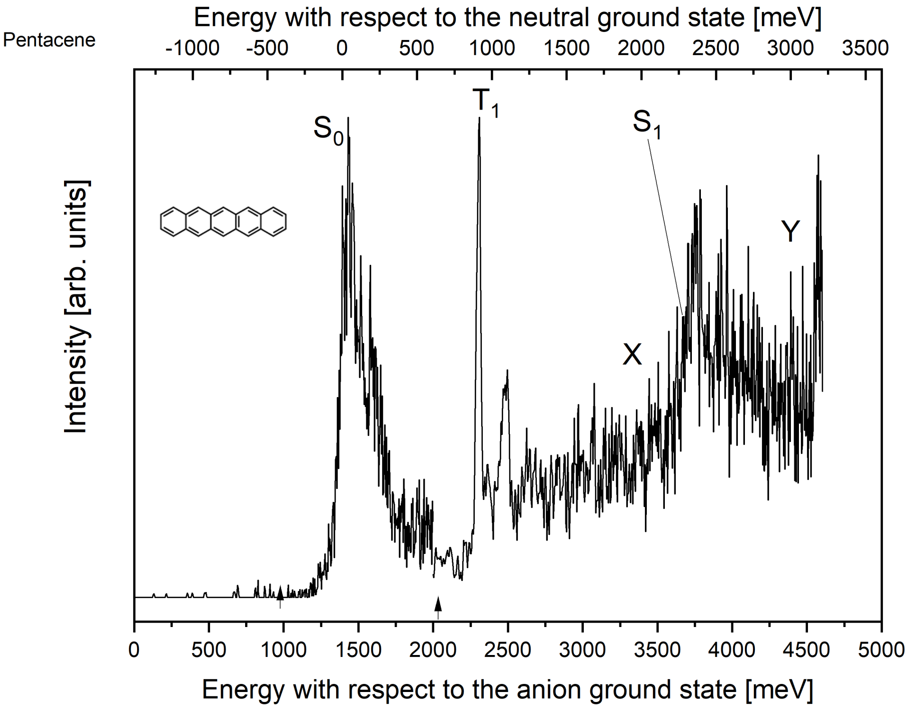

Figure 4.24: PD-PE overview spectrum of pentacene composed of two sections of two PD-PE spectra recorded with the detachment wavelengths 355 *nm* and 266 *nm*. Note the low-lying T_1 state with respect to the S_0 state and to the S_1 state, which allows singlet fission in pentacene crystals. For further explanations see text.

region between 2000 *meV* and 3000 *meV* seems to be less affected by auto-detachment as the S_0 region. The triplet T_1-peak at 916 *meV* (upper scale) is remarkably sharp in comparison to the other peaks. It has a few vibrational structures which slowly more and more merges into noise and background. Note the extremely small $T_1 - S_0$-energy gap, which fulfils the above-mentioned condition for a singlet fission. Our T_1 energy is unfortunately not in agreement with the value determined by Masubuchi et al. (960 *meV*). The deviation is with 44 *meV* and much bigger than for the EA values. The reason for this relatively large deviation remains unclear. In the range after the T_1-state does not yield any more clear peaks, but possible peaks show up in the noise (marked with X). This noise situation does, however, not allow to assign a possible T_2 triplet state. This situation is somewhat similar to the spectra of Konieczny of anthracene and tetracene, where it is known that the T_2 is below S_1. [Pau17].

In the immediate vicinity of the S_1-state an increasing electron activity and noise is observed. This might be due to an other anion-excited state excited with 266*nm*. This local distortion and the resulting signal modulation, makes it even difficult to clearly

Table 4.9: Overview of the electronic states of pentacene. The values without reference stem from this work. All values are given in *meV*

electronic state	configuration (ratio)	literature		experimental	
		theory	experimental	ΔE_{S_0}	ΔE_{D_0}
S_0 / EA	-		1392[a], 1430[b]	-	1392
T_1	-	-	960[b]	916	2308
S_1		2200[c]	2180[b], 2150[d]	2288	3680
T_2	-	-	-		
S_2			-		

[a] [CWK93] ion/molecule reaction equilibrium
[b] [MSN16] magnetic bottle PD-PES
[c] [MKD20] TDDFT
[d] [MRK+04] UV-VIS in thin film

assign the origin transition of the S_1-state. We assume that the S_1-state origin is the first onset before the maximum (marked with a line in figure 4.24). The such determined S_1-value of 2288 *meV* is in reasonable agreement with the theoretical literature value of 2200 *meV* [MRK$^+$04] and again deviates somewhat from the value determined by PD-PES (2150 *meV*)[MSN16]. As for the the difference of the S_1 value to that of Masubuchi, it may be due to the fact that here appears a smaller value for the S_0 position.

In conclusion, although already well-investigated, the PD-PE spectrum of pentacene yields interesting new information, and shows that even in the gas phase the T_1 and S_1 energy values would allow singlet-fission energetically .

Unfortunately experimental boundaries prohibited an observation of the dimer here, as well the usage of other laser-wavelengths, in order to circumvent the excitation of anion-excited-states.

But still now having an accurate EA one could try to estimate the energy of the intermolecular CT[11]-state in the dimer. The following equation for the intermolecular charge transfer (CT) energy in two π stacked molecules is relatively simple, but contains some assumption, for which the validity is unknown.[WS97] Those are

- i) That the two molecules are π stacked and are not shifted against each other
- ii) The assumption that the opposite charges are point charges
- iii) That the opposite charges move correlated through the molecules
- iv) That the intermolecular distance is a good description for the charge distance

---

[11] charge transfer

Whereas the above points are well fulfilled for small molecular complexes theirs validity is highly questionable for a pentacene dimer.

$$E_{CT} = IP_{5-Ac} - \int_d^\infty \frac{q^2}{4\pi\epsilon_0 r^2} dr - EA_{5-Ac} - \Delta E_{stab}$$

E_{CT}:	charge transfer state energy [eV]
IP_{5-Ac}:	ionisation energy [eV]
$\int f(r)dr$:	coulomb integral [eV]
d:	spacing of the molecules [m]
EA:	electron affinity[eV]
ΔE_{stab}	difference in stabilization energy [eV]

The energy of a possible CT-state can be estimated, by taking into account:

- i) the $IP_{5-Ac} = 6,61eV$ [SM84]
- ii) the EA of 1392 meV, determined in this work
- iii) the Coulomb integral by assuming an intermolecular distance of $3,1A$ (centre-to-centre) provides an value of about 4500 meV

In the following the unknown stabilization energy wil be neglected. This term takes into account that the separated charges in the monomers try to come closer to each other, than the centre-to-centre distance and further reduces the energy of the CT state.

The result is 718 mev for the position of the CT-state. This low CT energy value lies even below the T_1 state, which means that the singlet-fission process can happen directly from the singlet to triplet states without an CT-intermediate as the CT-energy in this approximation lies lower than a single triplet T_1-energy.

The question, however, arises whether the above equation initially set up for point charges really describes the CT energy in a dimer of such large molecules. Especially the assumption that the charge distance between the opposite charges is equivalent to the one-dimensional distance (say coordinate z) of the quasi-two-dimensional molecules (the molecular planes extend in in x and y directions) might be very wrong, since it assumes a full and permanent correlation of the motion of the two charges in the x and y directions. If this correlation of the charge motions in x and y is not possible due to for example quantum mechanical reasons, the electron and the hole might be most of the time in different x,y positions of the neighbouring molecules and the inter-charge distance is much larger than the molecular distance. This discussion shows that the above equation might not hold for the CT state in pentacene dimers and therefore it would have been very important to measure the dimer and determine the position of the CT state. Unfortunately this was not possible. In a retrospective view of the PD-PES measurements performed on the

5-Ac molecule, one has to say that several improvements of the experimental set-up could lead to better or more precise results (see Section "Conclusion"). As the here mentioned experimental procedures unfortunately were not accessible by the likes of our group till now, the only thing left is a advanced theoretical investigation. Yet, it is possible to compare the results presented here with the results for 3-Ac[12] and 4-Ac[13] raised by Paul Konieczny[Pau17]. An attempt at classification of 5-Ac in the series of the linear acenes is made in the next subsection.

---

[12] Anthracene

[13] Tetracene

Pentacene data compared with the data of tetracene and anthracene

As 5-Ac is a natural continuation of the series of acenes, it is reasonable to compare the change in excited states energies ot them. A comparing plot can be seen in Figure 4.25. All values are referenced to the S_0-ground state with respect to the neutral species. As it was not possible to gain information of higher excited states of 5-Ac the comparison is limited to the EA´s and the S_1 and T_1 states. As expected, the general trend is an decreasing energy of the excited states while extending the linear acene system. In fact a almost systematically decrease is observable from 3-Ac over 4-Ac down to 5-Ac. Simultaneous an increase in the EA values can be found. This seems consistent as a larger π-electron system should be able to hold an additional charge more preferably than a small one thus resulting in a higher EA-value. The consistent decrease in the T_1/S_1-splitting energy can

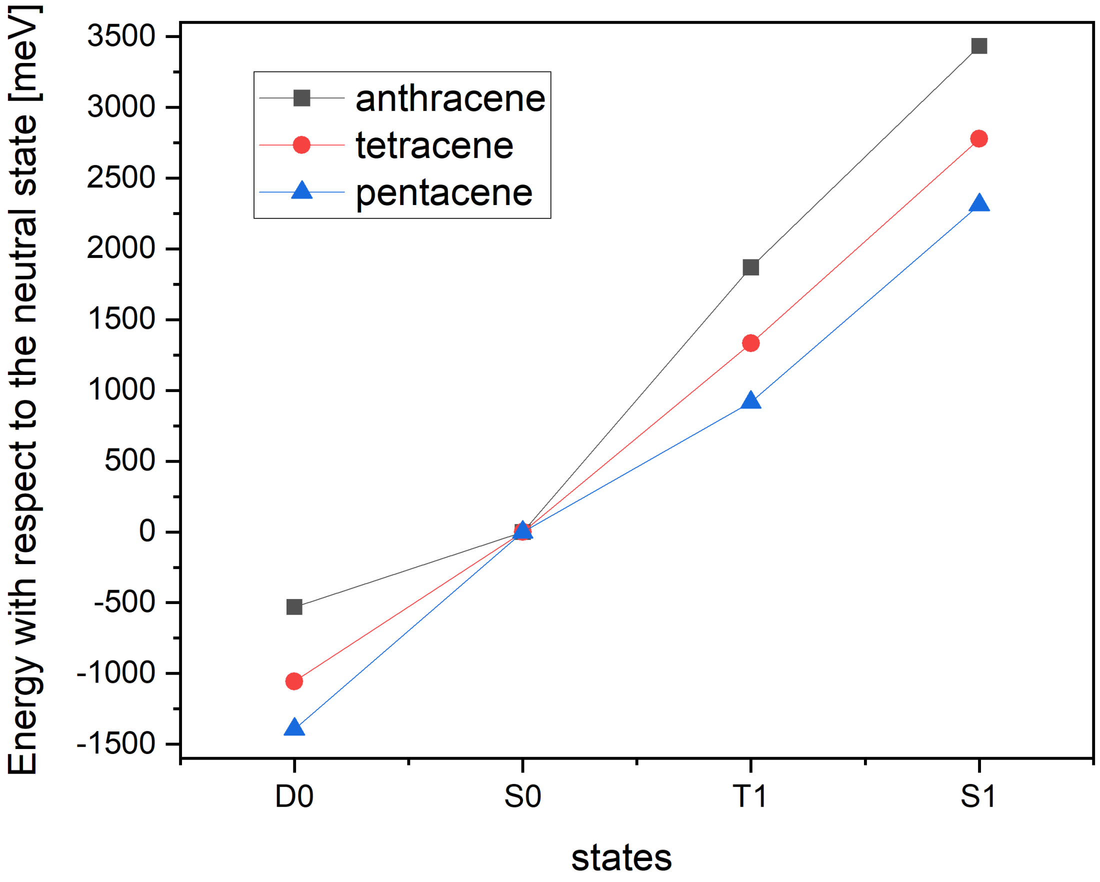

Figure 4.25: The excited state and electron affinity data of anthracene, tetracene([Pau17]) and pentacene. Note that all data are referenced to the S_0 states.

be vice versa interpreted as a yet good overlap of the participating orbitals, with a deflating trend regarding longer systems. The diminishing of the triplet energies seem to be nearly equidistant at a rate of 400 meV per additional ring. Based on these considerations, one could derivate the following assumptions:

- System-length affects the total energy values to decrease
- System-length slightly affects the T_1/S_1-splitting
- System-length increases the EA

Aside of these observations, it seems also that the EA greatly affects the absolute energy of triplet states. Due to a general lack of overall data regarding triplet states in organic molecules (gas phase), the nature of this statement is purely hypothetical.

4.6.6 Comparison of the Data of the Acenes

To obtain a general insight in the excited states dynamics, it is of utmost interest to find possible correlations between molecular geometries and the excited state energies. Because anion PD-PES is applied in this work, the main focus lies on triplet states T_1, T_2 and the electron affinity.

Comparison of the EAs

The EA's of the acenes varying over a wide range. In Figure 4.26 , all the acene spectra are shown. To concentrate on the neutral state energies all spectra were shifted so they are referenced to the S_0 ground state. The EA vales are added as labels at the S_0-state onsets. This means Figure 4.27 obtains all anion ground values as text labels and all neutral excited state values become directly visible by comparing the positions in the spectra.

In general the EA values does not change dramatically when going from dibenzanthracene, via benzanthracene to pyrene. Pyrene has the smallest EA (440 meV) of all investigated acenes. At the same time, the S_1-value of pyrene is the highest among the S_1 values of the here listed species.The EA of dibenzanthracene and benzanthracene differs the less among the regarded species, although there is quite a difference in structure as also in total atom numbers. BaP shows the first significant increase in EA and 5-Ac has the highest observed EA.

In a simple consideration, it can be assumed that sheer size of a molecule affects the corresponding EA. This is, however, obviously not the only and the predominant factor in absolute terms of EA.

If you compare the form and structure of the S_0 regions, it stands out that the vibrational progressions are quite sharp for pyrene, benzanthracene and DBA, while it is broader for 5-Ac and BaP. Eye-catching are also the auto-detachment (AD) effects in these molecules. While the AD effect is in pyrene is quite local, it is absent in BA, a hump with resolved sharp peaks on top for 5-Ac and broad in BaP.

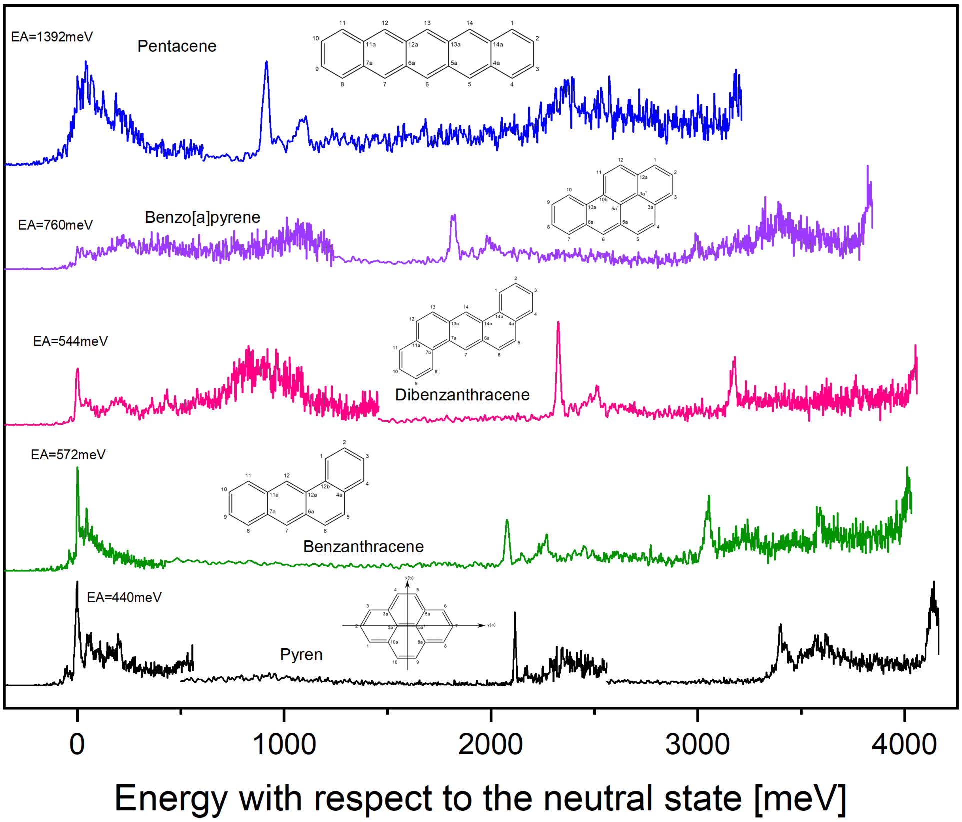

Figure 4.26: PD-PE spectra of the measured acene compounds. All spectra are shifted in order to agree with their S_0 origin positions. For further explanations see text.

Comparison of the T_1 Energies

The deviation in the singlet state energies of the acenes seem to be smaller than that for the T_1 states, with the exception of pentacene. Its variance pattern seems to be much smaller compared to the T_1 values. Also differences of the T_1/S_1 splittings are observed and (as indirectly stated before) are increasing in size with the molecular size.

In conclusion, in order to obtain a more detailed pattern on how molecular size and shape influences excited electronic state positions, EAs or respectively anion-excited states, further experimental and theoretical investigations are necessary to provide sound and accurate data for many molecules for a comparison to theoretical calculations.

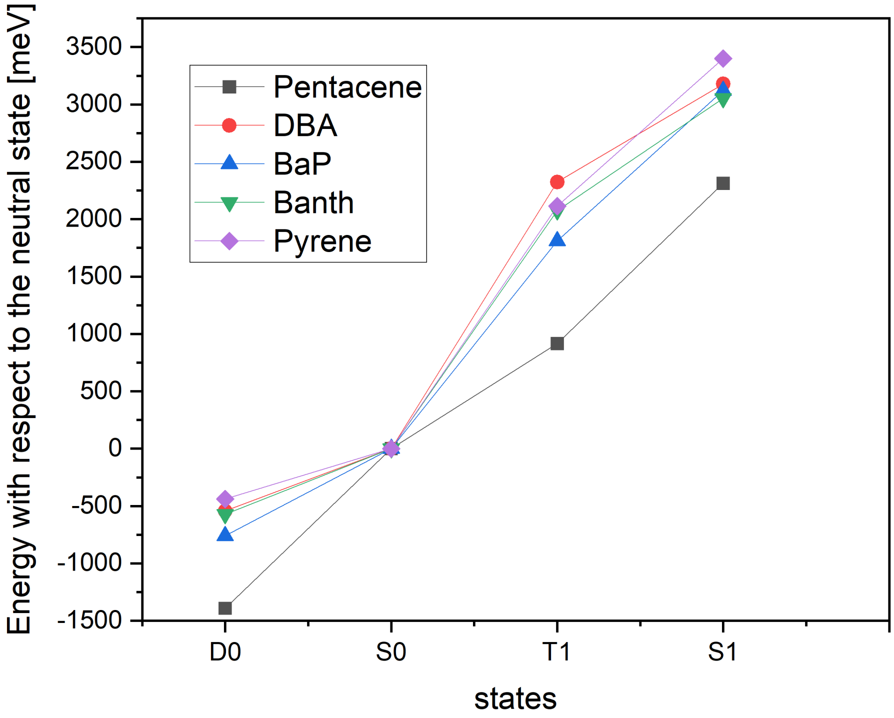

Figure 4.27: Comparision of the state energies of the measured acenes (y scale) including the electron affinity.

4.6.7 9,10-Diphenylanthracen

The measurement of 9,10-diphenylanthracene (abbreviated 910Dpa[14]) pursues the concept to investigate the electronic effects caused by phenyl substitutions on an anthracene core. The chemical structure of 910Dpa is shown in Figure 4.28. Its has an anthracene core just with two phenyl groups substituted at the 9 and 10 positions. The phenyl rings are bound to the anthracene by a single C-C bond in contrast to the acenes investigated above, where the phenyl rings are co-annealed to anthracene.

Already in 1965 910Dpa was investigated due to the chemo-luminescence of its anion [SB65]. Also the optical and electronic properties of neutral 910Dpa attracted attention, because it may be suited for tunable semiconducting devices. For example, single crystals of 910Dpa embedded in nano-rods were investigated, concerning a probable application as field effect transistors.[ZYL$^+$08]

Because 910Dpa performs efficient triplet-triplet annihilation as a dimer and in crystals, its seems to be a potent material for photon frequency up-conversion[XSD$^+$21]

In Figure 4.29, the PD-PES overview spectrum of 910Dpa is shown. It is composed of three sections of three PD-PE spectra, measured with the wavelengths 1064 nm, 355 nm and 266 nm. The very first peak with a steep onset at 750 meV is – as in all spectra of the radical anions – the transition from the ground state of the anion D_0 to the origin of the S_0 of the neutral molecule. This transition energy defines the EA of 910Dpa which had not been evaluated before. The peak and background activities in the region of 1000 meV

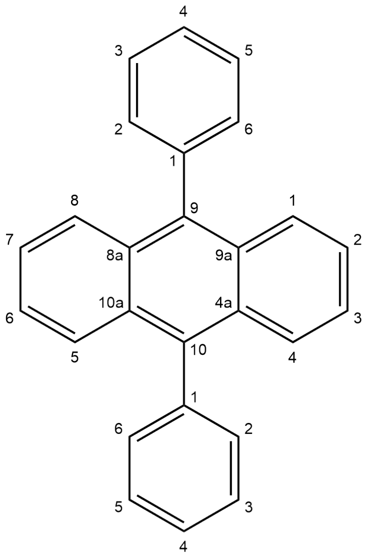

Figure 4.28: Chemical structure and atomic numbering of 9,10-diphenylanthracene (IUPAC).

---

[14] 9,10-Diphenylanthracene

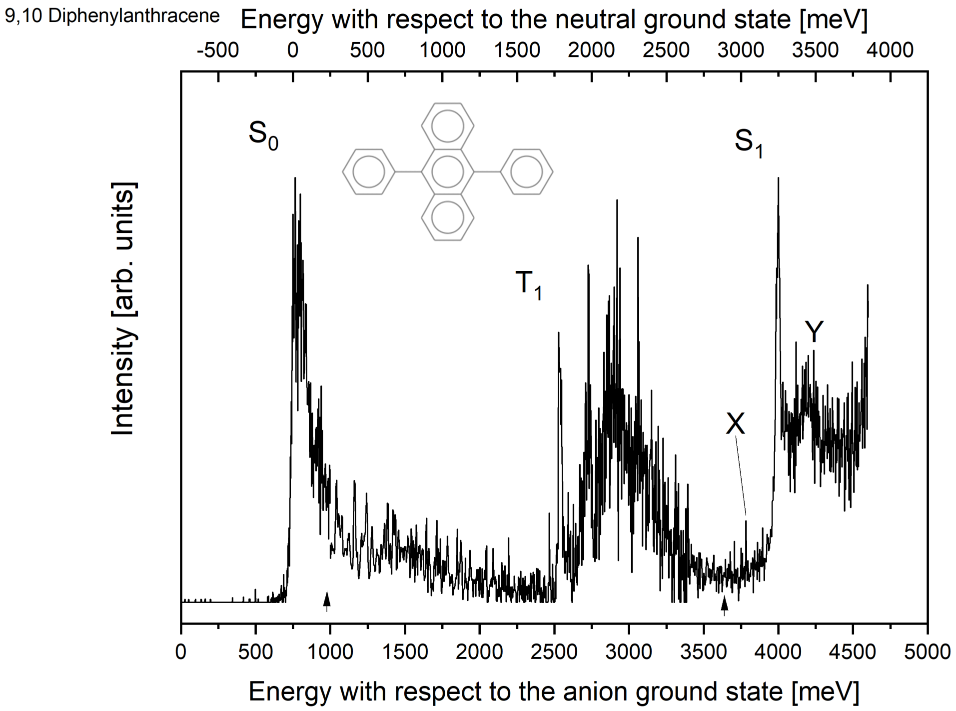

Figure 4.29: PD-PE overview spectrum of 9,10-diphenylanthracen. For further explanation see text.

to 2000 *meV* seem to be due to vibrational progressions, which are only partly resolved and might be due to the accidental excitation of an anion-excited state by the detachment wavelength of 355 *nm*.

The following sharp peak at 1779 *meV* is the lowest triplet state T_1 in good accordance to the experimental value of 1770 *meV* in solution [CKD83] and the theoretical value of 1720 *meV*.[OGMA21]. Note the vibrational progressions of sharp peaks which – at higher T_1 state energy – become so dense that they merge and form a hump on top of which still peaks remain. This strong and long-range activity just after the T_1 origin is with high probability also due to the accidental excitation of an anion-excited-state. It should be noted, that the PD-PE spectrum recorded with 1064 *nm*(at approx 900 *mev*)/355 *nm* (left side) and the PD-PE spectrum recorded with 266 *nm* (right side) are mounted together at 3375 *meV* (lower scale). The best indication for this site are the different signal levels. The small and thin peak at about 3050 *meV* is marked with X. It lies just before the S_1-region, and could be the T_2 state. Because of its minuscule intensity this is, however, very speculative.

The intense peak at 3249*meV* is assigned to the transition to the origin of the S_1 singlet state. This value agrees well with the S_1 energy of 3262 *meV* determined by an UV absorption measurement in non-polar solutions[JON47]. Note the occurrence of vibrational bands similar as for T_1. The energy difference of the first two peaks in S_1 is roughly the same than that for the first two peaks in T_1. This is a strong indication that in both cases the second peak is a vibronic band of the respective electronic state. Since the second peak in S_1 is, however, broad, it could be that around $3375 meV$ (see Y) there is another weak electronic origin transition close-by. Indeed, in the theoretical work of Chen-Hanson Ting [Tin67] a triplet state of 910Dpa lies around 3500 meV. This agreement supports that the y-marked region after the S_1-state could be the onset of the T_2-state.

In table 4.10 the values derived from the PD-PE spectra are compared to literature values. In conclusion, the PD-PE measurement on 910Dpa radical anions in the gas phase provided the previously unknown EA, as well as the direct observation of the transitions to T_1 and S_1. The energy values for the electronic origins found in the PD-PE spectra show good agreement with the solution (S_1) and solid state (T_1) values of previous work. Further weak peaks found in the PD-PE spectra may be assigned to transitions to other excited electronic states of 910Dpa if this assignment would be supported by theoretical calculations.

Table 4.10: Electronic state energies of 9,10-DPA: Comparison of literature values with values of this work (data without citation). All values are given in meV

electronic state	configuration (ratio)	literature		experimental	
		theory	experimental	ΔE_{S_0}	ΔE_{D_0}
S_0/eA (A_g)	-				750
T_1 (B_{1u}^-)	-	1720[a]1750[b]	1770[c]	1779	2529
S_1(B_{1u}^+)			3262[d]	3249	3999
T_2(B_{3g})	-	-	-		
S_2(B_{2u})			-		

[a] [XSD+21] TDDFT
[b] [Tin67] Pariser Parr method
[c] [CKD83] laser flash photolysis
[d] [JON47] UV absorption spectroscopy

4.6.8 2,6-Diphenylanthracene

Another molecule which fits into the series of the anthracene-derivatives investigated in this work is 2,6-diphenylanthracene (abbreviated 26Dpa[15]). Its chemical structure is shown in Figure 4.30. Note that the distance of the hydrogen atoms No. 1 in anthracene and No 2 in the right phenyl ring and equivalent the hydrogen atoms No. 3 in anthracene and No. 6, in the right phenyl ring have a relatively large distance in comparison to the corresponding distances in 9,10-diphenylanthracene. The equivalent H–H distances also exist at the left phenyl ring. As a result, in 26Dpa the H–H repulsion is smaller and the phenyl rings can be more planar than in 9,10-diphenylanthracene, but they are still rotated out of the plane. For the later discussion the question is whether the phenyl torsion shows up in the PD-PE spectra.

26Dpa was for the first time synthesised and then characterised by UV-Vis spectroscopy by Clar et al. [Cla61]. Later, an alternative synthesis was found by Hu et al. [LDW+15] who investigated 26Dpa as a thin film on a silicon wafer. The main potential applications of 26Dpa lie obviously in the field of organic semiconductors [LZD+15],[LDW+15] and OLED's.[FLW17] The two cited publications provide the only experimental data on the electronic properties of26Dpa. This means that especially so far no gas phase data exist.

In Figure 4.31 the PD-PE spectrum of 26Dpa is presented. For a optimised electron energy resolution the overview spectrum is composed of sections of two spectra recorded with 532 nm and 266 nm as detachment wavelengths. As usual the first onset at 884 meV represents the transition from the D_0 ground state of the radical anion to the origin of the S_0 state of the neutral molecule. This value is the first EA value of 26Dpa in the gas phase.

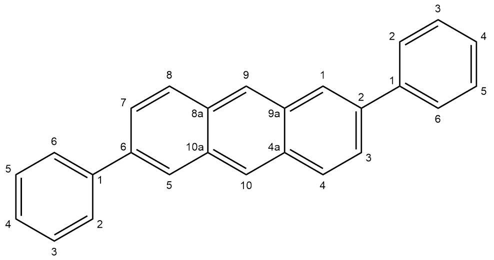

Figure 4.30: Chemical structure and atomic numbering of 2,6-diphenylanthracen (IUPAC).

For the transition to S_0 a high-energetic vibrational progression is observed. After three broad peaks the spectrum becomes quickly dense and unresolved (see range of 1250 meV

---

[15] 2,6-Diphenylanthracene

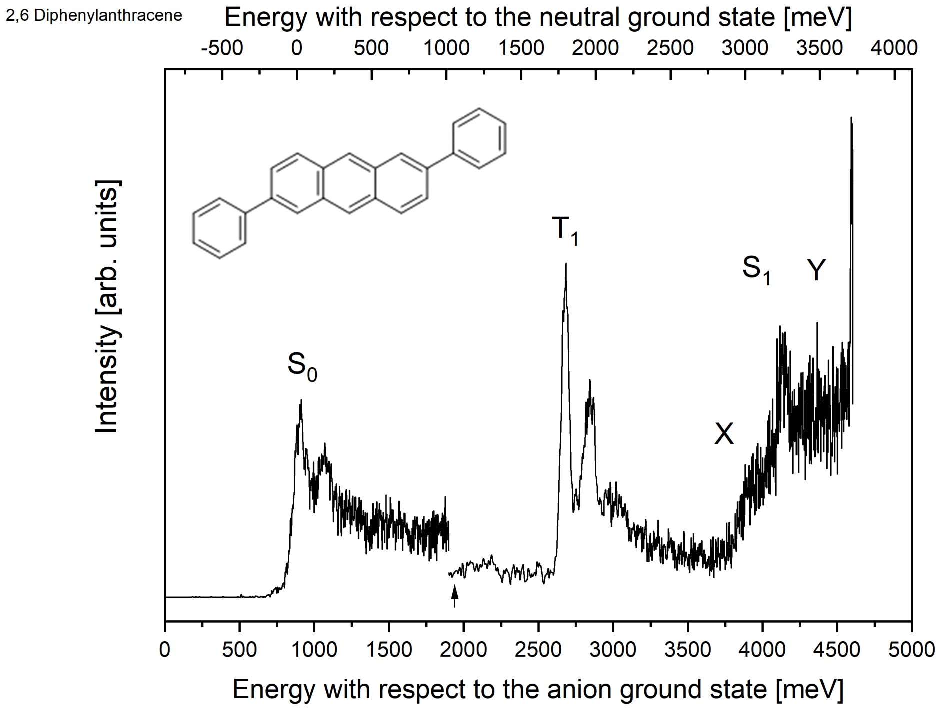

Figure 4.31: PD-PE overview spectrum 2,6-diphenylanthracen. The overview spectrum is composed of sections of two spectra recorded with 532 *nm* and 266 *nm*.

to 2000 *meV* (lower scale)). In addition, if comparing carefully the peak widths, it can be observed that the first peak of the transition to S_0 is broader than that of the first peak of the transition to T_1. The arising question is, what causes the excitation of vibrations and what causes the broad peak width in S_0?

In a first reaction, in analogy to other molecular spectra above, one could argue that the detachment wavelength of 532 *nm* accidentally excites a vibrational state of an electronically excited state of the anion. As a result, auto-detachment from this anion state occurs, which then leads to FC factors which are given by the accidentally hit vibration of the anion excited state and the S_0 state of the neutral molecule. If this explanation would be true, this case is not interesting for us and does not provide valuable molecular information.

A second alternative possibility for an explanation is, that the peak widths and the intensities of the vibrational structures in S_0 are a result of the undisturbed anion-to-neutral FC factors. Indeed – similar to the longer p-polyphenyl molecules – also in 26Dpa strong geometry changes may occur: By PD-PES investigations on p-terphenyl, p-tetraphenyl and p-quinquephenyl Koniezcny [?] could provide good evidences that in the neutral ground state the phenyl rings are stronger twisted against each other than in the anion ground state. Interestingly, in the anion and the excited electronic states of the p-polyphenyls this out-of-plane twist angle is smaller.

The same or a similar geometry change effect in the torsional coordinate of the phenyl rings is also possible in 26Dpa. In addition, the corresponding hindered phenyl rotation (classified as a vibration) is assumed to be so low-energetic that it should be not resolved by PD-PE spectra.

First this discussion will ne interrupted in order to identify the excited electronic states in the PD-PE spectrum. Afterwards an investigation of the transitions from the anion to the electronic states in regard to this geometry effect take place.

Remarkable is the first peak of the T_1-state (onset at 1800 meV (upper scale)) which has the highest observed intensity in the spectrum. Typically this is a result of a good transition moment for the PD-process to this state, meaning that the participating orbital transitions can be performed by a single electron excitations (compare 2.3.1, one photon-one electron-rule).

Regarding the literature, only values for solvent and thin-film UV-Vis experiments are available. The S_0-to-S_1 energy value in a thin film is 2799 meV [LDW+15] and in ethanol 3002 meV [Cla61]. The interpretation of a red-shift when going from solution to a thin film, in which the molecules have direct contact, is difficult. In ideal molecular packings (π stacking without displacement) H and J aggregates have been postulated [FK54]. In the fist type the transition moments (these are vectors) are side by side and aligned parallel or antiparallel. In the J aggregates the transition dipoles (vectors) are behind each other and also parallel or antiparallel. In H aggregates the transition-allowed vector combination (same direction) is blue shifted against the forbidden antiparallel combination and in J aggregates the allowed component (parallel vectors) it is red-shifted against the other forbidden component. Hence in these two special orientations blue-shift and red-shift can be observed. If the orientation of neighbouring molecules does not fit in the two ideal cases, the splitting of both components and their transition intensities can go through intermediate cases. In addition in a crystal theoretically also both combinations of the transition vectors can be observed. In the case of 26Dpa in solid state a red-shift is observed, which favours that in thin films the neighbouring molecules form J aggregates.

Back to the gas phase: concerning going from solution to gas phase, a possible trend would be a further blue-shift. Therefore, due to this expectation it is assumable that the noisy peak at 3212 meV is the gas phase the transition to S_1 and not the small step at 3000 meVwhich lies before the noisy peak. If this assignment is true, the small step before the S_1 transition (at 3000 meV) should be the T_2 state. This electronic state order would be then very similar to that of the anthracene core, where the anion-to-T_2 transition lies also close-below the transition to S_1 [Pau17]. Since 26Dpa shows bright fluorescence in solid state [LDW+15] it can be assumed that – as observed in the thin film experiment [LDW+15]– by excitonic coupling the excitonic transition allowed S_1 component shifts below the T_2 state. Note that the excitonic coupling between states in neighbouring molecules increases with the transition moment for the transition from S_0 state to the relevant state. Since the transition moment is large for singlet states and very small for triplet states, this means that due to the excitonic coupling singlet states shift strongly whereas triplet states do practically not shift. Further investigations on the lifetime or the configuration of the involved states could reveal the properties and the identity of the peak at 3000 meV.

Now coming back to the peak widths. The peak width of the first peak in the S_0 state is broader than the peak width of the first peak in the T_1 state. This effect is small, but notable and significant, especially since the electron energy resolution should be much better experimentally for the ground state PD-PE spectrum than for the T_1 state. The reasons for this are the different electron energies due to the two different wavelengths used: The energies of the electrons which stem from a S_0 population are more low-energetic than the energies of the electrons which stem from a T_1 population. Hence, it can be assumed that this width effect in S_0 is due to the envelope structure of the many excited low-energetic levels of the torsional vibration of the phenyl rings. In this argumentation a broader peak would mean that it consists of more quantum states of the torsional vibration motion and means more difference in the torsional geometries between the anion ground and the corresponding neutral state. Unfortunately the spectral regions of the transitions to the T_2 and the S_1 states are so noisy, that no informations about the torsional coordinates can be derived. It seems, however, that the geometry differences between the anion and the neutral states in the torsional coordinate are rather similar, in contrast to the p-polyphenyls, where the S_1 state was almost planar[Pau17].

All electronic state energies including literature data are collected in Table 4.11 below. In conclusion, for 26Dpa for the first time the EA, T_1 and S_1-state energies have been measured in the gas phase. It seems that also the position of the T_2 state is in gas phase below the S_1 state. It also seems that the phenyl torsion angle is different in the anion, the neutral ground and the excited states. If the PD-PE spectrum is – as assumed – dominated by anion-to-neutral FC factors the anion and the T_1 state have the best structural agreement in the torsional coordinate. It seems that the greatest geometry change

Table 4.11: Overview of the electronic state data of 2,6-DPA. The values without citation stem from this work. All values are given in *meV*

electronic state	configuration (ratio)	literature		experimental	
		theory	experimental	ΔE_{S_0}	ΔE_{D_0}
S_0/eA	-			-	884
T_1	-	-		1800	2684
S_1			3009[a],2799[b]	3212	4096
T_2	-	-	-		
S_2			-		

[a] [Cla61] UV-Vis in ethanol

[b] [LDW+15] UV-Vis of thin film on silica

according to the structures in the PD-PE spectrum takes place between the anion and the T_2 state.

A geometry shift in the low-energetic torsion vibration could also lead to a small error in the determination of the EA, since the maximum of the first spectral structure then does not correspond to the anion-to-S_0 origin transition: The true EA would then be at the onset. This is the reason that above the onset value of 884 *meV* was taken. The transition energies are less affected by this geometry shift, since all origin transitions are shifted in the same direction (to lower energies) and the differences do presumably not change very much.

Unfortunately it was not possible to produce enough dimers to investigate the excitonic coupling in such complexes. Such an experiment would have been enormously interesting because this subject was up to now never investigated in mass-selected compounds of a defined size and never from the radical anion.

4.6.9 9-Phenylanthracen

In the list of anthracene analogues, 9-phenylanthracene (abbreviated 9Pa[16]) is the next molecule which has been investigated by PD-PE spectroscopy. The chemical structure and the atomic numbering of 9Pa is shown in Figure 4.32). It has similar properties like the other substituted anthracene compounds, such as for example the phenyl group which is expected to be slightly twisted out-of-plane. In the following the molecular series 9-phenylanthracene, 9-(1-naphtyl)-anthracene and 99-bianthracene is investigated, a molecular series in which the substituted unit increases in size. With the size of the substituted unit increases the steric repulsion to the anthracene core. This should increase the twist angle between the two units. The out-of-plane twist angle and the effect of the substituted unit on the anthracene π system is one of the targets investigated in detail in the following.

9Pa has be used as a building block, in organic thin-film applications for example as a semiconductor intermediate [Vor20]. In other experiments it serves as an electron donor in optical active materials such as fluorophors [IKY16].

In addition, in the most recent work, 9Pa is used as a guest system for supramolecular photocatalysis, to generate triplet anthracene compounds for [4,2] cyclo-addition reactions [UOK+20].

Already 1976 9Pa was of spectroscopic interest, as its T_1 triplet state can be populated via a double-excitation methods [KKK76] in solution. Other data on 9Pa regarding the excited states rely on spectroscopy in thin films, in crystals and in solutions ([IKY16], [NS13], [KKK76], [UOK+20]). This means that the energy values obtained in this work can only be compared to condensed phase data.

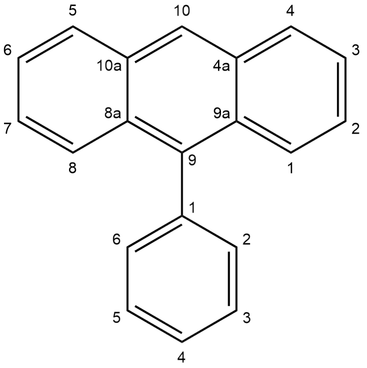

Figure 4.32: 9-phenylanthracene: Chemical structure and atomic numbering (IUPAC).

---

[16] 9-Phenylanthracene

The PD-PES spectrum of 9Pa is presented in Figure 4.33. In contrast to many spectra shown previously, it was recorded only with the detachment wavelength 266 *nm*. The reason for this is that the other available wavelengths (1064 *nm*, 532 *nm* and 355 *nm*) with high intensity excite anion-excited states, which then leads to very broad and ugly PD-PE spectra. In the spectrum recorded with 266 *nm*, the intensity of the S_0 state is rather low in comparison to the origin peaks of the other electronic states, which might partly be due to the fact that the electron energy resolution in this absolute electron energy range (about 4 *eV* electron energy) is rather low and the peaks are therefore broad.

The onset of the S_0-state lies at 576 *meV*, representing the EA of 9Pa. The lowest triplet state T_1 is observed at 1852 *meV*. Compared to the liquid phase value of 1785 *meV* [KKK76] it is blue shifted. This seems to be reasonable as a red-shift is typical when going from the gas to the aqueous phase. In the T_1 range between 1800 and 2500 *meV* (upper energy scale), a high-energetic vibrational progression up to two or even three quanta is visible, as well as an unresolved background-like activity most likely due to an autodetachment state.

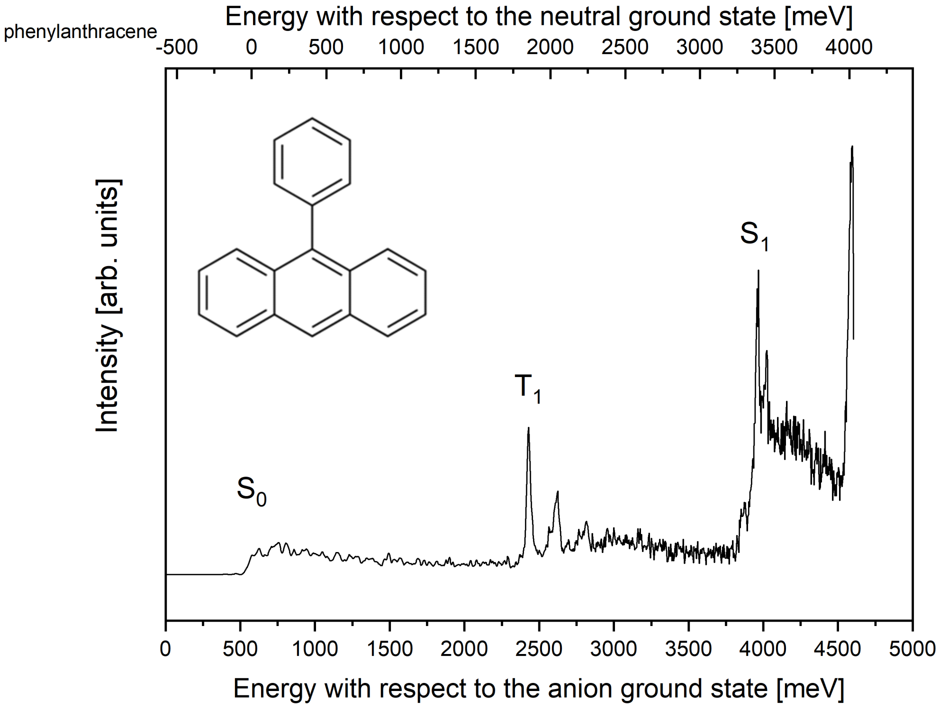

Figure 4.33: PD-PE spectrum of 9-phenylanthracen, recorded with the detachment wavelength 266 *nm*.

The S_1-peak at 3384 *meV* has the highest intensity in the spectrum and shows – in contradiction to the T_1-state vibrations – a lower-energetic vibrational progression. Possibly this low-energetic vibration (value?) is the frequency of the torsional phenyl vibration. The assignment of the T_2 state or other higher triplet states is difficult due to missing theoretical data. The small peak below S_1 is, however, not due to a hot band transition, and therefore a new electronic origin. In these past experiments with anthracene and anthracene derivatives, one could see a certain trend that the T_2-state lies just below the S_1-state [Pau17][Vog12][VKMW15]. So on this basis the structure in front of S_1 is assigned to the transition to the T_2-state.

At the very end of the energy scale, another sharp and high peak is present. Its nature stays unclear, due to the lack of theoretical data. It could be a transition to a singlet or triplet state. It could be unfortunately also caused by extremely low-energetic background electrons.

If one compares the PD-PE spectrum of 9Pa with the spectrum of anthracene [Pau17], the shifts of the corresponding peaks in 9Pa versus anthracene are minuscule. This situation leads to the assumption, that the π-system of 9Pa, is exclusively centred in the anthracene-structure and does not extend into the phenyl unit.

Table 4.12: Overview over the electronic state data of 9PA. The values without citation stem from this work. All values are given in meV

electronic state	configuration	literature		experimental	
		theory	experimental	ΔE_{S_0}	ΔE_{D_0}
S_0/eA	-			-	576
T_1	-	1785[d]		1852	2428
S_1		3220[a]	3228[a], 3130[b], 3090[c]	3384	3960
T_2	-	-	-		
S_2			-		

[a] [IKY16] theory B3LYP/UV-VIS in cyclohexane
[b] [NS13] UV-VIS in water/acetonitrile
[c] [UOK$^+$20] UV-VIS in dichlormethane
[d] [KKK76] double excitation in ethanol

The phenyl unit can only participate as a unit which can accept some surplus electron charge and by this slightly increase the EA ($EA_{anthracene} = 530\ meV$) In conclusion, the additional phenyl-group has nearly no effect on the energetic positions of the excited electronic states. This could be explained by a localisation of the anionic charge on the anthracene structure.

4.6.10 9-(1-Naphtyl)-Anthracene

The chemical structure of 9-(1-naphtyl)-anthracene, abbreviated 91NaAn[17], is shown in Figure 4.34. In comparison to the 9-phenyl-anthracene treated above, in 91NaAn the substituted naphtyl is now twice as large than the phenyl unit. As a consequence in 91NaAn there occurs a strong repulsion between the hydrogen atom in position 8 of the anthracene core and the hydrogen atom in position 8 of the naphtyl unit. This H-H repulsion in 91NaAn is expected to force the naphtyl group to twist out of plane by rotation around the C9-C1 axis, much more as this is the case for 9-phenyl-anthracene. Note, that in the latter molecule the shortest H-H distance between the anthracene core an the phenyl unit is considerably larger (see Figure 4.32).

As already mentioned before, many PAH's have optical properties for applications in OLED´s or other semiconducting devices. 91NaAn as well as other anthracene derivatives like 9-(2-naphtyl)-anthracene can be used for triplet up-conversion as shown in blue emitting OLED's [MZZ+15], [LSY+13].

Due to its very weak fluorescence the detection of the S_1-state origin of 91NaAn was first not found in a gas phase experiment [FKB57], only on later in ethanol solution by absorption spectroscopy [VBZ58].

The most interesting question arising for 91NaAn is how the twist angle between the anthracene core and the naphtyl side group influences the coupling between the two π systems. The strength of this interaction should especially affect the EA value, but possibly also the energetics of the excited electronic states. This and the similarity of the structure of 91NaAn with other substituted anthracene species raised the interest to investigate it with the PD-PES method. The PD-PE spectrum of 91NaAn recorded with a detachment wavelength of 266 nm is presented in Figure 4.35. Due to the fact that the PD-PE spectrum is not composed of sections of different spectra recorded with different wavelengths, the electron energy resolution is low for the transition from the anion ground state to the S_0 state (first peak on the left hand side) and increases to the right (compare the peak widths in Figure 4.35). The lower energy region of the spectrum around the transition to the S_0 state resembles in parts to the situation in the PD-PE spectrum of 9-phenyl-anthracene in section 4.2.9. Only some small differences exist: i) In Figure 4.35 the origin transition and a vibration of the S_0 state are somewhat better resolved and ii) there is less contribution of auto-detachment signal in the spectrum of 91NaAn than in the PD-PE spectrum of 9-phenyl-anthracene (see Figure 4.33).

The anion-to-S_0 origin transition lies within the accuracy of the energy calibration and with

---

[17] 9-(1-Naphtyl)-anthracene

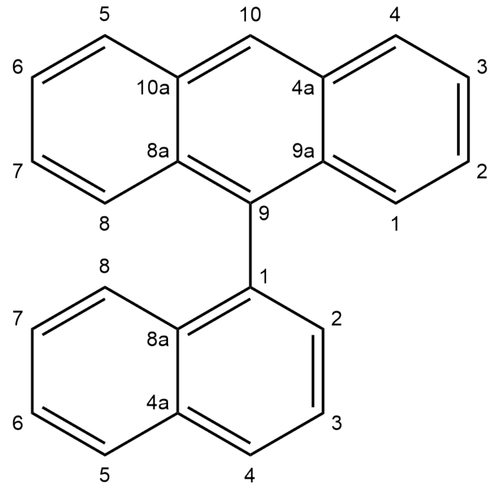

Figure 4.34: Chemical structure and atomic numbering of 9-(1-naphtyl)-anthracene (IUPAC).

the assumption that the FC factors allow the transition to the S_0 origin, at 652 ± 10 meV (lower scale) and defines the EA value of 91NaAn.

The peak at 1852 meV (upper scale) is the transition to the T_1-state. It is remarkably intense and followed by a vibronic transition, presumably a C-C- breathing mode (≈ 2000 cm^{-1}), which seems to be the same vibration than observed in the transition to the S_0 state. In the region of the T_1 state there seems to be also some auto-detachment signal modulating the baseline. According to the literature up to now the gas phase energy of the T_1 state was unknown.

The transition to the S_1 state at 3376 meV (upper scale) is very sharp and very intense. Its small width is a result of the very good resolution of the TOF spectrometer in this corresponding low-energy electron range. Due to this excellent resolution a vibronic transition about 50 meV above the S_1 origin is resolved, which might be the C9-C1 stretch vibration between the anthracene and the naphtyl group.

Right behind the S_1-state also a vibration with 250 meV ($\approx 2000 cm^{-1}$) is observed, presumably the same than in S_0 and T_1. Looking very close at the origin peak of the S_1 also a shoulder is observed (give value) which could be due to the torsion motion between the two units.

The available literature data on the S_1 state energy all rely on measurements in liquid phases, so a direct comparison of these data to the gas phase values of this work is difficult. The S_1 positions measured by UV-VIS spectroscopy in ethanol (3204 meV) [VBZ58] and in chloroform by fluorescence emission spectroscopy (3024 meV) [XLST13] are red-shifted against the value of this work (3376 meV), as is expected for such types of molecules.

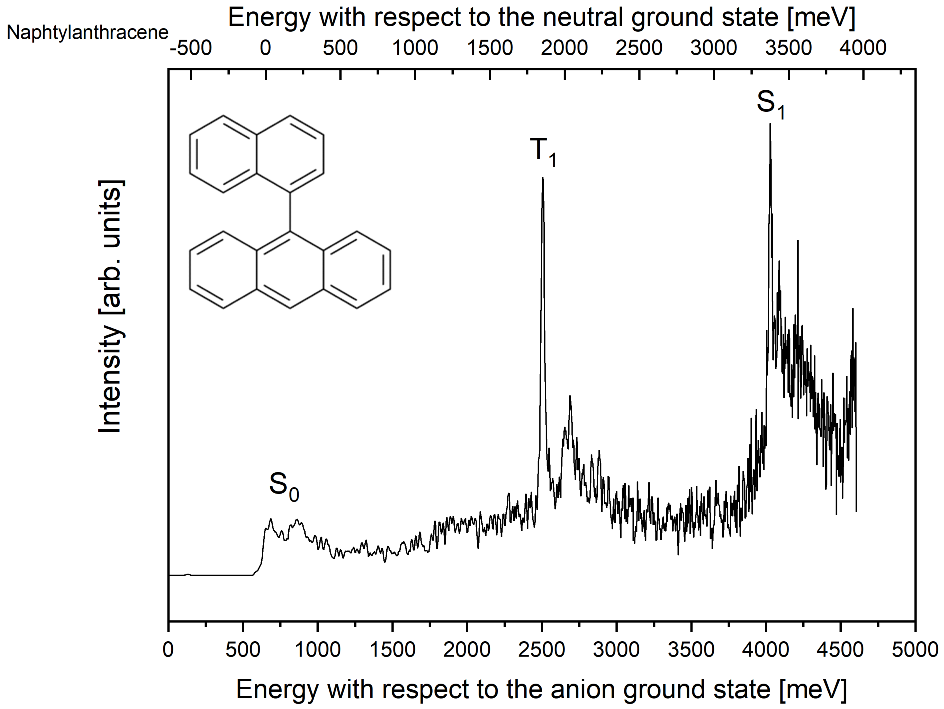

Figure 4.35: PD-PE spectrum of 1-(9-naphtyl)-anthracene recorded with 266nm

Right in front of the S_1 state, around 3100 meV (upper scale) several small peaks appear, which look like noise or hot-band transitions. Since hot-bands do obviously not contribute to the spectrum (see the zero line in front of the transition to the S_0 state) and the fact that in anthracene the T_2 state lies just below S_1, also in 91NaAn these small peaks can be assigned to the transition to the T_2 state. The fact that this transition is very small in intensity has an analogy to the intensity of the T_2 transition in anthracene, where only one of the two configurations of T_2 can be addressed by photo-detachment from the anion ground state configuration.The assignment of the peak at the end of the scale, is so far impossible and would need additional theoretical data.

In Table 4.13 the data of 91NaAn as determined in this work are compared to literature data. As a first comment concerning the consequences resulting from the PD-PE spectrum it can stated that the naphtyl group does not notably participate at the π system of anthracene, which suggests that the torsion angle of the two units against each other is large and that the FC intensities indicate that this torsion is not much involved in the photoexcitations from the anion to the neutral excited states.

Table 4.13: Overview over the electronic state data of 1-(9-naphtyl)-anthracene. The values without citation stem from this work. All values are given in meV

electronic state	configuration	literature		experimental	
		theory	experimental	ΔE_{S_0}	ΔE_{D_0}
S_0/eA	-			-	652
T_1	-	-		1852	2504
S_1			3204[a];3024[b]	3376	4028
T_2	-	-	-		
S_2			-		

[a] [VBZ58] UV-VIS

[b] [XLST13] fluorescence emission

4.6.11 9-9'-Bianthracen

The chemical structure of 9-9´-bianthracene, abbreviated 99Ba[18], is shown in Figure 4.36. Due to the fact that the hydrogen atoms at the positions 8 and 8´ as well as 1 and 1´ repel each other, the structure of 99Ba is such that the two anthracene units are rotated against each other along the C_9-$C_{9'}$ axis into a nearly perpendicular relative-position. This implicates that the two π systems are mostly decoupled and more or less independent.

Similar to other PAH's presented in this work, also 99Ba is used in OLED´s and in organic semiconductor devices. It is a cost-efficient intermediate for the synthesis of blue emitting OLED's as shown by Li and co-workers [LGL⁺19].

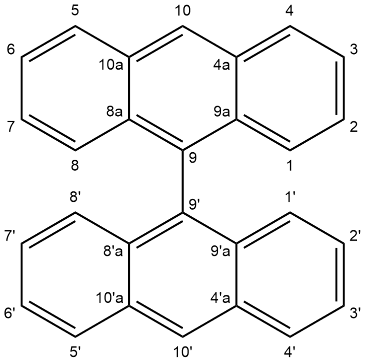

Figure 4.36: Chemical structure and atomic numbering of the 9-9´-bianthracene molecule (IUPAC).

The fact that anthracene has a relative high EA (530 ± 5 meV) [Pau17],[SW97] and a relative low IE 7.41 eV [Sch77] led to the assumption that a low-lying intra-molecular charge transfer (CT) state below the S_1 state may exist. This theoretically predicted CT state was not observed in the gas phase[KZ86]. The reason for this might have been, that in comparison to the geometry of the S_1 state in the CT state the anthracene-anthracene distance should be compressed by the attraction of the two opposite charges. As a result, even if the origin of the CT state would be energetically below the S_1 state, it cannot be populated directly by photoexcitation from S_0 or by a radiation-less process from the origin of the S_1. The reason for the latter is that the geometry difference between the two states results in a high barrier between them (see Figure 4.37).

Just recently, Lee and co-workers observed the charge transfer by time-resolved fluorescence detection in 99Ba, however, only in polar solvents [LLCJ19]. They could identify the SBCT[19]-band at about 480 nm (2583 meV above S_0). The reason that in polar

---

[18] 9,9'-Bianthracene

[19] symmetry breaking charge transfer

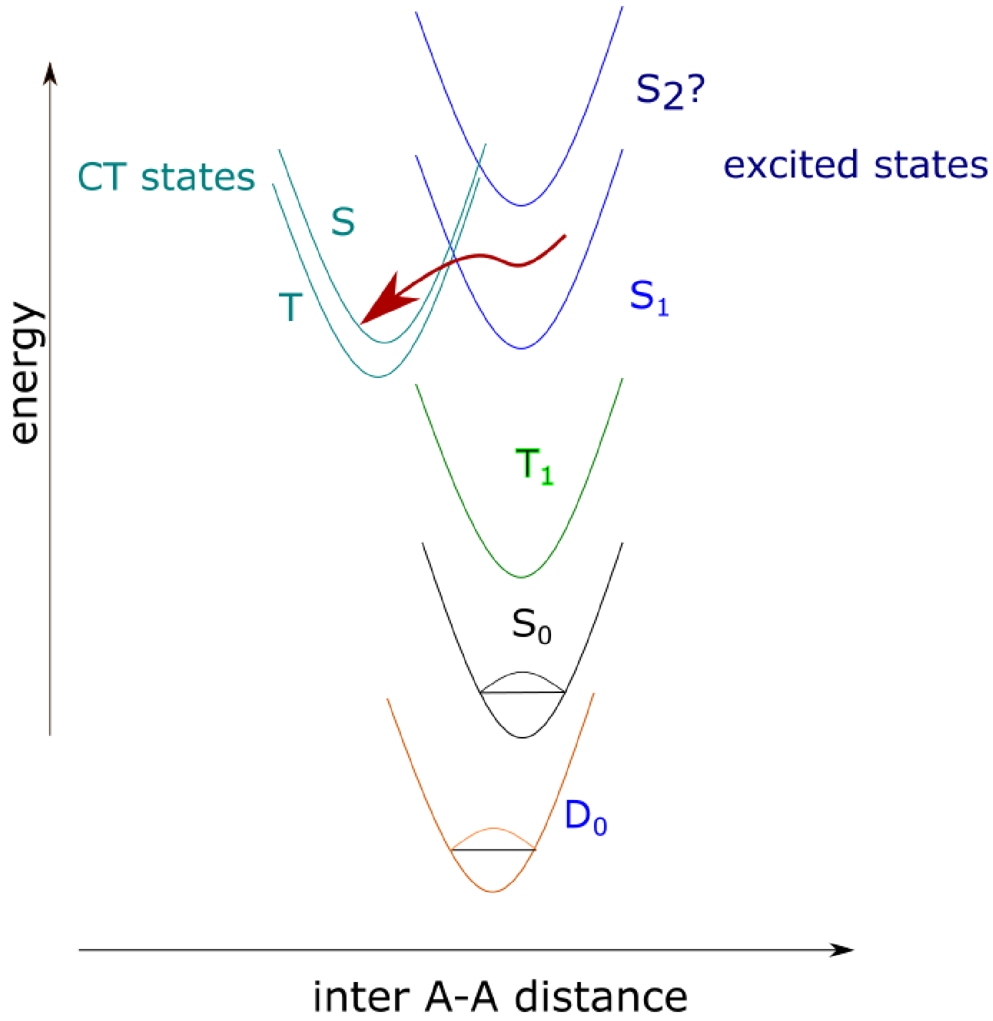

Figure 4.37: Schematic electronic state in 9-9´-bianthracene: Note the intersection between possible CT states and the excited state. The CT state can be adressed while exciting into higher electronic states.

solvents the CT state can be populated from the S_1 state and not in the gas phase is, that the CT state is stabilized by the solvent and pushed downwards so that the barrier between S_1 and the CT state is considerably lower or even vanishes. Additionally, the group of Zhao [ZCH+18] later observed a charge-transfer-induced ISC[20] to the T_1 state, which also depends on the solvent used. The explanation for this lies in the fact that in the charge-separated situation the two unpaired electrons are i) well-separated and ii) can have a parallel or anti-parallel spin. Due to the unpaired orbitals are disjunct and the unsaturated electrons are far apart this results in the consequence that the singlet-triplet splitting is very small and the singlet CT state and the triplet CT state are nearly isoenergetic[VKMW15] .This is expected to enhance the ISC between the singlet CT and

---

[20] inter system crossing

the triplet CT. The latter state then can relax by fast IC to the T_1 state.

It seems that the nearly orthogonal alignment of the two anthracene units promotes the CT and this special ISC-mechanism [ZSC+21]. In the same work a T_1-T_n-absorption could be observed at around 433 nm (2863 meV) which also seemed to have a charge transfer characteristics.

Due to this CT state and the CT-induced dynamics, 99Ba is an especially interesting molecule for spectroscopists. By the investigation of 99Ba radical anions with PD-PE spectroscopy it is possible to be able to directly access the CT state by photodetachment, because of the following reasons:

- i) The geometry of the anion of 99Ba might be compressed in comparison to that of the neutral ground state S_0. By this, the anion geometry might be close in geometry to the CT state allowing probably non-vanishing FC factors to the origin transition of the CT state.
- ii) The detachment process from the 99Ba anion to the neutral CT state is fully allowed because it is just the ionisation of the neutral anthracene unit in the presence of the second anthracene as an anion.

The hope that i) the geometry of the anion might be contracted is not so easily understandable: It is based on the expectation that in the anion ground state of a bi-chromophoric molecule a charge resonance effect may be present. Such charge resonance effects are well-known for radical cations [ON92] but their existence is still under discussion for negatively charged dimer complexes and nearly unknown for bi-chromophoric molecules such as 99Ba.

The typical pattern which allows the recognition of a charge resonance effect is the splitting between the bonding and the anti-bonding CR states. This splitting can be directly observed by optical excitation in the near IR wavelength range (0.5 - 1.0eV). Indeed an IR absorption in the radical anion of the bi-anthracene derivative 1,4,1´,4´-anthracenophane has been found in solution, which could be interpreted as a transition between the two CR states [SI72]. Since in this molecule the two anthracene units are coupled by two C-C- bridges, and hence much weaker than in 99Ba, it can be expected that such an CR absorption should also exists in 99Ba. It might be shifted to higher energies due to the strong coupling between the two anthracene units and the isolation in the gas phase. On the basis of these unique effects in 99Ba, and because of i) and ii) above there is a special interest in obtaining PD-PES-spectra of 99Ba. In Figure 4.38 the composed overview PD-PE spectrum of 99Ba is shown. It consists of three sections of different PD-PE spectra, which have been recorded with the detachment wavelengths 1064 nm, 355 nm and

266 *nm*. Figure 4.39 shows the complete spectrum recorded with 355 nm (upper trace, green) and the complete spectrum recorded with 266 nm (lower trace, blue) over the full energy range. In the latter spectrum it becomes evident that the excitation with 355 nm obviously excites an excited state in the anion or even several anion excited states. At this point it is important to point out, that autodetachment via anion excited states i) still follows the law of energy conservation and ii) the neutral molecule has to remain in an electronic state in a vibrational excitation which really exists in the neutral molecule. Hence although the FC factors can be manipulated by the autodetachment process the AD peak positions in the PD-PE spectrum represent vibronic states of the neutral molecule.

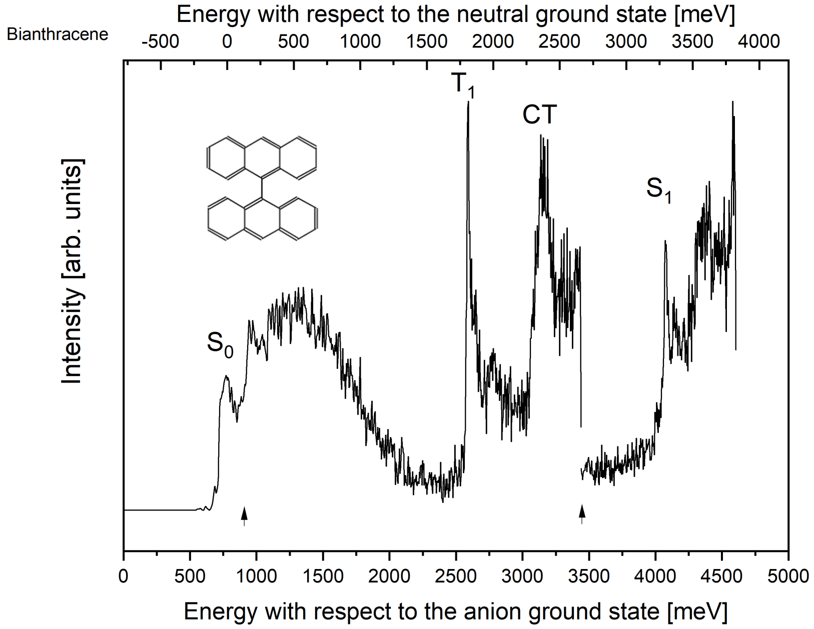

Figure 4.38: PD-PE overview spectrum of 9-9´-bianthracene.The spectrum is composed of sections of the spectra recorded with 1064 *nm*, 355 *nm* and 266 *nm*. Please note the transition behind the T_1 state, which we attribute to the intra-molecular charge transfer state CT. For further explanations see text

In Figure 4.39 in the lower trace the peak shape and the peak positions (compare to anthracene [Pau17]) agree with the normal expectation one would have for a PD-PE spectrum of 99Ba. This means that the detachment wavelength of 266 *nm*is obviously non-resonant with anion excited states in 99Ba.

To make the following discussion easier for the reader, forestalling the outcome of the assignments is necessary. You can assign the on-going structure directly behind the S_0 state to inter-anthracene vibrations in S_0 and the spectral structure CT above the T_1 state

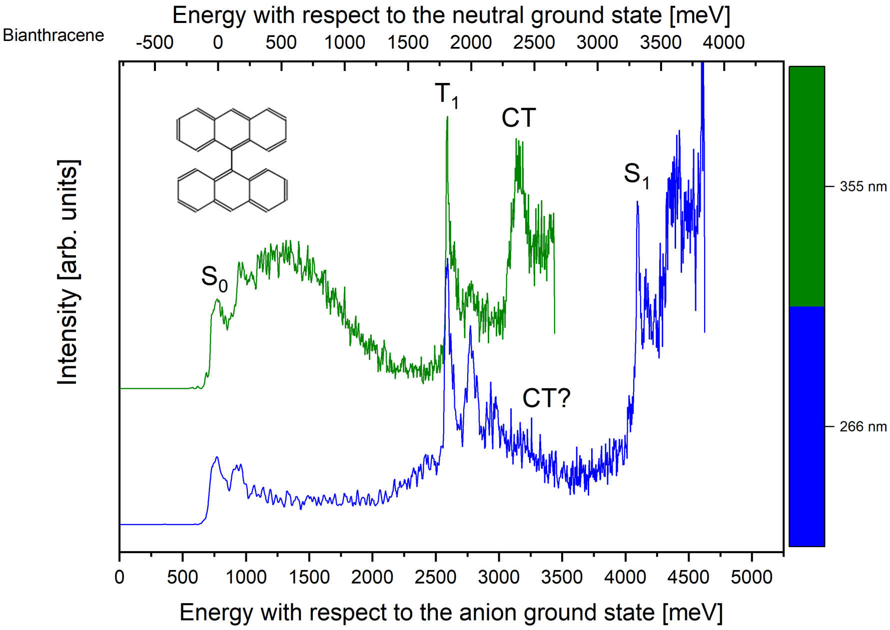

Figure 4.39: PD-PE spectra of 9-9´-bianthracene recorded with 355 *nm* (upper trace, green) and 266 *nm* (lower trace, blue). Note the change in intensity and the appearance/disappearance of the CT structure. For further explanations see text.

as the transition from the anion to the intra-molecular charge transfer (CT) triplet and singlet states of the in total neutral 99Ba molecule.

First proceeding as usual. The transition to the S_0 state is observed at 728 *meV* (this defines the EA of 99Ba). The best accuracy of the S_0 position and the EA value is achieved with the detachment wavelength of 1064 *nm* (energy value taken at half height of the left side of the first peak).

In the spectrum recorded with 355 *nm*the region from 800-1800 *meV* is filled with a strong signal (see Figure 4.38) which should correspond to vibrations of the S_0 state. There can be two reasons for this:

- i) the anion ground state is a charge resonance state and is geometry-shifted to the S_0 state and/or
- ii) the detachment wavelength resonantly excites a vibrational excited auto-detachment state of the anion which has FC overlap to high-energetic vibrational states of the S_0 state.

Concerning the first point i) already a positive statement was made above. Concerning ii) the question is, what is the nature of this vibrational excited auto-detachment state of the anion. Below each vibronic level of the CT state, there should be an anionic dipole-bound state. A detachment from such a dipole-bound state which corresponds to a vibronic state of one of the CT states is expected to have a preference to decay to the neutral CT state, but neither to the T_1 state (as observed) nor to the S_0 state. This means that the involvement of dipole-bound anion excited states resonantly excite with 355 nm but not with 266 nm agree with the presence and absence of the CT state in the corresponding spectra in Figure 4.39. An other explanation for the broad structure in S_0, but not in T_1 could be that the inner wing of the anti-bonding CR resonance state can reach up to 355 nm. If this anion upper CR state would be excited neither the T_1 state nor the CR states can be populated by the loss of the electron from the upper π^* charge resonance state.

In conclusion, it is possible that the situation in the 99Ba anion and in the neutral molecule is rather complicated due to the two CR states and the two CT states.

In the following, it is continued with the spectrum recorded with 266 nm because it seems to be almost free of auto-detachment effects.

The very intense T_1-state origin lies at 1864 meV followed by a vibronic transition of about 250 meV, presumably a vibration in the ring system.

The S_1-state is observed at 3344 meV, which is in good agreement to the gas phase value of Zewail et al. (3321 meV) [KZ86]. Behind the S_1 origin a small vibronic transition is observed at a distance of 50 meV.

Similar to other spectra of molecules with an anthracene core presented in this work, right in front of the S_1-state at directly at the rise lies again a minuscule peak. This could be the only weakly-allowed triplet-state T_2. However, further evidences like theoretical calculations are lacking to support this tentative assignment.

In the 355 nm spectrum, right after the first triplet-state, a very intense and relatively sharp peak appears. Since it is only present in the 355 nmspectrum a resonant excitation to an anion excited state followed by auto-detachment has to be present.

The question is, what is the nature of this anion excited state and what is the nature of the final state in the neutral molecule. Since the resonant excitation of neutral anthracene lies accidentally close to 355 nm (361.08 $nm \approx 3.4339$ eV, [LFSZ84]), it is reasonable to assume that the detachment wavelength 355 nm resonantly excites the neutral anthracene unit of the two units in 99Ba, and that then the excited anion undergoes auto-detachment to the CT state at 2408 meV by loosing the electron of the excited neutral anthracene unit. This resonant excitation of the neutral part of 99Ba is obviously so strong that it can compete with the detachment process of the anionic part of 99Ba. This leads to the conclusion that the peak at 2408 meV can be assigned to the two intramolecular CT triplet and singlet states. The PD-PE value of 2408 meV is in relative good agreement with the value found in polar solvent (2583 meV)[ZSC+21] if one considers that fluorescence can only come from the upper singlet CT component and that in both experiments – solvent and gas phase – geometry changes and FC factors may contribute to a difference between the observed signal rise and the position of the adiabatic onset. All obtained data, as well as literature data can be seen in table 4.14.

Table 4.14: Overview over the electronic state data of 99BA. The values without citation stem from this work. All values are given in meV

electronic state	configuration (ratio)	literature		experimental	
		theory	experimental	ΔE_{S_0}	ΔE_{D_0}
S_0/eA	-				728
T_1	-	-		1864	2592
CT	-	2583[a]		2408	3136
S_1			3321[b],3187[c],3171[c]	3344	4072
T_2	-	-	-		

[a] [ZSC+21] CT fluorescence in polar solvent

[b] [KZ86] super sonic jet, time resolved fluoresence

[c] [ZSC+21] uv-vis in acetonitrile/dichlormethane

4.6.12 Comparison of the anthracene derivatives

The high number of the investigated anthracene derivatives allows a comparison of their excited state energies and their electron affinities. As already found before in the works of Konieczny[Pau17] and Vosskötter [Ste15] there can be certain tendencies when the size or the substitution of conjugated molecules is changed. These tendencies are observed in PD-PE spectra as EA changes or/and changes of the electronic state positions in the compounds. For example Zhao and co-workers [ZSC+21] mentioned, a local excited state in 99Ba. The question is, whether the S_1 state in 99Ba is really local? The following comparison of the spectra of 99Ba and other anthracene derivatives adds further evidence of this local excitation. Figure 4.40 shows all acquired spectra (composed) of the anthracene derivatives and figure 4.41 graphically displays the excited state values for a better overview.

Electron Affinities

Coming from pure anthracene with a EA of 530 meV[Pau17],the electron affinity varies within a range of 300 meV, indicating that the addition of any phenyl group increases the EA of the system, therefore enhancing the local charge stabilizing effect. This is not surprising as generally a phenyl group is considered inductively withdrawing and resonance donating.

9Pa has the lowest electron affinity of 576 meV in the investigated series indicating a electron density withdrawing effect as well as a resonance donating via the phenyl group. So if another phenyl-group is added, resulting in 26Dpa or 910Dpa respectively results in a higher electron affinity, 884 meV and 750 meV. This indicates that an addition of a second phenyl-group has a much higher impact on the system as just one, if compared to the difference from anthracene to 9Pa (ΔEA = 46 meV), from anthracene to 910Dpa (ΔEA = 220 meV) and from anthracene to 910Dpa (ΔEA = 354 meV). Regarding the differences with respect to the anthracene molecule, the effect on the EA is not linear. Additional a positioning of the phenyl-groups in a way that increase the spatial size in one axis (like in 910Dpa) has a bigger impact on the EA. Nevertheless the effect seems to be the biggest in the diphenyl-derivates, as they inherit the highest and second highest EA in this series.

Regarding an addition of a naphtyl-group as for 91NaAn, the EA increase is higher as with just a phenyl-group ΔEA = 122 meV.

The effect of adding an anthracenyl-group to an anthracene has an even bigger effect as ΔEA = 198 meV resulting in an EA of 728 meV. This value affirms the perpendicular structure of the 99Ba-molecule, as the EA of 99Ba is not simply doubling related to the anthracene molecule, indicating a weak but existing coupling between the anthracene sub-systems. In conclusion, only regarding the investigated species revolving around anthracene, 3 major effects can be observed:

- Adding groups with a (-I)/(+M)-effect generally increases the EA.
- The EA increase is not linear.
- The positioning is crucial in the resulting effect.

Triplet T_1-states

As in this work, several before unknown gas phase values for the triplet states could be observed, also a comparison in the deviations regarding the excited states is interesting. Remarkable are the miniscule shifts in the position of the T_1-state, as the differences between them, as well with respect to the anthracene molecule are nearly 0 meV a first sight, the triplet state all over all derivates is nearly the same (comparing the red lines indicating the anthracene values). This is a quite unexpected behaviour, as it could be assumed that adding functional groups with inductive effects should also alter the symmetry and structure of the corresponding molecular orbitals resulting in deviations.
This issue corroborates among other things the claim of Zhao[ZSC$^+$21], 99Ba is firstly locally excited within the anthracene systems. Now it can also be claimed that regarding the lowest triplet states of anthracene analogues, the major configuration of the T_1-state is determined by the anthracene-subsystem.
However, also the vibrational progression seems to be the same all over the investigated molecules, with the exception of 99Ba (compare section 4.2.11) and 910Dpa were obviously affected by AD-states as the vibrational progression is modulated. For an overview refer to 4.40 and 4.41.

Singlet S_1-states

The comparison of the S_1-states displays a slightly different effect. The shifts of the S_1-states are slightly higher than the shifts of the triplets. However, it stands out that within the group of 99Ba,91NaAn and 9Pa the singlet value shifts just around 40 meV. So regarding this series, it also seems that the anthracene MO's are dominating the configuration of the singlet states. Furthermore the red-shifts of 26Dpa and 910Dpa are conspicuous, as they are further shifted to the red in comparison to the other three systems. The position of their singlet S_1-value is nearly identical, which leads to the assumption that the positioning of the phenyl groups barely has any effect on the singlet-energy. These shifts can be observed in 4.40 and 4.41.

Overall it seems, that the anthracene subsystem dominates the configurations for the singlet and triplet states regarding their respective energies. All this evidence affirms the claims of a locally excitation of the anthracene subsystem, even in other molecules than 99Ba as reported by [ZSC$^+$21]. For a better understanding and interpreting interrelationships, more data is needed, experimental and theoretical as well.

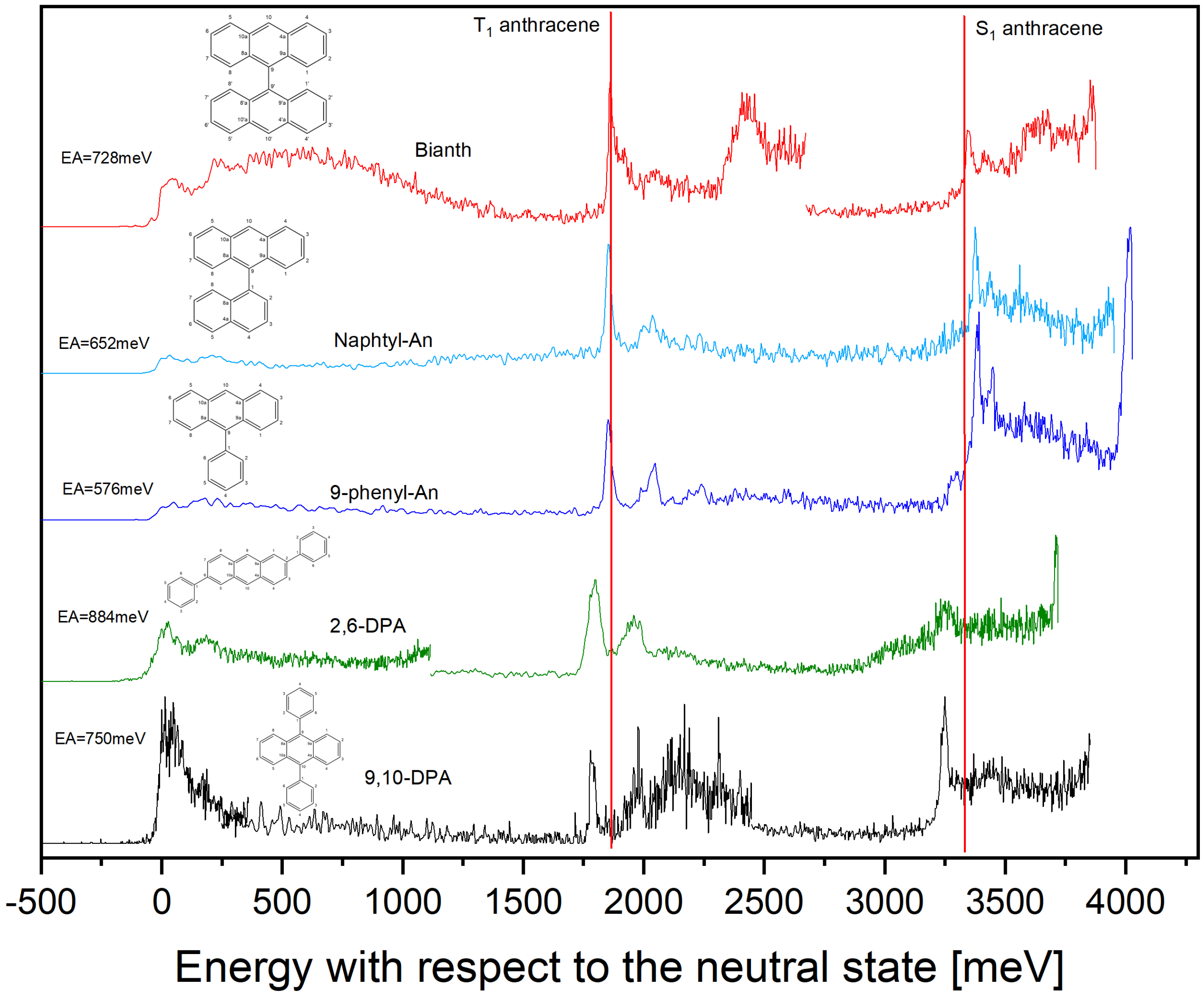

Figure 4.40: Photo-electron spectra of anthracene derivates. Note the position of the excited states. The charge seems to be localised on the anthracene system. Further explanation see text.

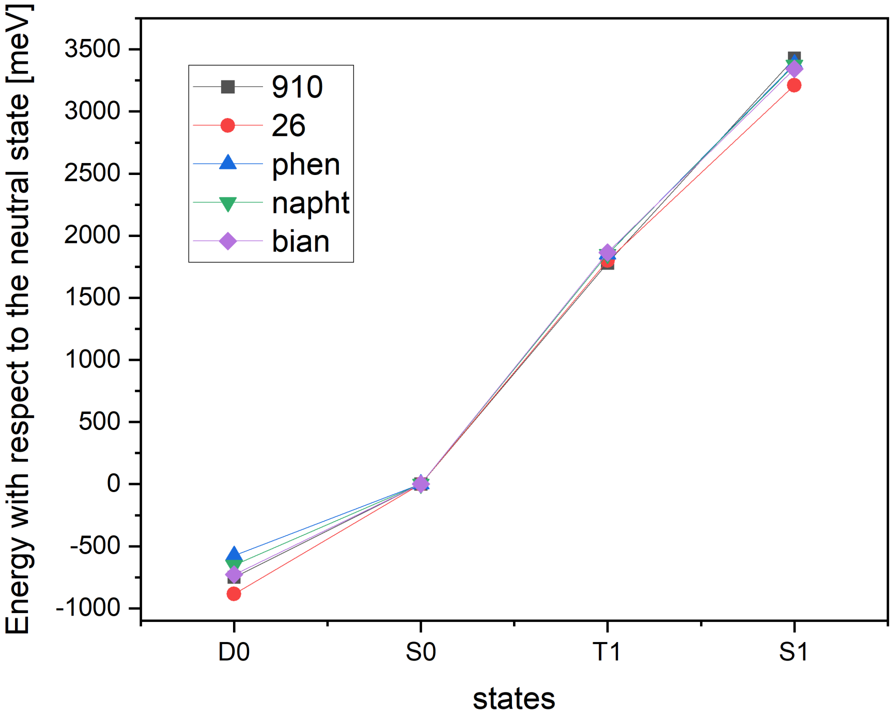

Figure 4.41: Comparison of the excited state values of the investigated anthracene derivatives.Note the miniscule shifts in the triplet energy. Further explanation see text.

4.7 Complex compounds

4.7.1 Copper phtalocyanine

Metalloporphyrines in general, had been studied intensively, not only due to their resemblance to biological active molecules, but also to their applications as semiconductors, especially Cu-Ph[21](comp. 4.42). One exemplary usage in biochemistry is to inhibit certain enzymes [Rot11]. The manifold usages in semiconductor applications include high charge mobility in thin films as Dimitrakopoulos and co-workers could display[DPK+99]. So the electronic properties of Cu-Ph are crucial, for the application as conducting material. However, vapour spectroscopy had been difficult to perform on molecules in this size, as temperatures around 400° C are needed for vaporizing, resulting in experimental challenges. Nevertheless, a PD-PES spectrum could be obtained, but regarding the electron configuration in the ground state a straightforward interpretation is confounded.

To establish a possible interpretation, the spectroscopical history of Cu-Ph is crucial.

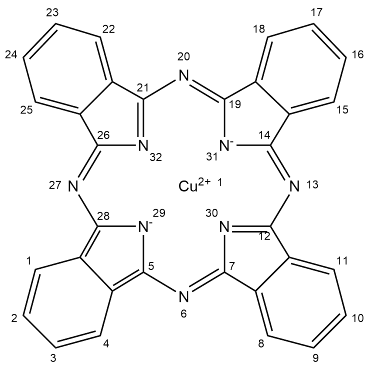

Figure 4.42: Chemical structure and atomic numbering of the copper(II) phtalocyanine molecule (IUPAC).

Beginning in the mid 60's, Steinfeld et Al. [EEGS66] were the first group to obtain absorption/emission spectra of metallo-porphyrine vapors. They observed no fluorescence just absorption at 15240 cm^{-1} (1889 meV) indicating a radiation less decay of the S_1-state. Shortly after in 1970 Schechtman was able to the record absorption spectra of thin Cu-Ph films, whereas he could identify this absorption band (q-band, $S_0 - S_1$-transition) at roughly the same energy (1.8 eV) and the soret-band ($S_0 - S_2$-transition,3700 meV) as well as other higher energetic transitions beyond the soret-band[SS70]. Both groups agreed in the point, that the additional electron from the copper metal, is responsible for the absence of a fluorescence, Steinfeld et Al proposed a intersystem crossing as a possible

---

[21] copper(II)-phtalocyanine

channel for a radiation less decay. Much later, Liao and Scheiner [LS01] did a theoretical study (DFT) of the metallo-porphyrins, with interesting results. The electron configuration in Cu-Ph shows that the there exists a SOMO[22](b_{1g}) between the HOMO(a_{1u}) and LUMO($2e_g$), indicating that the possible configurations of the ground state is a doublet, because of the SOMO. The nature of the ground state being a open shelled state, could be determined by ESR early on [CAS69], as well as by XANES performed by [CCB$^+$04]. This starting situation means, that a electron attachment to Cu-Ph leads either to singlet or a triplet state, both configuration that would hinder a direct observation of the forbidden state via anion-PD-PES. This raises the question, why the obtained spectrum seems to appear like a typical PD-PES spectrum. Interestingly, Liao and Scheiner claims that a one electron oxidation process in Cu-Ph always occurs out of the HOMO and not out of the SOMO although lying 500 meV above. From this point on, one can speculate that the SOMO, which can be associated to the copper-atom, possibly does not contribute to the configurations responsible for (some of) the excited states. This would possibly lead to a local excitation on which only the porphyrine contributes. The SOMO state then could be seen as a "spectating state", not interfering with the MO's participating in the excitation. This leads to the conclusion that the here recorded spectrum, in fact displays a PD-PES spectrum featuring the excited states of the molecule as intended by the method. However[UFN$^+$07] could detect plasmon-enhanced up conversion fluorescence of Cu-Ph thin films on gold surfaces, showing a internal energy transfer via the T_1-triplet state resulting in an upconversion to a higher singlet state and resulting in a S_1-fluorescence which could not be detected by other means. Their obtained values (although its difficult to directly compare solid state spectroscopy with the gas phase) are in accordance with the here obtained spectrum.

With this in mind, interpretation of the PD-PES-spectrum can be performed as above. So the first peak (compare figure 4.43) marks the EA of Cu-Ph, with a very high value of 2166 meV if compared to the smaller investigated systems before. Of course this is an effect of the sheer size of the complex. The peak at 1083 meV then can be interpreted as the T_1-state,with some vibrational progression up to the area of 1200 meV. The X-marked peak, seem to not be a vibration of the triplet state, and could possible be another triplet-state (e.g. the T_2-state), but due to a lack of data, this can not be affirmed. The broad structure at 1870 meV marks the positon of the S_1-state, in good accordance to [SS70] ($1,8eV$) and [EEGS66] (1889 meV). Also the data gained by [UFN$^+$07] (1700 meV) seems in accordance to the gas phas value here, as a redshift can be assumed transitioning

---

[22] semi occupied molecular orbital

from vapour to solids. A further interpretation of the area after the S_1-transition can not be established due to the increase of the baseline and the noise ration. Note that the theoretical values derive from the literature (experimental values) and therefore from the obtained values here. Compare Table 4.15 with all obtained data from literature and the data from literature sources.

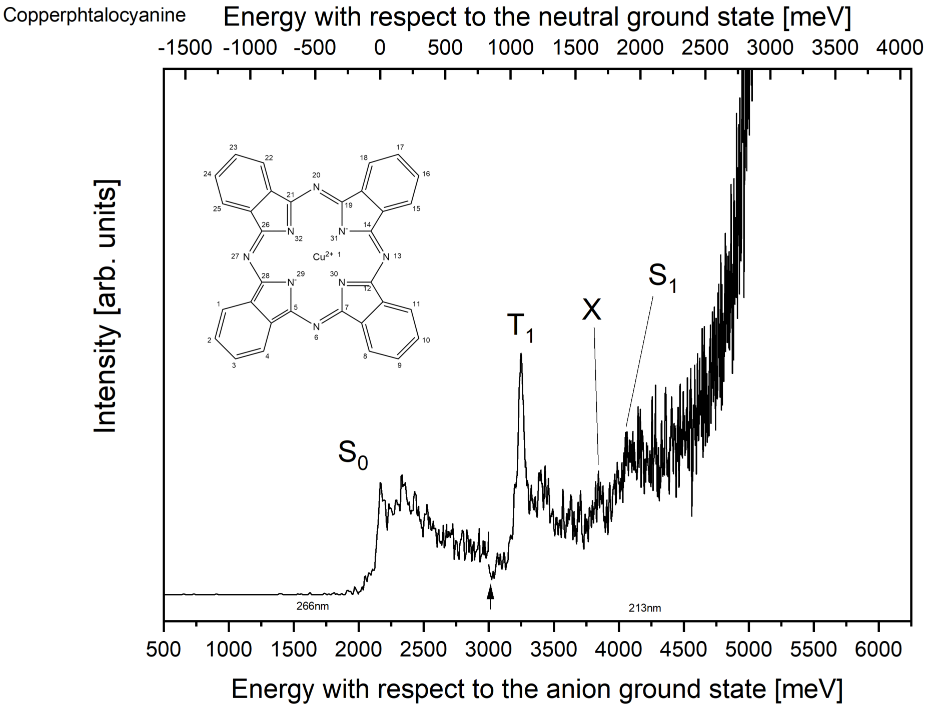

Figure 4.43: Photo electron spectrum of Pigment Blue-15. Used wavelength 266 *nm* and 213 *nm* composed at 1000 *meV* and 4600 *meV*

Table 4.15: Overview of the electronic states of Cu-Ph. The non cited values are out of this work. All values are indicated in *meV*

electronic state	configuration (ratio)	literature		experimental	
		theory	experimental	ΔE_{S_0}	ΔE_{D_0}
S_0/eA	-				2166
T_1	-	-	1100[a]	1083	3249
S_1		1460[b]	1700[a],1800[c],1889[d]	1870	4035
X	-	-	-	1676	3844
S_2			-		

[a] [UFN+07] plasmon enhanced upconversion on Au-substrate, electron tunneling microscopy
[b] [LS01] density functional theory
[c] [SS70] absorption uv-vis thin film
[d] [EEGS66] absorption uv-vis vapour

5 Appendix

5.1 Conclusions and Outlook

Radical anion-photo-detachment-spectroscopy wields the capability to contribute data on electronic structure of organic compounds which are otherwise inaccessible. The spectroscopy of forbidden states, such as triplets, can complement other studies and be insightful for the research of excited states in general.
So the major focus of this work had been to gather further, previously unknown, data on PAH's, complex compounds and heterocyclic compounds. In general these are not accessible by the means of classic spectroscopical methods. Also the superior aim of a systematic understanding of the interaction of structure and electronic states was tried to be served. In an attempt to meet the objectives mentioned above, this work contains

- The PD-spectra of four heterocyclic compounds (5Fi, 6Fi, f9one and DBF) and their comparison.
- The PD-spectra of ten PAH's (pyrene, benzantracene, BaP, DBA[1], 5-Ac, 910Dpa, 26Dpa, 9Pa, 91NaAn, 99Ba) and their comparison.
- The PD-spectrum of Cu-Ph and a possible interpretation.

In order to improve especially the time needed to obtain a radical-anion PD-PES, instrumental advancements were the key. These advancements could be achieved through the supervision of several theses which took place under the supervision of the author.
Including the bachelor theses by

- Marco Schmitt: first idea and setup for the needle discharge setup
- Laurin Henson: attempt to feed an electron gun via needle discharge
- Franziska Wichmann: improvement of the first needle setup (first pulsed setup) and first obtained interpretable mass-spectra

---

[1] Dibenz[a,h]anthracene

- Jan Meissner: attempting desorption via the needle discharge setup

and also the master theses by

- Nikita Schützek: redesign of the needle setup to the mounted-setup
- Jan Meissner: first obtained PD-PES spectra in a master thesis resulting in a publication [MKMW21]

The last mentioned thesis marked a milestone in the handling of the PD-PES-setup. Before the instrumental improvements, it was time consuming and difficult to obtain a spectrum (it took around days to a week just for the mass spectra to be obtained). The massively increased numbers in produced anion species often just took around 30 minutes to get a mass signal, prerequisite a positve EA.
In conclusion the usage of the mounted-discharge setup was the key to obtaining more spectra than before and can be seen as the core advancement in this work.

Spectroscopical advances

As just mentioned the savings in time made it possible to investigate more molecular systems thab ever before in a set time. With the intention of generating comparable datasets of molecules could be obtained. Yet, is has to be said that a successful interpretation of PD-PES-spectra is only possible to be interpreted by affirmation of other spectroscopical methods or theoretical investigation.
Nevertheless regarding the investigated heterocyclic compounds, the following could be observed:

- 5Fi and 6Fi are forming dipole bound states instead of anion radicals, due to their dipole moment, but the spectroscopy of these species opened up a pathway for a regio-selective dehydrogenation.
- For f9one a possible T_2-state was observed and the EA could be determined.
- The first lowest triplet states for DBF as well as its EA could be obtained.
- The direct comparison showed a systematic energy drop of the excited states from DBF to f9one

The biggest group of the investigated molecules had been the PAH's revolving around the anthracene sub system. So many spectra could be obtained in order to see overarching interrelationships. So concluding the acene, antracene-like derivates,

- The PD-PES of pyrene could be obtained as a benchmark measurement, gaining affirmation for the method itself.
- The EA of benzanthracene, as well as a hint on the positon of other triplet states.
- The T_1,T_2 and S_2-state for BaP.
- The EA, T_1 and T_2 state of DBA.
- The PD-PES spectra of 5-Ac in accordance to literature to fulfil the series of acenes (started with 3-Ac and 4-Ac).
- A comparison of the acene like molecules, showing that further data is needed for a systematic approach.
- The EA of 910Dpa, and the direct measurement of its T_1-state.
- The EA of 26Dpa and its triplet T_1 state, as well as the first vapour S_1-value.
- the first vapour values for the EA and T_1 of 9Pa
- the first vapour values for the EA and T_1 of 91NaAn
- charge transfer state of 99Ba, as well as the triplet state and EA
- a comparison of the anthracene derivates, indicating that the anthracene sub-system determines the excited states

This amount of data acquired made comparisons possible in this dimension. For a first investigation on trends in molecular structure and the position of excited states.
Furthermore, upgrades in the inlet system in chamber 1 enabled the investigation of substances with a high sublimation temperature. By that the Cu-Ph molecule could be investigated by PD-PES for the first time. Its EA could be obtained, as well as possible values for the S_1, T_1 and a hint on further excited states below the known q-band.
The raw amount of newly gained information on excited states and EA's indicate that the instrumental changes strongly improved the setup and made several new discoveries accessible.

Outlook

Summarizing the insights resulting from the conclusion of this work, several future improvements are conceivable. On one side, further instrumental developments are possible, on the other side further investigation of the molecular series here would also benefit future studies.

The enhancement of the experimental setup, has several approaches. So it is considerable, to further adjust the inlet-system to enable an access to bigger, possibly biological relevant molecule systems. A possible idea to achieve this claim could be the fusion of the mounted discharge valve without relying on the thermal sublimation of the sample. This could be done e.g. by means of desorption, but would also require intense investigation. As mentioned before (comp. 4.2.5), certain other measures would be beneficial:

- A fully tunable pico-second laser, for circumventing e.g. anion-exited states, and an overall better resolution of the respective peaks.
- Recreating the experiment with a higher repetition rate (e.g 20Hz).
- Upgrading the vacuum pumps, installing cryo-pumps.
- Additional detectors, possibly in a spherical orientation.

Also, an extended measurement-time could improve the signal noise-ratio, or as the last item suggest a more area-wide detection of electrons would accomplish the same. However, there are still ways to further improve the experiment.

The accomplishments by this work, mainly the easier execution of the experiment itself opened up possibilities to amass further spectroscopical data. As mentioned before in chapter 4.1, a systematic research on the regio-selective dehydrogenation of halogen-substituted heterocyclic compounds could also lead to interesting results. The series of anthracene derivate could be expanded in order to see overarching patterns in the respective excited states, but also other molecule systems like acenes or indoles could be investigated systematically. The sucessful measurement on copper(II)pthalocyanine could be complemented with other metalloporphyrins, on a way to bigger systems with biological relevance.

Bibliography

[ABDC20] Nancy Awwad, Anh Thy Bui, Evgeny O. Danilov, and Felix N. Castellano. Visible-light-initiated free-radical polymerization by homomolecular triplet-triplet annihilation. *Chem*, 6(11):3071–3085, 2020.

[ACBD+97] H. Abdoul-Carime, Y. Bouteiller, C. Desfrancois, L. Philippe, J. P. Schermann, Lauri Niinistö, Stenbjörn Styring, Cecilia Tommos, Kurt Warncke, and Bryan R. Wood. Excess electrons in polar cluster anions. *Acta Chemica Scandinavica*, 51:145–150, 1997.

[AK05] S. Fatma Aygün and Filiz Kabadayi. Determination of benzoapyrene in charcoal grilled meat samples by hplc with fluorescence detection. *International journal of food sciences and nutrition*, 56(8):581–585, 2005.

[AKMN04] Naoto Ando, Shinsuke Kokubo, Masaaki Mitsui, and Atsushi Nakajima. Photoelectron spectroscopy of pyrene cluster anions, (pyrene)n− (n=1–20). *Chemical Physics Letters*, 389(4-6):279–283, 2004.

[ASNM07] M. Abdel-Salam, M. Nakano, and A. Mizuno. Electric fields and corona currents in needle-to-meshed plate gaps. *Journal of Physics D: Applied Physics*, 40(11):3363–3370, 2007.

[BAB+19] Dominik B. Bucher, Aude Craik, Diana P. L., Mikael P. Backlund, Matthew J. Turner, Oren Ben Dor, David R. Glenn, and Ronald L. Walsworth. Quantum diamond spectrometer for nanoscale nmr and esr spectroscopy. *Nature Protocols*, 14(9):2707–2747, 2019.

[BBLN11] Marcus Baumann, Ian R. Baxendale, Steven V. Ley, and Nikzad Nikbin. An overview of the key routes to the best selling 5-membered ring heterocyclic pharmaceuticals. *Beilstein journal of organic chemistry*, 7:442–495, 2011.

[BBST81] M. Barber, R. S. Bordoli, R. D. Sedgwick, and A. N. Tyler. Fast atom bombardment of solids as an ion source in mass spectrometry. *Nature*, 293(5830):270–275, 1981.

[BBX$^+$16] A. M. Buytendyk, A. M. Buonaugurio, S-J Xu, J. M. Nilles, K. H. Bowen, N. Kirnosov, and L. Adamowicz. Computational and photoelectron spectroscopic study of the dipole-bound anions, indole(h2o)1,2 (.). *The Journal of chemical physics*, 145(2):024301, 2016.

[BC66] R. S. Becker and E. Chen. Extension of electron affinities and ionization potentials of aromatic hydrocarbons. *The Journal of chemical physics*, 45(7):2403–2410, 1966.

[Ber17] Bernd Günter Kosper. *Erzeugung von Radikalanionen aromatischer Chromophore: potentielle Mechanismen und experimentelle Durchführung.* Master thesis, Heinrich-Heine-Universität, Düsseldorf, August/2017.

[BGLR87] B. Bonno, F. Gérardot, J. L. Laporte, and Y. Rousset. Triplet exciton fusion in organic mixed crystals: the naphthalene as host and chrysene and 1,2,5,6-dibenzanthracene as guests system. *Journal of Photochemistry*, 38:157–165, 1987.

[BKP$^+$10] Christian Brand, Jochen Küpper, David W. Pratt, W. Leo Meerts, Daniel Krügler, Jörg Tatchen, and Michael Schmitt. Vibronic coupling in indole: I. theoretical description of the 1la-1lb interaction and the electronic spectrum. *Physical Chemistry Chemical Physics*, 12(19):4968–4979, 2010.

[BMS49] E. J. Bowen, E. Mikiewicz, and F. W. Smith. Resonance transfer of electronic energy in organic crystals. *Proceedings of the Physical Society. Section A*, 62(1):26–31, 1949.

[BNWS82] U. Boesl, H. J. Neusser, R. Weinkauf, and E. W. Schlag. Multiphoton mass spectrometry of metastables: direct observation of decay in a high-resolution time-of-flight instrument. *The Journal of Physical Chemistry*, 86(25):4857–4863, 1982.

[Bor07] Raffaele Borrelli. Franck–condon analysis of the sf6- electron photodetachment spectrum. *Chemical Physics Letters*, 445(4-6):84–88, 2007.

[BVZ73] A. Bree, V.V.B. Vilkos, and R. Zwarich. Some electronic spectra of dibenzofuran. *Journal of Molecular Spectroscopy*, 48(1):135–147, 1973.

[CAS69] Inan Chen, Martin Abkowitz, and James H. Sharp. Esr of alpha –copper phthalocyanine. ii. powder line shape and mo calculations. *The Journal of chemical physics*, 50(5):2237–2244, 1969.

[CBP12] Gareth R. Chalmers, R. Marc Bustin, and Ian M. Power. Characterization of gas shale pore systems by porosimetry, pycnometry, surface area, and field emission scanning electron microscopy/transmission electron microscopy image analyses: Examples from the barnett, woodford, haynesville, marcellus, and doig units: Aapg bulletin, 96(6), 1099-1119. *AAPG Bulletin*, 96(6):1099–1119, 2012.

[CCB$^+$04] A. Cossaro, D. Cvetko, G. Bavdek, L. Floreano, R. Gotter, A. Morgante, F. Evangelista, and A. Ruocco. Copper−phthalocyanine induced reconstruction of au(110) †. *The Journal of Physical Chemistry B*, 108(38):14671–14676, 2004.

[CDA$^+$13] Taner Cavlar, Tobias Deimling, Andrea Ablasser, Karl-Peter Hopfner, and Veit Hornung. Species-specific detection of the antiviral small-molecule compound cma by sting. *The EMBO journal*, 32(10):1440–1450, 2013.

[CKD83] S. K. Chattopadhyay, Ch.V. Kumar, and P. K. Das. Triplet-related photophysics of 9,10-diphenylanthracene. a kinetic study of reversible energy transfer from anthracene triplet by nanosecond laser flas. *Chemical Physics Letters*, 98(3):250–254, 1983.

[CKM10] Kyle N. Crabtree, Carrie A. Kauffman, and Benjamin J. McCall. Note: A modular and robust continuous supersonic expansion discharge source. *Review of Scientific Instruments*, 81(8):086103, 2010.

[Cla61] E. Clar. Asymmetric annellations—v. *Tetrahedron*, 16(1-4):113–118, 1961.

[CLG$^+$18] Sandra M. Ciborowski, Gaoxiang Liu, Jacob D. Graham, Allyson M. Buytendyk, and Kit H. Bowen. Dipole-bound anions: formed by rydberg electron transfer (ret) and studied by velocity map imaging–anion photoelectron spectroscopy (vmi–apes). *The European Physical Journal D*, 72(8), 2018.

[CO01] Loucas G. Christophorou and James K. Olthoff. Electron attachment cross sections and negative ion states of sf6. *International Journal of Mass Spectrometry*, 205(1-3):27–41, 2001.

[Con26] Edward Condon. A theory of intensity distribution in band systems. *Physical Review*, 28(6):1182–1201, 1926.

[CRT62] R. B. Campbell, J. M. Robertson, and J. Trotter. The crystal structure of hexacene, and a revision of the crystallographic data for tetracene. *Acta Crystallographica*, 15(3):289–290, 1962.

[CS13] Eric Clar and Regina Schoental. *Polycyclic Hydrocarbons: Volume 1.* Springer Berlin / Heidelberg, Berlin, Heidelberg, 2013.

[CWK93] Louis Crocker, Tiebang Wang, and Paul Kebarle. Electron affinities of some polycyclic aromatic hydrocarbons, obtained from electron-transfer equilibria. *Journal of the American Chemical Society*, 115(17):7818–7822, 1993.

[Dab99] Dabestani. *A compilation of physical, spectroscopic and photophysical properties of polycyclic aromatic hydrocarbons.* 1999.

[DD54] W. W. Dolan and W. P. Dyke. Temperature-and-field emission of electrons from metals. *Physical Review*, 95(2):327–332, 1954.

[DGA⁺12] P. Delahaye, A. Galata, J. Angot, G. Ban, L. Celona, J. Choinski, P. Gmaj, A. Jakubowski, P. Jardin, T. Kalvas, H. Koivisto, V. Kolhinen, T. Lamy, D. Lunney, L. Maunoury, A. M. Porcellato, G. F. Prete, O. Steckiewicz, P. Sortais, T. Thuillier, O. Tarvainen, E. Traykov, F. Varenne, and F. Wenander. Prospects for advanced electron cyclotron resonance and electron beam ion source charge breeding methods for eurisol. *The Review of scientific instruments*, 83(2):02A906, 2012.

[DM61] F. H. Dorman and J. D. Morrison. Double and triple ionization in molecules induced by electron impact. *The Journal of chemical physics*, 35(2):575–581, 1961.

[DPK⁺99] Dimitrakopoulos, Purushothaman, Kymissis, Callegari, and Shaw. Low-voltage organic transistors on plastic comprising high-dielectric constant gate insulators. *Science*, 283(5403):822–824, 1999.

[DPTP96] M. F. Denissenko, A. Pao, M. Tang, and G. P. Pfeifer. Preferential formation of benzoapyrene adducts at lung cancer mutational hotspots in p53. *Science (New York, N.Y.)*, 274(5286):430–432, 1996.

[Dra08] Klaus Dransfeld. *Physik II: Elektrodynamik und Spezielle Relativitätstheorie*. DE GRUYTER, Berlin/Boston, 7th ed. edition, 2008.

[EE17] Nnabuk Okon Eddy and Nsikak Bassey Essien. Computational chemistry study of toxicity of some m-tolyl acetate derivatives insecticides and molecular design of structurally related products. *In Silico Pharmacology*, 5(1):14, 2017.

[EEGS66] D. Eastwood, L. Edwards, M. Gouterman, and J. Steinfeld. Spectra of porphyrins. *Journal of Molecular Spectroscopy*, 20(4):381–390, 1966.

[EH40] R. W. Engstrom and W. S. Huxford. Time-lag analysis of the townsend discharge in argon with activated caesium electrodes. *Physical Review*, 58(1):67–77, 1940.

[Ein05] Albert Einstein. *Einstein's Proposal of the Photon Conceptfia Translation of the Annalen der Physik Paper of 1905*. 1905.

[ES68] Mostafa A. El-Sayed. Triplet state. its radiative and nonradiative properties. *Accounts of Chemical Research*, 1(1):8–16, 1968.

[Fab] Fabian Drenkow. Resonanzverstärkte multiphotonen-photoelektronenspektroskopie von schwerflüchtigen aromatischen dreiring-systemen.

[FD26] J. Franck and E. G. Dymond. Elementary processes of photochemical reactions. *Transactions of the Faraday Society*, 21(February):536, 1926.

[Fes58] Herman Feshbach. Unified theory of nuclear reactions. *Annals of Physics*, 5(4):357–390, 1958.

[FH67] J. Franck and G. Hertz. Über zusammenstöße zwischen elektronen und den molekülen des quecksilberdampfes und die ionisierungsspannung desselben. *Physik Journal*, 23(7):294–301, 1967.

[FK54] Th. Förster and K. Kasper. Ein konzentrationsumschlag der fluoreszenz. *Zeitschrift für Physikalische Chemie*, 1(5_6):275–277, 1954.

[FKB57] Milton Furst, Hartmut Kallmann, and Felix H. Brown. Fluorescence efficiencies of organic compounds. *The Journal of chemical physics*, 26(5):1321–1332, 1957.

[FLW17] Jianzhong Fan, Lili Lin, and Chuan-Kui Wang. Molecular stacking effect on photoluminescence quantum yield and charge mobility of organic semiconductors. *Physical Chemistry Chemical Physics*, 19(44):30147–30156, 2017.

[Fra18] Franziska Wichmann. *Entladungen als Ionenquellen.* bachelor thesis, Heinrich-Heine-Universität, Düsseldorf, 2018.

[FRE18] Moritz H. Futscher, Akshay Rao, and Bruno Ehrler. The potential of singlet fission photon multipliers as an alternative to silicon-based tandem solar cells. *ACS energy letters*, 3(10):2587–2592, 2018.

[GBA+11] Andrew Gall, Rudi Berera, Maxime T. A. Alexandre, Andrew A. Pascal, Luc Bordes, Maria M. Mendes-Pinto, Sandra Andrianambinintsoa, Katerina V. Stoitchkova, Alessandro Marin, Leonas Valkunas, Peter Horton, John T. M. Kennis, Rienk van Grondelle, Alexander Ruban, and Bruno Robert. Molecular adaptation of photoprotection: triplet states in light-harvesting proteins. *Biophysical Journal*, 101(4):934–942, 2011.

[GCL+97] Gregory, Clary, Liu, Brown, and Saykally. The water dipole moment in water clusters. *Science*, 275(5301):814–817, 1997.

[Git40] Sherwood Githens. The influence of discharge chamber structure upon the initiating mechanism the high frequency discharge. *Physical Review*, 57(9):822–828, 1940.

[GKKN09] E. A. Gastilovich, N. V. Korol'kova, V. G. Klimenko, and R. N. Nurmukhametov. Effect of the orbital structure and symmetry of electronic states on nonradiative s-t intersystem crossing: Dibenzofuran. *Optics and Spectroscopy*, 106(3):311–319, 2009.

[GM28] H. Geiger and W. Mller. Elektronenzhlrohr zur messung schwchster aktivitten. *Die Naturwissenschaften*, 16(31):617–618, 1928.

[GM56] R. H. Good and Erwin W. Müller. Field emission. In Wayne B. Nottingham, R. H. Good, Erwin W. Müller, R. Kollath, G. L. Weissler, W. P. Allis, L. B. Loeb, A. Engel, and P. F. Little, editors, *Electron-Emission Gas Discharges I / Elektronen-Emission Gasentladungen I*, Encyclopedia of Physics / Handbuch der Physik, pages 176–231. Springer, Berlin and Heidelberg, 1956.

[GMK$^+$14] Indrajit Ghosh, Arindam Mukhopadhyay, Apurba Lal Koner, Subhas Samanta, Werner M. Nau, and Jarugu Narasimha Moorthy. Excited-state properties of fluorenones: influence of substituents, solvent and macrocyclic encapsulation. *Physical Chemistry Chemical Physics*, 16(31):16436–16445, 2014.

[Gob71] Heinrich Gobrecht. *Lehrbuch der Experimentalphysik: Band 2: Elektrizität und Magnetismus*. DE GRUYTER, Berlin, 6. aufl., 6., neubearb. und erw. aufl. reprint 2013 edition, 1971.

[Gri13] David J. Griffiths. *Introduction to electrodynamics*. Always learning. Pearson, Boston, 4. ed., international ed. edition, 2013.

[HAAS03] Helge Haberkern, Knut R. Asmis, Michael Allan, and Petra Swiderek. Triplet states in oligomeric materials: Electron energy loss spectroscopy of thiophene and bithiophene and extrapolation to the polymer. *Physical Chemistry Chemical Physics*, 5(5):827–833, 2003.

[Hab94] Hellmut Haberland. *Clusters of Atoms and Molecules: Theory, Experiment, and Clusters of Atoms*, volume 52 of *Springer Series in Chemical Physics*. Springer Berlin Heidelberg, Berlin, Heidelberg, 1994.

[HDX$^+$13] Oliver T. Hofmann, Jan-Christoph Deinert, Yong Xu, Patrick Rinke, Julia Stähler, Martin Wolf, and Matthias Scheffler. Large work function reduction by adsorption of a molecule with a negative electron affinity: pyridine on zno(1010). *The Journal of chemical physics*, 139(17):174701, 2013.

[HKW$^+$12] Christian Hock, Jongjin B. Kim, Marissa L. Weichman, Tara I. Yacovitch, and Daniel M. Neumark. Slow photoelectron velocity-map imaging spectroscopy of cold negative ions. *The Journal of chemical physics*, 137(24):244201, 2012.

[HS83] John M. Hayes and Gerald J. Small. Supersonic jets, rotational cooling, and analytical chemistry. *Analytical Chemistry*, 55(4):565A–574A, 1983.

[IAR85] IARC. *Polynuclear aromatic compounds: This publication represents the views and expert opinions of an IARC Working Group on the Evaluation of the Carcinogenic Risk of Chemicals to Humans which met in Lyon*, volume 35 of *IARC monographs on the evaluation of the carcinogenic risk of chemicals to humans*. International Agency for Research on Cancer, Lyon, 1985.

[IKY16] Hideaki Iwahara, Tomokatsu Kushida, and Shigehiro Yamaguchi. A planarized 9-phenylanthracene: a simple electron-donating building block for fluorescent materials. *Chemical Communications*, 52(6):1124–1127, 2016.

[IS98] E. Illenberger and Boris M. Smirnov. Electron attachment to free and bound molecules. *Physics-Uspekhi*, 41(7):651–685, 1998.

[Jab33] A. Jablonski. Efficiency of anti-stokes fluorescence in dyes. *Nature*, 131(3319):839–840, 1933.

[Jan19] Jan Meissner. *Entladungen als Quelle zur Desorption.* bachelor thesis, Heinrich-Heine-Universität, Düsseldorf, 2019.

[JBD01] D. C. Jordan, C. T. Burns, and R. B. Doak. Corona discharge supersonic free-jet for iii–v nitride growth via metastable nitrogen molecules. *Journal of Applied Physics*, 89(2):883–892, 2001.

[JFV$^+$10] A.-V. Jung, C. Frochot, F. Villieras, B. S. Lartiges, S. Parant, M.-L. Viriot, and J.-L. Bersillon. Interaction of pyrene fluoroprobe with natural and synthetic humic substances: Examining the local molecular organization from photophysical and interfacial processes. *Chemosphere*, 80(3):228–234, 2010.

[JM08] John Arthur Joule and Keith Mills. *Heterocyclic chemistry.* Blackwell Science, Oxford, 4. ed., reprinted. edition, 2008.

[JON47] R. N. JONES. The ultraviolet absorption spectra of anthracene derivatives. *Chemical Reviews*, 41(2):353–371, 1947.

[JZS$^+$02] J.-P. Sun, Z.-X. Zhang, S.-M. Hou, G.-M. Zhang, and Z.-Q. Xue. Work function of tungsten carbide thin film calculated using field emission microscopy. *Tien Tzu Hsueh Pao/Acta Electronica Sinica*, 30(5):655–657, 2002.

[KC78] Cornelius E. Klots and R. N. Compton. Electron attachment to van der waals polymers of water. *The Journal of chemical physics*, 69(4):1644–1647, 1978.

[KD70] M. Krejči and M. Dressler. *Selective detectors in gas chromatography*, volume 13. 1970.

[Kha20a] Sulaiman Khalifeh. Optimized polymeric structures of organic active electronic components. In Sulaiman Khalifeh, editor, *Polymers in organic electronics*, pages 251–339. ChemTec Publishing, Toronto, 2020.

[Kha20b] Sulaiman Khalifeh, editor. *Polymers in organic electronics: Polymer selection for electronic, mechatronic & optoelectronic systems.* ChemTec Publishing, Toronto, 2020.

[KHF$^+$11] Juliane Köhler, Patrick Hemberger, Ingo Fischer, Giovanni Piani, and Lionel Poisson. Ultrafast dynamics of isolated fluorenone. *The journal of physical chemistry. A*, 115(50):14249–14253, 2011.

[KJ89] Gary R. Kinsel and Murray V. Johnston. Post source pulse focusing: a simple method to achieve improved resolution in a time-of-flight mass spectrometer. *International Journal of Mass Spectrometry and Ion Processes*, 91(2):157–176, 1989.

[KKK76] Shunsuke Kobayashi, Koichi Kikuchi, and Hiroshi Kokubun. Fluorescence of the antharacenes following tn → t1 excitation studied by a double excitation method. *Chemical Physics Letters*, 42(3):494–497, 1976.

[KLS09] Jeong Hyun Kim, Sang Hak Lee, and Jae Kyu Song. Photoelectron spectroscopy of pyrene anion clusters: autodetachment via excited states of anion and intermolecular interactions in anion clusters. *The Journal of chemical physics*, 130(12):124321, 2009.

[KMMJ91] G. R. Kinsel, C. D. Mowry, P. J. McKeown, and M. V. Johnston. Resolution enhancement in linear time-of-flight mass spectrometry by post-source pulse focusing. *International Journal of Mass Spectrometry and Ion Processes*, 104(1):35–44, 1991.

[Kor12] Sebastian Korff. Das geiger-müller-zählrohr : Eine wissenschaftshistorische analyse mit der replikationsmethode. *NTM*, 20(4):271–308, 2012.

[KRH$^+$21] Benedikt P. Klein, Lukas Ruppenthal, Samuel J. Hall, Lars E. Sattler, Sebastian M. Weber, Jan Herritsch, Andrea Jaegermann, Reinhard J. Maurer, Gerhard Hilt, and J. Michael Gottfried. Topology effects in molecular organic electronic materials: Pyrene and azupyrene*. *ChemPhysChem*, 22(11):1065–1073, 2021.

[KW96] Adam Kiejna and Kazimierz F. Wojciechowski. *Metal surface electron physics.* Elsevier, Oxford, 1. ed. edition, 1996.

[KZ86] Lutfur R. Khundkar and Ahmed H. Zewail. Exciton and vibronic effects in the spectroscopy of bianthracene in supersonic beams. *The Journal of chemical physics*, 84(3):1302–1311, 1986.

[Lau18] Laurin Hensen. *Elektronenemisson als Feed für eine Elektronenkanone.* bachelor thesis, Heinrich-Heine-Universität, Düsseldorf, 2018.

[LCG+20] Gaoxiang Liu, Sandra M. Ciborowski, Jacob D. Graham, Allyson M. Buytendyk, and Kit H. Bowen. Photoelectron spectroscopic study of dipole-bound and valence-bound nitromethane anions formed by rydberg electron transfer. *The Journal of chemical physics*, 153(4):044307, 2020.

[LCP+19] Gaoxiang Liu, Sandra M. Ciborowski, Cody Ross Pitts, Jacob D. Graham, Allyson M. Buytendyk, Thomas Lectka, and Kit H. Bowen. Observation of the dipole- and quadrupole-bound anions of 1,4-dicyanocyclohexane. *Physical Chemistry Chemical Physics*, 21(33):18310–18315, 2019.

[LDW+15] Jie Liu, Huanli Dong, Zongrui Wang, Deyang Ji, Changli Cheng, Hua Geng, Hantang Zhang, Yonggang Zhen, Lang Jiang, Hongbing Fu, Zhishan Bo, Wei Chen, Zhigang Shuai, and Wenping Hu. Thin film field-effect transistors of 2,6-diphenyl anthracene (dpa). *Chemical Communications*, 51(59):11777–11779, 2015.

[LFSZ84] W. R. Lambert, P. M. Felker, J. A. Syage, and A. H. Zewail. Jet spectroscopy of anthracene and deuterated anthracenes. *The Journal of chemical physics*, 81(5):2195–2208, 1984.

[LGL+19] Zhanfeng Li, Guoyue Gan, Zhitian Ling, Kunping Guo, Changfeng Si, Xiang Lv, Hua Wang, Bin Wei, and Yuying Hao. Easily available, low-cost 9,9′-bianthracene derivatives as efficient blue hosts and deep-blue emitters in oleds. *Organic Electronics*, 66:24–31, 2019.

[LL94] Michael A. Lieberman and Allan J. Lichtenberg. *Principles of plasma discharges and materials processing.* A Wiley Interscience publication. Wiley, New York, NY, 1994.

[LLCJ19] Changmin Lee, Taecheon Lyu, Cheol Ho Choi, and Taiha Joo. Symmetry-breaking charge transfer dynamics of 9,9’-bianthracene revealed by experiment and theory. *EPJ Web of Conferences*, 205:09008, 2019.

[LMDCQ10] Jutta Ludwig-Müller, Kathrin Denk, Jerry D. Cohen, and Marcel Quint. An inhibitor of tryptophan-dependent biosynthesis of indole-3-acetic acid alters seedling development in arabidopsis. *Journal of Plant Growth Regulation*, 29(2):242–248, 2010.

[LML84] Keith R. Lykke, Roy D. Mead, and W. C. Lineberger. Observation of dipole-bound states of negative ions. *Physical Review Letters*, 52(25):2221–2224, 1984.

[Lor40] Egon Lorenz. Intestinal carcinoma and other lesions in mice following oral administration of 1,2,5,6-dibenzanthracene and 20-methylcholanthrene1. *JNCI: Journal of the National Cancer Institute*, 1940.

[Lov58] J. E. Lovelock. *A sensitive detector for gas chromatography*, volume 1. 1958.

[LS01] Meng-Sheng Liao and Steve Scheiner. Electronic structure and bonding in metal phthalocyanines, metal=fe, co, ni, cu, zn, mg. *The Journal of chemical physics*, 114(22):9780–9791, 2001.

[LSY$^+$13] Zuo-Qin Liang, Bin Sun, Chang-Qing Ye, Xiao-Mei Wang, Xu-Tang Tao, Qin-Hua Wang, Ping Ding, Bao Wang, and Jing-Jing Wang. New anthracene derivatives as triplet acceptors for efficient green-to-blue low-power upconversion. *Chemphyschem : a European journal of chemical physics and physical chemistry*, 14(15):3517–3522, 2013.

[LZD$^+$15] Jie Liu, Hantang Zhang, Huanli Dong, Lingqiang Meng, Longfeng Jiang, Lang Jiang, Ying Wang, Junsheng Yu, Yanming Sun, Wenping Hu, and Alan J. Heeger. High mobility emissive organic semiconductor. *Nature Communications*, 6(1):10032, 2015.

[Mam01] B. A. Mamyrin. Time-of-flight mass spectrometry (concepts, achievements, and prospects). *International Journal of Mass Spectrometry*, 206(3):251–266, 2001.

[Mar17] Marco Schmidt. *Aufbau und Test einer alternativer Elektronenkanone*. bachelor thesis, 2017.

[MDB$^+$01] C. C. Mattheus, A. B. Dros, J. Baas, A. Meetsma, J. L. de Boer, and T. T. Palstra. Polymorphism in pentacene. *Acta crystallographica. Section C, Crystal structure communications*, 57(Pt 8):939–941, 2001.

[MG56] E. L. Murphy and R. H. Good. Thermionic emission, field emission, and the transition region. *Physical Review*, 102(6):1464–1473, 1956.

[Mid02] Wendy Middleton. *Reference data for engineers: Radio, electronics, computer, and communications.* Electronics & Electrical. Newnes, Boston and Oxford, 9th ed. edition, 2002.

[MIH02] Y. Matsushita, T. Ichimura, and T. Hikida. Photochemical and photophysical processes in the molecular cluster of fluorenone. *Chemical Physics Letters*, 360(1-2):65–71, 2002.

[MKD20] İskender Muz, Mustafa Kurban, and Mehmet Dalkilic. Dft and td-dft studies of new pentacene-based organic molecules as a donor material for bulk-heterojunction solar cells. *Journal of Computational Electronics*, 19(3):895–904, 2020.

[MKMW21] Jan Meissner, Bernd Kosper, Christel M. Marian, and Rainer Weinkauf. Lowest triplet and singlet states in n-methylacridone and n,n'-dimethylquinacridone: Theory and experiment. *The Journal of Physical Chemistry A*, 125(40):8777–8790, 2021.

[MMT16] Ana Maslać, Maja Maslać, and Mirta Tkalec. The impact of cadmium on photosynthetic performance and secondary metabolites in the lichens parmelia sulcata, flavoparmelia caperata and evernia prunastri. *Acta Botanica Croatica*, 75(2):186–193, 2016.

[MPW$^+$09] Boleslaw Marczynski, Beate Pesch, Michael Wilhelm, Bernd Rossbach, Ralf Preuss, Jens-Uwe Hahn, Sylvia Rabstein, Monika Raulf-Heimsoth, Albrecht Seidel, Hans-Peter Rihs, Ansgar Adams, Michael Scherenberg, Anja Erkes, Beate Engelhardt, Kurt Straif, Heiko Udo Käfferlein, Jürgen Angerer, and Thomas Brüning. Occupational exposure to polycyclic aromatic hydrocarbons and dna damage by industry: a nationwide study in germany. *Archives of Toxicology*, 83(10):947–957, 2009.

[MRK$^+$04] Ashok Maliakal, Krishnan Raghavachari, Howard Katz, Edwin Chandross, and Theo Siegrist. Photochemical stability of pentacene and a substituted pentacene in solution and in thin films. *Chemistry of Materials*, 16(24):4980–4986, 2004.

[MRS+20] Aline Murawski, Alexandra Roth, Gerda Schwedler, Maria I. H. Schmied-Tobies, Enrico Rucic, Nikola Pluym, Max Scherer, Gerhard Scherer, André Conrad, and Marike Kolossa-Gehring. Polycyclic aromatic hydrocarbons (pah) in urine of children and adolescents in germany - human biomonitoring results of the german environmental survey 2014-2017 (geres v). *International journal of hygiene and environmental health*, 226:113491, 2020.

[MSN16] Tsugunosuke Masubuchi, Yoshito Sugawara, and Atsushi Nakajima. Adiabatic electron affinity of pentacene and perfluoropentacene molecules studied by anion photoelectron spectroscopy: Molecular insights into electronic properties. *The Journal of chemical physics*, 145(24):244306, 2016.

[MZZ+15] Guangyuan Mu, Shaoqing Zhuang, Wenzhi Zhang, Yixin Wang, Bo Wang, Lei Wang, and Xunjin Zhu. Efficient blue organic light-emitting diodes based on triphenylimidazole substituted anthracene derivatives. *Organic Electronics*, 21:9–18, 2015.

[Nak72] Akira Nakajima. Fluorescence emission in the gas phase of several aromatic hydrocarbons. *Bulletin of the Chemical Society of Japan*, 45(6):1687–1695, 1972.

[Nic74] Bernhard Nickel. Delayed fluorescence from higher excited singlet states of 1,2-benzanthracene and fluoranthene. *Chemical Physics Letters*, 27(1):84–90, 1974.

[Nik02] Sascha Nikolov. *Frühwirkungen genotoxischer und nichtgenotoxischer Kanzerogene (Fluorene) auf die Zellteilung verschiedener 'Nicht-Targetgewebe´ bei jungen männlichen Ratten.* 2002.

[Nik19] Nikita Schützek. *Monitoring der Anionenerzeugung.* master thesis, Heinrich-Heine-Universität, Düsseldorf, 2019.

[NJK+] Miloslav Nič, Jiří Jirát, Bedřich Košata, Aubrey Jenkins, and Alan McNaught. Iupac compendium of chemical terminology.

[NS13] Palani Natarajan and Michael Schmittel. On-off luminescence signaling of hybrid organic-inorganic switches. *Inorganic chemistry*, 52(15):8579–8590, 2013.

[OBP+] Oleg Opanasyuk, Anders Barth, Thomas-Otavio Peulen, Suren Felekyan, Stanislav Kalinin, Hugo Sanabria, and Claus A. M. Seidel. Unraveling multi-state molecular dynamics in single-molecule fret experiments – part ii: Quantitative analysis of multi-state kinetic networks.

[OGMA21] Axel Olesund, Victor Gray, Jerker Mårtensson, and Bo Albinsson. Diphenylanthracene dimers for triplet-triplet annihilation photon upconversion: Mechanistic insights for intramolecular pathways and the importance of molecular geometry. *Journal of the American Chemical Society*, 143(15):5745–5754, 2021.

[ON92] Kazuhiko Ohashi and Nobuyuki Nishi. Photodepletion spectroscopy on charge resonance band of benzene clusters (c6h6)2+ and (c6h6)3+. *The Journal of Physical Chemistry*, 96(7):2931–2932, 1992.

[OSS+01] A. Oelsner, O. Schmidt, M. Schicketanz, M. Klais, G. Schönhense, V. Mergel, O. Jagutzki, and H. Schmidt-Böcking. Microspectroscopy and imaging using a delay line detector in time-of-flight photoemission microscopy. *Review of Scientific Instruments*, 72(10):3968–3974, 2001.

[OSS+20] Tsukasa Owada, Hisahiro Sasabe, Yoshihito Sukegawa, Taiki Watanabe, Tomohiro Maruyama, Yuichiro Watanabe, Daisuke Yokoyama, and Junji Kido. A terpyridine-modified chrysene derivative as an electron transporter to improve the lifetime in phosphorescent oleds. *Journal of Materials Chemistry C*, 8(9):3200–3205, 2020.

[PA99] P. V. Poliakov and B. R. Arnold. An application of time-resolved linear dichroism spectroscopy: The excited singlet state of 1,2:5,6-dibenzanthracene. *Spectroscopy Letters*, 32(5):747–762, 1999.

[Pas89] Friedrich Paschen. Ueber die zum funkenübergang in luft, wasserstoff und kohlensäure bei verschiedenen drucken erforderliche potentialdifferenz. *Annalen der Physik*, 273(5):69–96, 1889.

[Pau] Linus Pauling. The electron affinity of hydrogen and the second ionization potential of lithium.

[Pau17] Paul Konieczny. *Anionen-Photodetachment-Photoelektronen-Spektroskopie und Gasphasen UV-Vis-Spektroskopie an konjugierten molekularen Systemen.* 2017.

[Per63] Willis B. Person. Electron affinities of some halogen molecules and the charge–transfer frequency. *The Journal of chemical physics*, 38(1):109–116, 1963.

[PMLK14] Stanislav A. Pshenichnyuk, Alberto Modelli, Eleonora F. Lazneva, and Alexei S. Komolov. Resonance electron attachment to tetracyanoquinodimethane. *The journal of physical chemistry. A*, 118(34):6810–6818, 2014.

[Pro17] Prof. Christel M. Marian. theoretical investigation on the excited states of anthracene, 2017.

[PSO$^+$17] Johannes Passig, Julian Schade, Markus Oster, Matthias Fuchs, Sven Ehlert, Cornelia Jäger, Martin Sklorz, and Ralf Zimmermann. Aerosol mass spectrometer for simultaneous detection of polyaromatic hydrocarbons and inorganic components from individual particles. *Analytical Chemistry*, 89(12):6341–6345, 2017.

[Raj97] Jurij P. Rajzer. *Gas discharge physics.* Springer, Berlin, corr. 2. printing edition, 1997.

[RAM21] C. V. RAMAN. The colour of the sea. *Nature*, 108(2716):367, 1921.

[RBD20] John R. Rumble, Thomas J. Bruno, and Maria J. Doa, editors. *CRC handbook of chemistry and physics: A ready-reference book of chemical and physical data.* CRC Press, Taylor & Francis Group, Boca Raton and London and New York, 101st edition, 2020-2021 edition, 2020.

[Ric13] O. W. Richardson. *THE EMISSION OF ELECTRONS FROM TUNGSTEN AT HIGH TEMPERATURES: AN EXPERIMENTAL PROOF THAT THE ELECTRIC CURRENT IN METALS IS CARRIED BY ELECTRONS*, volume 38. 1913.

[Ron92] Jean Roncali. Conjugated poly(thiophenes): synthesis, functionalization, and applications. *Chemical Reviews*, 92(4):711–738, 1992.

[Rot11] Philip Roth. Neonatology. In Mark F. Ditmar and Richard Alan Polin, editors, *Pediatric secrets*, Secrets, pages 423–479. Mosby/Elsevier, Philadelphia, 2011.

[San14] Andrei Sanov. Laboratory-frame photoelectron angular distributions in anion photodetachment: insight into electronic structure and intermolecular interactions. *Annual review of physical chemistry*, 65:341–363, 2014.

[SB65] K. S. V. Santhanam and Allen J. Bard. Chemiluminescence of electrogenerated 9,10-diphenylanthracene anion radical 1. *Journal of the American Chemical Society*, 87(1):139–140, 1965.

[SBH+07] T. Siegrist, C. Besnard, S. Haas, M. Schiltz, P. Pattison, D. Chernyshov, B. Batlogg, and C. Kloc. A polymorph lost and found: The high-temperature crystal structure of pentacene. *Advanced Materials*, 19(16):2079–2082, 2007.

[SBZ21] Thorsten Streibel, Ulrich Boesl, and Ralf Zimmermann. Analytical application of resonance–enhanced multiphoton ionization mass spectrometry (rempi – ms). In Ralf Zimmermann and Luke Hanley, editors, *Photoionization and Photo–Induced Processes in Mass Spectrometry*, pages 125–158. Wiley, 2021.

[Sch77] W. Schmidt. Photoelectron spectra of polynuclear aromatics. v. correlations with ultraviolet absorption spectra in the catacondensed series. *The Journal of chemical physics*, 66(2):828–845, 1977.

[See34] M. G. Seelig. Dibenzanthracene 1:2:5:6 as a carcinogenic agent. *The American Journal of Cancer*, 20(4):827–833, 1934.

[SI72] Tadamasa Shida and Suehiro Iwata. Absorption spectra of dianthracene anion radical and anthracene dimer anion. *The Journal of chemical physics*, 56(6):2858–2864, 1972.

[SI20] Soichi Shirai and Shinji Inagaki. Ab initio study on the excited states of pyrene and its derivatives using multi-reference perturbation theory methods. *RSC Advances*, 10(22):12988–12998, 2020.

[Sie11] Swen Siegert. *Anionen-Photodetachment-Photoelektronen-Spektroskopie als neuer, systematischer Zugang zu dunklen, angeregten Neutralzuständen.* Cuvillier Verlag, Göttingen, 1st ed. edition, 2011.

[SJS+65] S. Singh, W. J. Jones, W. Siebrand, B. P. Stoicheff, and W. G. Schneider. Laser generation of excitons and fluorescence in anthracene crystals. *The Journal of chemical physics*, 42(1):330–342, 1965.

[SK13] M. A. Suhm and F. Kollipost. Femtisecond single-mole infrared spectroscopy of molecular clusters. *Physical Chemistry Chemical Physics*, 15(26):10702–10721, 2013.

[SM84] D. Stahl and F. Maquin. Charge-stripping mass spectrometry of molecular ions from polyacenes and molecular orbital theory. *Chemical Physics Letters*, 108(6):613–617, 1984.

[SMB$^+$16] Benoît Soep, Jean-Michel Mestdagh, Marc Briant, Marc-André Gaveau, and Lionel Poisson. Direct observation of slow intersystem crossing in an aromatic ketone, fluorenone. *Physical Chemistry Chemical Physics*, 18(33):22914–22920, 2016.

[SQ61] William Shockley and Hans J. Queisser. Detailed balance limit of efficiency of p–n junction solar cells. *Journal of Applied Physics*, 32(3):510–519, 1961.

[SS70] B. H. Schechtman and W. E. Spicer. Near infrared to vacuum ultraviolet absorption spectra and the optical constants of phthalocyanine and porphyrin films. *Journal of Molecular Spectroscopy*, 33(1):28–48, 1970.

[SSK$^+$20] Sivasamy Sethupathy, Ezhaveni Sathiyamoorthi, Yong-Guy Kim, Jin-Hyung Lee, and Jintae Lee. Antibiofilm and antivirulence properties of indoles against serratia marcescens. *Frontiers in microbiology*, 11:584812, 2020.

[Ste15] Stefan Vosskötter. *Hochaufösende Radikal-Anionen-Photo elektronen-Sp ektroskopie von konjugierten Aromaten: Simultane Spektroskopie von Singulett-undTriplett-Zuständen.* Dissertation, Heinrich-Heine-Universität, Düsseldorf, November/2015.

[SW97] J. Schiedt and R. Weinkauf. Photodetachment photoelectron spectroscopy of mass selected anions: anthracene and the anthracene-h2o cluster. *Chemical Physics Letters*, 266(1-2):201–205, 1997.

[SW99] J. Schiedt and R. Weinkauf. Resonant photodetachment via shape and feshbach resonances: p -benzoquinone anions as a model system. *The Journal of chemical physics*, 110(1):304–314, 1999.

[SWNS98] J. Schiedt, R. Weinkauf, D. M. Neumark, and E. W. Schlag. Anion spectroscopy of uracil, thymine and the amino-oxo and amino-hydroxy tautomers of cytosine and their water clusters. *Chemical Physics*, 239(1-3):511–524, 1998.

[SWS98] Joachim Schiedt, Rainer Weinkauf, and E. W. Schlag, editors. *Photodetachment-Photoelektronenspektroskopie: Erste Schritte zu größeren Systemen: Zugl.: München, Techn. Univ., Diss., 1998*, volume Bd. 9 of *Laserspektroskopie und Lasermassenspektrometrie.* Utz Wiss, München, 1998.

[TB21] J. S. Townsend and V. A. Bailey. Xcvii. the motion of electrons in gases. *The London, Edinburgh, and Dublin Philosophical Magazine and Journal of Science*, 42(252):873–891, 1921.

[Til78] Michael J. Tilby. Inhibition of coprinus cinereus by 5-fluoroindole. *Archives of Microbiology*, 118(3):301–303, 1978.

[Tin67] Chen-Hanson Ting. Electronic structure and intersystem crossing in 9,10-diphenylanthracene. *Chemical Physics Letters*, 1(8):335–336, 1967.

[TR97] Andreas Thöny and Michel J. Rossi. Gas-phase uv spectroscopy of anthracene, xanthone, pyrene, 1-bromopyrene and 1,2,4-trichlorobenzene at elevated temperatures. *Journal of Photochemistry and Photobiology A: Chemistry*, 104(1-3):25–33, 1997.

[TVC+98] J. Tóth, D. Varga, I. Cserny, L. Kövér, B. Gruzza, D. Zeze, C. Jardin, and G. Gergely. Resolution correction in eels. *Vacuum*, 50(3-4):473–479, 1998.

[TWI+88] Koichi Tanaka, Hiroaki Waki, Yutaka Ido, Satoshi Akita, Yoshikazu Yoshida, Tamio Yoshida, and T. Matsuo. Protein and polymer analyses up tom/z 100 000 by laser ionization time-of-flight mass spectrometry. *Rapid Communications in Mass Spectrometry*, 2(8):151–153, 1988.

[UFN+07] T. Uemura, M. Furumoto, T. Nakano, M. Akai-Kasaya, A. Saito, M. Aono, and Y. Kuwahara. Local-plasmon-enhanced up-conversion fluorescence from copper phthalocyanine. *Chemical Physics Letters*, 448(4-6):232–236, 2007.

[UOK+20] Tatsuhiro Uchikura, Mari Oshima, Minami Kawasaki, Kohei Takahashi, and Nobuharu Iwasawa. Supramolecular photocatalysis by utilizing the host-guest charge-transfer interaction: Visible-light-induced generation of triplet anthracenes for 4+2 cycloaddition reactions. *Angewandte Chemie (International ed. in English)*, 59(19):7403–7408, 2020.

[VBZ58] Frank A. Vingiello, Alexej BoŘkovec, and Walter Zajac. An unusual elbs-type reaction observed during a study of the cyclization of ketones 1,2. *Journal of the American Chemical Society*, 80(7):1714–1716, 1958.

[VKMW15] Stefan Vosskötter, Paul Konieczny, Christel M. Marian, and Rainer Weinkauf. Towards an understanding of the singlet-triplet splittings in conjugated hydrocarbons: azulene investigated by anion photoelectron spectroscopy and theoretical calculations. *Physical Chemistry Chemical Physics*, 17(36):23573–23581, 2015.

[Vog12] Ferdinand Vogeler. *Throwing light on dark states of organic molecules.* 2012.

[Vor20] Mikhail Vorona. *Anthracene-Based Molecules for Organic Thin-Film Transistor Integration: Anthracene-Based Molecules for Organic Thin-Film Transistor Integration.* PhD thesis, Université d'Ottawa / University of Ottawa, 2020.

[Wei89] Weinkauf. Zna-1989-44a-1219. 1989.

[Wig48] Eugene P. Wigner. On the behavior of cross sections near thresholds. *Physical Review*, 73(9):1002–1009, 1948.

[WM55] W. C. Wiley and I. H. McLaren. Time–of–flight mass spectrometer with improved resolution. *Review of Scientific Instruments*, 26(12):1150–1157, 1955.

[Wol] Wolfgang. dissertation_rosellen_revision.

[Wol81] Monika Wolf. Multi-channel-plates*. *Physik in unserer Zeit*, 12(3):90–95, 1981.

[WP92] Walter and Peterson. Shape resonance in ca- photodetachment and the electron affinity of ca(1s). *Physical review letters*, 68(15):2281–2284, 1992.

[WPTM06] K. Wegner, P. Piseri, H. Vahedi Tafreshi, and P. Milani. Cluster beam deposition: a tool for nanoscale science and technology. *Journal of Physics D: Applied Physics*, 39(22):R439–R459, 2006.

[WS97] R. Weinkauf and J. Schiedt. Energetics of photoinduced electron transfer in the indole.o2 cluster in gas phase: possible consequences for photoexcited tryptophan in solution. *Photochemistry and photobiology*, 66(5):569–575, 1997.

[WSM+96] R. Weinkauf, P. Schanen, A. Metsala, E. W. Schlag, M. Bürgle, and H. Kessler. Highly efficient charge transfer in peptide cations in the gas phase: Threshold effects and mechanism. *The Journal of Physical Chemistry*, 100(47):18567–18585, 1996.

[WSW98] Georges A. Wagnières, Willem M. Star, and Brian C. Wilson. In vivo fluorescence spectroscopy and imaging for oncological applications. *Photochemistry and photobiology*, 68(5):603, 1998.

[WW00] Lai-Sheng Wang and Xue-Bin Wang. Probing free multiply charged anions using photodetachment photoelectron spectroscopy. *The Journal of Physical Chemistry A*, 104(10):1978–1990, 2000.

[WW08] Yi-Lei Wang and Guo-Shi Wu. Improving the tddft calculation of low-lying excited states for polycyclic aromatic hydrocarbons using the tamm–dancoff approximation. *International Journal of Quantum Chemistry*, 108(3):430–439, 2008.

[WWB+17] Josefin Wilke, Martin Wilke, Christian Brand, J. Dominik Spiegel, Christel M. Marian, and Michael Schmitt. Modulation of the la/lb mixing in an indole derivative: A position-dependent study using 4-, 5-, and 6-fluoroindole. *The journal of physical chemistry. A*, 121(8):1597–1606, 2017.

[XLST13] Mizhi Xu, Xingbao Li, Zheming Sun, and Tao Tu. Suzuki-miyaura cross-coupling of bulky anthracenyl carboxylates by using pincer nickel n-heterocyclic carbene complexes: an efficient protocol to access fluorescent anthracene derivatives. *Chemical Communications*, 49(98):11539–11541, 2013.

[XSD+21] Pan Xia, Joseph Schwan, Thomas W. Dugger, Lorenzo Mangolini, and Ming Lee Tang. Air–stable silicon nanocrystal–based photon upconversion. *Advanced Optical Materials*, page 2100453, 2021.

[YCW+20] Yu Kun Yang, Yongjun Cheng, Yong Wu, Yi Zhi Qu, Jian Guo Wang, and Song Bin Zhang. Particle scattering and resonances involving avoided crossing. *New Journal of Physics*, 22(12):123022, 2020.

[YF84] Masamichi Yamashita and John B. Fenn. Electrospray ion source. another variation on the free-jet theme. *The Journal of Physical Chemistry*, 88(20):4451–4459, 1984.

[YTG+19] You-Jun Yu, Xun Tang, Hui-Ting Ge, Yi Yuan, Zuo-Quan Jiang, and Liang-Sheng Liao. Fluorenone-based thermally activated delayed fluorescence materials for orange-red emission. *Organic Electronics*, 73:240–246, 2019.

[YZQ+21] Dao-Fu Yuan, Yue-Rou Zhang, Chen-Hui Qian, Yuan Liu, and Lai-Sheng Wang. Probing the dipole-bound state in the 9-phenanthrolate anion by photodetachment spectroscopy, resonant two-photon photoelectron imaging, and resonant photoelectron spectroscopy. *The Journal of Physical Chemistry A*, 2021.

[ZBV74] R. Zwarich, A. Bree, and V. Vilkos. The vibrational spectra of 9-fluorenone. *Journal of Molecular Spectroscopy*, 51(1):38–49, 1974.

[ZCH+18] Jianzhang Zhao, Kepeng Chen, Yuqi Hou, Yuanyuan Che, Lang Liu, and Dianzeng Jia. Recent progress in heavy atom-free organic compounds showing unexpected intersystem crossing (isc) ability. *Organic & Biomolecular Chemistry*, 16(20):3692–3701, 2018.

[ZCL19] Guo-Hua Zhong, Xiao-Jia Chen, and Hai-Qing Lin. Superconductivity and its enhancement in polycyclic aromatic hydrocarbons. *Frontiers in Physics*, 7, 2019.

[ZHHK11] Jie Zhang, Colin Harthcock, Fangyuan Han, and Wei Kong. Zero kinetic energy photoelectron spectroscopy of jet cooled benzoapyrene from resonantly enhanced multiphoton ionization. *The Journal of chemical physics*, 135(24):244306, 2011.

[ZKC+04] Hua-Jin Zhai, Boggavarapu Kiran, Li-Feng Cui, Xi Li, David A. Dixon, and Lai-Sheng Wang. Electronic structure and chemical bonding in mo(n)- and mo(n) clusters (m = mo, w; n = 3-5): a photoelectron spectroscopy and ab initio study. *Journal of the American Chemical Society*, 126(49):16134–16141, 2004.

[ZLI+06] Xiuhui Zhang, Qianshu Li, Justin B. Ingels, Andrew C. Simmonett, Steven E. Wheeler, Yaoming Xie, R. Bruce King, Henry F. Schaefer, and F. Albert

Cotton. Remarkable electron accepting properties of the simplest benzenoid cyanocarbons: hexacyanobenzene, octacyanonaphthalene and decacyanoanthracene. *Chemical communications (Cambridge, England)*, (7):758–760, 2006.

[ZMJ$^+$96] J. Zobel, U. Mayer, K. Jung, H. Ehrhardt, H. Pritchard, C. Winstead, and V. McKoy. Absolute differential cross sections for electron-impact excitation of co near threshold: Ii. the rydberg states of co. *Journal of Physics B: Atomic, Molecular and Optical Physics*, 29(4):839–856, 1996.

[ZSC$^+$21] Xiaoyu Zhao, Andrey A. Sukhanov, Kepeng Chen, Xinyu Geng, Yu Dong, Violeta K. Voronkova, Jianzhang Zhao, and Lang Liu. Effect of molecular conformation on the efficiency of the spin orbital charge recombination-induced intersystem crossing in bianthryls. *Dyes and Pigments*, 187:109121, 2021.

[ZYL$^+$08] Xiujuan Zhang, Guodong Yuan, Quansong Li, Bo Wang, Xiaohong Zhang, Ruiqin Zhang, Jack C. Chang, Chun-sing Lee, and Shuit-tong Lee. Single-crystal 9,10-diphenylanthracene nanoribbons and nanorods. *Chemistry of Materials*, 20(22):6945–6950, 2008.

Abbreviations

26Dpa 2,6-Diphenylanthracene

3-Ac Anthracene

4-Ac Tetracene

5-Ac Pentacene

5Fi 5-Fluoroindole

6Fi 6-Fluoroindole

910Dpa 9,10-Diphenylanthracene

91NaAn 9-(1-Naphtyl)-anthracene

9Pa 9-Phenylanthracene

99Ba 9,9'-Bianthracene

f9one 9H-Fluorenone

AD auto detachment

BaP Benz[a]anthracene

CT charge transfer

DBA Dibenz[a,h]anthracene

DBF Dibenzofurane

DFT density functional theory

CCD charge coupled device

Cu-Ph copper(II)-phtalocyanine

EA electron affinity

ECD electron capture detector

EELS electron energy loss spectroscopy

ESI-MS electrospray ionization mass spectrometry

ESR electron spin resonance

FC franck condon

FWHM full wide half maximum

HOMO highest occupied molecular orbital

ISC inter system crossing

IE ionization energy

LUMO lowest unoccupied molecular orbital

MALDI-MS matrix assisted laser desorption ionization mass spectrometry

MCP micro channel plate

MS Mass Spectrometry

OLED Organic light transmitting Diode

PAH Poly aromatic Hydrocarbons

PD Photodetachment

PE Photoelectron

PES Photoelectron Spectroscopy

PS post source focussing effect

REMPI resonance enhanced multi photon ionisation

SBCT symmetry breaking charge transfer

SOMO semi occupied molecular orbital

TADF thermally activated delayed fluorescence

TOF time-of-flight

List of Figures

List of Tables